THE TRANSIENT RECEPTOR POTENTIAL VANILLOID-1 CHANNEL IN STRESS-INDUCED ASTROCYTE MIGRATION

By

Karen W. Ho

Dissertation

Submitted to the Faculty of the

Graduate School of Vanderbilt University

in partial fulfillment of the requirements

for the degree of

DOCTOR OF PHILOSOPHY

in

Pharmacology

December, 2014

Nashville, Tennessee

Approved by:

David J. Calkins, Ph.D.
Bruce D. Carter, Ph.D.
Kevin Currie, Ph.D.
Vsevolod V. Gurevich, Ph.D.
Rebecca M. Sappington, Ph.D.
Gregg Stanwood, Ph.D.

ACKNOWLEDGEMENTS

Throughout this journey, there have been many people who have helped and guided me along the way. I would like to thank my advisor, Dr. David Calkins for his commitment to training and mentoring. His boundless energy, enthusiasm and passion for science have contributed to many of my successes. I appreciate his trust and confidence in my abilities to give me the freedom to pursue my research interests. The training and support I received from him are instrumental in my growth and development as a scientist. I would also like to thank the members of my committee. Dr. Gregg Stanwood, who chaired my committee, provided great help and thoughtful guidance throughout my graduate studies. Dr. Seva Gurevich and his knowledge of receptor theory pushed me to consider different aspects of TRPV1 pharmacology. Dr. Kevin Currie and Dr. Bruce Carter asked great questions that gave me another perspective regarding TRPV1 function and signaling. Dr. Rebecca Sappington taught me multiple techniques including primary cell isolations that became an integral part of my project. She always provided great advice and knowledge regarding the visual system, glaucoma and TRPV1.

Additionally, I also benefited tremendously from the support from a wonderful team of researchers in the Calkins Lab. I owe a great deal of gratitude to Dr. Wendi Lambert for her guidance and help throughout the years. She was always willing to listen, help me troubleshoot techniques and brainstorm new ideas and approaches. I am thankful for her knowledge and endless patience. Dr. Carl Weitlauf provided me with a novel perspective on my project, data analysis and interpretation. I also appreciate his guidance and advice on navigating the job market. Brian Carlson provided a great deal of help with the animal work and making sure I had the reagents and supplies for my experiments. Nick Ward is a fellow graduate student and a wonderful colleague. I am fortunate to have worked with so many incredible people.

I am also grateful to the Pharmacology department for their strong training program, and the Pharmacology training grant for helping fund my research. I am especially grateful to Karen Gieg, Joey Neil and Dr. Joey Barnett for their help and support. Part of my training is also attributed to the Vanderbilt Eye Institute, and I appreciate the support from Vanessa Alderson. I am also grateful to the Cell Imaging Shared Resource core at Vanderbilt, and my research has benefitted from their resources.

I am also thankful to the wonderful friends who have made my time in Nashville an exciting, interesting and fun one. And lastly, I would like to thank my parents, Wing and Joanna Ho. None of this would be possible without their infinite love and support. I am forever grateful.

TABLE OF CONTENTS

LIST OF FIGURES

ABBREVIATIONS

CNS	Central nervous system
RGC	Retinal ganglion cell
NFL	Nerve fiber layer
pNF	Phosphorylated neurofilament
MBP	Myelin basic protein
GFAP	Glial fibrillary protein
MTOC	Microtubule organizing center
TRP	Transient receptor potential
CAP	Capsaicin
RTX	Resiniferatoxin
CPZ	Capsazepine
IRTX	Iodo-resiniferatoxin
EPSC	Excitatory postsynaptic current
LTD	Long term depression
LTP	Long term potentiation
PBS	Phosphate buffered saline
EGTA	Ethylene glycol-bis (2-aminoethylether)-N,N,N',N'-tetraacetic acid
DIC	Differential interference contrast
DAPI	4',6-Diamidino-2-phenylindole
SEM	Standard error of the mean
AKAP	A-kinase anchor proteins
BrDU	Bromodeoxyuridine

CHAPTER 1

BACKGROUND AND INTRODUCTION*

1.1 Astrocyte Characterization

The central nervous system (CNS) is comprised of neurons and glia, non-neuronal cells that support neurons. Astrocytes are the main glia found in the CNS and account for 20-50% of the brain volume (Tower and Young, 1973). They are distinguished by their stellate morphology and exist in distinct, non-overlapping domains where they can establish networks with the vasculature and other cell types. Astrocytes exhibit incredible morphological and functional heterogeneity. The two main classes of astrocytes are protoplasmic and fibrous (Figure 1.1). Protoplasmic astrocytes are found in grey matter and contain many finely branched processes, whereas fibrous astrocytes are located in white matter and have longer processes (Robel et al., 2011b). However, at least nine morphological subtypes of astrocytes have been identified across regions in the CNS (Emsley and Macklis, 2006). Species-dependent differences in morphology also exist as humanoid astrocytes display increased complexity including a larger cell size and a greater number of processes than their rodent counterparts (Matyash and Kettenmann, 2010). Functional heterogeneity also exists amongst various astrocyte subtypes including differences in expression of neurotransmitter receptors, gap junction coupling and calcium signaling (Matyash and Kettenmann, 2010).

Despite their heterogeneity, astrocytes are vital in maintaining homeostasis of the extracellular environment and provide both metabolic and structural support to neurons.

* Portions of this chapter have been published previously in Ho KW, Ward NJ, Calkins DJ. TRPV1: a stress response protein in the central nervous system (2012) Amer J Neurodegener Dis 1(1):1-14.

Some of their main functions include providing ionic and fluid support, recycling neurotransmitters and serving as a metabolic and energy reserve. Once believed to mainly provide support to neurons, astrocytes are increasingly recognized to have much broader functions from modulating synaptic activity to contributing to neurodegeneration.

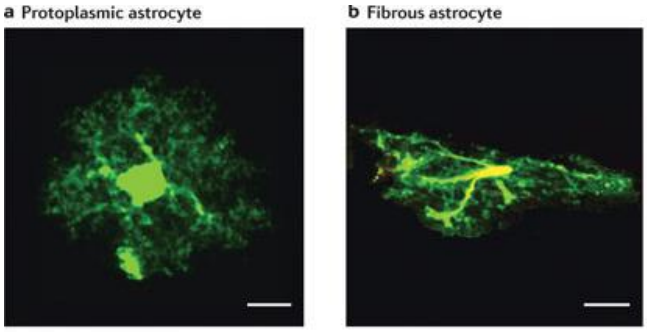

Figure 1.1. General astrocyte subtypes. Protoplasmic and fibrous are the main classifications of astrocyte subtypes. The morphology of astrocytes in normal CNS tissue is visualized with green fluorescent protein under the control of an astrocyte-specific promoter. Protoplasmic astrocytes are found in grey matter and possess finer, more branched processes than the fibrous astrocytes found in white matter. Scale: 10 μm.

Figure from Robel et al., 2011b and used in accordance with Copyright Clearance Center's RightsLink service.

1.2 Astrocyte Function

Astrocytes are coupled to other cell types and can serve as a connection between cells to facilitate communication. For example, astrocyte endfeet contact blood vessels while their processes can envelop axons of neurons, which allow astrocytes to serve as a link between neurons and the vasculature. Astrocytes are also connected to astrocytes and other cell types by

a network of gap junctions that facilitates communication and exchange of molecules between cells.

As a result of this network, astrocytes perform a variety of functions that support neuronal health and maintain homeostasis (Figure 1.2). In fact, extensive communication exists between astrocytes and neurons. For example, since astrocyte processes envelop neuronal processes and synapses, astrocytes facilitate neurotransmitter recycling and can modulate synaptic transmission. They also support neuronal survival by producing and releasing neurotropic factors, as well as providing energy substrates. Through their contact with the vasculature, astrocytes are also involved in maintenance of the blood-brain barrier and can modulate vascular dynamics in response to neuronal activity. Astrocytes are also important in maintaining ionic homeostasis and buffering the extracellular space through potassium buffering and fluid and pH regulation.

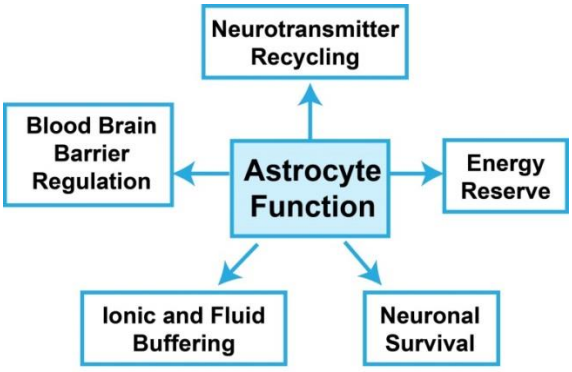

Figure 1.2. Common astrocyte functions. Astrocytes have multiple supportive functions to maintain CNS homeostasis.

During times of increased neuronal activity, the extracellular space accumulates excessive levels of glutamate and potassium. If they are not removed, these compounds can

affect neuronal synaptic transmission and channel kinetics. Astrocytes are responsible for clearing a majority of these compounds through a number of channels and transporters expressed on the cell surface (Figure 1.3). In fact, about 80% of glutamate in the extracellular space is cleared by perisynaptic astrocytes while the remaining 20% is taken up by neurons (Parpura and Verkhratsky, 2012). To take up excess glutamate, astrocytes express glutamate transporters like GLAST (or EAAT1) and GLT-1 (or EAAT2; Perego et al., 2000). Glutamate is then converted to its precursor, glutamine via glutamine synthetase. Glutamine is then released to neurons, which reconvert glutamine to active neurotransmitters. Similarly, astrocytes also mediate GABA recycling, whereby GABA is first converted to glutamate and then to glutamine, which is recycled to neurons (Sickmann et al., 2010). In addition to glutamate, astrocytes also mediate clearance of potassium. Potassium influx into astrocytes occurs through inward rectifying potassium channels (Walz, 2000). Unlike glutamate which is recycled, potassium is redistributed via gap junctions throughout the astrocyte network and is released into areas with low potassium concentrations.

In addition to neurotransmitter recycling, astrocytes also mediate synaptic pruning of neurons. Transcriptome profiling indicates astrocytes express genes involved in metabolism, lipid synthesis and phagocytosis (Cahoy et al., 2008). Proteins involved in phagocytosis like MEGF10 and MERTK can mediate dendritic pruning by astrocytes (Chung et al., 2013). Astrocytes can engulf synaptic material and deletion of MEGF10 and MERTK results in an excessive number of synapses in retinal neurons in the dorsal lateral geniculate nucleus (Chung et al., 2013). Phagocytosis of neuronal synapses and debris by astrocytes can also be mediated by the Draper signaling pathway and the Crk/Mbc/dCed-12 complex (Tasdemir-Yilmaz and Freeman, 2014).

Astrocytes also provide metabolic support to neurons by serving as energy reserves. This concept is known as the lactate shuttle (Belanger et al., 2011). During glutamatergic synaptic transmission, glutamate accumulates in the extracellular space and is transported into astrocytes via the Na^+-dependent glutamate transporters. The increased Na^+ activates the Na^+/K^+-ATPase pump that increases ATP consumption and glycolysis. Glycolysis is supported by the glucose transporter, Glut1 that facilitates uptake of glucose into astrocytes from the vasculature (Allen and Messier, 2013). Once glucose is taken up by astrocytes, it can be stored as glycogen or converted to lactate that is then released to neurons as an energy substrate.

Astrocytes are also coupled to blood vessels and help establish a link between neurons and the vasculature (Figure 1.4). Neuronal activity can induce an increase in astrocyte intracellular calcium, which triggers the production of arachidonic acid in astrocytes (Strokin et al., 2003). Arachidonic acid can generate prostaglandins or epoxyeicosatrienoic acids for vasodilation and 20-hydroxyeicosatetraenoic acid for vasoconstriction (Belanger et al., 2011). The endfeet of astrocytes envelop blood vessels and interact with endothelial cells that make up the blood brain barrier. (Figure 1.4). The blood brain barrier can provide neurons with nutrients and facilitate the removal of waste products. However, the passage of molecules into the CNS is restricted by tight junctions formed between endothelial cells. This limits the influx of potentially harmful substances from reaching neurons and helps maintain homeostasis of the CNS. Extensive communication and information exchange exist between endothelial cells and astrocytes (Figure 1.4; Abbott et al., 2006). Since astrocytes also interact with neurons, they serve as intermediates between neurons and the vasculature.

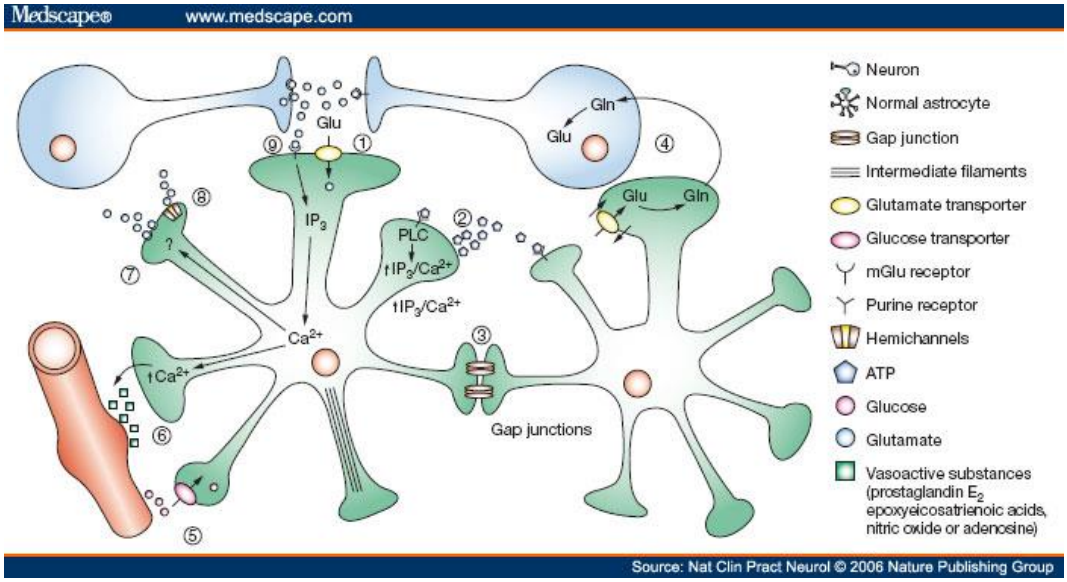

Figure 1.3. Astrocyte communication and interactions. Astrocytes communicate with both neurons and blood vessels. Neurons release glutamate that induces an increase in astrocyte intracellular calcium (1). Astrocytes communicate with other astrocytes through release of ATP (2) and a network of gap junctions (3). Astrocyte can provide metabolic support through glutamate recycling (4) and uptake of glucose (5). Astrocytes also mediate vascular dynamics (6), as well as take up and release glutamate (7, 8).

Figure from Maragakis and Rothstein, 2006 and used in accordance with Copyright Clearance Center's RightsLink service.

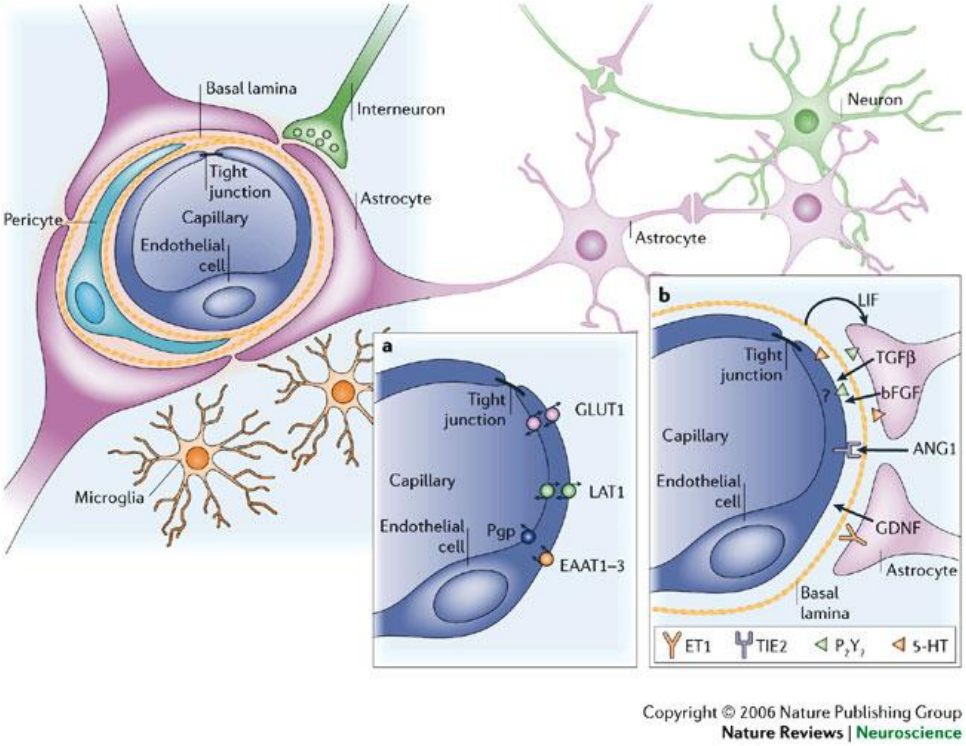

Figure 1.4. Components of the blood brain barrier. Astrocytes are one of the cell types that comprise the blood brain barrier. Astrocyte endfeet encircle endothelial cells. Both astrocyte and endothelial cells release factors to facilitate communication between the two cell types. Figure from Abbot et al., 2006 and used in accordance with Copyright Clearance Center's RightsLink service.

In addition to potassium and glutamate, astrocytes also regulate fluid and pH balance. Fluid accumulation in the brain can increase intracranial pressure and lead to tissue damage, but astrocytes reduce brain edema by maintaining water balance. Astrocytes express water channels like aquaporins, especially aquaporin 4 at their endfeet to regulate fluid redistribution (Fukuda and Badaut, 2012). In addition to aquaporins, astrocyte also express the Na^+/H^+ and Na^+/HCO_3^- transporters to regulate pH (Chesler, 2003). For these transporters, the movement of sodium is coupled to transport for H^+ or $HCO3^-$ in an isoelectic exchange. A change in pH can occur

through cellular respiration and activity. If not regulated, a drop in pH can affect enzyme function and ion channel activity, and ultimately influence cell viability (Chesler, 2003).

1.3 Astrocytes in the Retina and Optic Nerve

Astrocytes are found throughout the CNS, including the retina and optic nerve. In the retina, astrocytes are located in the nerve fiber layer where their processes envelop the axons of retinal ganglion cells (RGCs; Figure 1.5). The axons of RGCs converge to form the optic nerve, and the axon terminals synapse in the visual cortex. Retinal and optic nerve astrocytes both originate in the brain. During development, astrocytes migrate from the brain, down the optic nerve and into the retina (Watanabe and Raff, 1988). They enter the retina at the optic disk and migrate centrifugally to the periphery. By secreting factors like VEGF, astrocytes provide a template for endothelial cells to migrate and form the developing vasculature (Dorrell et al., 2002; Jiang et al., 1994; Ling et al., 1989; West et al., 2005).

The macroglia of the retina are comprised of astrocytes and Muller cells. Both cell types have similar functions and express similar genes. Although less focus has been placed on retinal astrocytes, studies have suggested that they exhibit similar properties to astrocytes found in the brain. In the retina, astrocytes are distributed across the surface where their processes surround RGC axons (Figure 1.6). In the mature retina, mechanical stimulation can lead to calcium wave propagation in astrocytes through release of ATP to modulate neuronal activity (Newman, 2001). Whether the modulation is excitatory or inhibitory depends on the type of RGC being recorded, although glial calcium waves generally reduced firing rates of RGCs (Newman and Zahs, 1998). Astrocytes are also involved in angiogenesis and maintenance of the blood-retinal barrier. Protection and rescue of astrocytes helped revascularize the retina and prevent pathological

neovascularization in the vitreous in a model of oxygen-induced retinopathy (Dorrell et al., 2010). Retinal astrocytes express aquaporin 4, suggesting they might be involved in osmosis and fluid redistribution (Nagelhus et al., 1998). They also express the glutamate transporters, EAAT4 and GLAST, as well as glutamine synthetase suggesting that retinal astrocytes also mediate glutamate recycling and uptake (Derouiche and Rauen, 1995; Ward et al., 2004).

In the optic nerve head, astrocytes are perpendicular to RGC axons and form columns through which the axons pass (Figure 1.7 and 1.8). Astrocytes provide structural support to RGC axons by synthesizing extracellular matrix molecules such as collagen and elastin (Hernandez, 1992; Hernandez et al., 1991). Astrocytes can extend processes through the extracellular matrix and contact other cell types, including RGC axons at the Nodes of Ranvier (Butt et al., 1994; Hernandez, 2000). The release of ATP and glutamate during an action potential can increase intracellular calcium in optic nerve astrocytes that propagates to neighboring glia (Hamilton et al., 2008). Astrocytes in the optic nerve also help buffer and regulate extracellular potassium levels during synaptic transmission. Inhibition of glial inward rectifying potassium channels increases extracellular potassium accumulation and prolongs axon recovery following compound action potentials (Bay and Butt, 2012).

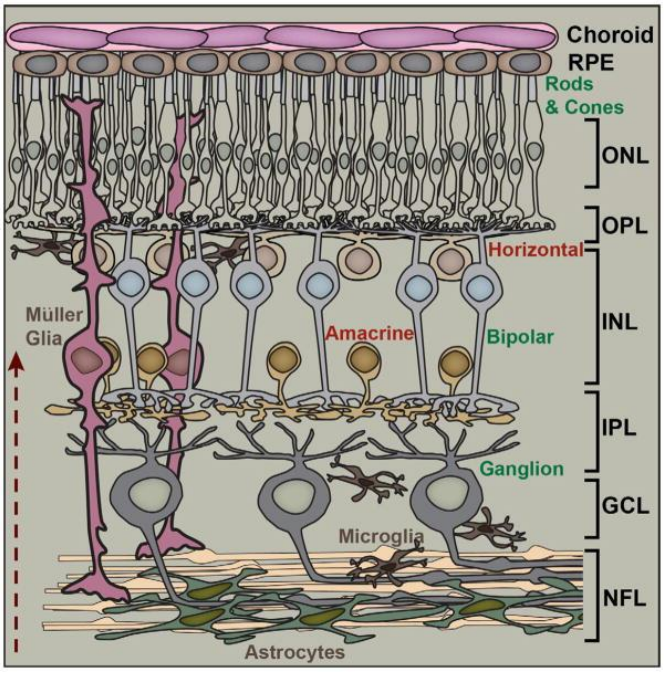

Figure 1.5. Retinal layers and cell types. Astrocytes are located in the nerve fiber layer (NFL) with the RGC axons.

Figure from Calkins 2006 and used in accordance with Copyright Clearance Center's RightsLink service.

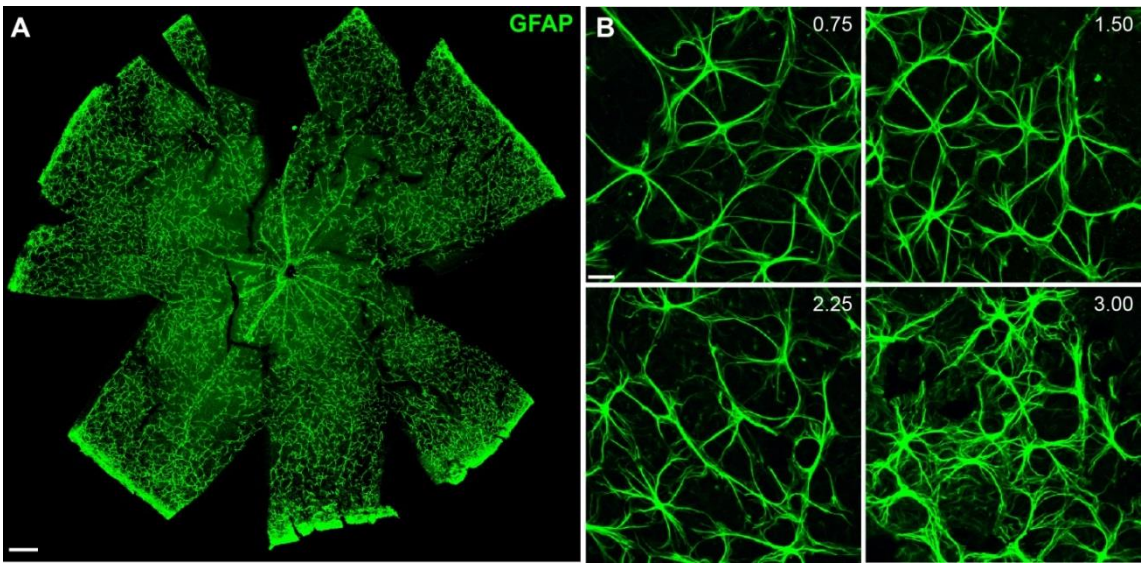

Figure 1.6. Astrocytes distribution in the retina. Confocal micrographs show the astrocyte plexus as labeled with GFAP (green) in the retina **(A)**. Astrocyte morphologies at various eccentricities from the retina are shown **(B)**. Scale: 500µm for A; 20µm for B.

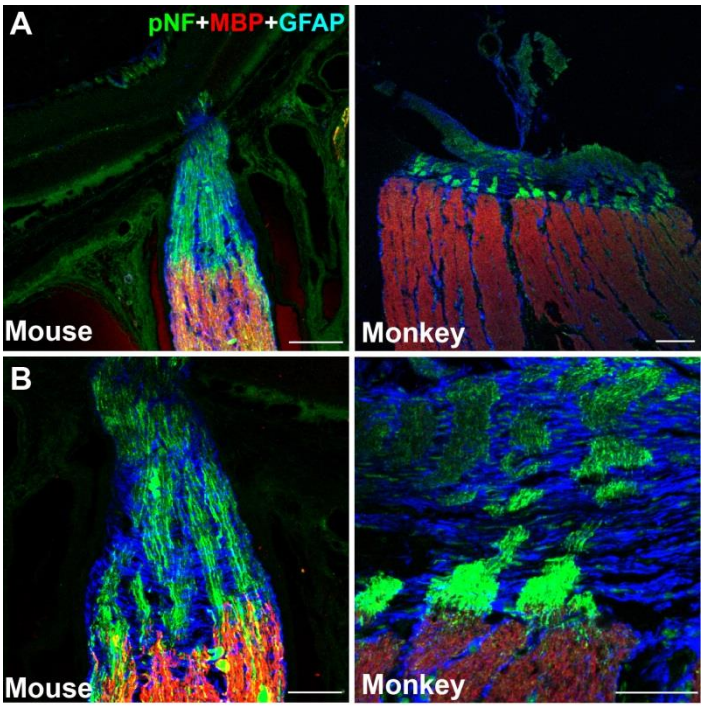

Figure 1.7. Astrocyte distribution in optic nerves. Confocal micrographs show astrocyte distribution in mouse and monkey longitudinal optic nerve sections. Mouse and monkey optic nerves are immunolabeled for phosphorylated neurofilaments (pNF; green), myelin basic protein (MBP; red) and glial fibrillary acidic protein (GFAP; blue) (**A**). High magnification images of the optic nerve head are shown (**B**). Scale: 100µm for A; 50µm for B.

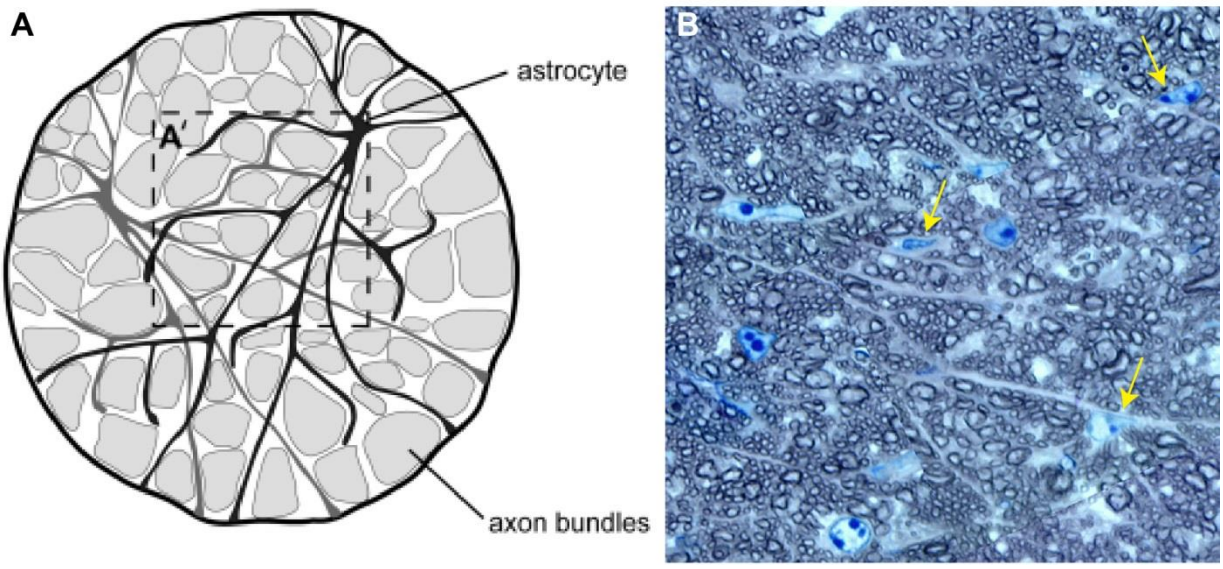

Figure 1.8. Astrocyte in optic nerve cross sections. A schematic depicts the orientation of astrocyte somas and processes relative to the axon bundles of RGCs **(A)**. The presence of astrocytes surrounding axon bundles in the optic nerve is further shown (yellow arrows; B). Figure from Sun et al., 2013a and used in accordance with Copyright Clearance Center's RightsLink service.

1.4 The Astrocyte Stress Response

In addition to their physiological contributions, astrocytes also serve a variety of functions under pathophysiological conditions. Following injury, astrocytes undergo a stress response known as reactive gliosis, which is characterized by both morphological and functional changes. A variety of stressors including ischemia, infection and apoptosis can trigger gliosis (Figure 1.9). Additionally, injury responses from other cells including microglia and leukocytes can release factors to induce astrocyte reactivity. Excessive astrogliosis has also been implicated in neurodegeneration. In Alzheimer's disease, exposure to amyloid-β can triggers gliosis, leading to reactive hypertrophic astrocytes encircling the neuritic plaque (DeWitt et al., 1998;

Nagele et al., 2004; Rodriguez et al., 2009). Increased astrogliosis has also been found in the substantia nigra, potentially contributing to the inflammatory state in Parkinson's disease (Koprich et al., 2008; McGeer and McGeer, 2008; Mena and Garcia de Yebenes, 2008). In glaucoma, reactive astrocytes in the retina and optic nerve are an early indication of pathology and contribute to axon loss (Inman and Horner, 2007; Son et al., 2010).

One defining characteristic of gliosis is astrocyte hypertrophy, which refers to a thickening of astrocyte soma and processes (Figure 1.10). Astrocyte hypertrophy can be due to increased expression of intermediate filaments including GFAP, vimentin and nestin. Astrocytes devoid of GFAP and vimentin have shorter processes compared to wild-type astrocytes following cortical lesion, although the volume occupied by reactive astrocytes is similar (Wilhelmsson et al., 2004). The processes of reactive astrocytes from GFAP and vimentin double-knockouts also appear as fine strands rather than as thick processes in a mouse model of Alzheimer's Disease (Kraft et al., 2013).

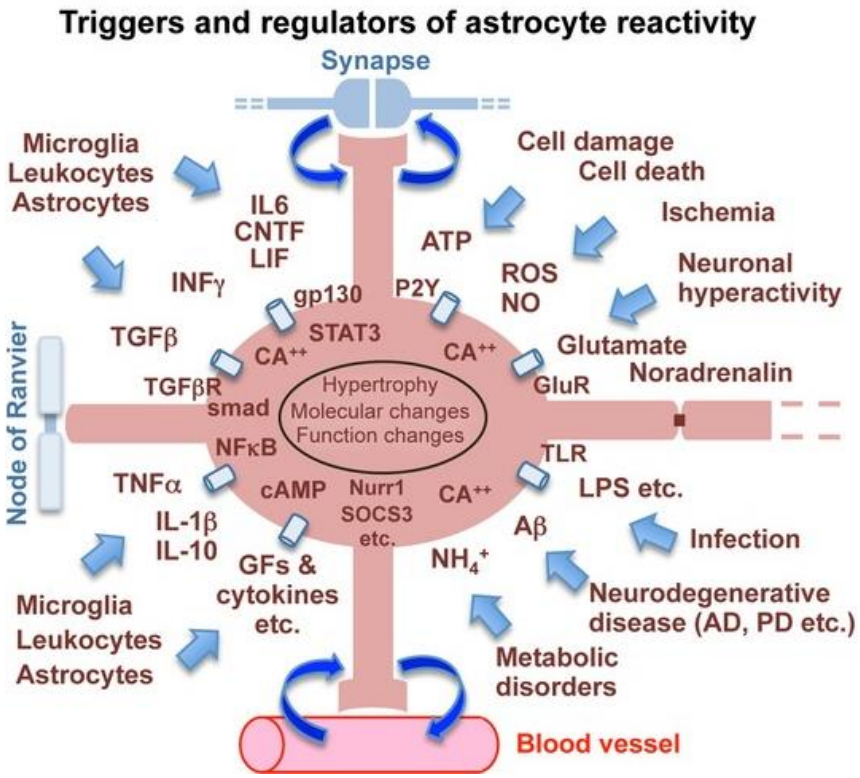

Figure 1.9. Triggers of astrocyte reactivity.

Figure from Sofroniew and Vinters, 2010 and used in accordance with Copyright Clearance Center's RightsLink service.

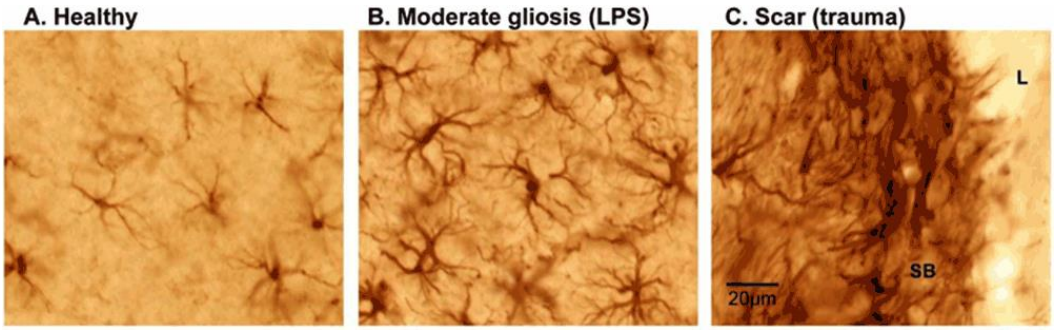

Figure 1.10. Grades of astrocyte reactivity following injury. Moderate gliosis induced by lipopolysaccharide results in astrocytes hypertrophy. More severe types of trauma, however, can lead to formation of a glial scar.

Figure from Verkhratsky et al., 2012 and used in accordance with Copyright Clearance Center's RightsLink service.

In addition to hypertrophy and glial scarring, astrocytes also undergo multiple functional changes (Figure 1.11). For example, they can secrete multiple pro-inflammatory cytokines like TNF-α, IL-1β and IL-6 and also chemokines including RANTES and IL-8 (Dong and Benveniste, 2001). These cytokines and chemokines have both beneficial and detrimental effects on neurons. TNF-α is a pro-inflammatory cytokine and can reduce the length and branching of hippocampal neurons *in vitro* (Neumann et al., 2002). It can also initiate a signaling cascade that leads to caspase activation and apoptosis in dopaminergic neurons (Mogi et al., 2000). However, there is evidence that TNF-α might also exert neuroprotective effects (Figiel, 2008). For example, TNF-α can activate NF-κB to lead to transcription of anti-apoptotic genes including Bcl-2and cIAP2 (Tamatani et al., 1999; Wang et al., 1998). It can also induce production of neuroprotective factors like NGF, GDNF and BDNF in astrocytes (Appel et al., 1997; Saha et al., 2006). Like TNF-α, IL-6 can be both pro- and anti-inflammatory depending on the signaling pathway that is activated (Scheller et al., 2011). IL-1β, on the other hand, is regarded as a pro-inflammatory cytokine that initiates multiple inflammatory responses (Allan et al., 2005). Increased levels of IL-1β have been observed in multiple neurodegenerative diseases (Luheshi et al., 2009). These cytokines can activate other astrocytes as well as microglia, which further exacerbate reactive gliosis.

Glial clearance of glutamate is also impacted by stress and injury. Expression of glutamate transporters, EAAT1 and EAAT2 is down-regulated in astrocytes in the glial scar and following traumatic brain injury, leading to reduced glutamate uptake (Schreiner et al., 2013; van

Landeghem et al., 2006). In models of Amyotrophic Lateral Sclerosis, reactive astrocytes reduce expression of glutamate transporters as well as release glutamate and nitric oxide. Both actions lead to excitotoxicity and apoptosis of neurons (Barbeito et al., 2004). Although some inconsistencies exist, expression of glutamate transporters in reactive astrocytes is generally reduced in epilepsy, stroke and other neurodegenerative diseases (Maragakis and Rothstein, 2004). A reduction in expression of glutamate transporters impacts the ability of astrocytes to clear the glutamate released during synaptic transmission, thereby contributing to neuronal excitotoxicity.

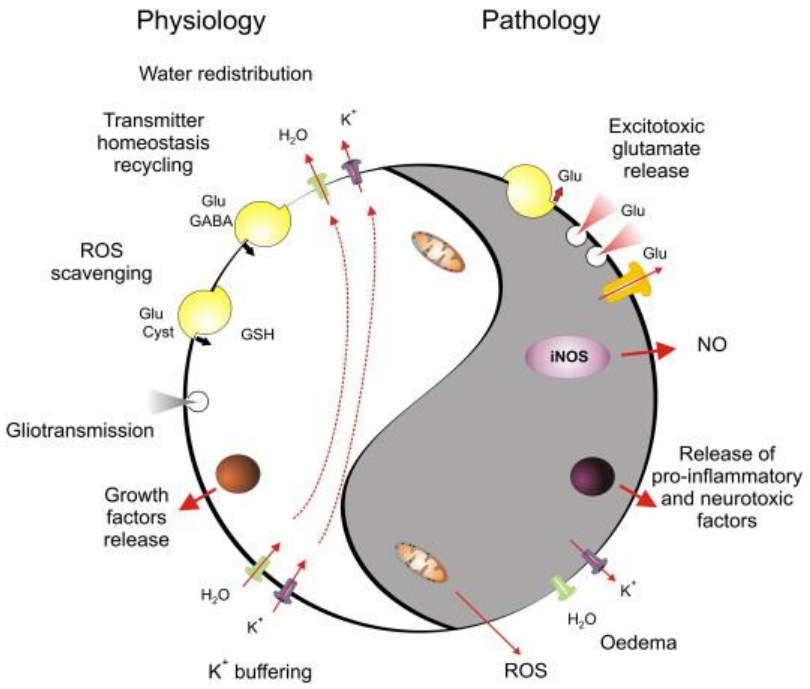

Figure 1.11. Functional changes in reactive astrocytes. Under physiological conditions, astrocytes help maintain homeostasis. Following injury, however, astrocytes can adopt functional changes that can be detrimental for neuronal survival.

Figure from Heneka et al., 2010 and used in accordance with Copyright Clearance Center's RightsLink service.

1.5 Relevance of Astrocyte Migration in Disease

A moderate injury will cause astrocyte hypertrophy, but in response to more severe injuries, astrocytes may also migrate to the injury site. Astrocyte migration within the CNS can underlie glial scar formation seen following spinal cord injury and traumatic brain injury (Di Giovanni et al., 2005; Yuan and He, 2013). Glial scar formation can exert both beneficial and detrimental effects on neuronal survival. For example, the scar can isolate the area of damage and help repair the blood-brain barrier, but it can lead to expression of extracellular matrix proteins like chondroitin sulfate proteoglycans that act as a barrier against axon regeneration (Silver and Miller, 2004). Astrocyte motility can be influenced by matrix metalloproteinases that degrade the extracellular matrix. For example, matrix metalloproteinase-9 knockouts display reduced astrocyte migration and decreased chondroitin sulfate proteoglycan expression and glial scarring following spinal cord injury (Hsu et al., 2008). Likewise, knockout of aquaporin-4 can also reduce motility as well as glial scarring after cortical stab injury (Saadoun et al., 2005). In addition to migration, astrocytes can also affect the response of other cell types involved in glial scarring. Following cortical stab injury, reactive astrocytes can secrete growth factors and cytokines to guide other migrating cells to the injury site (Wang et al., 2004). However, astrocytes can inhibit migration of both Schwann cells and oligodendrocyte precursor cells through increased production of cadherins that anchor the cells and decrease their motility (Fok-Seang et al., 1995; Wilby et al., 1999). Schwann cells and oligodendrocytes are recruited to myelinate the axon following injury, and reducing their migration to the damage site might impact nerve repair.

In addition to glial scar formation, astrocyte migration is important in the metastasis of gliomas. Gliomas account for about 70% of all brain tumors, and less than 3% of patients

survive five years after diagnosis (Ohgaki and Kleihues, 2005). One reason for the high mortality is the invasive and aggressive nature of glioma cells. Surgical removal of the tumor is usually unsuccessful, mostly because the malignant cells have already invaded the normal brain tissue. This leads to a recurrence of tumors usually within 1 cm of the resection site (Demuth and Berens, 2004). Increased cell motility contributes to the invasiveness of gliomas. Glioma cells upregulate genes that mediate migration, including genes involved in extracellular matrix remodeling and cell adhesion, such as matrix metalloproteinases, tenascin C, integrin and cadherins (Demuth and Berens, 2004). They can also migrate long distances at speeds of up to 100 μm/h along the surface of blood vessels with intermittent periods of proliferation in response to cues from the brain vasculature (Farin et al., 2006). Migrating glioma cells have an increased resistance to apoptosis, thus reducing the success of chemotherapy and many cytotoxic treatments (Mariani et al., 2001). These factors contribute to the invasive nature of gliomas and render the tumors difficult to manage. Drugs directed against matrix metalloproteinases or angiogenic targets, as well as treatments including surgery, radiotherapy, chemotherapy and immunotherapy have not significantly increased survival rate, and prognoses for high grade gliomas remain poor (Demuth and Berens, 2004; Ehtesham et al., 2004; Lefranc et al., 2009).

Astrocyte migration has also been observed in eye diseases including age-related macular degeneration and glaucoma. Under physiological conditions, retinal astrocytes are localized to the nerve fiber layer. However, in age-related macular degeneration and retinal detachment, retinal astrocytes can be found in the vitreous cavity, suggesting that they have migrated from the nerve fiber layer to the vitreous (Morino et al., 1990; Ramirez et al., 2001). Ischemia can occur in age-related macular degeneration and results in a high metabolic need. It has been suggested

that astrocytes migrate into the vitreous to help meet that metabolic demand and send nutrients to the retina through intercellular gap junctions (Ramirez et al., 2001).

Glaucoma is a blinding disease that results from degeneration of the RGCs and their axons, and an estimated 79.6 million people will be affected by the disease by 2020 (Quigley and Broman, 2006). Currently, there is no cure for glaucoma, and once vision is lost, it is nearly impossible to restore. Increased intraocular pressure is one risk factor and currently the only modifiable factor for glaucoma. Indeed, many glaucoma treatments attempt to lower intraocular pressure (Lee and Higginbotham, 2005). Like other neurodegenerative diseases, astrocyte reactivity is seen in both the retina and optic nerve in glaucoma (Inman and Horner, 2007; Son et al., 2010). In response to elevated hydrostatic pressure *in vitro*, astrocytes increase migration and proteolytic degradation of the extracellular matrix (Tezel et al., 2001a). Reactive astrocytes in the optic nerve can migrate into the nerve bundles and occupy the spaces left by degenerating RGC axons (Miao et al., 2010). Like in gliomas, genes involved in migration, including tenascin C, integrins, neural cell adhesion molecule, matrix metalloproteinases and myosin light chain kinase also show differential expression in glaucomatous astrocytes (Hernandez et al., 2008; Miao et al., 2010).

Reactive astrocytes can migrate in response to injury, and can exert both beneficial and detrimental effects on neuronal survival. Astrocytes can release inflammatory mediators like nitric oxide and TNF-α, but can also increase production of protective factors like brain-derived neurotrophic factor (Crish et al., 2013; Liu and Neufeld, 2000; Tezel and Wax, 2000). Astrocytes in the glial scar impede axon regeneration but can also repair the blood-brain barrier and isolate the area of damage to minimize the impact on healthy surrounding tissue (Silver and Miller, 2004). By better understanding the mechanisms and signaling pathways that underlie

astrocyte migration, perhaps novel therapeutic interventions can be developed to temper glial scar formation, glioma metastasis and other detrimental effects of astrocyte motility.

1.6 Cell Migration

Cell migration requires a coordinated cascade involving multiple receptors, proteins and signaling pathways, and can essentially be divided into six general steps (Figure 1.12):

1. Establishment of direction and polarity
2. Protrusion of the leading edge
3. Attachment to the extracellular matrix
4. Contraction of the cell
5. Release of the cell rear
6. Recycling of proteins to the front of the cell

The first step in migration is to establish directionality. One way polarity is created is through detection of a chemotactic gradient. Cells can migrate in response to a variety of stimuli including growth factors, chemokines and other extracellular molecules. For example, astrocytes can migrate in response to platelet derived growth factor, transforming growth factor β and the nucleotide UTP (Bressler et al., 1985; Morganti-Kossmann et al., 1992; Wang et al., 2005b). Astrocytes also express chemokine receptors CXCR4, CCR1, CCR5, and CX3CR1 that would enable the cell to detect chemokines and migrate (Dorf et al., 2000). Activation of multiple signaling proteins, including CDC42, Par6 and PKC, can reorient the microtubule organizing center (MTOC) in the direction of migration to establish polarity in astrocytes (Etienne-Manneville and Hall, 2003).

Upon establishing polarity, cell protrusion occurs to form the leading edge. Cell protrusion is generally mediated by remodeling of the cytoskeleton. In astrocytes, the leading edge is formed primarily by polymerization of microtubules radiating from the MTOC, although actin assembly can also modulate this process (Baorto et al., 1992; Etienne-Manneville, 2013). The leading edge then must contact and adhere to the extracellular matrix. This is mediated by the formation of focal adhesions that link actin stress fibers to integrins, which are receptors for the extracellular matrix. Astrocytes express multiple integrins including $\alpha1\beta1$, $\alpha3\beta1$, $\alpha5\beta1$ and $\alpha6\beta1$ to bind laminin, collagen and fibronectin (Tawil et al., 1993; Tawil et al., 1994). Adherence to the extracellular matrix may be regulated by signaling pathways, such as the JAK-STAT pathway with the transcription activator Stat3 (Buffo et al., 2010). Astrocytes from Stat3-/- mice display reduced migration and increased expression of E-cadherin, which might increase adhesion of cells to inhibit motility (Okada et al., 2006).

Once the leading edge adheres to the extracellular matrix, the cell undergoes contraction. The contractile forces are usually generated by interactions between actin and myosin II. Myosin II can bind actin and move actin fibers in an anti-parallel direction (Vicente-Manzanares et al., 2009). Microtubules can indirectly influence this process by modulating signaling proteins like RhoA, which activates myosin (Liu et al., 1998). These contractile forces can push the cell forward in the direction of migration. Once the cell has moved, it has to detach from the extracellular matrix. Cell detachment is mediated by disassembly of focal adhesions while retraction of the cell rear is mediated by actin-myosin interactions (Broussard et al., 2008; Mitchison and Cramer, 1996).

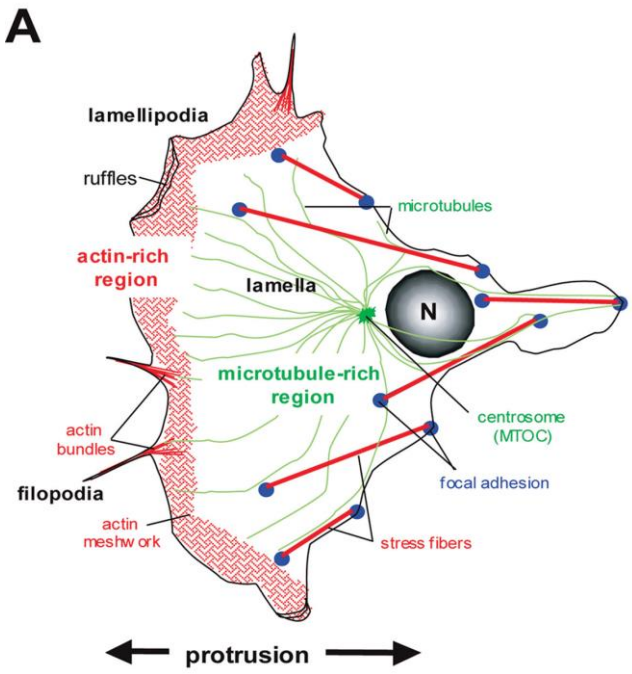

Figure 1.12. The cytoskeleton of a migrating cell. This schematic shows the localization of actin (red), microtubules (green) and focal adhesions (blue) in a migrating cell.

From Etienne-Manneville, 2004a and used in accordance with Copyright Clearance Center's RightsLink service.

1.7 Components of Cell Migration

In addition to providing the structural framework of the cell and mediating normal cellular function, the cytoskeletal rearrangement that occurs following injury is a key driving force underlying migration. The astrocyte cytoskeleton is made up of three main components: actin, microtubules and intermediate filaments. Each of these components plays a role in migration. Additionally, a variety of receptors, proteins and signaling pathways all converge to mediate the cytoskeletal rearrangements that occur during migration.

Actin: Actin can transition between two states: monomeric (G-actin) and filamentous (F-actin). Actin polymerization occurs through addition of actin monomers at the barbed (+) end of the filament, while disassembly occurs at the pointed (-) end in an ATP-dependent process (Dominguez and Holmes, 2011). The actin cytoskeleton can also undergo various modifications that are mediated by multiple actin binding proteins. Actin binding proteins can facilitate assembly/disassembly by sequestering G-actin monomers to prevent polymerization, dissociating F-actin into G-actin, capping the barbed or pointed ends to prevent turnover, severing actin into shorter filaments and crosslinking actin to promote filament polymerization and branching (dos Remedios et al., 2003).

The actin cytoskeleton mediates multiple aspects of astrocyte function. Disruption of actin dynamics can reduce the propagation of calcium waves (Cotrina et al., 1998). Similarly, inhibition of actin polymerization with cytochalasin D affects the morphological clustering of the glutamate transporter, GLT-1 to disrupt glutamate uptake and recycling (Zhou and Sutherland, 2004). The actin cytoskeleton is also involved in gating ion channels, including outwardly rectifying chloride-selective channels and calcium channels (Johnson and Byerly, 1993; Lascola et al., 1998). In neocortical astrocytes, polymerization or stabilization of actin increased the probability of chloride channels being in the open state, which was reduced when actin polymerization was inhibited (Lascola et al., 1998). Actin can also modulate voltage-gated calcium channels, as stabilization of actin can prolong calcium channel activity and reduce its inactivation (Johnson and Byerly, 1993).

In addition to normal astrocyte function, actin has also been shown to mediate gliosis. Following scratch wound or stab injury, astrocytes increased expression of palladin, an actin-

binding protein (Boukhelifa et al., 2003). Palladin was also increased along the edge of the injury and correlated with increased actin assembly (Boukhelifa et al., 2003). Addition of IL-6 can result in actin reorganization and loss of stress fibers without affecting overall actin levels (John et al., 2004). Consequently, IL-6 slowed astrocyte migration following scratch injury. During migration, astrocytes treated with IL-6 randomly extended and collapsed their processes and lacked coordination, while control cells were able to protrude a process, contact the extracellular matrix and push forward (John et al., 2004).

Microtubules: Microtubules are formed from the polymerization of α- and β- tubulin in a process that is dependent on GTP. Like actin, microtubule filaments are polarized – tubulin monomers are usually added to the plus-end and dissociated from the slower minus-end. When microtubules transition from growth to shrinkage, the process is known as catastrophe, and the transition from shrinkage to growth is referred to as rescue (van der Vaart et al., 2009). They can also undergo a process known as dynamic instability, which is characterized by rapid growth and disassembly. Microtubules interact with microtubule-associated proteins that stabilize and cross-link microtubules. Generally, microtubule-associated proteins can regulate shrinkage speeds and modulate the frequencies of catastrophe and rescue to promote disassembly or growth (van der Vaart et al., 2009).

Microtubules can regulate a variety of cellular functions including morphology, cell division and intracellular transport (Nogales, 2000). Addition of colchicine to inhibit microtubule polymerization reduced expression of the microtubule-associated protein, MAP-2 and shortened astrocyte processes (Couchie et al., 1985). Microtubule disassembly can also cause vimentin filaments to condense and aggregate into bundles in glioma cells (Sorci et al.,

2000). In addition to mediating morphology, microtubules help position the centrosome during cell division. The motor protein, dynein can interact with microtubules to generate a pulling force that reorients the centrosome in astrocytes (Etienne-Manneville, 2004). Microtubules are also involved in cellular transport, and provide the tracks for the motor proteins dynein and kinesin to transport membrane-bound vesicles or organelles (Goldstein and Yang, 2000).

Similar to actin, microtubules can also regulate aspects of gliosis. Reactive astrocytes have been shown to increase expression of MAP2, a protein usually found in dendrites of neurons (Geisert et al., 1990). Stabilization of microtubules can reduce astrocyte reactivity, glial scarring and promote axon regeneration following spinal cord injury (Hellal et al., 2011). Addition of taxol to stabilize microtubules reduced the levels of both glycosaminoglycan and chondroitin sulfate proteoglycan (Hellal et al., 2011). Following sciatic nerve injury, addition of taxol induced axon regeneration in dorsal root ganglion neurons and neurons from the Raphe spinal tract compared to the retraction observed in vehicle-treated neurons (Hellal et al., 2011).

Intermediate Filaments: Intermediate filaments are a diverse group of proteins and are classified into five types based on amino acid sequence. The main type found in astrocytes is Type III intermediate filaments which include vimentin, nestin and GFAP (Eliasson et al., 1999). Intermediate filaments are formed by one filament strand coiling around another to create a dimer. Dimers then associate to form tetramers, and tetramers associate to form protofilaments which combine together to form the filament (The Cell: A Molecular Approach. 2nd edition. Cooper GM). In vimentin knockout animals, astrocytes retained expression of GFAP though expression was lowered. GFAP filaments were also less condensed with increased spacing between each filament (Eliasson et al., 1999). Unlike GFAP, vimentin cannot form filaments

without associating with another Type III filament. Examples include vimentin-GFAP and vimentin-nestin interactions (Eliasson et al., 1999). In cortical astrocytes, intermediate filament organization within the cell appears to be dependent on microtubules, as stabilization or depolymerization of microtubules resulted in a re-distribution of intermediate filaments and inhibited astrocyte process extension in the presence of dibutyryl cyclic AMP (Goetschy et al., 1986). Microtubule-associated proteins like MAP2 can also interact with intermediate filaments to regulate the movement and transport of intermediate filaments along microtubules (Chang and Goldman, 2004).

Intermediate filaments form both a cytoplasmic and a nuclear network, thus connecting cell-to-cell junctional complexes at the plasma membrane to the nuclear matrix in order to modulate the dynamics and structural integrity of cells (Herrmann et al., 2007; Middeldorp and Hol, 2011). The cytoplasmic intermediate filament network can act to stabilize cell morphology and reinforce microtubules (Herrmann et al., 2007). In astrocytes, GFAP is the major intermediate filament, and recent work has suggested this protein can affect a multitude of functions including maintenance of cell shape, astrocyte motility, proliferation and vesicular trafficking (Middeldorp and Hol, 2011). GFAP can also modulate neuronal function via astrocyte-mediated changes in synaptic plasticity, regulation of the blood brain barrier and CNS myelination (Middeldorp and Hol, 2011).

Increased expression of intermediate filaments, like GFAP, is a hallmark of astrocyte reactivity. Astrocytes from vimentin/GFAP double knockout mice exhibit a reduction in hypertrophy and had shorter processes following cortical lesion, and this was accompanied by increased synaptic regeneration (Wilhelmsson et al., 2004). In addition to mediating hypertrophy, intermediate filaments are involved in the transient swelling of astrocytes in

response to osmotic stress. Spinal cord astrocytes that lacked GFAP swelled slower compared to wild-type in hypotonic or high potassium solutions (Anderova et al., 2001). Intermediate filaments have also been shown to mediate migration. For example in glioma cells, induced expression of GFAP reduced migration and elongated cell processes (Elobeid et al., 2000). Studies using vimentin knockout mice showed reduced migration and altered arrangement of actin and focal adhesions in fibroblasts (Eckes et al., 1998). In astrocytes, nestin, vimentin and GFAP interact with actin to position the nucleus following scratch injury (Dupin et al., 2011). Astrocytes that lack either GFAP or vimentin also have reduced speed but maintained their sense of direction (Lepekhin et al., 2001).

Focal Adhesions: To migrate effectively, a cell needs to contact and adhere to the extracellular matrix. Focal adhesions help mediate this process by linking actin stress fibers to integrins and proteoglycans (Figure 1.13). They are comprised of a variety of proteins including scaffolding proteins, GTPases and kinases. Focal adhesions can vary in size. Smaller focal adhesions, known as focal contacts, localize to the cell periphery and are regulated by the small GTPases CDC42 and Rac (Nobes and Hall, 1995). Focal contacts can develop into larger complexes known as focal adhesions. Focal adhesions are found both peripherally and centrally within a cell and are regulated by the GTPase Rho (Chrzanowska-Wodnicka and Burridge, 1996; Ridley and Hall, 1992). Downstream effectors of Rho that modulate such events include PI 3-kinase and actin binding proteins including cofilin (for review, see (Raftopoulou and Hall, 2004). In addition to GTPases, other proteins that modulate focal adhesions include kinases like focal adhesion kinase and src, and scaffold proteins such as paxilin (Frame et al., 2002; Shen and Schaller, 1999; Turner, 2000).

Once the leading edge of the cell contacts the extracellular matrix, small focal contacts that contain mainly paxilin and α-actinin are established (Laukaitis et al., 2001). Tenascin C can mediate this process by interacting with extracellular matrix molecules like fibronectin (Midwood and Schwarzbauer, 2002). Tenascin C can also modulate focal adhesion kinase and RhoA, and induce loss of focal adhesions (Chung et al., 1996; Midwood and Schwarzbauer, 2002). Other proteins, including talin, vinculin, and focal adhesion kinase, are then recruited to form focal adhesions and stabilize the leading edge (Wozniak et al., 2004; Zaidel-Bar et al., 2003). Once focal adhesions form, they have to be disassembled to allow migration. Src and calpains can modulate focal adhesion turnover. For example, src kinase generally leads to cell detachment and one mechanism is through phosphorylation of integrins (Parsons and Parsons, 1997). The calpain proteases also lead to disassembly by cleaving proteins found in focal adhesions including talin and α-actinin (Bhatt et al., 2002; Dourdin et al., 2001).

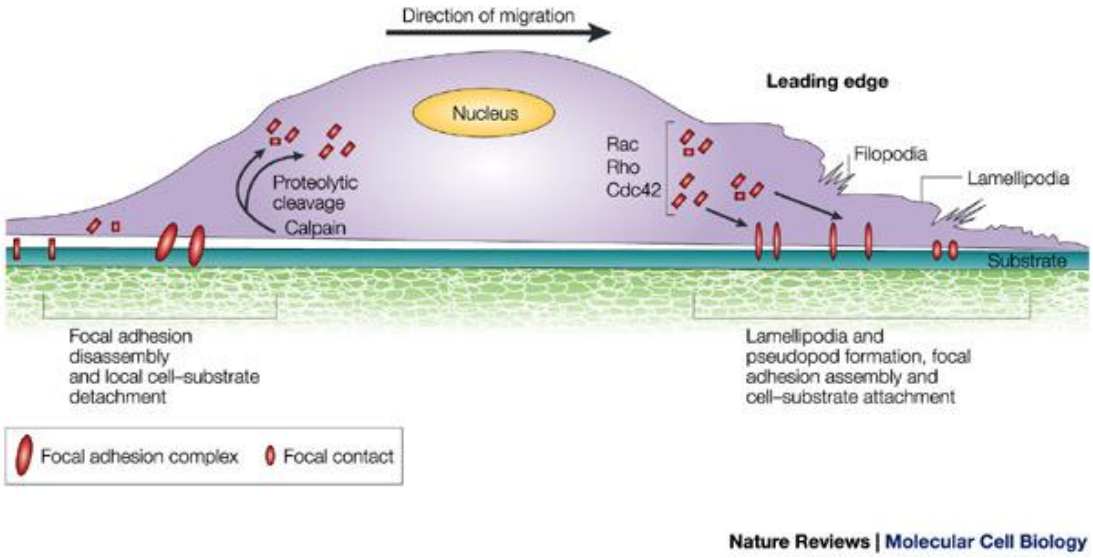

Figure 1.13. Focal adhesion dynamics in a migrating cell. This diagram illustrates focal adhesion assembly at the leading edge, and disassembly at the cell rear. This process is mediated by various proteins including calpains, Rac, Rho and CDC42.

Figure from (Frame et al., 2002) and used in accordance with Copyright Clearance Center's RightsLink Service.

1.8 Calcium Signaling in Astrocytes

Astrocytes can respond to a wide variety of stimuli with increases in calcium. For example, mechanical stimulation increases intracellular calcium in retinal astrocytes (Newman, 2001). This increase in calcium can spread to neighboring astrocytes via both intracellular and extracellular pathways. Intracellularly, inositol triphosphate (IP3) can pass through gap junctions and activate IP3 receptors in the endoplasmic reticulum to release calcium from intracellular stores (Scemes and Giaume, 2006). In the extracellular pathway, glutamate and ATP are released and bind to glutamate and purinergic receptors on the plasma membrane to increase calcium (Scemes and Giaume, 2006). In addition to mediating intercellular communication, calcium is also important for astrocytes in modulating synaptic transmission. Glutamate that is released into the extracellular space during neuronal synaptic activity can bind metabotropic glutamate receptors on astrocytes. This leads to increased intracellular calcium and the subsequent release of gliotransmitters, including glutamate, ATP and D-serine to modulate neuronal activity. This enables astrocytes to interact with pre- and post-synaptic neurons at the synaptic cleft and form a unit known as the tripartite synapse. The tripartite synapse mediates the bi-directional communication between neurons and astrocytes (Perea et al., 2009).

Calcium signaling is an important component of the astrocyte stress response. Indeed, reactive astrocytes can exhibit aberrant calcium dynamics in neurodegenerative diseases (Agulhon et al., 2012). Reactive astrocytes also increase expression of L-type calcium channels following brain injury (Westenbroek et al., 1998). Inhibition of L-type calcium channel with the drug verapamil can reduce GFAP upregulation in astrocytes following cortical lesion (Klepper et al., 1995). Calcium influx through L-type calcium channels also activates calpains to induce astrogliosis and GFAP expression following injury (Du et al., 1999). The IP3 receptor can also mediate reactive gliosis as astrocytes from IP3 receptor knockouts have reduced GFAP expression following neocortical stab wound injury (Kanemaru et al., 2013). In addition to hypertrophy, calcium increases are necessary for astrocytes to release IL-6 (Codeluppi et al., 2014). Also, functional voltage-gated calcium channels and ryanodine receptors are required for glial cell migration (Lohr et al., 2005; Matyash et al., 2002).

In addition to gliosis, calcium is an important signaling molecule in cell migration. A migrating cell can exhibit a calcium gradient that is higher posteriorly (Brundage et al., 1991). This calcium gradient might be important in establishing cell polarity and mediating retraction at the cell rear. Calcium microdomains at the leading edge of the cell are important for turning the cell and creating directionality (Wei et al., 2009). The calcium binding protein, S100A4 can interact with myosin-IIA to mediate cell protrusion (Li and Bresnick, 2006). Additionally, many proteins that regulate the cytoskeleton are contain calcium-binding sites and are, in turn, regulated by calcium. For example the actin crosslinking protein, α-actinin and the actin severing protein, gelsolin contain two and three calcium-binding sites respectively (Lamb et al., 1993; Noegel et al., 1987). Focal adhesion dynamics are also modulated by calcium. Calcium-activated proteins like CaMKII, calcineurin and calpains can modulate focal adhesion assembly

and turnover (Conklin et al., 2005; Easley et al., 2008; Glading et al., 2002). Since calcium mediates multiple aspects of astrocyte function during physiology and following injury, astrocytes express a variety of channels and receptors to regulate calcium levels (Figure 1.14). These calcium channels include transporters, metabotropic receptors and ligand-gated and voltage-gated channels.

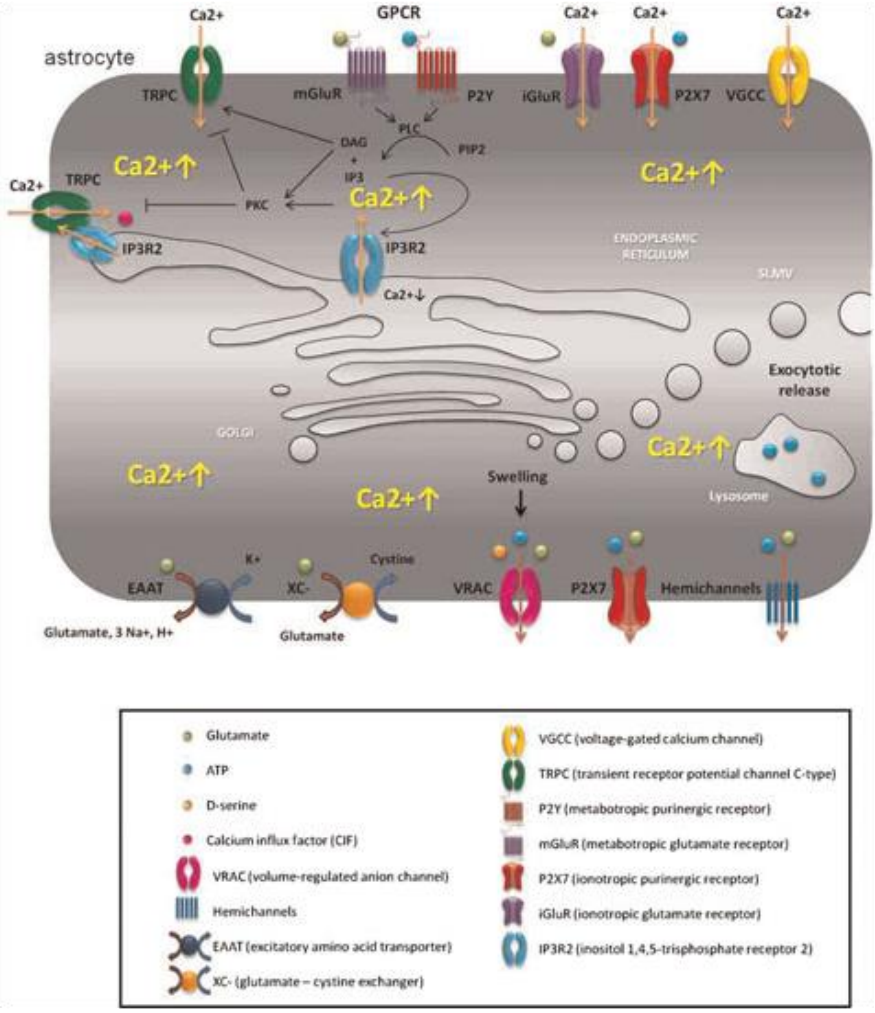

Figure 1.14. Calcium channels and receptors in astrocytes.

From Achour SB et al., 2010 and used in accordance with Copyright Clearance Center's RightsLink service.

1.9 The Transient Receptor Potential Vanilloid 1 Channel

One family of calcium channels expressed by astrocytes is the transient receptor potential (TRP) family. TRP channels are a diverse group that regulates cation entry and contributes to a vast variety of physiological functions. There are 28 mammalian TRPs, divided into 6 subfamilies based on homology: canonical (TRPC1-7), vanilloid (TRPV1-6), melastatin (TRPM1-8), ankyrin (TRPA1), polycystin (TRPP1-3) and mucolipin (TRPML1-3). All six members share a common structure of six transmembrane domains with a hydrophobic pore located between the fifth and sixth domains. TRP channels can respond to a variety of external stimuli including temperature, osmolality, mechanical force, chemoattractants and ischemia (Christensen and Corey, 2007; Jost et al., 1992; Liu et al., 2007; Simard et al., 2007; Wang and Poo, 2005). Characterized by an increased calcium flux, TRP activation has been implicated in many calcium-mediated events including synaptic transmission, neuronal death, axon pathfinding and visual transduction (Aarts and Tymianski, 2005; Clapham et al., 2001; Cui and Yuan, 2007; Montell, 2005; Munsch et al., 2003).

Similar to other TRP channels, TRPV1 displays robust calcium conductance and has a 10-fold greater selectivity for calcium versus sodium (Kauer and Gibson, 2009). TRPV1 is known for its role in pain sensation where it modulates levels of intracellular calcium in nociceptive neurons (Caterina et al., 1997; Hagenacker et al., 2008). Activation of TRPV1 in nociceptive neurons induces release of neurotransmitters and neuropeptides involved in pain transmission, including substance P and calcitonin gene-related peptide, thereby making TRPV1 an attractive target for hyperalgesic drugs (Gazzieri et al., 2007; Nakanishi et al., 2010)).

1.10 TRPV1 pharmacology

TRPV1 was first isolated as the receptor for capsaicin (CAP), the prototypical TRPV1 agonist (Caterina et al., 1997). Subsequent research has demonstrated that in TRPV1 knockout animals, capsaicin-induced activity such as nociceptive behavior, glutamate transmission, ethanol avoidance, wound healing and vasoconstriction is eliminated (Caterina et al., 2000; Ellingson et al., 2009; Keeble and Brain, 2006; Musella et al., 2009; Sumioka et al., 2014). One of the most potent agonists of TRPV1 is resiniferatoxin (RTX), a plant toxin isolated from the plant *Euphorbia resinifera.* RTX has a molecular structure similar to and recognizes the same vanilloid binding sites on TRPV1 as CAP, but is about 20-fold more potent than CAP (Raisinghani et al., 2005; Szallasi et al., 1993). Endogenous ligands of TRPV1 include endocannabinoids (anandamide and N-arachidonolydopamine), lipoxygenase products, protons and heat.

Capsazepine (CPZ) was one of the first competitive antagonists of CAP and RTX found. CPZ can block vanilloid-induced activity in multiple cell types including nociceptive neurons in the dorsal root ganglion, corneal epithelial cells, hippocampal interneurons and microglia (Bevan et al., 1992; Dickenson and Dray, 1991; Gibson et al., 2008; Kim et al., 2006; Yang et al., 2010b)). Iodination of a moiety on RTX led to the discovery of iodo-resiniferatoxin (IRTX), another TRPV1-selective antagonist. Binding experiments revealed that IRTX is 40 times more potent than CPZ, and can displace vanilloid binding as well as block vanilloid-induced activity in neurons from the dorsal root ganglia, microglia, dopaminergic neurons and other cell types (Kim et al., 2006; Marinelli et al., 2003; Seabrook et al., 2002; Wahl et al., 2001). Endogenous inhibitors of TRPV1 include PIP_2 and adenosine (Puntambekar et al., 2004; Rosenbaum and Simon, 2007).

1.11 Structure and Modulation of TRPV1

Structural analysis of TRPV1 indicates a compact transmembrane region and a large basket-like intracellular domain (Moiseenkova-Bell et al., 2008). Figure 1.15 shows the structure of TRPV1. TRPV1 contains six transmembrane domains. The N-terminal tail has numerous phosphorylation sites and ankyrin repeats that serve as binding sites for calmodulin and ATP (Lishko et al., 2007). The C-terminal tail has a TRP domain and binding sites for both calmodulin and PIP_2, an endogenous TRPV1 inhibitor (Garcia-Sanz et al., 2004; Numazaki et al., 2003; Ufret-Vincenty et al., 2011). Within the extracellular loop domain, the amino acid residues Glu600 and Glu648 can regulate TRPV1 activation by protons, allowing for pH sensitivity (Jordt et al., 2000). Agonist activation is also mediated intracellularly, as lipophilic capsaicin readily crosses the membrane to bind several sites on TRPV1 (Jung et al., 1999). Mutation and deletion studies have identified multiple residues critical for activation. Deletion of Thr550 in transmembrane region 4 can reduce capsaicin sensitivity (Gavva et al., 2004). Deletion of Arg114 and Glu761 in the N- and C-termini can block capsaicin-induced currents without affecting its activation by heat (Jung et al., 2002). Mutations of Tyr511 and Ser512 can abolish capsaicin responses, yet leave activation by heat and protons intact (Jordt and Julius, 2002).

Phosphorylation is also important in modulating the channel allowing for rapid responses to external stimuli or environmental changes. Generally, phosphorylation sensitizes while dephosphorylation desensitizes the channel. PKC phosphorylation at Ser800 reverses desensitization of TRPV1 from prolonged capsaicin treatment and increases the sensitivity of TRPV1 to agonists (Mandadi et al., 2006; Varga et al., 2006). Forskolin-mediated activation of PKA can decrease capsaicin-induced desensitization of TRPV1, a phenomenon that is blocked

by a PKA inhibitor (Mohapatra and Nau, 2003). PKA can also reduce desensitization by direct phosphorylation of TRPV1 at Ser116 (Bhave et al., 2002). In addition, PKC or PKA activation through stimulation of multiple receptors including the protease-activated receptor PAR2, bradykinin B1 and B2, purinergic P2 receptors, chemokine receptor CCL3 and endothelin receptors have all been shown to increase sensitivity of the channel (Amadesi et al., 2006; Tominaga et al., 2001; Vellani et al., 2004; Yamamoto et al., 2006; Zhang et al., 2005a). Src kinase, CaMKII and PI3K can all phosphorylate TRPV1 and increase sensitivity as well (Price et al., 2005; Van Buren et al., 2005; Zhang et al., 2005b). On the other hand, dephosphorylation by calcineurin/PP2B and increases in intracellular calcium can desensitize the channel (Koplas et al., 1997; Mohapatra and Nau, 2005).

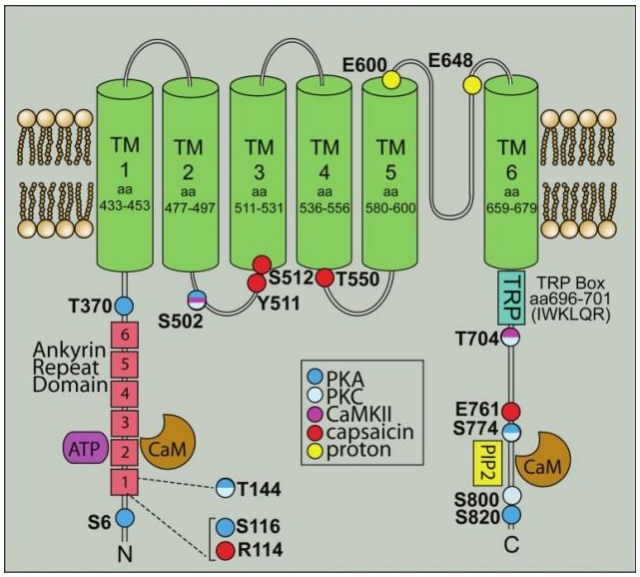

Figure 1.15. Structure of TRPV1. TRPV1 has six transmembrane domains with the pore region between the fifth and sixth domains. Binding sites for kinases, capsaicin, protons and other factors are shown.

From Ho KW et al. 2012 and used in accordance with the Creative Commons Attribution Noncommercial License.

1.12 TRPV1 in CNS function

TRPV1 has been shown to mediate both neuronal and glial function in the CNS (Ho et al., 2012). In neurons, TRPV1 can mediate synaptic transmission and plasticity. In substantia nigral and hypothalamic brain slices, capsaicin increases presynaptic calcium to enhance presynaptic activity and glutamate release (Marinelli et al., 2003; Medvedeva et al., 2008; Sasamura et al., 1998). In addition to glutamate release, TRPV1 has also been implicated in dopamine release. In the ventral tegmental area, capsaicin enhances both the release of dopamine at the nucleus accumbens and also the firing of dopaminergic neurons (Marinelli et al., 2005). In striatal medium spiny neurons and sensory neurons, TRPV1 enhances the frequency of glutamatergic excitatory post-synaptic currents (EPSC) that were potentiated by PKC-mediated decreases in desensitization (Musella et al., 2009; Sikand and Premkumar, 2007) TRPV1-mediated increases in EPSC frequencies have also been observed in the substantia gelatinosa, periaqueductal gray, medial preoptic nucleus, substantia nigra and locus coeruleus (Jiang et al., 2009; Karlsson et al., 2005; Marinelli et al., 2003; Marinelli et al., 2002; Xing and Li, 2007).

By modulating synaptic transmission, TRPV1 can influence synaptic plasticity and survival. In hippocampal neurons, TRPV1 activation by capsaicin or 12-(S)-HPETE is necessary to cause long term depression (LTD) by high frequency stimulation. This effect was notably absent in TRPV1-null mice (Gibson et al., 2008). As a result of this finding, the authors propose a model in which glutamate induces post-synaptic release of 12-(S)-HPETE into the synaptic cleft to activate pre-synaptic TRPV1 channels. Activated TRPV1 subsequently decreases pre-

synaptic glutamate release through a calcium-dependent pathway. Another study found that in the dentate gyrus and in the medium spiny neurons of the nucleus accumbens, post-synaptic activation of TRPV1 by anandamide leads to LTD through calcium-mediated endocytosis of AMPA receptors (Chavez et al., 2010; Grueter et al., 2010). In the developing superior colliculus, IRTX blocks the induction of tetanus-induced LTD, while RTX reduces the amplitude of field excitatory postsynaptic potentials (Maione et al., 2009). In TRPV1 knockout mice, there is a reduction in long term potentiation (LTP) compared to wild-type mice in the CA1 region of the hippocampus (Marsch et al., 2007). These previous studies indicate that TRPV1 facilitates LTD; however, another study found that CAP and RTX amplify LTP and suppressed LTD in the CA1 region of the hippocampus (Li et al., 2008).

In glia, spinal cord astrocyte and microglial reactivity is reduced in TRPV1 knockout mice in models of acute, inflammatory and neuropathic pain (Chen et al., 2009). TRPV1 activation by CAP can also increase both microglial and astrocyte reactivity in the trigeminal nucleus caudalis (Kuroi et al., 2012). However in the mesencephalon, CAP reduces microglial activation and production of reactive oxygen species to increase survival of dopaminergic neurons following 1-methyl-4-phenylpyridinium-induced toxicity in a model of Parkinson's Disease (Park et al., 2012). Treatments of CAP can up-regulate bradykinin B1, a receptor involved in nociception and inflammation, as well as IL-1β levels in rat spinal cord microglia (Talbot et al., 2012). Addition of cannabidiol can also increase phagocytosis by brain and spinal cord microglia, a process that could be reduced with addition of CPZ (Hassan et al., 2014). TRPV1 activation, however, can induce microglial apoptosis by increasing intracellular calcium and release of cytochrome C (Kim et al., 2006).

In addition to microglia, TRPV1 can also mediate astrocyte function. In a mouse model of Amyotrophic Lateral Sclerosis, transplanted neural stem cells can reduce astrocyte activation by releasing endogenous ligands of TRPV1 to activate the channel (Nizzardo et al., 2014). TRPV1 is also expressed in astrocytes, mainly in thick cellular processes, in the sensory circumventricular organs, where channel activation can increase c-fos expression (Mannari et al., 2013). Cortical astrocytes also express TRPV1 to mediate changes in current induced by low pH through an influx of sodium rather than calcium (Huang et al., 2010). Additionally, TRPV1 expression is also found in astrocytes in the spinal cord, hippocampus and retina (Doly et al., 2004; Leonelli et al., 2009; Sun et al., 2013).

1.13 TRPV1 in the Retina

During retinal development, TRPV1 is expressed in the retinal neuroblastic layer and can modulate cellular apoptosis (Leonelli et al., 2009). TRPV1 inhibition with CPZ can reduce apoptosis in the retina of newborn rats without affecting cell division (Leonelli et al., 2011). In the mature retina, TRPV1 is expressed in multiple retinal cell types including neurons (RGCs, photoreceptors), interneurons (amacrine cells), endothelial cells and glia (astrocytes and microglia) (Leonelli et al., 2009; Sappington and Calkins, 2008; Sappington et al., 2009; Zimov and Yazulla, 2004, 2007). TRPV1 activation has both beneficial and detrimental effects on retinal neuronal function. In RGCs, TRPV1 activation with CAP can reduce cell loss following intravitreal injections of N-methyl-d-aspartic acid (Sakamoto et al., 2014). Deletion of TRPV1 exacerbates deficits in RGC anterograde transport as well as axon loss in a model of optic neuropathy (Ward et al., 2014). Similarly, a neuroprotective role for TRPV1 has been suggested following ischemia-reperfusion of the retina – addition of CPZ reduces the neuroprotective effect

of anandamide, an endogenous TRPV1 ligand (Nucci et al., 2007). However, TRPV1 activation has also been shown to mediate neurodegeneration. Capsaicin treatment in retinal explants can increase nitric oxide levels and induce RGC apoptosis (Leonelli et al., 2013). TRPV1 also contributes to apoptosis of the RGCs by increasing intracellular calcium following exposure to elevated hydrostatic pressure (Sappington et al., 2009).

In retinal glia, TRPV1 can modulate reactivity. For example, injection of CPZ reduces Muller glial reactivity and GFAP expression in the retina following axotomy (Leonelli et al., 2010). Likewise, TRPV1 antagonism can reduce NF-κB translocation and IL-6 secretion in microglia following exposure to elevated hydrostatic pressure (Sappington and Calkins, 2008).

1.14 TRPV1, an Intrinsic Stress Response Protein in Astrocytes

Decades of research have established the importance of calcium in mediating astrocyte function and cell motility. TRPV1 is a cation channel with a high calcium permeability and is known to be expressed in retinal astrocytes (Leonelli et al., 2009). Previous studies performed by our lab have determined that TRPV1 is part of the intrinsic stress response of RGCs (Ward et al., 2014), but the function of the channel in the astrocyte stress response is unknown. Because of the importance of calcium in astrocyte function and reactivity, the *objective* of this project is to determine the contribution of TRPV1 to astrocyte function following injury. My *central hypothesis* is that TRPV1 influences astrocyte stress response by modulating migration, calcium influx and cytoskeletal dynamics in response to injury. The specific aims of this project are:

Aim 1: Determine the contribution of TRPV1 activation to astrocyte migration. *My working hypothesis* is that mechanical injury activates TRPV1 to contribute to astrocyte

migration. Using the scratch wound assay as a model of injury-induced migration, I will measure whether astrocyte motility is modulated by (a) TRPV1 agonists and antagonists, (b) genetic knockout of TRPV1 and (c) chelation of intracellular and extracellular calcium.

Aim 2: Quantify the contribution of TRPV1 to calcium influx following injury. *My working hypothesis* is that TRPV1 modulates calcium levels in astrocytes following injury. Using calcium imaging and the scratch wound model, I will measure (a) the influx of calcium following injury, and if calcium levels are influenced by (b) TRPV1 pharmacological agents and (c) genetic knockout of TRPV1.

Aim 3: Determine the effects of TRPV1 modulation on cytoskeletal dynamics in response to injury. *My working hypothesis* is that TRPV1 modulates cytoskeletal dynamics in astrocytes following injury. Using immunocytochemistry and confocal microscopy, I will visualize changes in the actin and tubulin cytoskeleton in astrocytes following (a) scratch injury, (b) with addition of TRPV1 agonists and antagonists and (c) genetic knockout of TRPV1.

CHAPTER II

CHARACTERIZATION AND EXPRESSION OF THE TRPV1 CHANNEL IN ASTROCYTES*

2.1 Introduction

Neurodegeneration is the progressive loss of structure or function of neurons. While neuronal dysfunction and death are fundamental to neurodegeneration, the role of glia in this process is still being elucidated (Gionfriddo et al., 2009; Sappington et al., 2006; Tezel et al., 2001b). To better understand the mechanisms of neurodegeneration and the neuron-glia interactions that mediate this process, the Calkins Lab uses the retinal neuron, RGCs as the prototypical neuron. RGC somas are located in the retina, while their axons comprise the optic nerve and their axon terminals synapse in the brain. The retina and optic nerve are part of the CNS and are readily accessible for experimental manipulation. Various disease states including ischemia, optic neuropathy, excitotoxicity, traumatic injury and mechanical stress have all been modeled in the eye (Calzada et al., 2002; Downs et al., 2008; Gionfriddo et al., 2009; Levkovitch-Verbin, 2004). Glaucoma, a group of optic neuropathies that involves the degeneration of RGCs and their axons, exhibits a pathology similar to other neurodegenerative diseases (Howell et al., 2013; Nickells et al., 2012). The pathogenesis in glaucoma occurs in a distal to proximal fashion, with loss of anterograde transport at the central projection sites as one of the earliest signs of dysfunction and loss of RGC bodies as one of the end stages of

* Portions of this chapter have been published previously in Ho KW, Lambert WS and Calkins DJ. Activation of the TRPV1 cation channel contributes to stress-induced astrocyte migration (2014) Glia 62(9):1435-51.

degeneration (Calkins, 2012; Crish et al., 2010). Other neurodegenerative outcomes in glaucoma are shown in Figure 2.1, further demonstrating the practicality of the eye as a model tissue for CNS neurodegeneration.

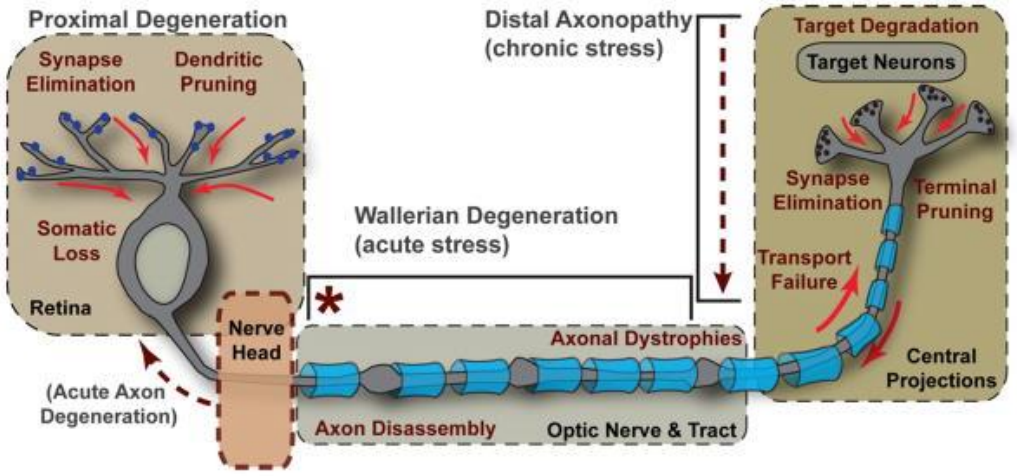

Figure 2.1 Neurodegeneration in glaucoma. Pathogenesis displays a distal-to-proximal progression, and exhibits outcomes similar to other neurodegenerative diseases.
Figure from Calkins, 2012 and used in accordance with Copyright Clearance Center's RightsLink service.

Previous work in our lab examining neuronal and glial responses to injury suggests that the TRPV1 channel may play a key role in glaucomatous neurodegeneration. In the retina, TRPV1 is found in neurons including photoreceptors and RGCs, interneurons like amacrine cells, and glia including astrocytes and microglia (Leonelli et al., 2009; Sappington and Calkins, 2008; Sappington et al., 2009; Zimov and Yazulla, 2004, 2007). Using quantitative PCR, we have shown that whole mouse retinas express TRPV1 and other TRPV channel family members (Figure 2.2). Expression of TRPV5 was not detected, possibly because the assay used did not

detect splice variants in the retina or that retinal expression is below the limit of target detection for this assay (Flicek et al., 2014). Using immunohistochemistry, we localized TRPV1 protein to microglia and RGCs within the retina, demonstrating expression that is diffuse throughout the RGC soma and more punctate in the dendrites and axons (Sappington et al., 2009). In microglia exposed to elevated hydrostatic pressure to mimic glaucomatous stress, we found that TRPV1 mediates the translocation of NF-κB to the nucleus and release of IL-6 (Sappington and Calkins, 2008). More recently, we have shown that TRPV1 is neuroprotective to RGCs in an animal model of glaucoma. Deficits in anterograde transport and axon loss in response to increased intraocular pressure are greater in TRPV1-/- animals compared to wild-type, strongly suggesting TRPV1 is part of an intrinsic stress response within the retina and optic nerve (Ward et al., 2014).

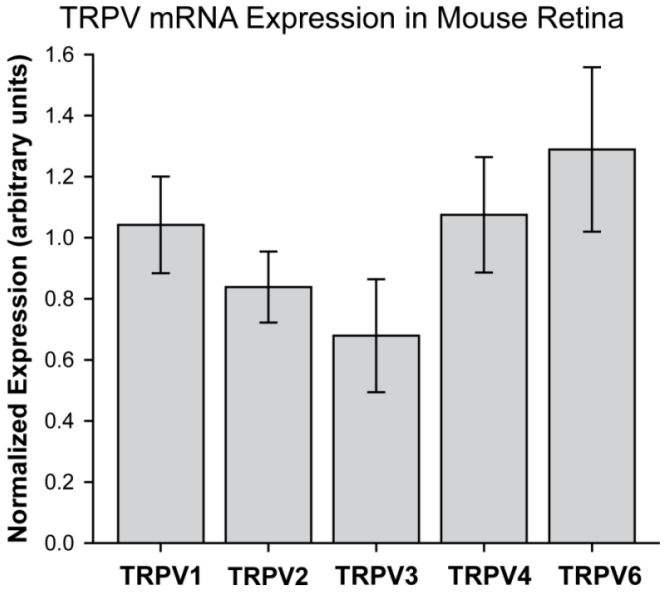

Figure 2.2. TRPV mRNA in whole retinas. C57BL/6 whole retinas express TRPV channel mRNA. Bar graph shows mRNA expression of the TRPV family normalized to GAPDH in mouse retinas.

Similar to RGCs and microglia, astrocytes undergo a stress response known as reactive gliosis in disease and following injury. Reactive astrocytes are hypertrophic, demonstrating increased expression of intermediate filaments, as well as increased proliferation, migration, extracellular matrix remodeling and cytokine secretion. In age-related macular degeneration, reactive astrocytes within the retina can phagocytose RGCs as well as migrate from their location in the nerve fiber layer into the vitreous (Ramirez et al., 2001). Retinal astrocytes also become reactive in glaucoma, where they increase expression of GFAP but do not proliferate (Inman and Horner, 2007). They also reduce IL-6 secretion and increase expression of TNF-α, both of which modulate RGC survival (Sappington et al., 2006; Tezel et al., 2001b). Proteomic-based analysis showed retinal astrocytes upregulate inflammatory mediators such as NF-κB as well (Tezel et al., 2012).

Astrocytes in the optic nerve also undergo gliosis and increase expression of intermediate filaments following injury or disease (Son et al., 2010). Reactive astrocytes contribute to remodeling of the optic nerve head through release of extracellular matrix proteins. In glaucomatous tissue, astrocytes increase expression of both neural cell adhesion molecule, a protein involved in cell anchoring, and collagen (Morrison et al., 1990; Ricard et al., 2000). Levels of integrins and glycosaminoglycans and the synthesis of matrix metalloproteinases are altered as well (Agapova et al., 2001; Morrison, 2006; Tezel et al., 1999). In response to elevated hydrostatic pressure, optic nerve astrocytes can also increase migration and degrade the extracellular matrix as they move (Tezel et al., 2001a). In addition to extracellular matrix

remodeling, reactive astrocytes might also be involved in inflammatory responses. Like in the retina, astrocytes in the optic nerve upregulate production of TNF-α, which induces expression of nitric oxide synthase (Yuan and Neufeld, 2000).

Since astrocytes in both the retina and optic nerve can undergo a stress response in diseases like glaucoma and age-related macular degeneration, we wanted to determine if TRPV1 mediates an intrinsic stress response in these glial populations as it does in RGCs. TRPV1 expression has been shown in rat retinal astrocytes, but its expression in astrocytes in other species or in optic nerve has not been determined (Leonelli et al., 2009). Preliminary work in our lab demonstrated expression of TRPV1 mRNA in mouse optic nerves using fluorescent *in situ* hybridization (Figure 2.3). In young (3 month) and older (9 month) optic nerves, TRPV1 message was found in astrocyte somas and either colocalized with GFAP or was surrounded by GFAP. While these results suggest optic nerve astrocytes express TRPV1, mRNA expression does not necessarily mean a functional protein is expressed. Therefore, to further investigate whether TRPV1 mediates an intrinsic stress response in retinal and optic nerve astrocytes, I wanted to determine if retinal and optic nerve astrocytes express this protein. This chapter will describe the expression of TRPV1 protein in retinal and optic nerve tissue, the isolation and characterization of retinal and optic nerve astrocyte cultures, and the expression of TRPV1 protein in these cultures.

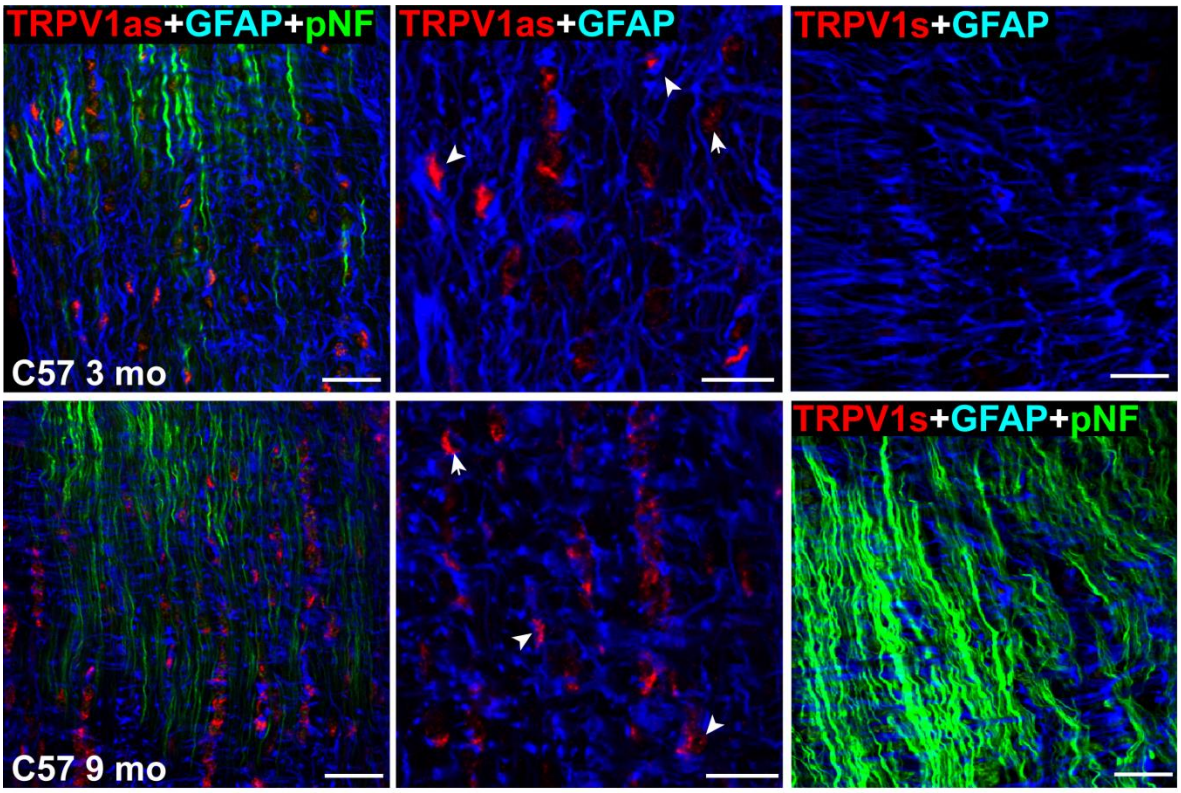

Figure 2.3. TRPV1 mRNA in optic nerve astrocytes. Fluorescent *in situ* hybridization show that TRPV1 mRNA (red) is found in GFAP-positive (blue) optic nerve astrocytes (arrowheads) in 3 month and 9 month mouse optic nerves. mRNA was absent in tissue labeled with sense TRPV1. Axons are labeled with phosphorylated neurofilaments (green). Scale: 20 µm.

2.2 Methods

Animals

All animal procedures were approved by the Vanderbilt University Medical Center Institutional Animal Care and Use Committee. Adult (1-month-old) male Trpv1−/− (B6.129X1-Trpv1^{tm1Jul}/J) mice, which were created on a C57BL/6 background, were obtained from Jackson Laboratories and age-matched C57BL/6 mice were obtained from Charles River Laboratories (Wilmington, MA). Timed-pregnant Sprague-Dawley rats were also obtained from Charles River

Laboratories. Animals were maintained in a 12 hour light/dark cycle with standard rodent chow available *ad libitum* as described (Crish et al., 2010; Sappington et al., 2010).

Immunohistochemistry

Perfused optic nerves or retina from Sprague-Dawley rats, C57 mice or Macaque monkeys were washed in phosphate-buffered saline (PBS) and blocked with 5% normal serum with 0.1% Triton-X 100 in PBS for 2 hours at room temperature. Tissue was then placed in primary antibody solution containing 3% normal serum, 0.1% Triton X-100 in PBS for least 4 days at 4˚C. The following primary antibodies and dilutions were used: TRPV1 (for rat, Novus Biologicals, Littleton, CO, 1:1000; for mouse, Neuromics, Edina, MN, 1:100), TRPV2 (Alomone Labs, Jerusalem, Israel, 1:200), TRPV3 (Alomone Labs, Jerusalem, Israel, 1:200), TRPV4 (Alomone Labs, Jerusalem, Israel, 1:200), TRPV5 (Alomone Labs, Jerusalem, Israel, 1:200), TRPV6 (Santa Cruz Biotechnology Inc, Dallas, TX, 1:200), glial fibrillary acidic protein (GFAP; EMD Millipore, Billerica, MA 1:500), phosphorylated neurofilament (pNF, SMI-31, Sternberger Monoclonal, Baltimore, MD, 1:1,000). Tissue was then washed with PBS and placed into the appropriate DyLight-conjugated secondary antibodies (Jackson Immunoresearch, West Grove, PA 1:150) with 1% normal serum and 0.1% Triton X-100 in PBS overnight at 4˚C. Samples were washed with PBS and then coverslipped with Fluoromount–G (SouthernBiotech, Birmingham, AL). Confocal images were captured using an Olympus FV-1000 inverted microscope.

Isolation of primary retinal astrocytes

Primary astrocytes were isolated with immunomagnetic separation as previously described (Figure 2.4; Sappington et al., 2006). Retinas from post-natal day 1 to 3 Sprague-Dawley rats were harvested in DMEM/Glu plus 5% glucose (Corning Cellgro, Manassas, VA) and then centrifuged at 70 x g for 6 min. The tissue was then dissociated with 1 mg/mL papain and 0.005% DNase at 37˚C for 15 minutes, followed by mechanical trituration. The cells were centrifuged at 250 x g for 8 minutes, and then incubated with a mouse anti-astrocyte antibody that recognizes a 180-200 kDa protein on the astrocyte cell surface (Leinco Technologies, St. Louis, MO, 4 µg/mL) for 10 minutes on ice to isolate astrocytes. Cells were centrifuged and incubated with 20 µL anti-mouse IgM microbeads (Miltenyi Biotec, Auburn, CA). Cell suspensions were centrifuged again, and then loaded onto pre-equilibrated magnetic columns (Miltenyi Biotech) and allowed to flow through. The columns were washed with DMEM/Glu plus 5% glucose, and then eluted. Isolated cells were seeded onto poly-D-lysine-coated (Sigma-Aldrich, St. Louis, MO, 0.01mg/mL) T25 flasks and grown until confluent in astrocyte media [DMEM/F12 (Mediatech, Inc. Manassas, VA), 1X G5 supplement (Life Technologies, Grand Island, NY) and 0.1% gentamicin (Life Technologies, Grand Island, NY) plus 10% FBS (Mediatech, Inc. Manassas, VA)]. Media was changed the day after seeding and then every other day. Once confluent, cells were passaged with 0.25% trypsin/2.21 mM EDTA (Mediatech, Inc. Manassas, VA) and then seeded onto poly-D-lysine-coated wells to be used for experiments.

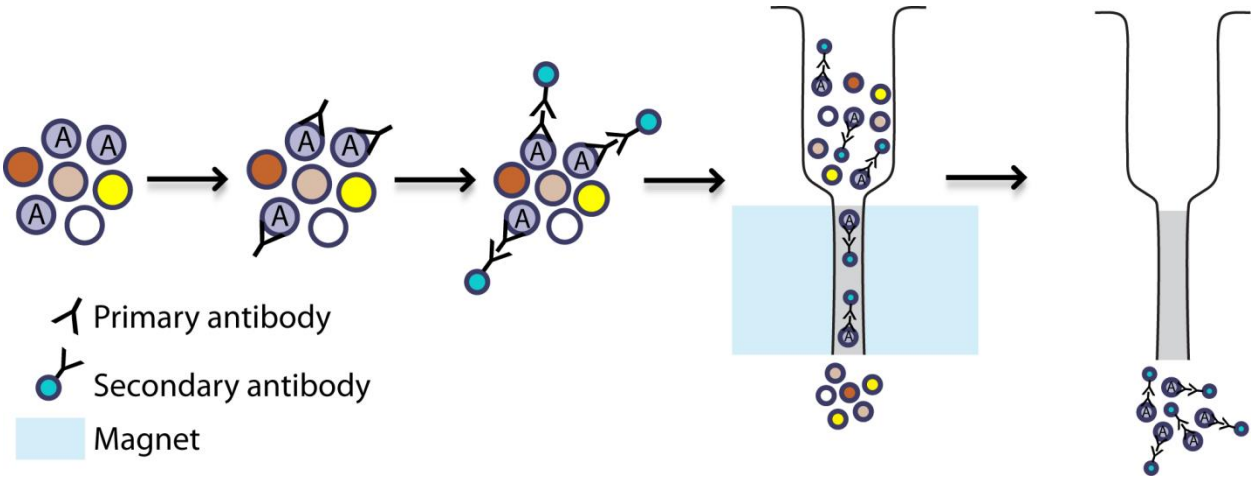

Figure 2.4. Isolation of primary retinal astrocytes. Retinal astrocytes were isolated with immunomagnetic separation. Postnatal retinas were dissociated. Astrocytes were identified with a cell-specific antibody, followed by a magnetic secondary antibody. The cell suspension was placed in column with magnetic beads. Labeled cells were retained and non-labeled cells were washed out. Labeled cells were then washed and eluted.

Genotyping of TRPV1-/- animals

The TRPV1-/- mouse was generated from a germ-line mutation that resulted from a deletion of an exon encoding part of the fifth and all of the sixth transmembrane domains, which include the pore-loop region. The background for the TRPV1-/- are C57BL/6, which were used as controls, and mice were genotyped prior to use (Caterina et al., 2000). Ear clippings (3 mm x 3 mm) were collected, and DNA was extracted with the DNeasy Blood and Tissue Kit (Qiagen, MD). DNA concentration was determined with a NanoDrop 8000 (Thermo Scientific, Wilmington, DE), and then used in a PCR reaction. Each PCR reaction contained the following: 2.5 µL 10X PCR Buffer (Life Technologies, Grand Island, NY), 0.75 µL 50 mM $MgCl_2$ (Life Technologies, Grand Island, NY), 0.5 µL 10 mM dNTP mix (Promega, Madison, WI), 0.5 µL of

each primer (10 μM working stocks; Integrated DNA Technologies, Coralville, IA), 0.1μL Platinum Taq polymerase (Life Technologies, Grand Island, NY), 40 ng of extracted template DNA, and the correct amount of DNase/RNAse free water to bring the reaction volume to 25 μL. The primers used were recommended by Jackson Laboratories for detection of the TRPV1-/- gene truncation. Two forward primers were used to distinguish between wild-type (Jackson Laboratory, Bar Harbor, Maine, oIMR1561; 5' CCT GCT CAA CAT GCT CAT TG 3') and knockout (Jackson Laboratory, Bar Harbor, Maine, oIMR0297; 5' CAC GAG ACT AGT GAG ACG TG 3') gene products. Both forward primers shared a reverse primer (Jackson Laboratory, Bar Harbor, Maine, oIMR1562; 5' TCC TCA TGC ACT TCA GGA AA 3'). Wild-type animals yield a product size of 984 bp and TRPV1-/- animals results in a product size of 600 bp. GAPDH gene was used as positive control with the following primers: forward (5' TTG GCA TTG TGG AAG GGC TC 3') and reverse (5' TGC TGT TGA AGT CGC AGG AGA C 3') to produce a 363 bp product. PCR reactions were performed using a Mastercycler gradient thermocycler (Eppendorf AG, Hamburg, Germany) with the following cycling steps:

Step 1: Denaturing: 94ºC for 3 minutes

Step 2: Denaturing: 94ºC for 30 seconds

Step 3: Annealing: 65ºC for 1 minute

Step 4: Extension: 72ºC for 1 minute

Step 5: Repeat steps 2-4 40 times

Step 6: Extension: 72ºC for 2 minutes

Step 7: Finish, holding reactions at 4ºC

The PCR products from this reaction were then used as template DNA for a second PCR reaction using the same steps described above. This was necessary because one round of PCR did not

yield enough product for detection on an agarose gel. The second PCR reaction used 2.5 to 3.0 µL of template DNA from the first round PCR and the same reagents and primers. Products from the second round of PCR were separated on a 1.5% agarose gel with addition of ethidium bromide. Gels were imaged on a Gel Doc XR+ (Bio-Rad, Hercules, CA) gel reader with the expected following products: GAPDH 363 bp for a positive control (data not shown), C57 984 bp, TRPV1-/- 600 bp.

Isolation of primary optic nerve astrocytes

To isolate optic nerve astrocytes, both optic nerves from a mouse were dissected and minced with a razor blade as previously described (Figure 2.5; Lambert et al., 2001). Tissue was then placed into a well of a 24-well plate coated with 0.1mg/mL poly-D-lysine in astrocyte media with 10% FBS. Over time, astrocytes migrate out from the optic nerve explants and proliferate. Once confluent, cells were passaged with 0.25% trypsin/2.21 mM EDTA and then seeded onto poly-D-lysine-coated T25 flasks. The cells were placed in serum-free astrocyte media to reduce the viability of other cell types including oligodendrocytes and microglia, and to increase purity of the astrocyte cultures. The cultures were placed into full astrocyte media with 10% FBS the following day and allowed to proliferate.

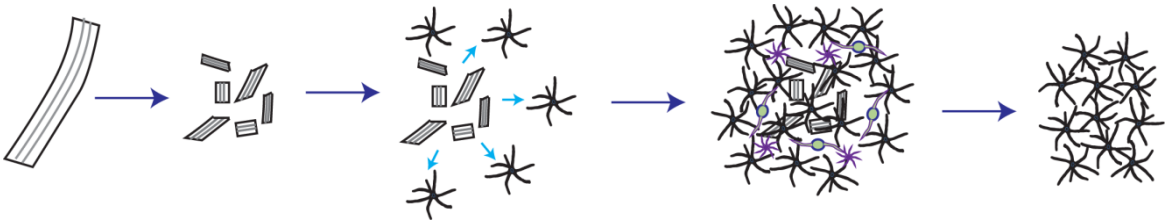

Figure 2.5. Isolation of primary optic nerve astrocytes. Astrocytes were isolated from optic

nerve explants. Astrocytes will migrate from minced optic nerve tissue. Cell purity was increased with subsequent passaging of cells and incubation in serum-free media.

Immunocytochemistry

Cultured astrocytes were fixed with 4% paraformaldehyde in PBS for 20 minutes. Cells were washed in PBS and blocked with 5% normal serum with 0.1% Triton-X 100 in PBS for 2 hours at room temperature. Cells were then placed in primary antibody in a solution containing 3% normal serum, 0.1% Triton X-100 in PBS overnight at 4˚C. The following primary antibodies and dilutions were used: glutamine synthetase (GluSyn, Santa Cruz Biotechnology, Dallas, TX, 1:250), ionized calcium binding adaptor molecule 1 (Iba-1, Abcam, Cambridge, MA, 1:400), phosphorylated neurofilaments (pNF, SMI-31, Sternberger Monoclonal, Baltimore, MD, 1:1,000), GFAP (EMD Millipore, Billerica, MA 1:500), nestin (Santa Cruz Biotechnology, Dallas, TX, 1:200), myelin basic protein (MBP, Novus Biologicals, Littleton, CO, 1:500), TRPV1 (Novus Biologicals, Littleton, CO, 1:1000). The next day cells were washed with PBS and incubated with appropriate DyLight-conjugated secondary antibodies (Jackson Immunoresearch, West Grove, PA 1:150) in 1% normal serum and 0.1% Triton X-100 in PBS overnight at 4˚C. Cells were washed with PBS, counterstained with DAPI (1:100, Molecular Probes, Eugene, OR), and then washed with PBS before being coverslipped with Fluoromount–G (SouthernBiotech, Birmingham, AL). Confocal images were captured using an Olympus FV-1000 inverted microscope.

Western Blot

Protein lysates were collected from primary astrocytes in RIPA buffer [50 mM Tris-HCl, 150 mM NaCl, 5 mM EDTA, 0.2 mM sodium vanadate, 1% NP-40, 0.1% SDS, 0.5% sodium deoxycholate, 1 mM phenylmethylsulfonyl fluoride, protease inhibitor cocktail (Roche, Basal, Switzerland)]. Protein concentration was determined with the bicinchoninic acid protein assay kit (Thermo Scientific, Wilmington, DE). Samples (40µg) were prepared with addition of protein loading buffer (Li-Cor Inc., Lincoln, NE) and 10% β-mercaptoethanol (Sigma, St. Louis, MO), and denatured at 70˚C for 5 minutes. Samples were then separated by SDS-PAGE in 4% to 20% gradient Tris-glycine precast gel (Bio-Rad, Hercules, CA) following the Western blot protocol from Li-Cor Inc. Blots were incubated in primary antibodies: TRPV1 (Novus Biologicals, Littleton, CO, 1:2000), GFAP (EMD Millipore, Billerica, MA 1:5,000), β-actin (Life Technologies, Grand Island, NY, 1:2000). Proteins were detected using IRDye 680 or IRDye 800CW secondary antibodies, Odyssey Blocking Buffer and a Li-Cor Odyssey Infrared Imaging System (Li-Cor Inc., Lincoln, NE) following manufacturer's protocol.

2.3 Results

Expression of TRPV channels in vivo in retinal astrocytes

The TRPV family of ion channels is comprised of six members. We have shown expression of TRPV family members 1 to 4 and 6 in whole retina using quantitative PCR. Other groups have found that retinal astrocytes express TRPV1 but not TRPV2 or TRPV4 (Leonelli et al., 2009; Ryskamp et al., 2011). To determine which TRPV family members are expressed specifically in retinal astrocytes, I performed immunochemistry on mouse retinal whole mounts

(Figure 2.6). While quantitative PCR demonstrated that whole retinas expressed TRPV mRNA, immunochemistry elucidates the expression and localization of TRPV protein in retinal astrocytes. Consistent with previous results, TRPV2 and TRPV4 was not detected in retinal astrocytes (Figure 2.6; Leonelli et al., 2009; Ryskamp et al., 2011). I found that retinal astrocytes express TRPV1, TRPV5 and TRPV6, all of which colocalized with GFAP, but TRPV2, TRPV3 and TRPV4 expression was absent. TRPV1 and TRPV5 demonstrated diffuse labeling throughout the cell soma (filled arrowheads) and processes (arrows), while TRPV6 appeared to have greatest expression in astrocyte processes with weak expression in astrocyte cell somas. TRPV1, TRPV5 and TRPV6 were also present in the RGC somas, which are located in the retinal ganglion cell layer beneath astrocytes. Astrocytes did not express TRPV2, TRPV3 or TRPV4. TRPV2 was found in RGC somas and axons, while TRPV4 was expressed in both in RGC somas as well as in the endfeet of Muller cells (arrowheads). TRPV3 was not expressed by either RGCs or astrocytes in mouse whole mount retinas (Figure 2.6).

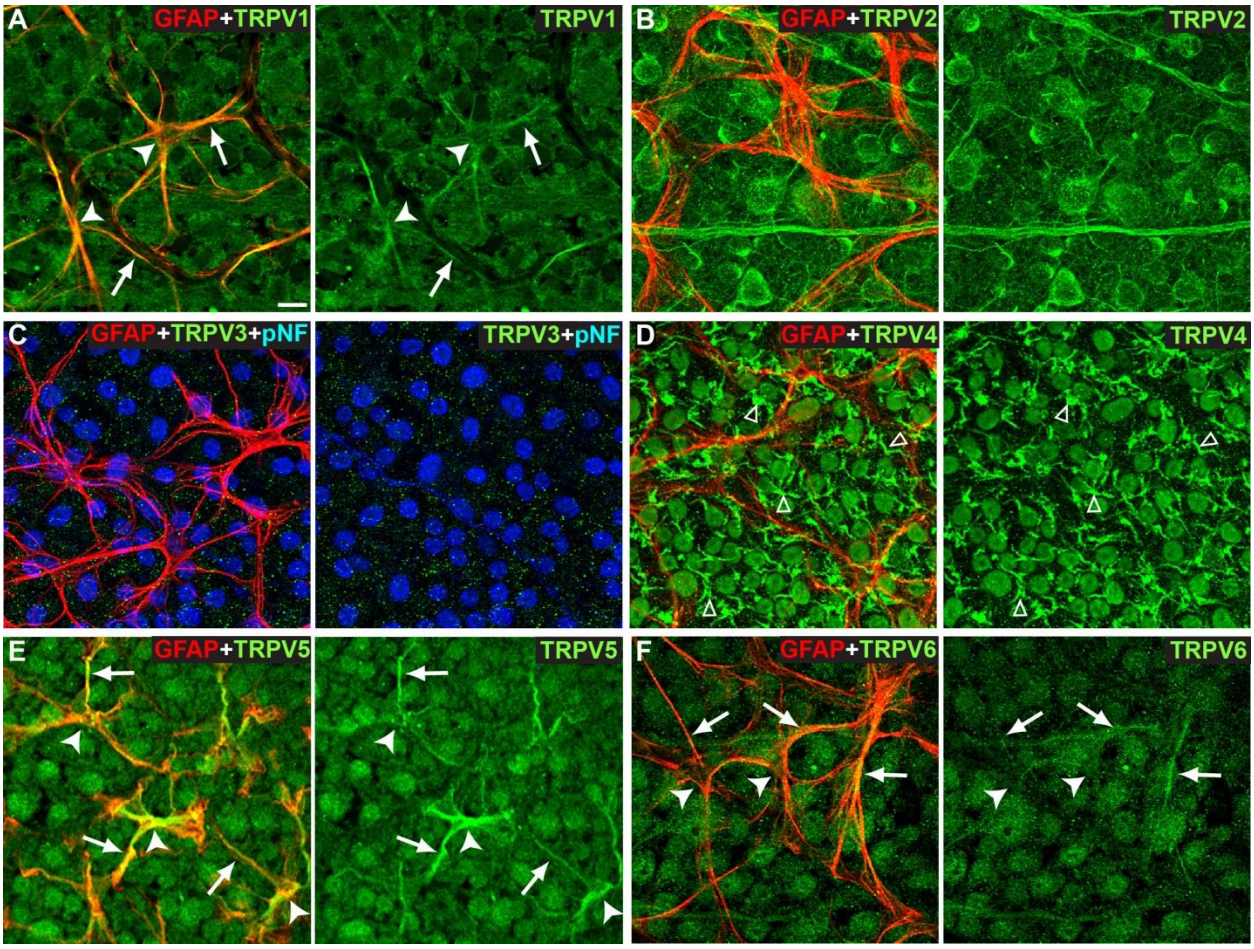

Figure 2.6. TRPV channels in astrocytes. Confocal micrographs show expression of TRPV1, TRPV2, TRPV3, TRPV4, TRPV5 and TRPV6 (green; A-F) in mouse retinal whole mounts. Astrocytes are positive for GFAP (red). TRPV expression and colocalization with GFAP is present in astrocyte soma (filled arrowheads) and processes (arrow) and Muller cell endfeet (arrowheads). Scale: 10 µm.

Since the primary retinal astrocyte cultures I used for my *in vitro* studies are isolated from rat retinas, I was interested in further characterizing the expression of TRPV1 in rat retinal astrocytes. Immunochemistry and confocal micrographs indicate that rat retinal astrocytes express TRPV1 (Figure 2.7A and 2.7B). Like in mouse, TRPV1 is diffusely expressed

throughout astrocyte soma (filled arrowheads) and processes (arrows). The channel is also found in RGC somas and axons, where is colocalizes with pNF (Figure 2.7A). High magnification images and orthogonal views demonstrate discrete areas of colocalization between TRPV1 and GFAP in astrocytes in both rat and mouse (Figure 2.7B and 2.7C).

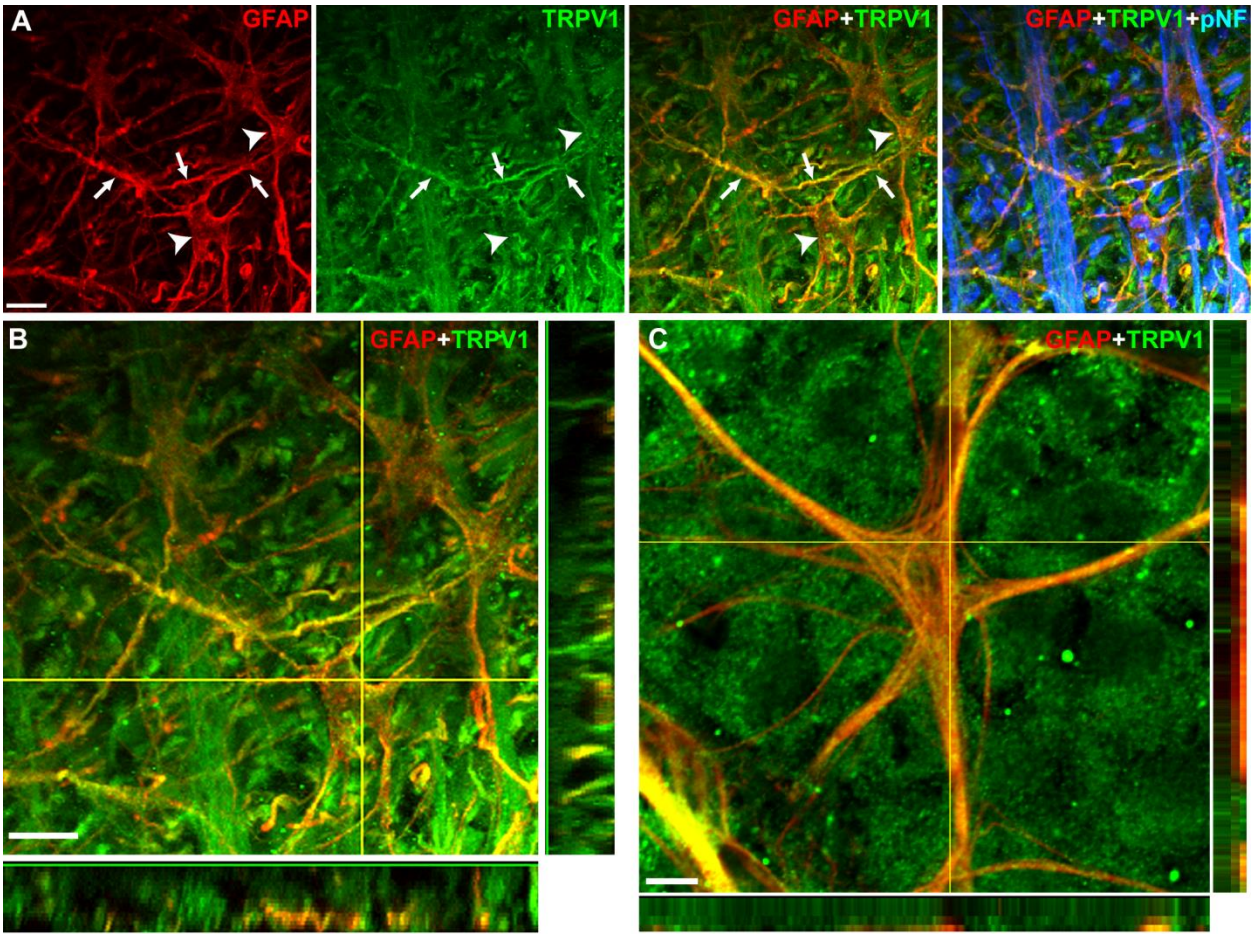

Figure 2.7. TRPV1 expression in retinal astrocytes. Whole-mounted rat (**A, B**) and mouse (**C**) retinas demonstrate TRPV1 labeling (green) throughout processes (arrows) and somas (arrowheads) of GFAP-positive astrocytes (red). Phosphorylated neurofilaments (pNF) label RGC soma (blue). Higher magnification and orthogonal views (**B, C**) show discrete

colocalization of TRPV1 within GFAP-labeled astrocyte processes (yellow puncta). Scale: 10 μm (A and B); 5 μm (C).

Optic nerve astrocytes express TRPV1 in vivo

The optic nerve is comprised of axons from RGC, and is believed to be an initial site of injury in glaucoma, our lab's disease of interest (Morgan, 2000; Quigley et al., 1981). Increased intraocular pressure is believed to target the optic nerve head and optic nerve, leading to axon degeneration and apoptosis of RGCs (Weber et al., 2008). In glaucoma, as well as diabetic retinopathy, astrocyte reactivity in the optic nerve has been observed prior to overt changes within the brain or retina and is one of the earlier signs of pathogenesis (Fernandez et al., 2012a, b; Hernandez, 2000; Son et al., 2010). To determine if TRPV1 may mediate an intrinsic stress response in optic nerve astrocytes, my *in vitro* studies utilized cultures of primary optic nerve astrocytes. However, prior to those studies I first had to characterize TRPV1 expression in mouse, rat and monkey optic nerve head and optic nerve tissue (Figure 2.8 and 2.9).

In mouse optic nerve head, TRPV1 expression was observed in discrete pockets in GFAP-positive astrocytes, while axonal expression appeared more diffuse (Figure 2.8). In contrast, TRPV1 expression in rat optic nerve head astrocytes appears more diffuse than in the mouse optic nerve head, although areas of discrete TRPV1 labeling are still observed (arrows). Axonal expression of TRPV1 in the rat optic nerve head was similar to mouse. Intense areas of TRPV1 labeling that did not colocalize with GFAP and did not appear to be within RGC axon bundles were also observed in rat optic nerve head tissue. In monkey optic nerve head, TRPV1 was extensively colocalized with GFAP. Of the three species examined, monkey optic nerve head demonstrated higher astrocyte TRPV1 expression than mouse or rat.

Within the optic nerve proper, TRPV1 expression in mouse was localized to discrete pockets in GFAP-positive astrocytes, similar to what was observed in the optic nerve head (Figure 2.9). Colocalization of TRPV1 and GFAP appeared within axonal bundles. Axonal expression of TRPV1 in mouse optic nerve appeared more punctate than in the nerve head. This staining pattern suggests TRPV1may localize at the Nodes of Ranvier. In rat optic nerve astrocytes, TRPV1 expression appeared diffuse and moderately colocalized with GFAP. Colocalization of TRPV1 and GFAP appeared concentrated along axonal bundles more so than within the bundles. Diffuse TRPV1 expression was also observed in monkey optic nerve astrocytes, and colocalization with GFAP appeared more concentrated along axonal bundles with very little astrocyte TRPV1 expression within axon bundles. TRPV1 protein also appeared in the somas of non-GFAP positive cells (arrowheads), indicating possible expression in oligodendrocytes (Figure 2.9).

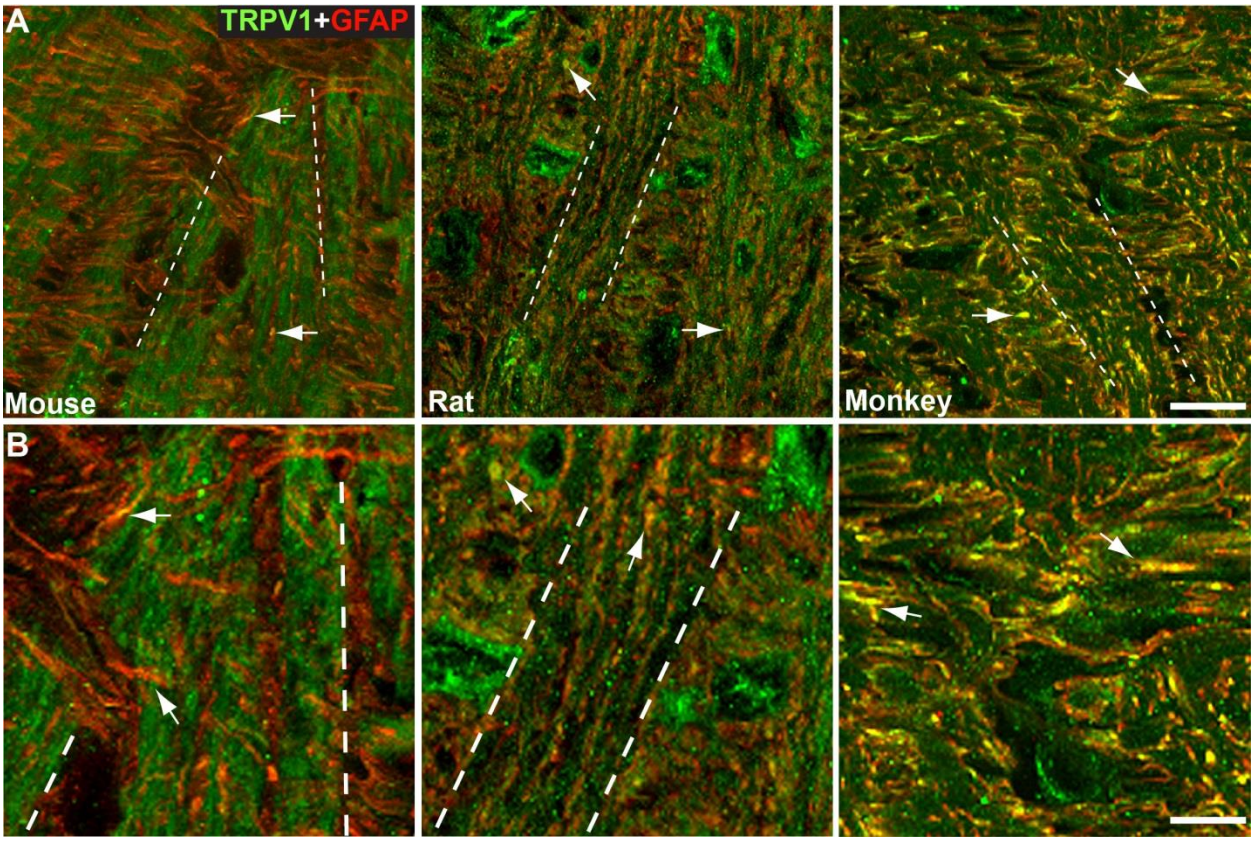

Figure 2.8. TRPV1 expression in optic nerve head astrocytes. Mouse, rat and monkey optic nerve heads are immunolabeled for TRPV1 (green) and GFAP (red). TRPV1colocalizes with GFAP (arrows). Dotted lines denote the axons of RGCs. Scale: 20 µm (A); 10 µm (B).

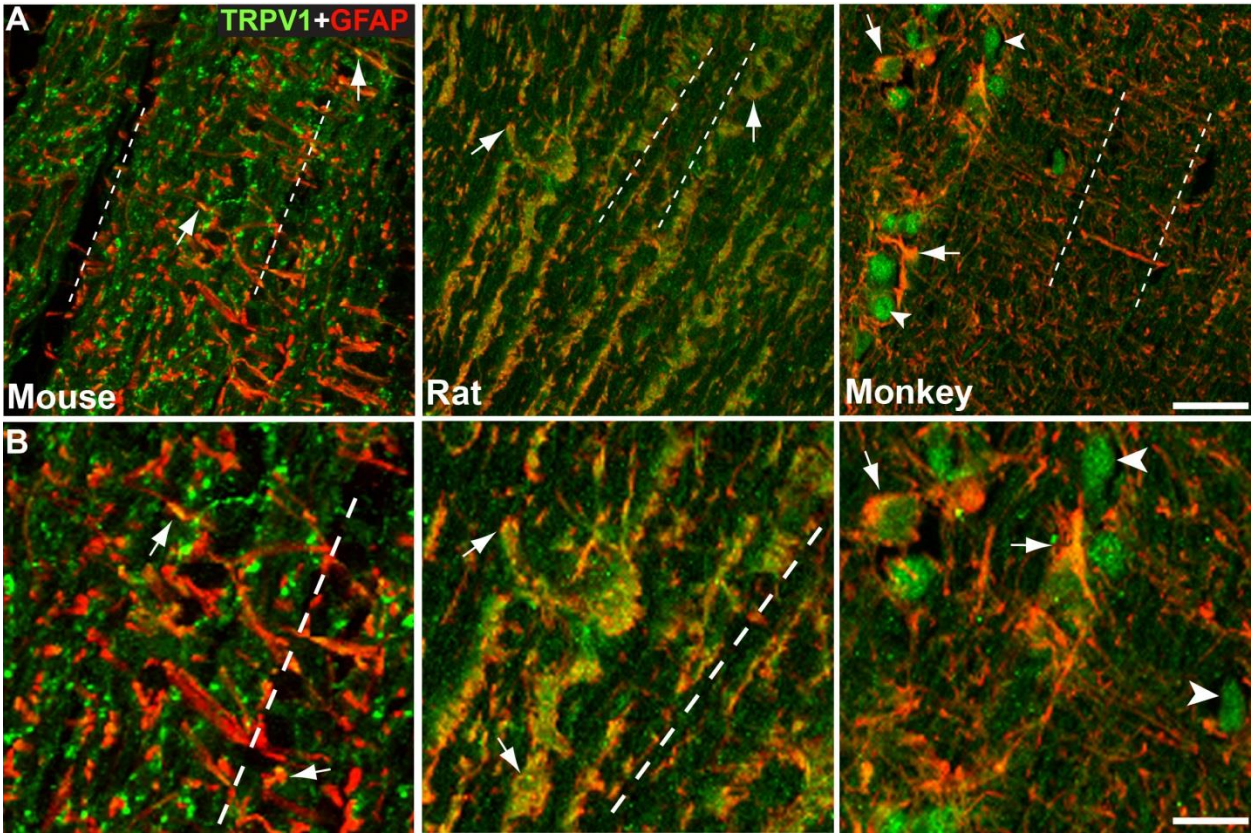

Figure 2.9. TRPV1 expression in optic nerve astrocytes. Mouse, rat and monkey optic nerves are immunolabeled for TRPV1 (green) and GFAP (red). TRPV1colocalizes with GFAP (arrows) but is also observed in non-GFAP positive cells (arrowheads). Dotted lines denote the axons of RGCs. Scale: 20 µm (A); 10 µm (B).

Primary cell cultures express astrocyte-specific genes

Since TRPV1 is expressed in retinal and optic nerve astrocytes *in vivo*, I was interested in characterizing the channel's expression *in vitro* in isolated primary astrocytes. I was able to isolate and culture three primary astrocyte populations: post-natal rat retinal astrocytes, adult C57 wild-type optic nerve astrocytes, and adult TRPV1-/- optic nerve astrocytes. The formation of the extracellular matrix and the presence of Muller cells in adult retinas make isolating retinal astrocytes more difficult. There is increased cell death and decreased cell viability as well the

presence of Muller cells. Also, the mouse retina is smaller than rats and would require twice the number of animals to produce similar cell numbers. Therefore, optic nerve rather than retinal astrocytes were isolated from adult mice.

Purity of the retinal astrocyte primary cultures was assessed with immunocytochemistry using antibodies against proteins expressed by glia and neurons present in the retina: glutamine synthetase (macroglia), Iba-1 (microglia) and pNF (neurons; Figure 2.10). Both astrocytes and Muller cells express glutamine synthetase, however the two cell types differ based on morphology. Muller cells are more fibrous and elongated while astrocytes are more globular and amoeboid shaped (Figure 2.10 and 2.11; Hicks and Courtois, 1990).

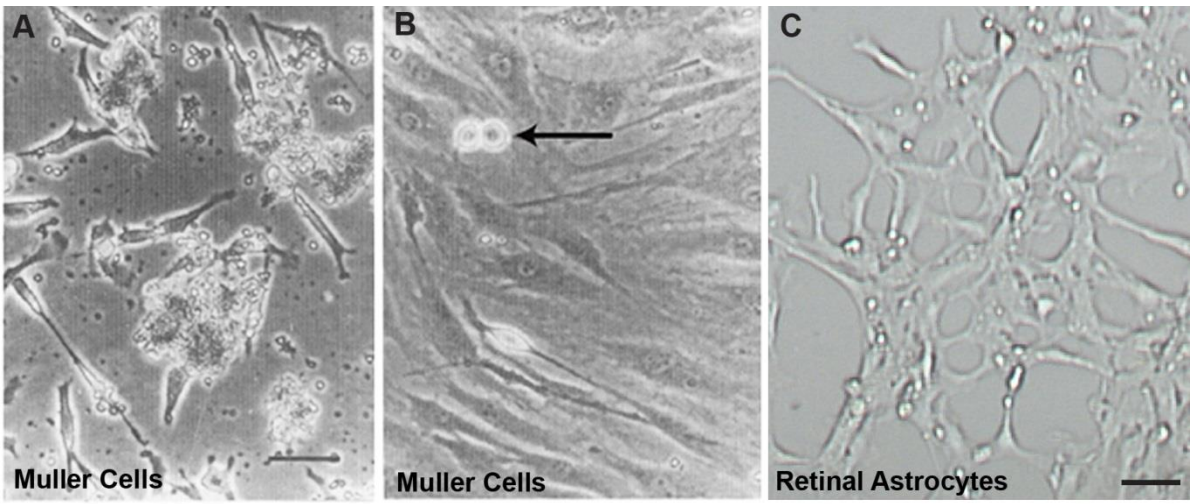

Figure 2.10. Morphology of cultured Muller cells. Phase-contrast images show Muller cells after 4 days in culture (**A**) or 2 passages (**B**). DIC images showing retinal astrocytes in culture (**C**) Arrow indicates a dividing cell.

Figure from Hicks and Courtois, 1990 and used in accordance with Copyright Clearance Center's RightsLink service.

Isolated retinal astrocytes do not express Iba-1 or pNF, indicating the absence of both microglia and neurons respectively, in the culture (Figure 2.11). My isolated rat retinal cultures express GFAP, further validating their astrocyte identity (Figure 2.12). The astrocyte cell population is heterogeneous, as shown by the range of morphologies as well as patterns of GFAP expression. While the cells are generally amoeboid shaped, some cells have well defined processes. Cell size also varies within the same culture. In some astrocytes, GFAP is filamentous and expressed throughout the cell, while in others labeling appears diffuse. The intensity of GFAP labeling also varied; some cells had uniform labeling throughout while others had intense labeling in the perinuclear area and less intense labeling in the cell processes (Figure 2.12).

The purity of optic nerve cultures from C57 and TRPV1-/- mice was also determined using immunohistochemistry with antibodies for optic nerve glia: GFAP and nestin for astrocytes, myelin basic protein (MBP) for oligodendrocytes and Iba-1 for microglia (Figure 2.13). Cells isolated from C57 and TRPV1-/- optic nerve explants expressed both GFAP and nestin, suggesting these cells are astrocytes (Figure 2.13A and 2.13B). Both intermediate filaments were expressed throughout the astrocytes, and while GFAP expression was more diffuse, nestin labeling was more filamentous. Expression of Iba-1 or MBP was not observed in my optic nerve cultures, indicating the absence of microglia and oligodendrocytes, respectively (Figure 2.13C and 2.13D).

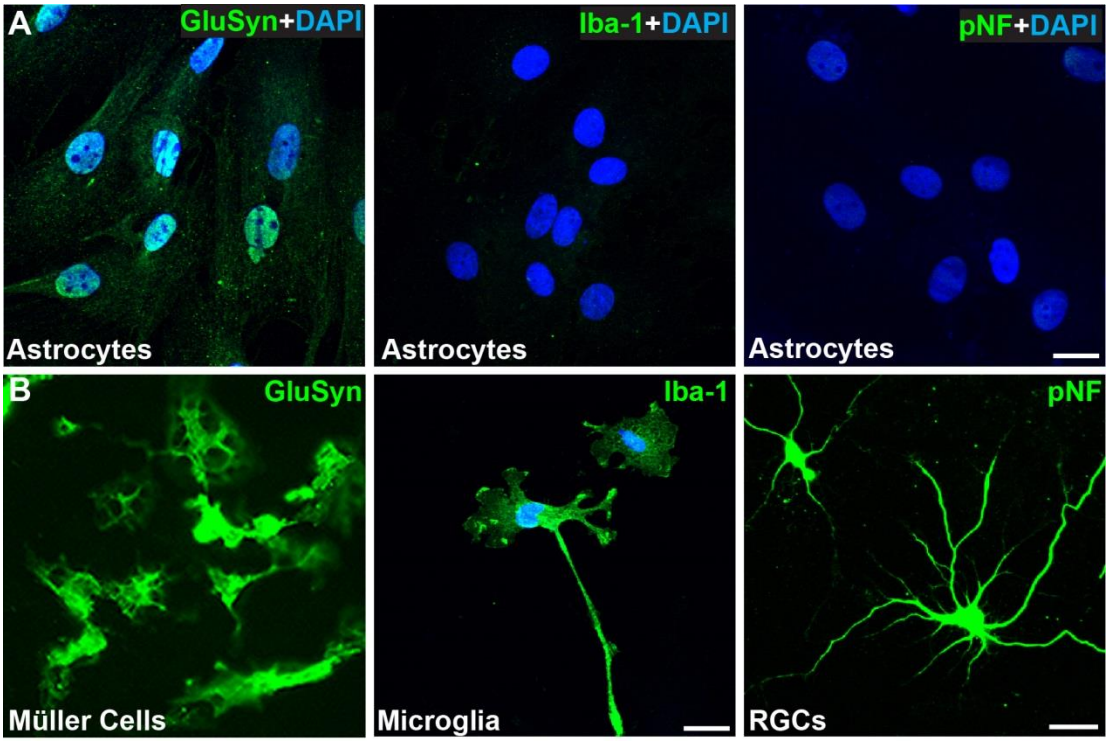

Figure 2.11. Purity of retinal astrocyte cultures. Confocal micrographs show that retinal astrocytes express glutamine synthetase but not Iba-1 or pNF (**A**). Muller cells also express glutamine synthetase, while microglia express Iba-1 and RGCs express pNF (green; **B**). Scale: 20µm. Muller cell image courtesy of D'anne Duncan in Rebecca Sappington's lab.

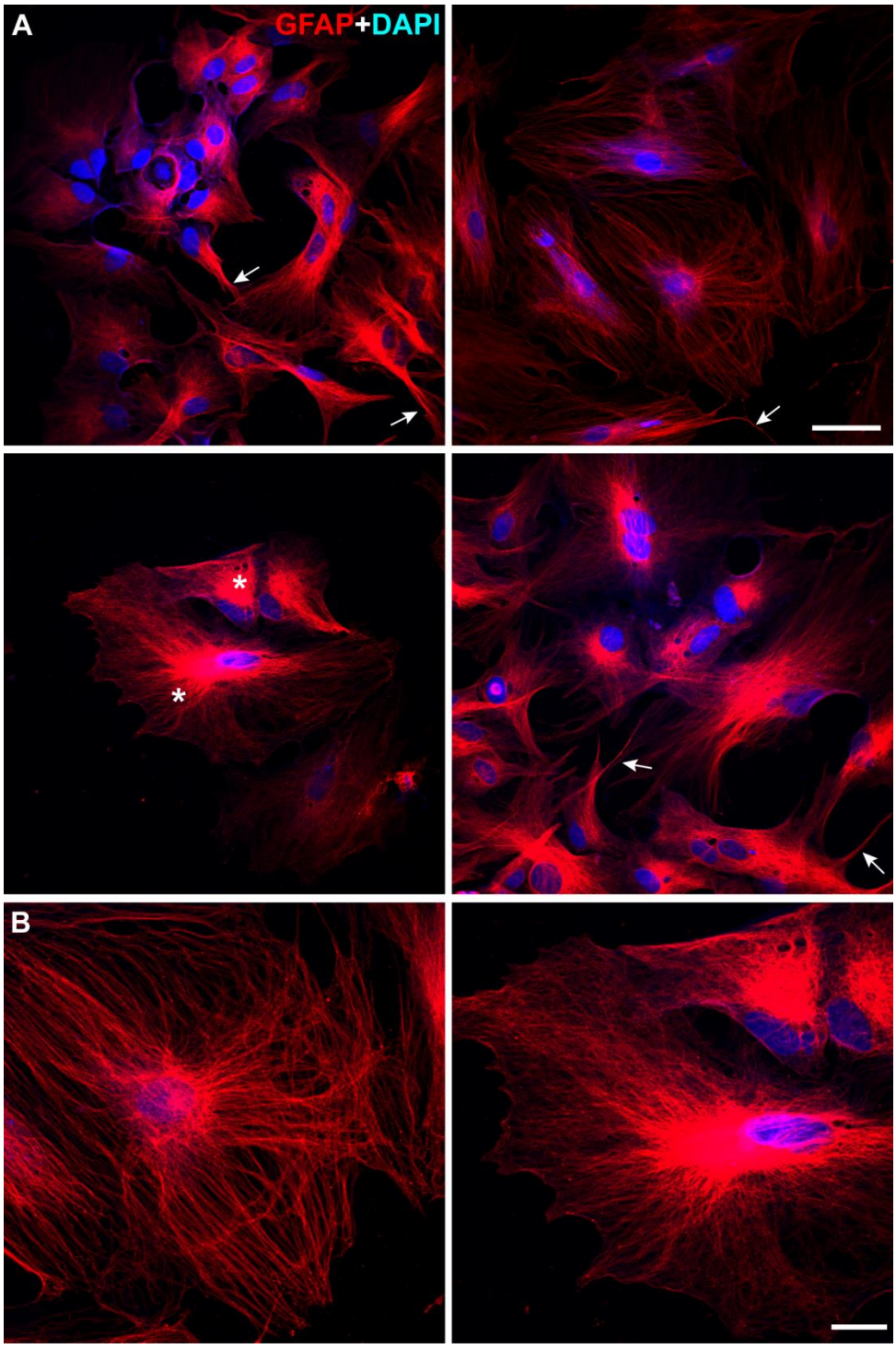

Figure 2.12. Heterogeneity of retinal astrocyte cultures. Astrocyte cultures are labeled with GFAP (red), and DAPI (blue) identifies the nucleus (**A**). Arrows indicate well defined processes.

Asterisks indicate different cell sizes in same culture. The variations in GFAP distribution throughout astrocytes is shown in **B**. Scale: 20 μm.

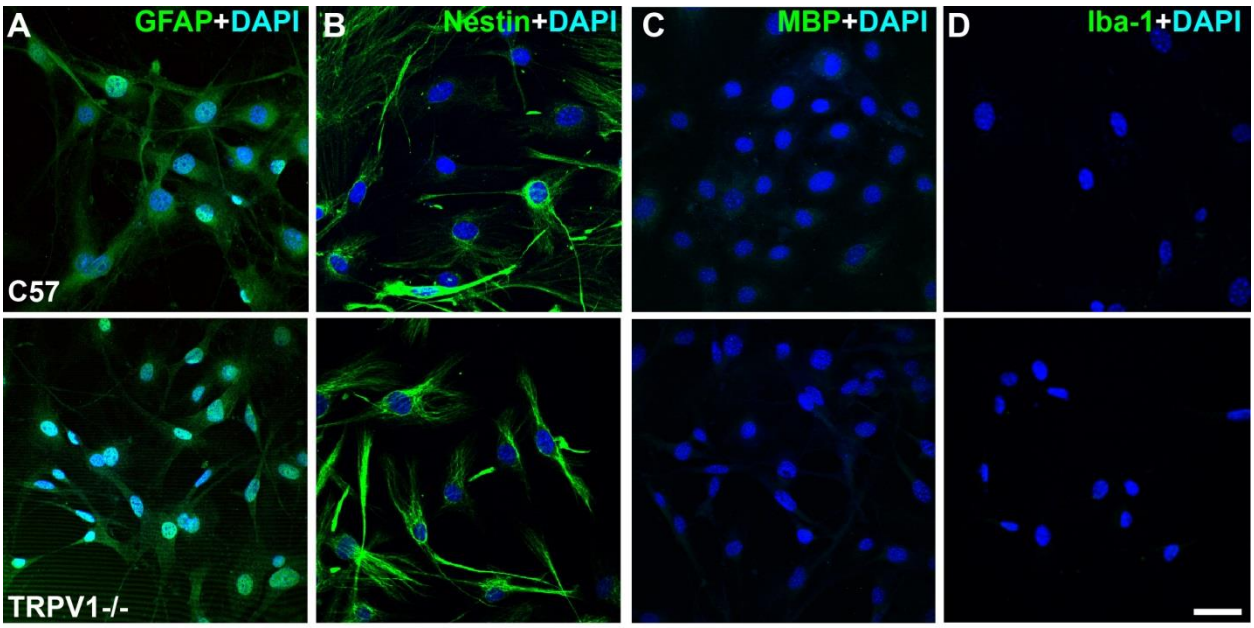

Figure 2.13. Purity of optic nerve astrocytes. Isolated cells express GFAP and nestin. Optic nerve astrocytes isolated from C57 and TRPV1-/- mice are positive for GFAP (green; **A**) and nestin (green; **B**), but do not express the oligodendrocyte marker, myelin basic protein (MBP; **C**) or the microglial marker, Iba-1 (**D**). Nuclei are labeled with DAPI (blue). Scale: 50 μm.

Astrocyte cultures express TRPV1 channel

After validating the purity of my primary astrocyte cultures, I wanted to determine the pattern of TRPV1 expression *in vitro*. Immunocytochemistry showed that in rat retinal astrocyte cultures, GFAP labeling was filamentous throughout the cell body and processes, while TRPV1 exhibited more punctate and diffuse labeling (Figure 2.14A). Merged confocal images indicated that the two proteins have discrete areas of co-localization. Higher magnification images were

then taken to allow for better visualization to discern the finer details of TRPV1 and GFAP expression. The filamentous expression of GFAP and the more diffuse punctate pattern of expression for TRPV1 are highlighted (Figure 2.14B). Orthogonal views indicate that TRPV1 and GFAP maintained distinct areas of expression but co-localization occurred in discrete pockets within the soma and processes in isolated astrocytes, much like the pattern seen in astrocytes from rodent retinal whole mounts (Figure 2.7 and 2.14). Western blots from these primary cultures further confirmed the presence of TRPV1 and GFAP protein in rat retinal astrocytes (Figure 2.14C). Full-length TRPV1 has a molecular weight of 90 to 113 kDa due to glycosylation states (Sappington et al., 2009). We detected four TRPV1 isoforms in our astrocytes, similar to those found in neuroblastoma cells (Lilja et al., 2007) with the band below 75 kDa having been specifically reported in astrocytes (Huang et al., 2010; Lilja et al., 2007). The bands present in the GFAP Western blot have molecular weights of about 55 and 60 kDa, and likely represent different splice isoforms or phosphorylation or glycosylation states of GFAP (Korolainen et al., 2005; Tura et al., 2009).

Next, I was interested in characterizing the expression of TRPV1 in primary optic nerve astrocytes (Figure 2.15A). Immunolabeling for GFAP in both C57 and TRPV1-/- astrocytes was diffuse and punctate throughout the cell. TRPV1-/- astrocytes appeared to have more perinuclear GFAP labeling. This was in contrast to rat retinal astrocytes which exhibited more filamentous GFAP expression (Figures 2.14 and 2.15A). Similar to retinal astrocytes, TRPV1 expression was diffuse in C57 optic nerve astrocytes and localized to both the soma and processes. As expected TRPV1 label was absent in TRPV1-/- optic nerve astrocytes (Figure 2.15A). Knockout of the TRPV1 gene was confirmed with genotyping (Figure 2.15B). Using primers near the

deletion site and a common reverse primer yielded a gene product at 984 bp in C57 mice and product at 600 bp in TRPV1-/- mice. GAPDH was used as a positive control (data not shown).

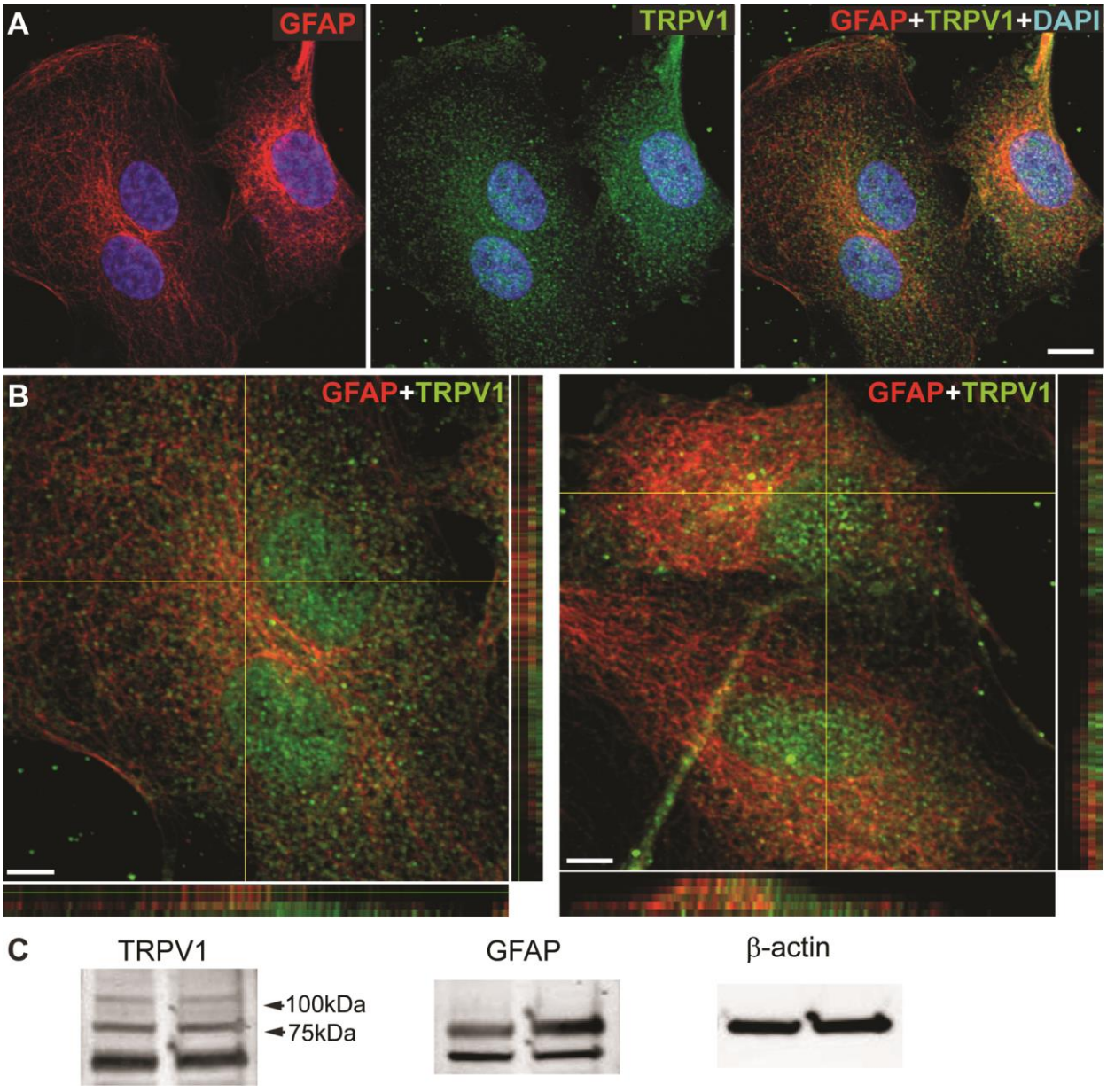

Figure 2.14. TRPV1 expression in cultured retinal astrocytes. Cultures of primary rat retinal astrocytes (**A**) expressing GFAP (red) demonstrate diffuse TRPV1 labeling (green). Higher magnification and orthogonal views (**B**) demonstrate patches of TRPV1 (green) or GFAP (red)

label as well as colocalization (**B**; yellow). Western blot analysis (**C**) shows expression of TRPV1 and GFAP in cultured astrocytes; β-actin is shown as loading control. Bands for TRPV1 include the expected weight near 100 kDa, a 75 kDa isoform, and a lower weight doublet specific for astrocytes. Scale: 10 μm (**A**); 5 μm (**B**).

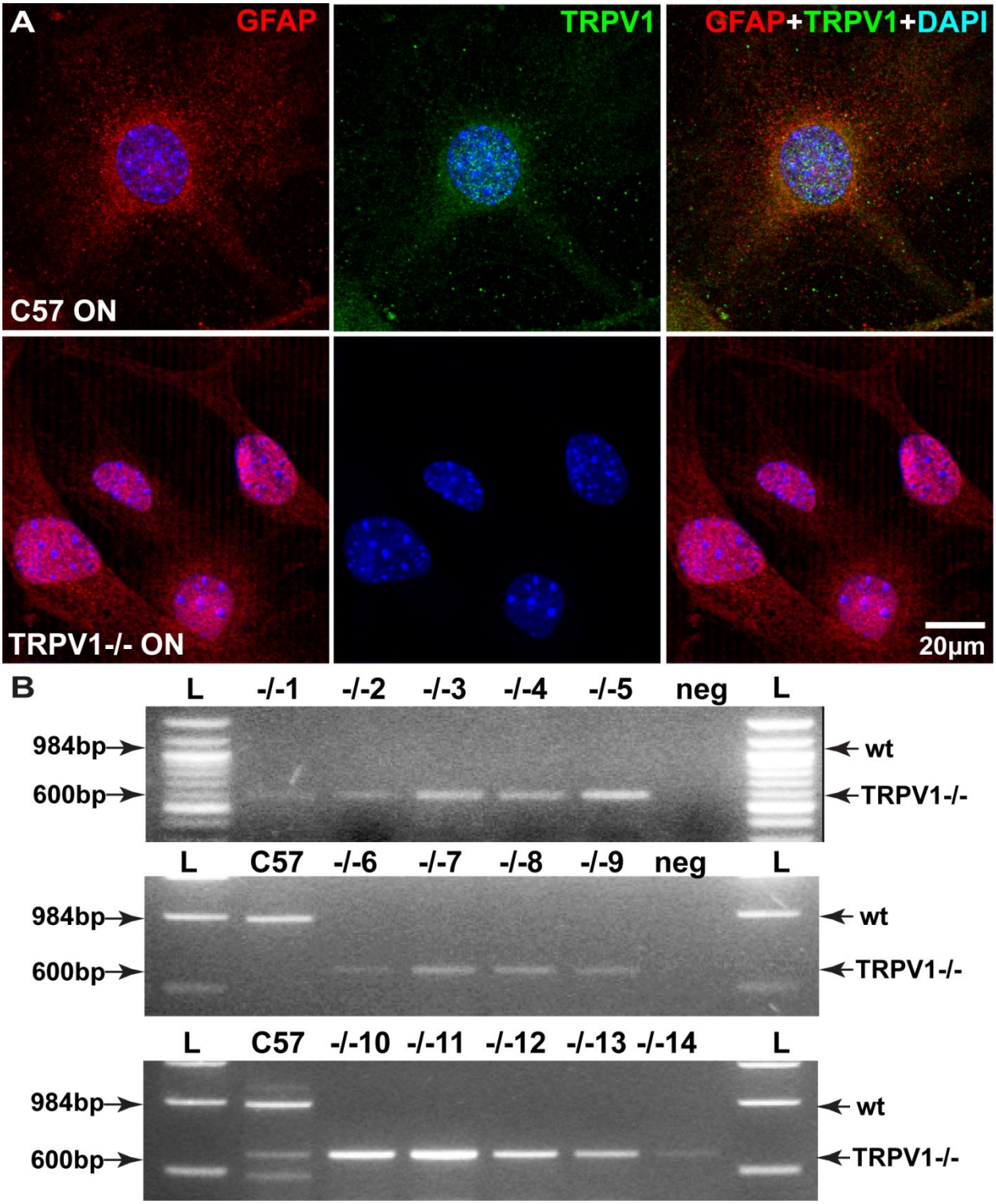

Figure 2.15. TRPV1 expression in cultured optic nerve astrocytes . Cultures of primary optic nerve astrocytes from C57 and TRPV1-/- mice (**A**) express GFAP (red). TRPV1 (green) is

expressed by C57 optic nerve astrocytes but is absent in TRPV1-/- astrocytes. Scale: 20 μm. Genotyping (**B**) confirms that TRPV1-/- mice have a deletion in the TRPV1 gene as shown by the different-sized PCR products generated using DNA from C57 and TRPV1-/- mice. L: 100 bp ladder (top gel), 1 kb ladder (bottom gels). neg: negative control (water added in place of DNA).

2.4 Discussion

Astrocytes in the retina and other parts of the CNS are known to express TRPV1 (Huang et al., 2010; Leonelli et al., 2009; Mannari et al., 2013; Sun et al., 2013). Here, I show that retinal astrocytes express TRPV1, TRPV5 and TRPV6 channels (Figure 2.6A, E and F). TRPV5 and TRPV6 are more calcium-selective than TRPV1 (den Dekker et al., 2003), but their function in astrocytes is unknown. The expression of TRPV2 in astrocytes depends on the astrocyte population studied. Cerebellar astrocytes express TRPV2, which can be activated by temperature > 50˚C and the lipid, lysophosphatidylcholine to increase intracellular calcium levels (Shibasaki et al., 2013). In contrast, TRPV2 expression has not been shown in retinal astrocytes (Leonelli et al., 2009). Consistent with that study, TRPV2 expression was not detected in my retinal astrocytes (Figure 2.6). Similar to TRPV2, the expression of TRPV4 also varies across astrocyte populations. Although retinal astrocytes do not express TRPV4 (Figure 2.6D; Ryskamp et al., 2011), TRPV4 is found in astrocytes in the cortex and hippocampus (Bai and Lipski, 2010; Benfenati et al., 2007; Butenko et al., 2012). Less is known about TRPV3 in retinal astrocytes. In addition to TRPV channels, astrocytes in the brain also express TRPA1, which modulates astrocyte calcium levels and TRPC1-6, which are involved in store-operated calcium entry and calcium regulation (Beskina et al., 2007; Grimaldi et al., 2003; Malarkey et al., 2008; Miyano et al., 2010; Shigetomi et al., 2012). Expression of TRPA and TRPC channels,

however, has not been studied in astrocytes in the retina or optic nerve. Since astrocytes are important in mediating neuronal function and synaptic transmission, and calcium is a key signaling molecule, it would be interesting to profile the expression and localization of other TRP channels in astrocytes.

TRPV1 localized to astrocyte cell bodies and processes identified by GFAP co-label in both mouse and rat whole-mounted retina (Figure 2.6 and 2.7). Retinal ganglion cells labeled with pNF also express TRPV1 (Figure 2.7), consistent with previous work (Leonelli et al., 2010; Sappington et al., 2009). Higher magnification images and orthogonal views show discrete pockets of colocalization of GFAP and TRPV1 in astrocyte cell bodies and processes in both mouse and rat (Figure 2.7). This is similar to the expression pattern seen in retinal cultures, which also exhibited punctate localization of TRPV1 and GFAP (Figure 2.14). Other groups have found that TRPV1 is punctate and more concentrated in astrocytes in the perivascular area in retinal sections (Leonelli et al., 2009). TRPV1 expression in the astrocyte cytoplasm and in the endfeet that contacts the vasculature has also been seen *in vivo* in the spinal dorsal horn, temporal cortex and hippocampus (Doly et al., 2004; Sun et al., 2013). In the sensory circumventricular organs, however, TRPV1 has higher expression in the thick astrocyte processes than in the finer ones (Mannari et al., 2013). Within both retina and optic nerve primary astrocytes cultures, TRPV1 was diffusely expressed throughout the astrocyte soma and processes (Figure 2.13 and 2.14). This expression pattern was similar to cultured cortical astrocytes, where TRPV1 expression was extensive in the membrane and cytoplasm, but was more limited in the processes (Huang et al., 2010).

In the optic nerve head and optic nerve tissue, TRPV1 expression in astrocytes was generally more punctate than in the retina and appeared to be species-dependent (Figure 2.9).

TRPV1 either localized to discrete areas within astrocytes (mouse) or was diffusely expressed throughout astrocytes (rat and monkey). The punctate expression of TRPV1 observed in some optic nerve astrocytes has also been seen in astrocytes in the spinal dorsal horn and brain tissue (Doly et al., 2004; Huang et al., 2010). Extensive co-labeling with GFAP was observed in monkey optic nerve head astrocytes compared to mouse or rat (Figure 2.9). The optic nerve head architecture is different and more complex in monkeys than in rodents, which might account for the differences in expression pattern. The antigenicity of TRPV1 might also be different between monkey and rodents and resulted in greater antibody recognition. There is also vast heterogeneity in astrocytes within different tissues. Across regions in the CNS, astrocytes can be classified into as many as nine groups (radial, Bergmann glia, protoplasmic, fibrous, velate, marginal glia, perivascular, ependymal and tanycytes) based on morphology (Emsley and Macklis, 2006). Comparing TRP expression amongst the different types of astrocytes within the CNS could help elucidate the role of these channels in normal glial function.

Species differences also exist between primate and rodent astrocytes. Astrocytes from human tissue are more complex than rodents. Human protoplasmic astrocytes are 2.6 times greater in diameter and have 10 times more GFAP-positive processes than rodents (Oberheim et al., 2009). Because human astrocytes are larger and more complex, the number of synapses an astrocyte can cover is also greater - 270,000 to 2 million synapses compared to 20,000 to 120,000 synapses for rodents (Oberheim et al., 2009). Calcium wave propagation in human astrocytes is also 4 times faster than rodents (Oberheim et al., 2009). Additionally, two novel astrocyte subtypes exist in primates that are not present in rodents: interlaminar and varicose projection astrocytes. Interlaminar astrocytes are found in cortical layer 1 and are characterized by one to two long columnar processes in addition to several shorter processes that radiate from

the soma (Colombo, 1996; Colombo et al., 1995; Oberheim et al., 2009). Varicose projection astrocytes are present in layers 5-6, and have a feature of one to five long, evenly spaced processes radiating from the soma (Oberheim et al., 2009). This suggests that astrocytes are fundamentally different in terms of morphology and function depending on species. Even within the same species, multiple subtypes exist which further emphasizes the heterogeneity of astrocyte populations.

Astrocyte properties can also differ between mouse and rat. In a scratch wound model, rat astrocytes demonstrated higher expression of GFAP and increased proliferation following injury when compared to mouse astrocytes (Puschmann et al., 2010). Rat astrocytes also exhibit higher mRNA and protein levels for GFAP, nestin and vimentin than mouse astrocytes under basal conditions *in vitro* (Ahlemeyer et al., 2013). Following 28 days in culture, levels of the glutamate transporters, GLAST and GLT-1 decreased in mouse but not rat astrocytes (Ahlemeyer et al., 2013). These data suggest that astrocytes, while similar in mouse and rat, are fundamentally different in the expression of certain genes and in their response to injury.

In the optic nerve, two subtypes of astrocytes (type 1 and type 2) have been identified based on antigenicity and morphology. Type 2 astrocytes can bind tetanus toxin and the antibody for A2B5, a cell surface ganglioside, while Type 1 astrocytes usually do not (Raff et al., 1983). Type 1 astrocyte can be further divided into Type 1A and 1B based on their expression of neural cell adhesion molecule (NCAM). Type 1A astrocytes express GFAP, but not NCAM or A2B5 while Type 1B express both GFAP and NCAM but not A2B5 (Kobayashi et al., 1997). Type 1B is the main astrocyte in the optic nerve head, while Type 2 astrocytes make up more than 65% of the optic nerve (Kobayashi et al., 1997; Miller et al., 1985). Type 1 astrocytes are morphologically similar to protoplasmic astrocytes while Type 2 are more like fibrous astrocytes

(Miller and Raff, 1984). Since optic nerve cultures were isolated from adult mice, both astrocyte subtypes would be present. Since Type 1 and Type 2 astrocytes can be distinguished with the antibody A2B5, it would be interesting to immunolabel for A2B5 to determine the percentage of each subtype present in the optic nerve cultures. Furthermore, co-immunolabeling for A2B5 and TRPV1 can be done to determine if there are differences in expression of TRPV1 between the two subtypes.

Subtypes of astrocytes have also been found in retina. In primates, two morphological classes of astrocytes have been determined: elongated and stellate (Ogden, 1978). Elongated astrocytes have processes that are parallel to the axon bundles and without vascular contact, while processes of stellate astrocytes form contacts with the vasculature (Ogden, 1978). In rabbit retina, however, three subtypes have been identified: class A, B and C (Robinson and Dreher, 1989). Class A astrocytes are perivascular and coupled with the vasculature. Class B do not contact either the vasculature or axons, and Class C mainly associate with axons (Robinson and Dreher, 1989). Less is known about retinal astrocyte subtypes in rodents, and one possible experiment would be to classify the different astrocyte morphologies present in rodent retina using immunolabeling with astrocyte markers including GFAP, S100β and glutamine synthetase.

Astrocytes from different regions of the eye and across different species exhibit a high degree of heterogeneity. Although both retinal and optic nerve astrocytes express TRPV1, expression patterns vary from diffuse to punctate and discrete pockets depending on location and species. This chapter established the presence of TRPV1 protein in retinal and optic nerve astrocytes both *in vivo* and *in vitro*. Subsequent chapters will examine the role of TRPV1 in an intrinsic stress response in astrocytes.

CHAPTER III

THE CONTRIBUTION OF THE TRPV1 CHANNEL IN ASTROCYTE MIGRATION*

3.1 Introduction

Astrocytes distribute widely across the CNS and provide both metabolic and structural support to neurons as part of normal physiology. For example, by establishing networks with the vasculature and with other glia, astrocytes contribute to the exchange of ions and small molecules to maintain homeostasis and facilitate cell-cell communication (Giaume et al., 2010). Astrocytes can also modulate synaptic transmission between neurons through potassium uptake, neurotransmitter recycling, and the release of gliotransmitters such as glutamate and ATP (Hamilton and Attwell, 2010; Wang et al., 2012). In response to neuronal stress or injury, astrocytes undergo reactive hypertrophy of the cell soma and processes (Sofroniew, 2009; Sofroniew and Vinters, 2010). These morphological changes are associated with an upregulation and redistribution of cytoskeletal proteins, including GFAP and actin.

Along with changes in morphology, reactive astrocytes undergo a series of functional changes, including increased motility. Astrocyte migration within the CNS can underlie glial scar formation in spinal cord injury and traumatic brain injury, and can be both beneficial and detrimental to neurons (Hsu et al., 2008; Saadoun et al., 2005; Silver and Miller, 2004). In addition to injuries, astrocyte migration is also important in the metastasis of gliomas, which account for about 70% of all brain tumors (Ohgaki and Kleihues, 2005). Glioma cells are

* Portions of this chapter have been published previously in Ho KW, Lambert WS and Calkins DJ. Activation of the TRPV1 cation channel contributes to stress-induced astrocyte migration (2014) Glia 62(9):1435-51.

particularly invasive and aggressive, leading to high mortality rates for patients. Increased cell motility contributes to this invasiveness, as glioma cells upregulate genes that mediate migration, cell adhesion and extracellular matrix remodeling (Demuth and Berens, 2004; Farin et al., 2006; Mariani et al., 2001). Astrocyte migration has also been observed in eye diseases including age-related macular degeneration and glaucoma (Miao et al., 2010; Morino et al., 1990; Ramirez et al., 2001). In age-related macular degeneration and retinal detachment, retinal astrocytes can migrate from their location in the nerve fiber layer to the vitreous (Morino et al., 1990; Ramirez et al., 2001). In glaucoma, astrocytes in the optic nerve can become reactive and migrate into the nerve bundles (Miao et al., 2010). And like in gliomas, glaucomatous astrocytes have differential expression of genes involved in migration and extracellular matrix remodeling (Hernandez et al., 2008; Miao et al., 2010).

Migration is a stress response of astrocytes following injury, and this motility can be both beneficial and harmful to neurons (Demuth and Berens, 2004; Ehtesham et al., 2004; Fok-Seang et al., 1995; Lefranc et al., 2009; Ramirez et al., 2001; Wang et al., 2004; Wilby et al., 1999). By better understanding the mechanisms that mediate astrocyte migration, novel therapeutic interventions can be developed to temper glial reactivity to improve pathological outcomes associated with injury and disease.

Astrocyte migration is mediated by a variety of signaling pathways and involves cytoskeletal proteins and proteins that mediate adhesion, cell polarity and extracellular matrix remodeling (Laczko et al., 2007; Milner et al., 1999; Ogier et al., 2006; Osmani et al., 2006; Raftopoulou and Hall, 2004; Ricard et al., 2000). Calcium is a key signaling messenger and can regulate many of these pathways. Astrocytes are known to express a number of potent Ca^{2+} modulators, including TRPV1 (Chen et al., 2009; Doly et al., 2004; Ho et al., 2012; Huang et al.,

2010; Mannari et al., 2013). Since retinal and optic nerve astrocytes express TRPV1 (Chapter 2; Leonelli et al., 2009), we asked whether this channel could play a role in mediating astrocyte migration in response to injury. We induced migration of isolated retinal astrocytes using a scratch wound assay and examined how modulation of TRPV1 activation with subunit-specific agonists (CAP and RTX) and antagonists (IRTX and CPZ) affected the rate of migration. We also examined the rate of migration in astrocytes isolated from the optic nerve head of C57BL/6 mice and TRPV1 -/- mice following scratch injury.

3.2 Methods

Scratch wound model of injury-induced migration

To test astrocyte migration following injury, I used the scratch wound model. Unlike the transwell assay which relies on chemotaxis, the scratch wound assay is a wound healing model. In the transwell assay, cells are seeded onto one side of a transwell chamber and allowed to migrate to the opposite side in response to a chemotactic signal. By counting the number of cells on the opposite side, migration is determined. In the scratch wound model however, a single scratch is made through the astrocyte monolayer. In response to this injury, cells release factors into the extracellular environment to induce migration of adjacent cells.

Retinal and optic nerve astrocytes were isolated as previously described in Chapter 2. Confluent primary astrocytes were passaged with 0.25% trypsin/2.21 mM EDTA and seeded onto cover glass chambers (ThermoScientific, Rochester, NY) coated with 0.01 mg/mL poly-D-lysine. Once confluent, astrocytes were serum-starved in 0.5% FBS overnight. A single scratch with a 1 mL pipet tip was then made through the astrocyte monolayer, and cultures were washed three times with serum-free DMEM/F-12 to remove debris (Figure 3.1). Cultures were then

incubated in astrocyte media plus 0.5% FBS in addition to pharmacological agents. The following TRPV1-specific agonists were applied immediately following the scratch: capsaicin (CAP; Sigma-Aldrich, St. Louis, MO, 100 pM-10 μM in ethanol) and resiniferatoxin (RTX; Thermo Fisher Scientific, Wilmington, DE, 100 pM-10 μM in ethanol). The following TRPV1-specific antagonists were applied 15 minutes prior to scratch: capsazepine (CPZ; Tocris Bioscience, Bristol, UK, 1 μM-10 μM in ethanol) and 5'-iodo resiniferatoxin (IRTX; Tocris Bioscience, Bristol, UK, 300 nM-3 μM in ethanol). The following calcium chelators were used: ethylene glycol-*bis* (2-aminoethylether)-*N*,*N*,*N*',*N*'-tetraacetic acid (EGTA, Sigma-Aldrich, St. Louis, MO, 100 μM-1 mM in water) and BAPTA-AM (Life Technologies, Grand Island, NY, 1 μM-10 μM in dimethyl sulfoxide). BAPTA was applied 15 minutes prior to scratch, while EGTA was added immediately after. Differential interference contrast (DIC) images were taken on an inverted Nikon Eclipse Ti microscope at 6 to 12 hour intervals post-scratch to monitor wound closure. A minimum of five images per well were taken, and each treatment was performed in triplicate. Images were taken until the wound for one or more treatments reached 70-100% closure, typically 24 to 48 hours post-wound.

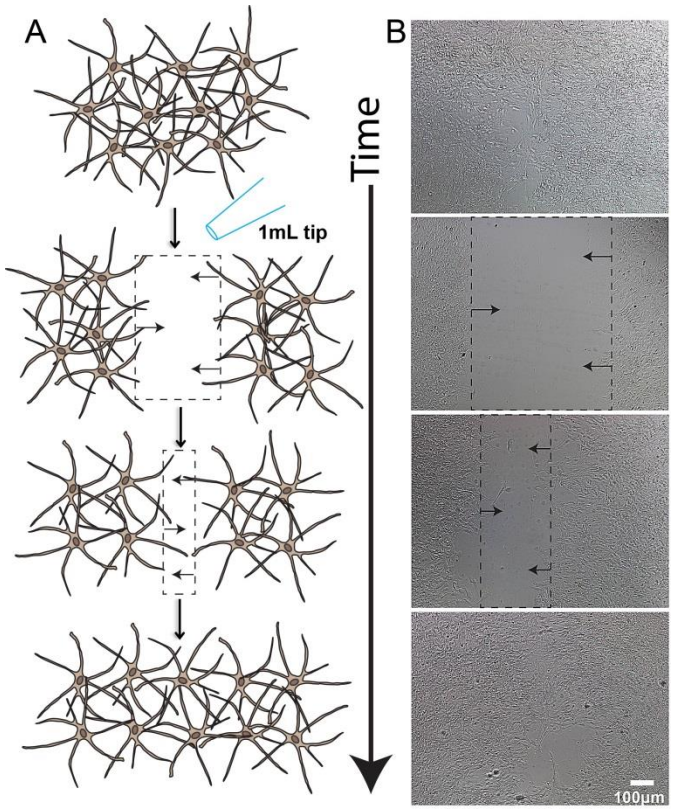

Figure 3.1. The scratch wound assay of injury-induced migration. **(A)** A schematic of the assay where a wound is made through the astrocyte cell layer with a pipet tip is shown. In response to the injury, astrocytes on either side of the injury would migrate over time to close the wound. **(B)** DIC images illustrate this assay in live astrocyte cultures.

Quantification of proliferation in scratch wound assay

To quantify proliferation, astrocyte cultures were fixed in 4% paraformaldehyde for 20 minutes following scratch injury and treatment with TRPV1 pharmacological agents. Cells were then placed in primary antibody for Ki-67 (ThermoScientific, Rochester, NY, 1:200) overnight at 4˚C, followed by incubation in the appropriate DyLight-conjugated secondary antibodies (Jackson Immunoresearch, West Grove, PA 1:150). Staining with 4',6-diamidino-2-phenylindole (DAPI; Life Technologies, Grand Island, NY, 1:100) in water was also performed to visualize

nuclei. Confocal images were taken using an Olympus FV-1000 inverted microscope. Cells positive for Ki-67 and DAPI were counted with ImageJ (Schneider et al., 2012). Five images per replicate were taken, and each treatment condition had at least three replicates. The amount of proliferation is represented as percent Ki-67-positive cells per total DAPI-positive cells in a field.

Quantification of astrocyte migration

To quantify astrocyte migration, DIC images for a given treatment were analyzed in blinded fashion to determine the area of the wound at each time point. Briefly, using ImageJ (Schneider et al., 2012) a rectangle was drawn over the cell-free area of the image, which was defined as the area that was minimally 95% free of astrocyte processes. This "cell-free" area was verified post-hoc by measuring total astrocyte cytoplasmic area and comparing it to any residual cytoplasmic area within the cell-free area. Across all scratch wounds and conditions examined, this cell free area excluded 97.8 ± 1.8% of the astrocyte processes calculated by cytoplasmic area. Although a 1 mL pipet tip was used to make the scratch wound in all assays, variations in tip diameter resulted in a range of initial cell-free areas within each preparation. To control for this variability, I restricted my analysis to scratch wound preparations with initial cell-free areas within the standard deviation of vehicle astrocytes for that assay. Excluding preparations that fell outside the standard deviation left 10 to 15 images for analysis. Rarely, a preparation required 1-2 additional rectangles to account for partial wound closure or asymmetric closure. In these cases, the areas of the rectangles were summed for total astrocyte-free area.

Next, I graphed the cell-free area at each time point, and linear regression was then performed to determine the best-fitting line for cell-free area over time. The slope of each line and its associated error was considered the rate of migration. These were compared between

treatments to determine significance using GraphPad Prism (GraphPad Software, Inc., La Jolla, CA). For each treatment, I calculated average cell-free area ± standard error of the mean (SEM) versus time post-scratch; this is shown in my figures along with the best-fitting regression line.

Statistical analysis

Data is presented as mean ± standard error of the mean (SEM) for each treatment. Statistical analysis and p-values for comparing mean cell-free areas were obtained using one-way ANOVA with Bonferroni's Multiple Comparison Test or t-tests for data meeting criteria for normalcy or using non-parametric rank statistics for data failing normalcy using SigmaPlot 11.0 for Windows (Systat Software Inc., Chicago, IL) or GraphPad Prism (GraphPad Software, Inc., La Jolla, CA).

3.3 Results

Proliferation in scratch wound assay is reduced with low serum conditions

In response to injury, astrocytes can also proliferate in the scratch wound assay (Liang et al., 2007). In order to reduce astrocyte proliferation, I performed the scratch wound assay in low serum (0.5%) conditions. To verify reduced proliferation in low serum conditions, I measured proliferation in astrocyte cultures following scratch injury under normal (10%) and low (0.5%) serum conditions. Proliferation was examined by immunolabeling for Ki-67, which recognizes a nuclear antigen found in dividing cells but is absent in quiescent cells (Figure 3.2A; Scholzen and Gerdes, 2000). Incubation in 0.5% serum reduced proliferation compared to 10% serum in both naïve (1.63 ± 0.63% vs. 17.98 ± 1.67% respectively; $p < 0.001$) and 24 hours after injury (5.68 ± 1.48% vs. 16.90 ± 2.42%, respectively; $p = 0.005$) conditions. In normal 10% serum

conditions, scratch injury did not change the amount of proliferation compared to naive unscratched astrocytes (17.98 ± 1.67% vs. 16.90 ± 2.42%; Figure 3.2B). Under low serum (0.5%) conditions, proliferation increased from 1.63 ± 0.63% to 5.68 ± 1.48% following scratch injury, although this was not significant ($p = 0.918$). The average total number of cells was similar for naïve (96.00 ± 10.26 vs 116.95 ± 12.33 cells) and scratched (52.35 ± 3.63 vs 56.85 ± 5.54 cells) under low and normal serum conditions, respectively ($p > 0.262$; Figure 3.2C). The reduction in the number of cells following scratch was due to the lower concentration of cells at the leading edges.

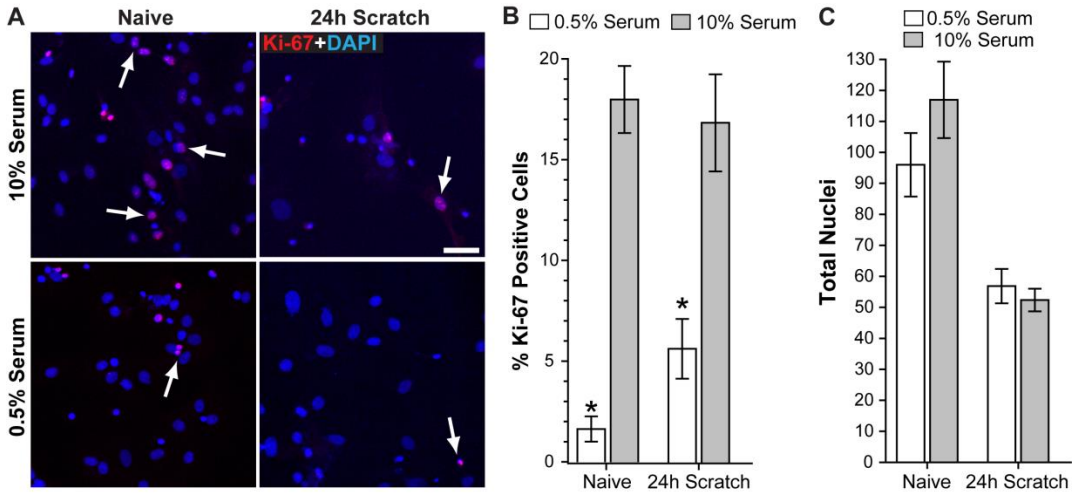

Figure 3.2. Proliferation in scratch wound model. **(A)** Confocal micrographs show naïve astrocytes and injured astrocytes cultured under normal (10%) and low (0.5%) serum conditions that have been immunolabeled for Ki-67 (red) and DAPI (blue). Scale: 50 µm. **(B)** Bar graph shows the percent of Ki-67 positive cells for each treatment condition. * $p \leq 0.005$ vs. 10% serum (n=4). **(C)** Bar graph shows the total number of nuclei for each treatment.

TRPV1 agonism has modest effects on astrocyte migration

Next, to determine if pharmacological activation of TRPV1 would affect migration, I treated astrocytes immediately following scratch with the specific agonists CAP or RTX (Caterina et al., 2000; Caterina et al., 1997; Raisinghani et al., 2005; Szallasi and Blumberg, 1989). Addition of CAP at the concentrations tested had no effect on cell morphology compared to vehicle throughout the duration of the experiment (Figure 3.3). At 24 hours following injury, CAP-treated astrocytes had processes and morphologies similar to vehicle, and no cell detachment was observed (Figure 3.3B and 3.3C).

Representative images show that scratch injury induces a wound through the astrocyte cell layer (Figure 3.4A and 3.4B). Astrocyte migration to reduce the cell-free area following scratch wound was similar for vehicle and CAP-treated cells at the time points measured (Figure 3.4A and 3.4B). Initial wound areas for vehicle treated cells in the CAP experiments averaged $6.49 \pm 0.338 \times 10^5$ μm^2 (Figure 3.4C). Preparations treated with CAP with an initial wound area that did not fall within the standard deviation of vehicle were excluded from analysis, leaving at least 14 independent images per time point for analysis. At 24 hours post-injury, treatment with 100 nM, 1 μM and 10 μM CAP induced closure of 74 ± 4.21%, 64 ± 5.77% and 46 ± 4.60% respectively, compared to 62 ± 6.34% closure with vehicle (Figure 3.4C). This difference in percent closure was not significant ($p \geq 0.097$). In terms of migration rate following CAP treatment (Figure 3.4D), a range of concentrations from 100 pM to 1 μM showed non-significant accelerations of 8-23% ($p \geq 0.26$). This trend towards acceleration was reversed at the highest concentration (10 μM), which resulted in a non-significant trend toward a reduced migration rate (~ 9%) compared to vehicle ($p = 0.66$).

To confirm the results with CAP and further assess TRPV1's role in injury-induced migration, I tested the effects of RTX, another TRPV1 agonist. Much like CAP treatment, cell morphology was not affected by the addition of RTX at the concentrations tested when compared to vehicle (Figure 3.5). Again, representative DIC images show that scratch injury induces a wound that is reduced over time as the cells migrate for both vehicle and RTX (Figure 3.6A and 3.6B). Initial wound areas for vehicle averaged $8.60 \pm 0.45 \times 10^5$ μm^2 (Figure 3.6C). All preparations treated with RTX had initial wound areas that fell within the standard deviation of the vehicle, therefore no preparations were excluded from analysis. Treatment with 100 pM or 1 nm RTX induced closure of 59 ± 4.05% and 52 ± 3.32%, similar to the 52 ± 5.05% closure with vehicle ($p \geq 0.289$; Figure 3.6C). As with CAP, the highest concentration of RTX used (10μM) appeared to reduce closure to 38 ± 1.74% at 24 h ($p = 0.056$). When comparing migration rates, treatment with 100 pM or 1 μM RTX accelerated migration 26% and 11% relative to vehicle, respectively ($p \geq 0.268$; Figure 3.6D). Migration rates for 1, 10 and 100 nM RTX were similar to vehicle ($p > 0.823$). Despite a near 30% average reduction in migration rate when 10 μM RTX was applied, this effect was not significant ($p = 0.186$).

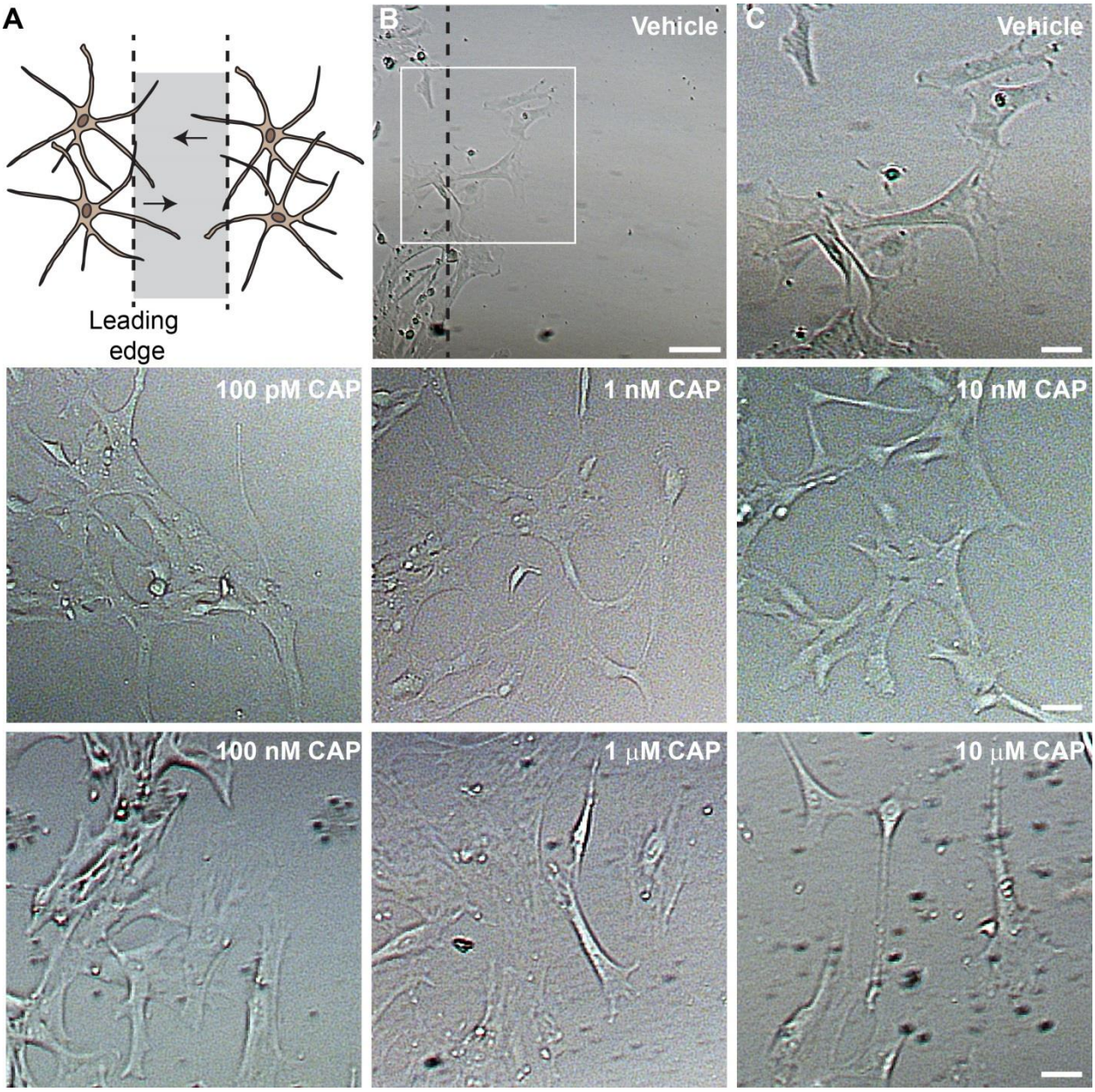

Figure 3.3. Cell morphologies following CAP treatment. In response to injury, cells at the leading edge migrate in the scratch wound assay (**A**). DIC micrograph shows live, vehicle-treated cells at 24 hours following injury. High magnification images were captured at the leading edge (solid box; **B**). Morphologies are shown for cells treated with vehicle and multiple concentrations of CAP (**C**). Scale: 50 μm for **B**, 20 μm for **C**.

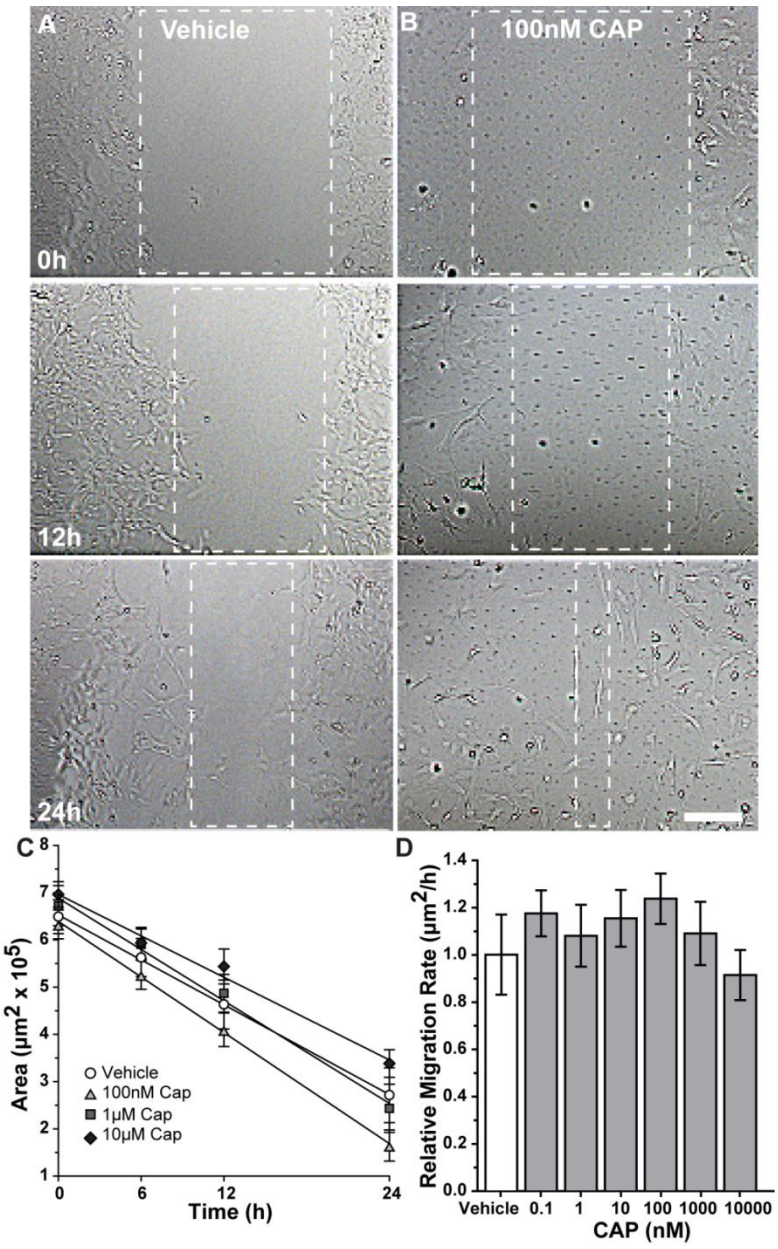

Figure 3.4. Effects of CAP on astrocyte migration. DIC micrographs show astrocytes treated with **(A)** vehicle and **(B)** 100 nM CAP at 0, 12 and 24 hours following scratch injury. Dotted boxes indicate the cell-free area. Scale bar: 100 μm. **(C)** Scatter plots with the best-fit linear regression line show the change in area over time for astrocytes treated with vehicle, 100 nM, 1 μM and 10 μM CAP. **(D)** Bar graphs show the relative migration rate (or the slope of the best-fit linear regression line) for vehicle and multiple concentrations of CAP.

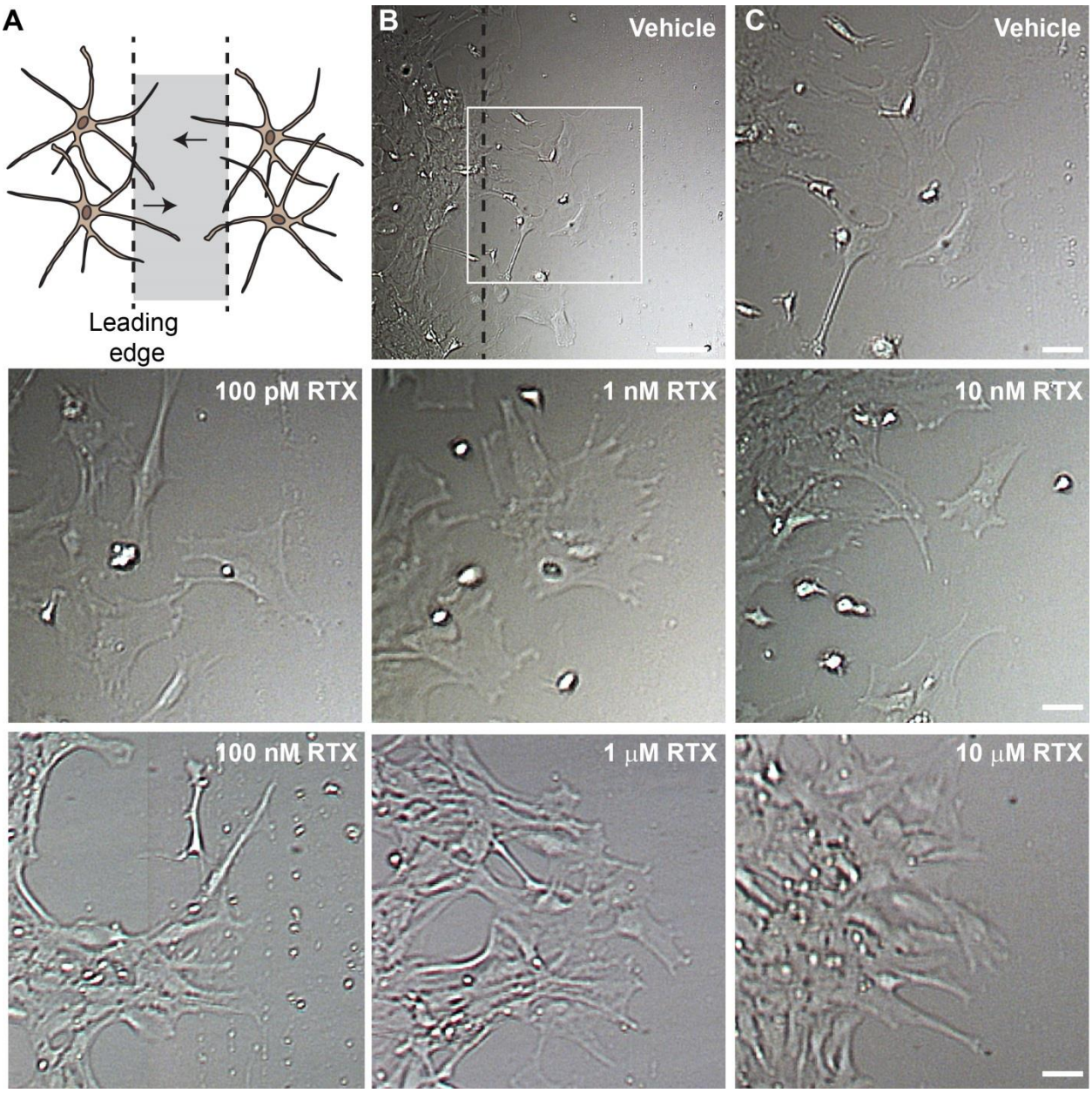

Figure 3.5. Cell morphologies following RTX treatment. In response to injury, cells at the leading edge migrate in the scratch wound assay (**A**). DIC micrograph shows live, vehicle-treated cells at 24 hours following injury. High magnification images were captured at the leading edge (solid box; **B**). Morphologies are shown for cells treated with vehicle and multiple concentrations of RTX (**C**). Scale: 50 μm for **B**, 20 μm for **C**.

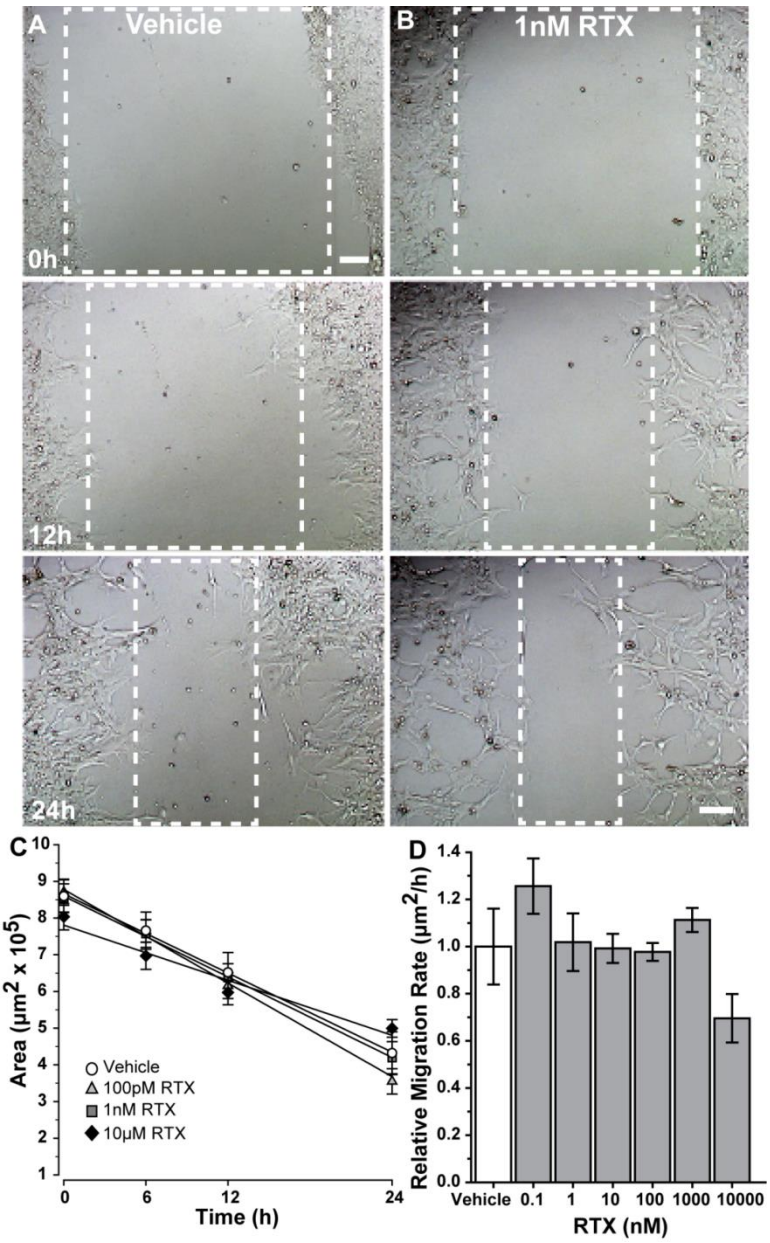

Figure 3.6. Effects of RTX on astrocyte migration. DIC micrographs show astrocytes treated with **(A)** vehicle and **(B)** 1 nM RTX at 0, 12 and 24 hours following scratch injury. Dotted boxes indicate the cell-free area. Scale bar: 100 μm. **(C)** Scatter plots with the best-fit linear regression line show the change in area over time for astrocytes treated with vehicle, 100 pM, 1 nM and 10 μM RTX. **(D)** Bar graphs show the relative migration rate (or the slope of the best-fit linear regression line) for vehicle and multiple concentrations of RTX.

Effects of TRPV1 agonists on astrocyte proliferation

Although proliferation following scratch injury was low, averaging only 5.68% in 0.5% serum conditions (Figure 3.2), I also immunolabeled for Ki-67 to test whether proliferation was affected by addition of CAP and RTX. Representative confocal micrographs show that Ki-67 and DAPI labeled nuclei in both vehicle and CAP treated astrocytes (Figure 3.7A). Similar labeling was observed following RTX treatment (data not shown). The percentage of Ki-67 positive cells averaged 5.91 ± 1.76 to 13.07 ± 2.41 % in CAP-treated cells and was similar to vehicle (7.93 ± 2.41%; $p > 0.075$; Figure 3.7B). Quantification of the percentage of Ki-67 positive cells following RTX treatment shows that proliferation is similar for both 100 pM and 1 nM RTX when compared to vehicle ($p \geq 0.572$). Addition of 10 μM RTX however, reduced proliferation from 7.33 ± 1.13% to 3.75 ± 0.59% compared to vehicle ($p = 0.03$; Figure 3.7C). The average number of total nuclei for CAP treated cells ranged from 24.36 ± 1.73 to 42.81 ± 4.32, and was similar to the vehicle average of 38.00 ± 1.66 cells ($p = 0.295$; data not shown). The same was true for RTX-treated cells ($p > 0.125$).

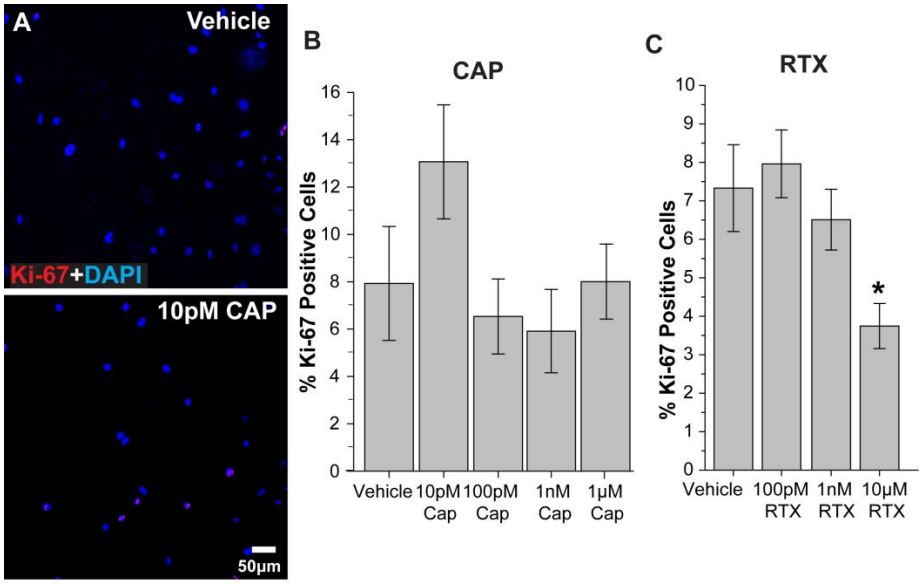

Figure 3.7. Effects of TRPV1 agonists on astrocyte proliferation following injury. **(A)** Confocal micrographs show vehicle- and 10 pM CAP-treated astrocytes immunolabeled for Ki-67 (red) and DAPI (blue) following scratch. **(B)** Bar graph shows the percent of Ki-67 positive cells for vehicle and multiple concentrations of CAP. **(C)** Bar graph shows the percent of Ki-67 positive cells for vehicle and different RTX concentrations. * p = 0.03 vs. vehicle.

Antagonism of TRPV1 reduces retinal astrocyte migration

In addition to activating TRPV1 and measuring migration, I also treated isolated retinal astrocytes with the TRPV1-specific antagonists CPZ or IRTX 15 minutes prior to the scratch to discern whether blocking channel activation would influence injury-induced migration (Seabrook et al., 2002; Wahl et al., 2001; Walpole et al., 1994).

Addition of CPZ did not affect cell morphology compared to vehicle throughout the duration of the experiment (Figure 3.8). Figure 3.9 shows representative images of CPZ-treated astrocytes following scratch wound. In the vehicle group, the initial cell-free area was reduced at 36 hours by astrocytes migrating from the edges (Figure 3.9A). Treatment with 10 µM CPZ

reduced wound closure, resulting in a considerably larger cell-free area at 36 hours compared to vehicle (Figure 3.9B). All preparations treated with CPZ had initial wound areas that were within the standard deviation of the vehicle, therefore no preparations were excluded from analysis. For the vehicle group in the CPZ experiments, an initial wound area of 9.4 ± 0.09 x10^5 μm^2 was reduced $75 \pm 3.13\%$ at 36 hours following injury (Figure 3.9C). While treatment with 1 μM CPZ resulted in similar closure at 36 hours ($77 \pm 4.87\%$, $p = 0.65$), both 5 and 10 μM CPZ significantly reduced closure to $44 \pm 3.41\%$ and $38 \pm 3.10\%$ ($p \leq 0.001$), respectively. Accordingly, the rate of astrocyte migration also differed with increasing concentrations of CPZ (Figure 3.9D). Compared to vehicle, 5 and 10 μM CPZ reduced migration rate by 41% and 44%, respectively ($p \leq 0.006$). This effect was dose-dependent as the 15% reduction with 1 μM CPZ was not significant ($p = 0.064$).

To further determine the effects of inhibiting TRPV1, I tested the effects of a second antagonist, IRTX on astrocyte migration. The addition of IRTX at various concentrations did not affect cell morphology compared to vehicle (Figure 3.8). Like with 5 and 10 μM CPZ, treatment with 3 μM IRTX reduced migration, resulting in a larger cell-free area over time compared to vehicle (Figure 3.10A and 3.10B). All preparations treated with IRTX had initial wound areas that fell within the standard deviation of the vehicle, therefore no preparations were excluded from analysis. Vehicle-treated cells had an initial wound area that averaged 12.54 ± 0.31 μm^2 x10^5 and showed a closure of $76 \pm 2.93\%$ at 36 hours after injury. Treatment with 300 nM or 1 μM IRTX had no effect on wound closure compared to vehicle ($67 \pm 4.16\%$ and $75 \pm 4.02\%$ respectively, $p > 0.08$), while 3 μM IRTX significantly reduced closure to $52 \pm 2.23\%$ of initial wound area ($p \leq 0.001$; Figure 3.10C). Similarly, while 300 nM and 1 μM had little effect on

migration rate compared to vehicle ($p \geq 0.687$), 3 μM IRTX significantly reduced the rate by 28% again illustrating a dose-dependent effect ($p = 0.035$; Figure 3.10D).

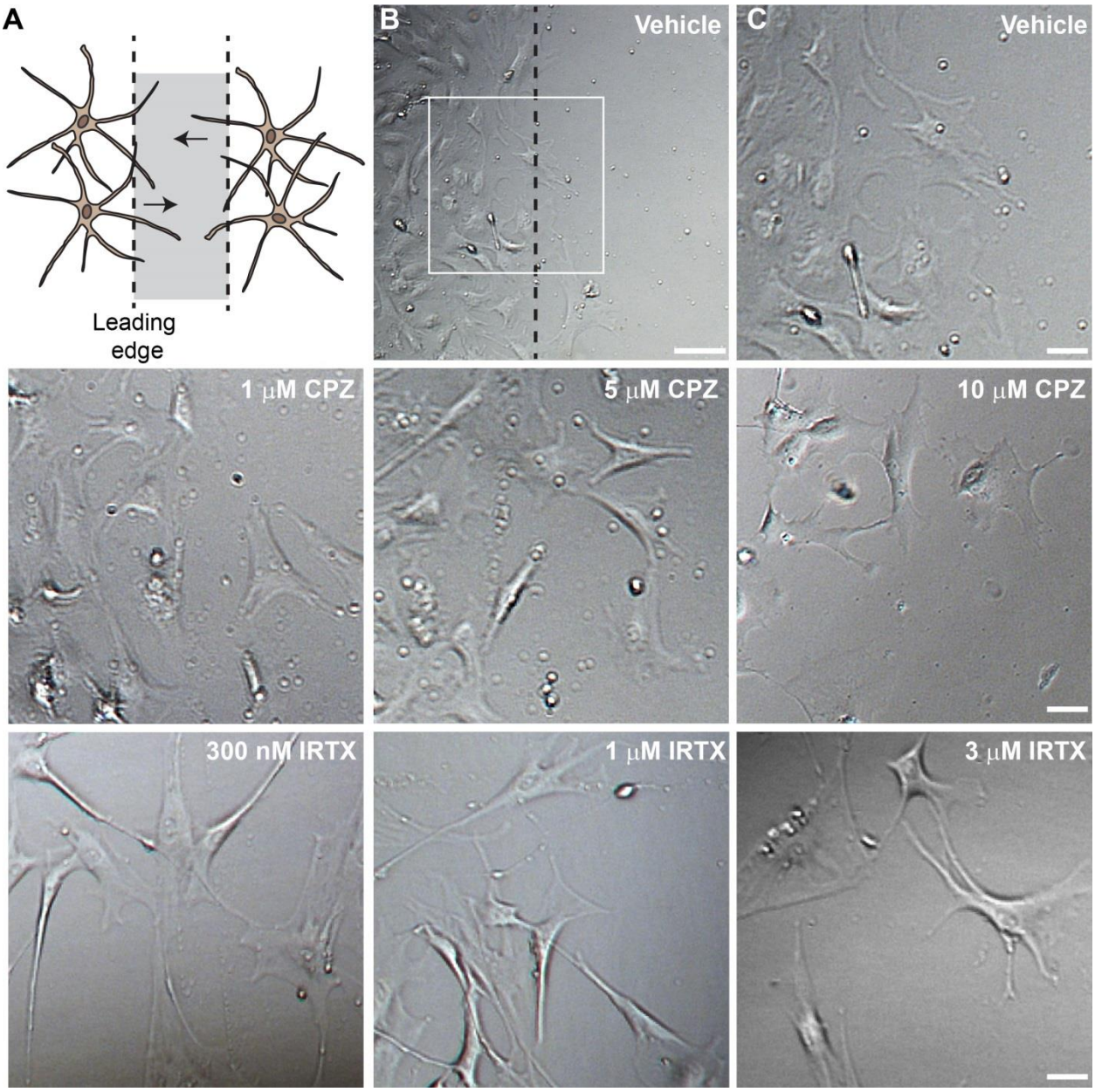

Figure 3.8. Cell morphologies following CPZ and IRTX treatments. In response to injury, cells at the leading edge migrate in the scratch wound assay (**A**). DIC micrograph shows live, vehicle-treated cells at 24 hours following injury. High magnification images were captured at the

leading edge (solid box; **B**). Morphologies are shown for cells treated with vehicle and multiple concentrations of CPZ or IRTX (**C**). Scale: 50 μm for **B**, 20 μm for **C**.

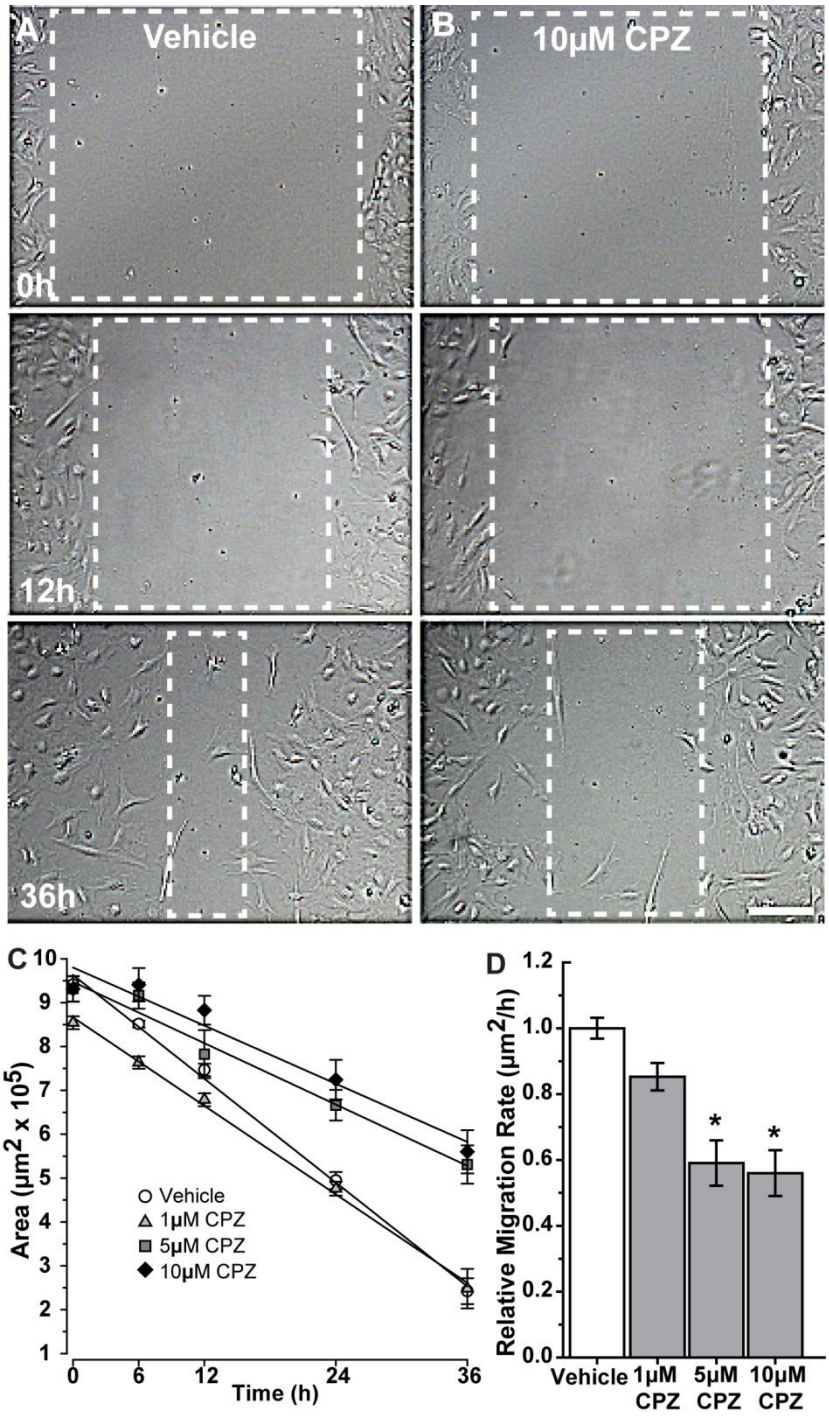

Figure 3.9. Effects of CPZ on astrocyte migration. DIC micrographs show astrocytes treated with **(A)** vehicle and **(B)** 10 µM CPZ at 0, 12 and 36 hours following scratch injury. Dotted boxes indicate the cell-free area. Scale bar: 100 µm. **(C)** Scatter plots with the best-fit linear regression line show the change in area over time for astrocytes treated with vehicle, 1, 5 and 10 µM CPZ. **(D)** Bar graphs show the relative migration rate (or the slope of the best-fit linear regression line) for vehicle and CPZ. * $p \leq 0.006$ vs. vehicle.

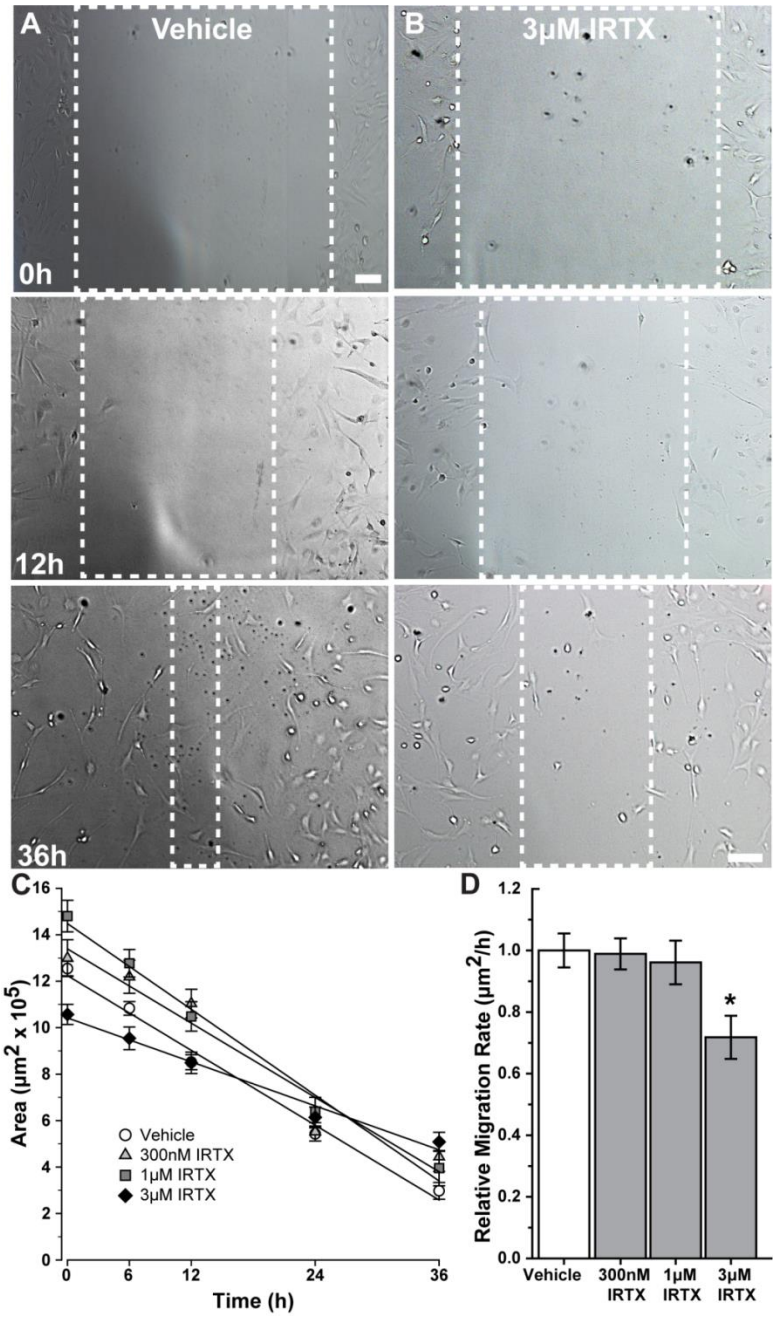

Figure 3.10. Effects of IRTX on astrocyte migration. DIC micrographs show astrocytes treated with **(A)** vehicle and **(B)** 3 μM RTX at 0, 12 and 36 hours following scratch injury. Dotted boxes indicate the cell-free area. Scale bar: 100 μm. **(C)** Scatter plots with the best-fit linear regression line show the change in area over time for astrocytes treated with vehicle, 300 nM, 1

and 3 μM RTX. **(D)** Bar graphs show the relative migration rate (or the slope of the best-fit linear regression line) for vehicle and IRTX. * p = *0.035* vs. vehicle.

Effects of TRPV1 antagonists on astrocyte proliferation

To further determine whether TRPV1 affects injury-induced proliferation, I tested whether the addition of the antagonists CPZ and IRTX influenced astrocyte proliferation following scratch injury. Again, Ki-67 immunolabeling was present in the nucleus of both vehicle and CPZ-treated cells (Figure 3.11A), as well as in IRTX-treated cells (data not shown). Quantification of the number of cells positive for Ki-67 normalized to total nuclei indicated that proliferation averaged 7.70 ± 1.38% for vehicle in the CPZ experiments (Figure 3.11B). Addition of CPZ reduced proliferation to 3.31 ± 0.51% for 5 μM and to 1.73 ± 0.96% for 10 μM CPZ. This reduced proliferation in response to 10 μM CPZ was significant compared to vehicle ($p < 0.02$; Figure 3.11B). Similarly, addition of 3 μM IRTX reduced the percent of Ki-67 positive cells relative to vehicle (1.11 ± 0.92% vs. 3.60 ± 0.71% respectively), but this reduction was not significant ($p > 0.09$; Figure 3.11C). Total number of nuclei was similar to vehicle controls for all concentrations of CPZ ($p > 0.48$) and IRTX ($p > 0.07$; data not shown).

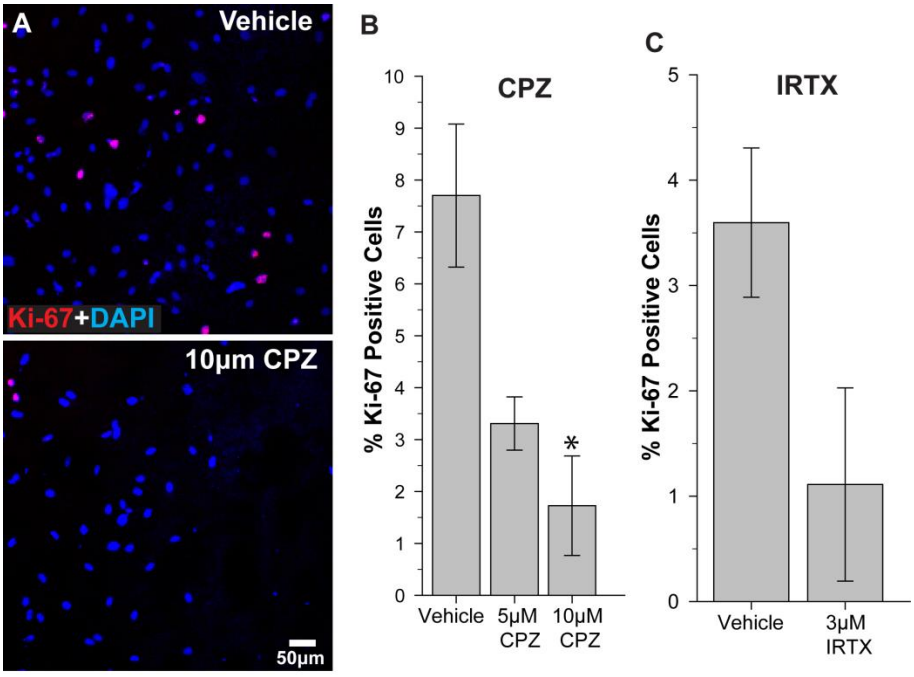

Figure 3.11. Effects of TRPV1 antagonists on astrocyte proliferation following injury. **(A)** Confocal micrographs show vehicle- and 10 μM CPZ-treated astrocytes that have been immunolabeled for Ki-67 (red) and DAPI (blue) following scratch injury. **(B)** Bar graph showing the percent of Ki-67 positive cells for vehicle and 5 and 10 μM CPZ. *$p < 0.02$ compared to vehicle. **(C)** Bar graph showing the percent of Ki-67 positive cells for vehicle and 3 μM IRTX**.**

Genetic knockout of TRPV1 slightly reduces retinal astrocyte migration

To complement my pharmacological experiments, I next examined whether genetic deletion of TRPV1 affected astrocyte migration in the scratch wound model. To this end, I used optic nerve astrocytes isolated from C57 wild-type and TRPV1-/- mice at one month of age. For the characterization, purity and genotyping of these astrocytes, see Chapter 2.

Similar to the prior experiments in retinal astrocytes, scratch injury induced a wound through the astrocyte cell layer that closed over time as migration occurred. Representative

images show that C57 wild-type and TRPV1-/- astrocytes have similar morphologies after injury (Figure 3.12). The change in cell-free area following injury was also similar (Figure 3.13A and 3.13B). Initial areas for C57 astrocytes averaged 10.54 ± 0.92 x10^5 μm^2. Like with the pharmacological experiments, initial areas for TRPV1-/- astrocytes that were not within the standard deviation of C57 astrocytes were excluded, leaving at least ten images per time point for each replicate (n= 9 animals for C57 and 10 for TRPV1-/-). Wound closure was similar between C57 and TRPV-/- astrocytes (80 ± 6.37% versus 78 ± 7.16%, respectively; p=0.90) following scratch injury (Figure 3.13C). Although migration rate was reduced by 14% in TRPV1-/- astrocytes compared to C57, this reduction was not significant (p > 0.39; Figure 3.13D).

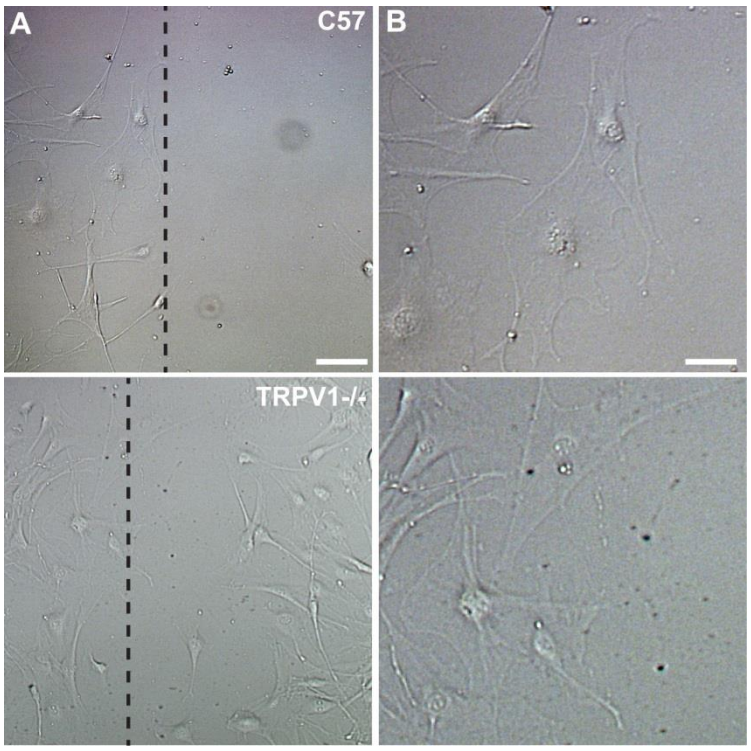

Figure 3.12. Comparison of cell morphologies in C57 and TRPV1-/- astrocytes. DIC micrographs show live astrocytes from C57 and TRPV1-/- optic nerves at 24 hours following

scratch injury (**A**). High magnification images were captured at the leading edge (dotted lines). High magnification images are shown for C57 and TRPV1-/- (**B**). Scale: 20 µm.

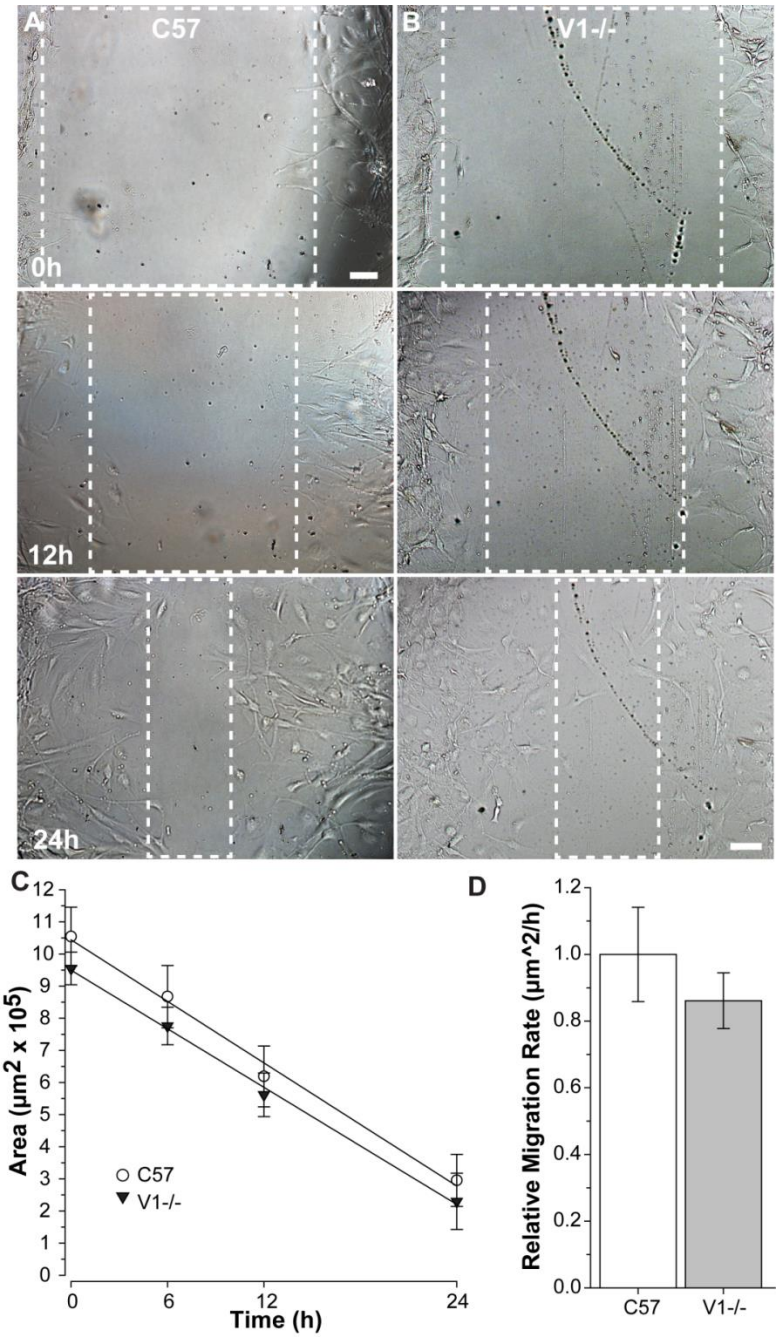

Figure 3.13. Injury-induced migration in TRPV1-/- astrocytes. DIC micrographs show astrocytes from **(A)** C57 wild-type and **(B)** TRPV1-/- optic nerves at 0, 12 and 24 hours

following scratch injury. Dotted boxes indicate the cell-free area. Scale bar: 100 μm. **(C)** Scatter plots with the best-fit linear regression line show the change in area over time for C57 and TRPV1-/- astrocytes. **(D)** Bar graphs show the relative migration rate (or the slope of the best-fit linear regression line) for C57 and TRPV1-/- astrocytes.

Chelation of extracellular calcium reduces astrocyte migration

Given that calcium is a key regulator of cytoskeletal reorganization and cell motility (Conklin et al., 2005; Easley et al., 2008; Lee et al., 1999; Martini and Valdeolmillos, 2010), I next determined the effects of calcium on injury-induced astrocyte migration by using EGTA or BAPTA-AM to chelate extracellular and intracellular calcium, respectively. Higher concentration of EGTA (10 mM) or BAPTA (10 μM) lead to cell rounding and detachment in my cultures, therefore lower concentrations were used in the scratch wound assay (Figure 3.14C and 3.14D). Astrocyte morphology was not affected by EGTA compared to vehicle at the concentrations tested (Figure 3.14B and 3.14C).

Representative images of astrocytes treated with vehicle and 1 mM EGTA are shown in Figure 3.10. As before, scratch injury induces a wound that becomes smaller as vehicle-treated astrocytes migrate (Figure 3.14A). Addition of 1 mM EGTA reduced migration, resulting in a larger cell-free area at 48 hours compared to control (Figure 3.14B). Initial wound areas in vehicle treated cells averaged $7.1 \pm 0.31 \times 10^5$ μm^2 (Figure 3.14C). Preparations treated with EGTA with initial wound sizes that did not fall within the standard deviation of vehicle areas were excluded from analysis, leaving at least 10 independent images per time point for analysis. For the vehicle group, the initial wound area was reduced 65 ± 7.67% at 48 h following injury (Figure 3.14C). Treatment with 100 μM EGTA led to 71 ± 6.32% closure after 48 h ($p = 0.29$),

while 1 mM EGTA resulted in 40 ± 9.31% closure ($p = 0.052$). Although the reduced percent wound closure did not significantly differ with EGTA treatment, the 35% reduction in migration rate for 1 mM EGTA was significant compared to vehicle ($p = 0.048$; Figure 3.14D). The modest increase in rate with 100 μM EGTA (9%) was not significant ($p = 0.48$).

Next, I tested if chelation of intracellular calcium with BAPTA-AM affected migration. BAPTA-AM treatment did not affect astrocyte morphology when compared to vehicle at the concentrations used (Figure 3.14B and 3.14D). Scratch injury induced cells to migrate to close the wound over time, resulting in a smaller cell-free are that was similar for vehicle and 10 μM BAPTA-AM at 36 hours (Figure 3.16A and 3.16B). Vehicle-treated cells had initial wound areas that averaged $8.3 \pm 0.20 \times 10^5$ μm^2 (Figure 3.16C). All preparations treated with BAPTA-AM had initial wound areas that fell within the standard deviation of the vehicle; therefore no preparations were excluded from analysis. In contrast to EGTA, chelation of intracellular Ca^{2+} with 1 μM or 10 μM BAPTA-AM had little effect on migration with 65 ± 3.62% and 70 ± 6.63% closure respectively, at 36 hours compared to 73 ± 3.94% for vehicle ($p \geq 0.106$; Figure 3.16C). Accordingly, migration rate following BAPTA-AM treatment was also similar to vehicle ($p \geq 0.53$; Figure 3.16D).

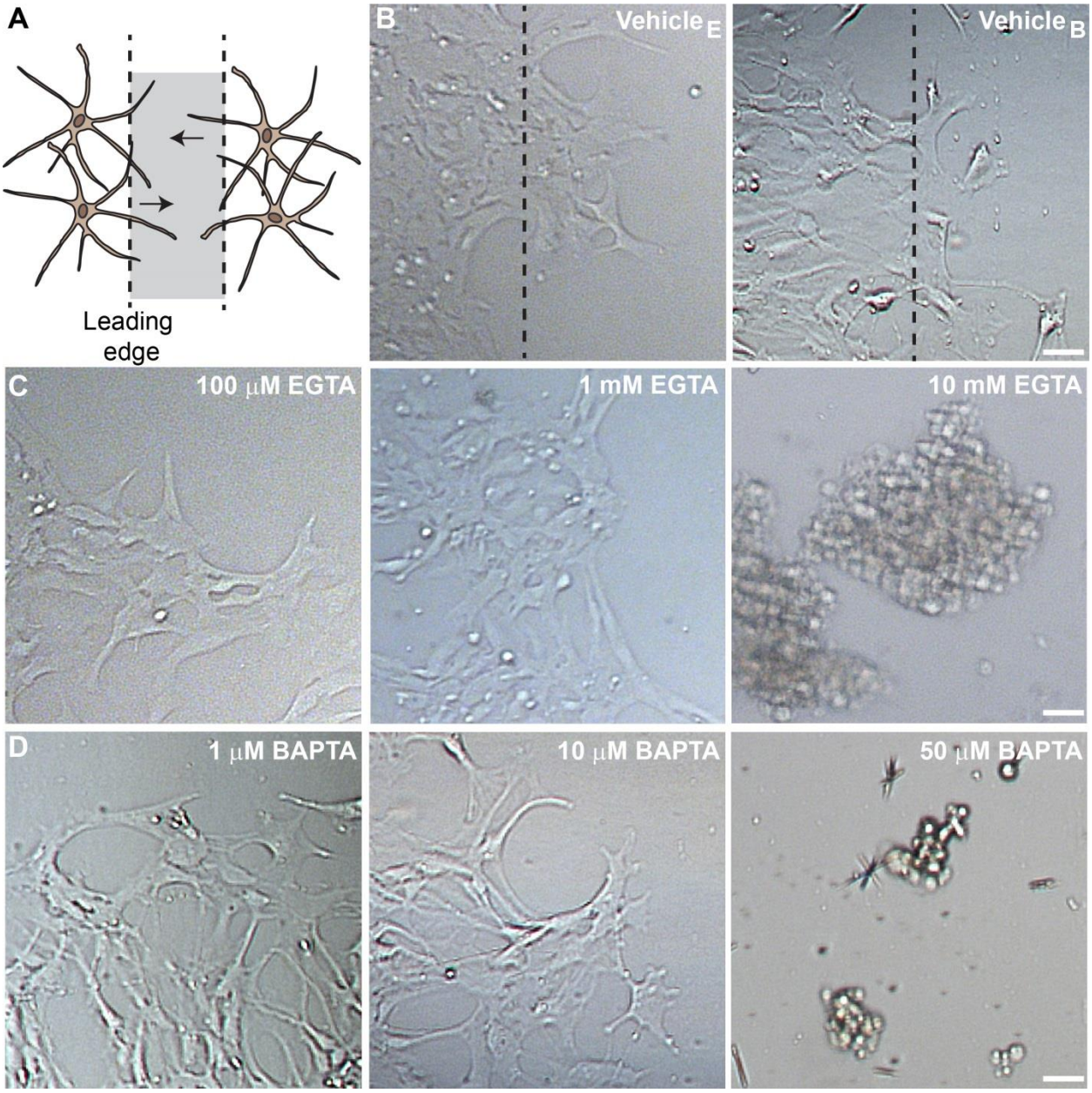

Figure 3.14. Astrocyte morphologies following addition of calcium chelators. In response to injury, cells at the leading edge migrate in the scratch wound assay (**A**). High magnification images were captured at the leading edge (dotted line) at 24 hours for vehicle EGTA and vehicle BAPTA cells (**B**). Morphologies are shown for cells treated with vehicle and multiple concentrations of EGTA (**C**) or BAPTA (**D**). Scale: 50 μm for **B**, 20 μm for **C** and **D**.

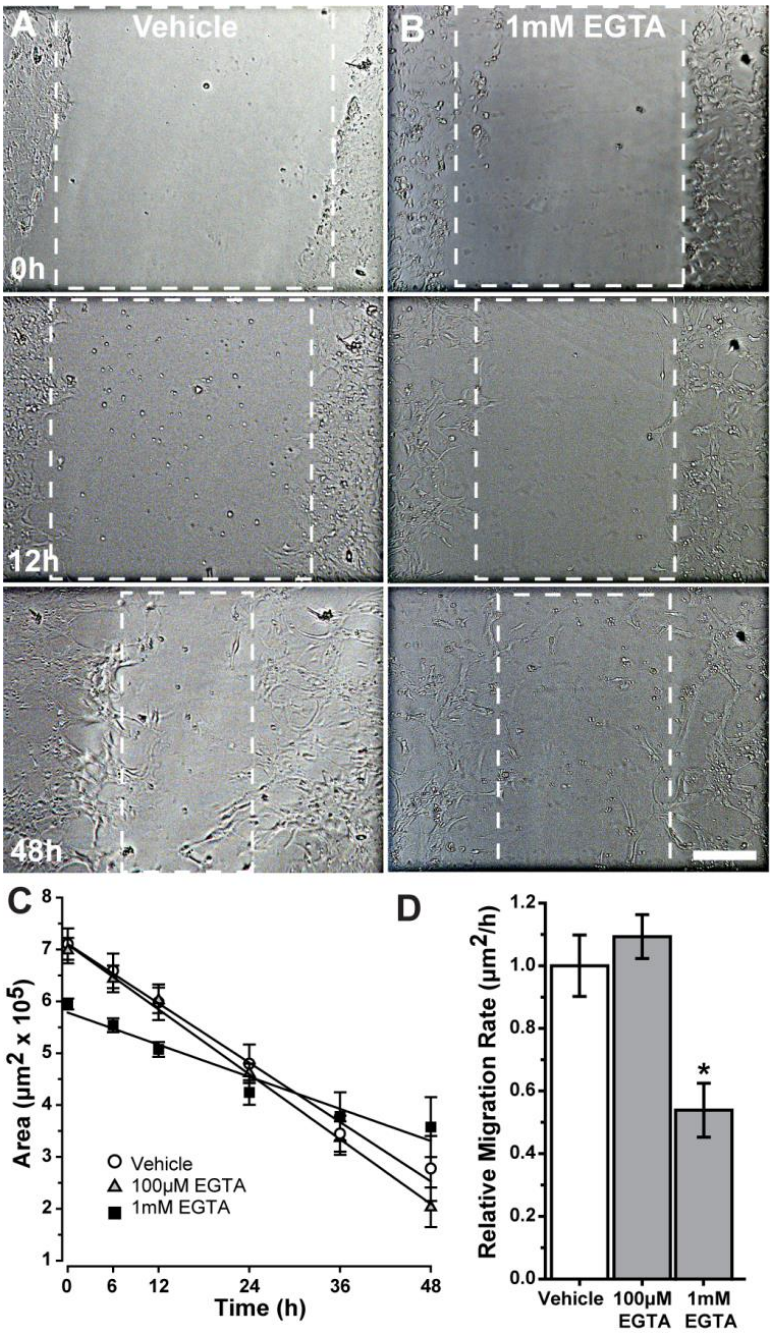

Figure 3.15. Effects of EGTA on astrocyte migration. DIC micrographs show astrocytes treated with **(A)** vehicle and **(B)** 1 mM EGTA at 0, 12 and 48 hours following scratch injury. Dotted boxes indicate the cell-free area. Scale bar: 100 µm. **(C)** Scatter plots with the best-fit linear regression line show the change in area over time for vehicle, 100 µM and 1 mM EGTA-

treated astrocytes. **(D)** Bar graphs show the relative migration rate (or the slope of the best-fit linear regression line) for vehicle and EGTA. *p = 0.048 vs. vehicle.

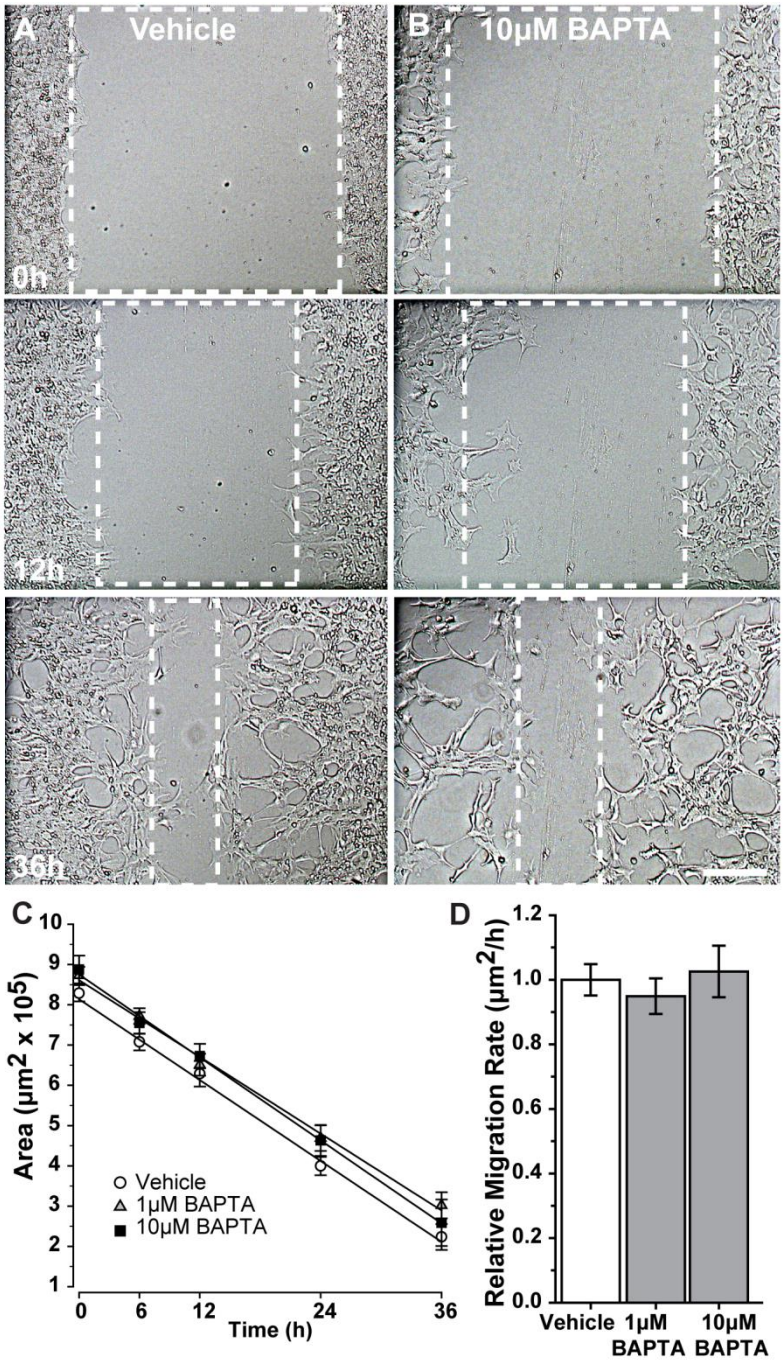

Figure 3.16. Effects of BAPTA-AM on astrocyte migration. DIC micrographs show astrocytes treated with **(A)** vehicle and **(B)** 10 µM BAPTA-AM at 0, 12 and 36 hours following scratch injury. Dotted boxes indicate the cell-free area. Scale bar: 100 µm. **(C)** Scatter plots with the best-fit linear regression line show the change in area over time for astrocytes treated with vehicle, 1 µM and 10 µM BAPTA-AM. **(D)** Bar graphs show the relative migration rate (or the slope of the best-fit linear regression line) for vehicle and BAPTA-AM.

3.4 Discussion

This chapter discusses the contribution of TRPV1 to astrocyte migration using the scratch wound model. Although astrocytes can also proliferate in response to injury, this was reduced with low serum conditions (Figure 3.2). TRPV1 pharmacological agents also affected proliferation compared to vehicle, but only at the highest concentrations tested (Figure 3.7 and 3.11). For migration, TRPV1 agonism with CAP and RTX had modest effects on motility (Figure 3.4 and 3.6) while antagonism of TRPV1 with CPZ and IRTX significantly reduced migration (Figure 3.9 and 3.10). Astrocytes from TRPV1-/- mice, however, showed minimal changes in migration relative to C57 wild-type astrocytes (Figure 3.13). This process is partly dependent on extracellular calcium as chelation of extracellular, but not intracellular, calcium reduced motility (Figure 3.15 and 3.16)

Several groups have shown that TRPV1 contributes to cell migration. In hepatoblastoma cells, Waning et al. showed that although CAP alone did not increase cell migration, it did enhance migration in response to hepatocyte growth factor, an effect that was inhibited by the TRPV1 antagonist CPZ (Waning et al., 2007). Yang et al. showed that TRPV1 mediated migration of corneal epithelial cells after scratch wound injury (Yang et al., 2010b). While CPZ

alone did not affect migration, it did prevent the CAP-induced increase in migration (Yang et al., 2010b). Similarly, in pulmonary arterial smooth muscle cells, TRPV1 activation increased migration, which was blocked by CPZ (Martin et al., 2012). I found that, in our retinal astrocytes, agonism with either CAP or RTX had little effect on migration following injury (Figure 3.4 and 3.6) However, TRPV1 antagonism with CPZ or IRTX slowed migration and reduced wound closure over time (Figure 3.9 and 3.10). Together, these data suggest TRPV1 may be activated by the injury itself, and that further activation by agonists is not possible. This endogenous activation could be mediated by other factors present in the wound milieu. Possible candidates include the endocannabinoids, such as anandamide, which are produced and released by astrocytes and can also influence their migration (Song and Zhong, 2000; Walter et al., 2002).

Although CAP and RTX did not significantly affect migration rate, high concentrations (10μM) modestly reduced motility. This could be a result of TRPV1 desensitization, which can occur following vanilloid-induced activation. There are two types of desensitization: acute, which is a reduced response following a continuous application of drug, or tachyphylaxis, which is a reduced response after repeated applications of drug. Although acute desensitization represents a fast response, both types can share common signaling molecules. Desensitization of TRPV1 depends on calcium, as chelation of extracellular or intracellular calcium can attenuate both types of desensitization (Koplas et al., 1997). Multiple proteins are involved in TRPV1 desensitization including the kinases PKA, PKC, CaMKII, and the phosphatase calcineurin (Bonnington and McNaughton, 2003; Mandadi et al., 2004; Mohapatra and Nau, 2003, 2005). Other proteins involved include ATP, calmodulin and phosphatidylinositol 4,5-bisphosphate (Lau et al., 2012; Liu et al., 2005). Following activation, TRPV1 can also be internalized through a clathrin- and dynamin-independent pathway that leads to degradation of the receptor in

lysosomes (Sanz-Salvador et al., 2012). In addition to internalization, TRPV1 can also undergo a conformational change that affects agonist binding, although the precise structural changes that occur are currently unknown (Vyklicky et al., 2008; Yang et al., 2014). For example, [^{3}H]RTX displays reduced binding to desensitized TRPV1 (Jung et al., 2004). In the scratch wound experiments, 10 µM CAP and 10 µM RTX caused a modest decrease in migration, suggesting that at these higher concentrations, TRPV1 might be desensitized and its activity reduced so that the observed changes in migration were similar to treatment with antagonists.

Consistent with results from *in vitro* studies, *in vivo* models of cellular migration have also implicated TRPV1. For example, intradermal injection of capsaicin increased migration of dendritic cells into the draining lymph nodes, an effect that was abolished in TRPV1-/- mice (Basu and Srivastava, 2005). *In vivo* migration and proliferation of corneal epithelial cells were also reduced in TRPV1-/- mice, thus reducing corneal healing following epithelial debridement (Sumioka et al., 2014). We induced scratch injury in optic nerve astrocytes isolated from TRPV1-/- mice, but observed only modest changes in migration compared to C57 wild-type optic nerve astrocytes (Figure 3.9). This suggests genetic compensation may be occurring. In addition to TRPV1, other TRPV channels have been shown to mediate migration, including TRPV4 and members of the TRPM and TRPC families, all of which are expressed by astrocytes (Beskina et al., 2007; Fiorio Pla and Gkika, 2013; Malarkey et al., 2008; Martin et al., 2012; Shirakawa et al., 2010).

Additionally, although CPZ and IRTX are well-characterized TRPV1 antagonists and have been used to study TRPV1-mediated effects, the antagonists might be binding to other channels or receptors. CPZ for example, can also bind nicotinic acetylcholine receptors, TRPM8 and voltage-gated calcium channels (Docherty et al., 1997; Liu and Simon, 1997; Mustafa and

Oriowo, 2005). In TRPV1-/- mice, [^{3}H]RTX binding is still seen throughout the CNS especially in the spinal cord, dorsal root ganglia and hypothalamus and indicates nonspecific binding in these regions (Roberts et al., 2004). Since IRTX is an analog of RTX, nonspecific binding of IRTX could be present as well.

It is also possible that the difference in astrocyte population used in my assays could contribute to the results. The cells in the pharmacological experiments were isolated from post-natal, rat retina while the TRPV1-/- astrocytes were derived from adult, mouse optic nerves. Although retinal and optic nerve astrocytes both come from the same pool of progenitors and migrate from the brain during development, they are subtypes of astrocyte that express different genes and might have different functions as well (Hochstim et al., 2008; Ling et al., 1989; Ye and Hernandez, 1995). Optic nerve astrocytes have been shown to migrate in response to injury especially in glaucoma, while less is known about retinal astrocytes (Miao et al., 2010; Tezel et al., 2001a). Repeating the pharmacological studies in optic nerve astrocytes isolated from young adult wild-type mice would help us better understand any inherent differences between these two astrocyte populations.

Migration can be modulated by calcium, and in my scratch wound experiments, chelation of extracellular but not intracellular calcium reduces migration (Figure 3.10 and 3.11). One reason for this could be the buffering effect of BAPTA, and the concentrations of BAPTA used might not be sufficient to buffer against the increases in calcium. It is conceivable that a concentration higher than 10 μM might be required to sufficiently chelate the injury-induced increases in calcium, However, the assay used does not allow for much higher concentrations as seen by the cell rounding and detachment observed when 50 μM BAPTA was used (Figure 3.14D). The influx of calcium may also induce changes in membrane potential that might

activate voltage-gated ion channels, including calcium channels to mediate migration (Akerman, 1978; Matsuda et al., 1982). When extracellular calcium is chelated with EGTA, this calcium influx is reduced. Since less calcium is entering the cell, this might reduce migration in a process similar to the addition of TRPV1 antagonists. Additionally, it is possible that TRPV1 may be tethered to or near the plasma membrane by scaffold proteins in order to bring signaling partners in closer proximity to the channel. For example, TRPV1 can bind to AKAP, an A-kinase anchoring protein that facilitates modulation by adenylyl cyclase and PKA, PKC and calcineurin phosphorylation to regulate the channel (Jeske et al., 2008; Jeske et al., 2009b; Zhang et al., 2008). Disruption of this signaling complex can impair sensitization of TRPV1 by inflammatory mediators such as forskolin, prostaglandin E_2 and bradykinin (Efendiev et al., 2013; Schnizler et al., 2008; Zhang et al., 2008). The formation of this complex at the plasma membrane might also bring various signaling proteins closer to the influx of calcium, and allow calcium to activate other proteins before chelation by BAPTA. Chelation of extracellular calcium by EGTA would reduce calcium influx and the subsequent signaling pathways.

Calcium levels and EGTA can also affect other proteins involved in migration. For example, chelation of calcium with 4 mM EGTA translocates E-cadherin from adhesion sites to the cytosol and thereby reducing cell attachment (Nakagawa et al., 2001). In addition to cadherins, calcium also regulates integrin-mediated cell adhesion. For example, increased intracellular calcium increases affinity of $\alpha 4$ integrin for ligands such as vascular cell adhesion molecule-1 (Hyduk et al., 2007). Chelation of calcium with EGTA and Quin-2 on the other hand, inhibits $\beta 1$ integrin activation and reduces adhesion of granulocytes to fibronectin (Rowin et al., 1998). This suggests that chelation of calcium with EGTA might also reduce adhesion of retinal astrocytes to slow cell migration in my experiments.

While addition of the TRPV1 agonist CAP did not have a significant effect on proliferation following scratch injury, application of the highest concentration of RTX (10 μM) significantly reduced proliferation (Figure 3.5). In general, TRPV1 antagonists also reduced astrocyte proliferation, but only 10 μM CPZ was significantly reduced compared to vehicle. This indicates that TRPV1 might be mediating multiple aspects of astrocyte reactivity following injury. Addition of 10 μM CPZ reduced both migration and proliferation, and although IRTX reduced migration, the decrease in proliferation was not significant (Figure 3.9, 3.10 and 3.11). A similar trend occurred for 10 μM RTX – proliferation was reduced but the decrease in migration rate was not significant (Figure 3.6 and 3.7). This suggests a possible correlation between reduced migration and reduced proliferation might exist and warrants further analysis. Although the scratch wound assay is an assay to determine changes in migration, proliferation can be tested further with other assays. One such assay utilizes bromodeoxyuridine (BrdU), an analog of thymidine to label dividing cells. Labeled BrdU is incorporated into the DNA of dividing cells in place of thymidine, and assessing the extent of BrdU labeling shows the amount of proliferation. Since BrdU labeling requires active DNA synthesis, it is commonly used to measure proliferation in living cells or tissue (Rothaeusler and Baumgarth, 2007). On the other hand, Ki-67 labels an antigen that is found only in dividing cells undergoing mitosis (Scholzen and Gerdes, 2000). Therefore, Ki-67 labeling does not require active DNA synthesis, and cells can be fixed, permeabilized and then labeled for Ki-67.

TRPV1 has been shown to modulate proliferation in other studies. Proliferation of corneal epithelial cells is reduced in TRPV1-/- mice compared to wild-type following epithelial debridement (Sumioka et al., 2014). In the spared nerve injury model of neuropathic pain, microglia increase proliferation following injury. Although the TRPV1 agonist RTX did not

significantly affect migration following injury compared to vehicle, RTX did increase microglial proliferation under basal, uninjured conditions (Suter et al., 2009). In MCF-7 breast cancer cells, TRPV1 overexpression does not affect proliferation compared to wild-type (Wu et al., 2014). However, increasing concentrations of CAP increases proliferation in the LNCaP prostate cancer cell line, but reduces proliferation in the PC-3 prostate cancer line (Malagarie-Cazenave et al., 2009; Sanchez et al., 2006).

The effects of TRPV1 on proliferation could be mediated through an influx of calcium as calcium has been linked to cell division and cell cycle regulation. Calcium channel inhibitors like mibefradil, amlodipine, diltiazem and verapamil can reduce proliferation (Panner and Wurster, 2006; Taylor and Simpson, 1992). Also, knockdown of TRPC1 and TRPC6 can block entry into the G1 and G2/M phase of the cell cycle respectively in other cell systems (Cai et al., 2009; Kuang et al., 2012). Calcium channels can interact with cell cycle proteins as well. For example, cyclin-dependent kinase 1/cyclin B directly interacts with and phosphorylates IP3 receptors in the endoplasmic reticulum (Malathi et al., 2005). In addition, chelation of calcium with EGTA or addition of calcineurin inhibitors decreases fibroblast growth factor-induced expression of cyclin A and E (Tomono et al., 1998).

Increased migration as well as proliferation is a stress response of reactive astrocytes, and is found in multiple types of injury and diseases including glial scar formation, metastasis of gliomas, glaucoma and age-related macular degeneration (Demuth and Berens, 2004; Ramirez et al., 2001; Tezel et al., 2001a; Yuan and He, 2013). Reactive astrocytes can be both beneficial and detrimental to neuronal survival. They can secrete neurotrophic factors to aid neuronal survival and repair the blood-brain barrier but they can also release cytokines and impede axon regeneration. A better understanding of the mechanisms and signaling pathways that underlie

astrocyte migration can potentially lead to novel therapeutic interventions to target scar formation and gliosis in neurodegenerative diseases. It might allow us to temper the detrimental effects associated with gliosis, while retaining the benefits and promoting CNS re

CHAPTER IV

THE CONTRIBUTION OF THE TRPV1 CHANNEL TO INJURY-INDUCED CALCIUM INFLUX*

4.1 Introduction

Calcium is an important regulator of many cellular functions in both neuronal and non-neuronal cell types. For example, calcium can mediate muscle contraction, neurotransmitter and gliotransmitter release, and cell-cell communication in astrocytes (Berchtold et al., 2000; Catterall and Few, 2008; Newman, 2001; Volterra et al., 2014). Calcium activates signaling molecules like PKA, PKC, calmodulin, CaMKII, and calcineurin to trigger downstream cascades and changes in cellular function (Crabtree, 2001; Dunn et al., 2009; Griffith, 2004; Luo and Weinstein, 1993). Additionally, calcium regulates cytoskeletal dynamics that can drive cell migration and intermediate filament expression (Rodnight et al., 1997; Wei et al., 2012). In astrocytes, calcium mediates the release of gliotransmitters to modulate synaptic transmission (Volterra et al., 2014). Elevations in calcium also mediate intercellular communication in astrocytes through the propagation of calcium waves (Newman, 2001). While calcium is an important signaling component that regulates many aspects of astrocyte function under physiological conditions, it also plays a role in reactive gliosis following injury. For example, the injury milieu can contain factors such as glutamate, ATP, endothelin and cytokines that increase intracellular calcium (Cornell-Bell et al., 1990; Goldman et al., 1991; Guthrie et al., 1999;

* Portions of this chapter have been published previously in Ho KW, Lambert WS and Calkins DJ. Activation of the TRPV1 cation channel contributes to stress-induced astrocyte migration (2014) Glia 62(9):1435-51.

Holliday and Gruol, 1993; Koller et al., 1996). Mechanical injury or stretch can also increase astrocyte intracellular calcium levels (Charles et al., 1991; Rzigalinski et al., 1998).

Astrocytes, like most cells, express a variety of receptors and channels that regulate calcium homeostasis and contribute to calcium increases following injury. These include G-protein coupled receptors, such as metabotropic glutamate receptors, as well as voltage-gated calcium channels (Bradley and Challiss, 2012; Latour et al., 2003). Ligand-gated channels like the purinergic P2X receptors can also regulate calcium levels (Fumagalli et al., 2003). In addition to these receptors, astrocytes also express multiple calcium transporters including the plasma membrane Ca^{2+}-ATPase and Na^{+}/Ca^{2+} exchanger (Fresu et al., 1999; Goldman et al., 1994). Increases in cytoplasmic calcium can also occur through release from intracellular stores within the endoplasmic reticulum. The IP3 receptor type 2 is the main channel that regulates intracellular calcium stores in astrocytes (Petravicz et al., 2008). In addition to IP3 receptors, ryanodine receptors can also be found in the endoplasmic reticulum (Matyash et al., 2002; Turner et al., 2003). Intracellular stores that become depleted can be replenished by store-operated channels in the plasma membrane, such as ligand gated TRPC channels (Golovina, 2005; Huang et al., 2006; Malarkey et al., 2008; Smyth et al., 2010; Yuan et al., 2007; Zeng et al., 2008). Multiple isoforms of the TRPC family have been found in astrocytes (Beskina et al., 2007; Grimaldi et al., 2003; Malarkey et al., 2008; Miyano et al., 2010; Shigetomi et al., 2012).

Another member of the TRP family expressed by astrocytes is TRPV1 (Chapter 2; Doly et al., 2004; Huang et al., 2010; Leonelli et al., 2010; Mannari et al., 2013). TRPV1 activation increases intracellular calcium in a variety of cell types, including endothelial cells, corneal epithelial cells, bronchial epithelial cells, glioma cells and dorsal root ganglion neurons (Amantini et al., 2007; Chard et al., 1995; Himi et al., 2012; Reilly et al., 2005; Zhang et al.,

2007). In these cells, TRPV1 modulates cell adhesion, migration, cytokine release and apoptosis. In neurons, TRPV1 can mediate the release of glutamate and substance P (Ferrini et al., 2007; Medvedeva et al., 2008). Endogenous TRPV1 ligands include protons, endocannabinoids and arachidonate metabolites (Edwards et al., 2012; Rousseau et al., 2005; Ryu et al., 2007); however, TRPV1 can also be activated in response to injury. For instance, in retinal ganglion cells and microglia TRPV1 is activated in response to elevated hydrostatic pressure and can increase intracellular calcium (Sappington and Calkins, 2008; Sappington et al., 2009). Elevated hydrostatic pressure can also increase calcium in cultured optic nerve head astrocytes, an effect that was attenuated with ruthenium red, a non-specific TRP channel inhibitor (Mandal et al., 2010). In Chapter 3, I showed that astrocytes migrate in response to injury, and that this effect is to some extent, mediated by TRPV1 and is dependent on extracellular calcium. As a next step, this chapter will examine calcium dynamics following TRPV1 activation in primary cultured astrocytes under physiological conditions and following scratch wound injury. Because TRPV1 antagonism reduced injury-induced astrocyte migration, I will also examine the effect of TRPV1 antagonists on calcium influx following injury.

4.2 Methods

Calcium imaging

Primary retinal and optic nerve astrocytes were isolated and prepared as previously described in Chapter 2. Once confluent, astrocytes were plated onto 8-well cover glass chambers (ThermoScientific, Rochester, NY) coated with 0.01 mg/mL poly-D-lysine. Intracellular calcium was monitored with the fluorescent indicator, fura-2 AM (Molecular Probes, Eugene, OR). Upon binding calcium, fura-2 increases fluorescence at 340 nm and decreases fluorescence at

380 nm. Therefore, a smaller 340/380 ratio indicates low calcium levels while a larger 340/380 ratio shows high calcium levels (Levkovitch-Verbin, 2004). Astrocyte cultures were loaded with 5 μM fura-2 AM for 30 minutes at 37˚C, rinsed and incubated in DMEM/F12 minus phenol-red with the appropriate pharmacological reagents. Cultures were then placed onto a Nikon Eclipse Ti inverted microscope for imaging. The cells were excited at the 340 and 380 nm wavelengths, and emission was collected at 510 nm at 3 second intervals with a Roper Scientific black and white camera (Photometrics, Tucson, AZ). A baseline recording of approximately 30 seconds was taken. To test for pharmacological effects, 100 μL of media was replaced with an equivalent volume containing the appropriate reagents to achieve the concentrations indicated. For scratch wound experiments, a 10 μL pipet tip was used to make a scratch through the astrocyte monolayer. Each experiment had at least 4 replicates, and at least 8 C57 and TRPV1-/- mice were used.

Quantification of calcium imaging

Image analysis was done with NIS Elements software (Nikon, Melville, NY). Regions of interest were drawn at 50, 100, 200 and 400 μm from the edge of the scratch injury (≥ 6 regions per distance), and the 340/380 fluorescence ratio was determined over time for each region (Figure 4.1). Ratios acquired during the scratch and 5 seconds prior to and after injury were excluded due to artifacts in the extracellular environment. Basal calcium levels were determined by averaging the ratios taken prior to scratch injury for each replicate. Time-to-peak measurements were calculated based on the time after injury required to reach maximum ratios for each treatment.

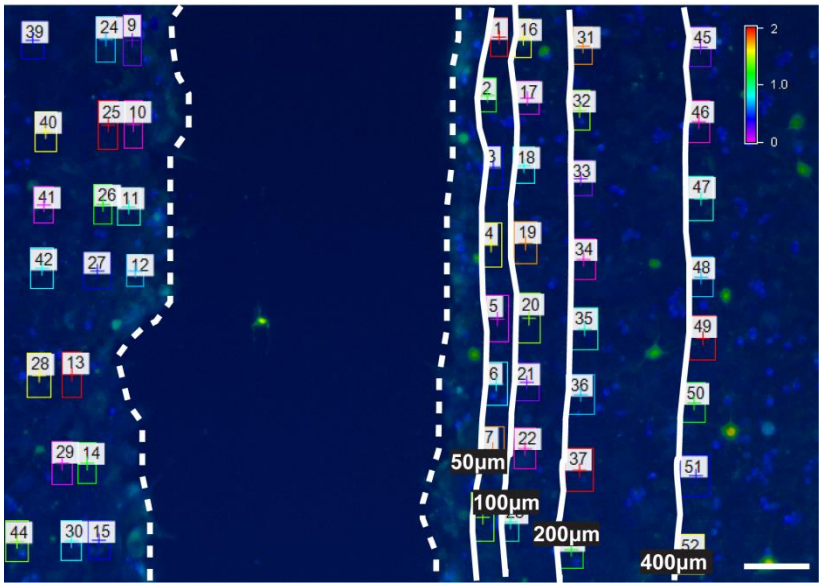

Figure 4.1. Calcium imaging quantification and analysis. Astrocytes were loaded with fura-2 AM, and then scratched. Regions of interest were drawn at 50, 100, 200 and 400 µm (solid lines) from the wound edge (dotted line). The scale shows 340/380 nm ratio from low (violet-blue) to high (orange-red) calcium levels. Scale: 100 µm.

Statistical analysis

Data for calcium levels is presented as mean ± SEM for each treatment. Statistical analysis and p-values for comparing calcium levels were obtained using ANOVA or t-tests for data meeting criteria for normalcy or using non-parametric rank statistics for data failing normalcy using SigmaPlot 11.0 for Windows (Systat Software Inc., Chicago, IL) or GraphPad Prism (GraphPad Software, Inc., La Jolla, CA).

4.3 Results

Effects of TRPV1 agonists on physiological calcium levels in astrocytes

Since TRPV1 is a calcium-selective ion channel, I first tested if activation of TRPV1 with CAP and RTX changed calcium levels in astrocytes under physiological conditions. Fluorescent micrographs of astrocytes loaded with fura-2 are shown in Figure 4.2. Fura-2 ratios appeared similar between the four basal conditions. Addition of 1 μM CAP or 100 nM and 1 μM RTX (Figure 4.2) did not appear to change calcium levels compared to vehicle at 10 and 60 seconds following drug application as fura-2 ratios remained similar between the four treatments. The change in calcium over time following treatment is quantified in Figure 4.3. Following the addition of CAP to the astrocyte culture, there was a drop in the 340/380 ratio that appeared to indicate calcium reduction. However, the change in ratio following application was similar for both vehicle and 1 μM CAP, indicating that any changes measured in the fura-2 ratio were due to drug application artifacts rather than changes in calcium (Figure 4.3A). Likewise, the change in calcium ratio was similar for vehicle and 1 μM RTX (Figure 4.3B), indicating this concentration of TRPV1 agonist had no impact under physiological conditions. However, addition of 100 nM RTX induced a slight increase in calcium over time. By 145-170 seconds following application, the average change in calcium levels for 100 nM RTX was 85.99 ± 4.40% greater than vehicle ($p = 0.04$; Figure 4.3B).

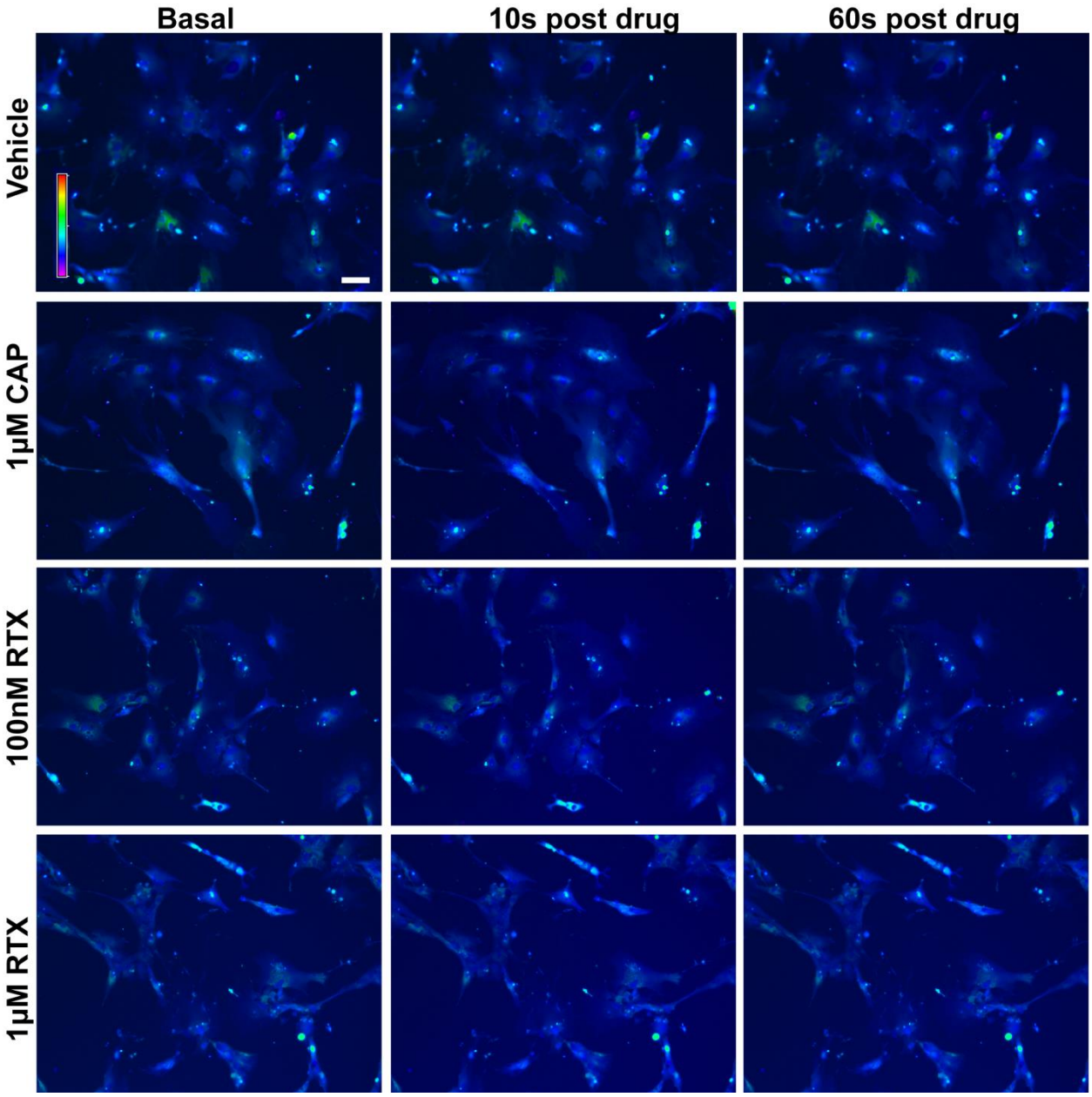

Figure 4.2. Effects of CAP and RTX on basal astrocyte calcium levels. Astrocytes were loaded with fura-2, and the scale shows 340/380 nm ratio from low (violet-blue) to high (orange-red) calcium levels. Fluorescent micrographs were captured under resting condition and at 10 and 60 seconds following addition of vehicle, 1 μM CAP or 100 nM and 1 μM RTX. Scale: 100 μm.

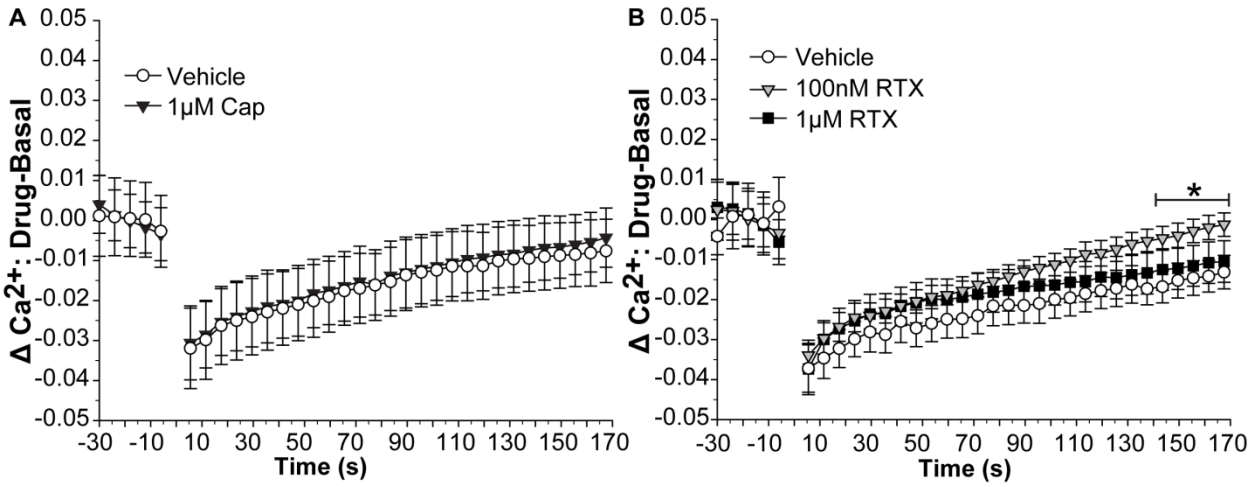

Figure 4.3. Quantification of CAP and RTX on physiological calcium levels. TRPV1 activation has modest effects on calcium levels under physiological conditions in astrocyte cultures. Calcium levels expressed as the 340/380 ratio are shown before and after addition of drug (time = 0 seconds) for cells treated with 1 μM CAP (A) or 100 nM and 1 μM RTX (**B**). * p = 0.04.

Antagonism of TRPV1 reduces and slows calcium influx following injury

Although TRPV1 activation did not affect calcium levels under basal conditions, TRPV1 may act as a stress response protein and increase intracellular calcium levels following injury. Since TRPV1 inhibition reduces astrocyte migration, I next wanted to determine if TRPV1 modulates astrocyte calcium influx following scratch injury. Figure 4.4 shows examples of astrocyte cultures loaded with fura-2 before and after scratch. At 10 seconds following scratch wound, intracellular calcium increased throughout the culture, but especially near the leading edge (Figure 4.4B). Pre-treatment with the TRPV1-specific antagonists CPZ (10 μM; Figure 4.4C) and IRTX (3 μM; Figure 4.4D) appeared to reduce this increase.

I quantified the 340/380 nm calcium ratio over time at discrete distances from the scratch-wound edge (50, 100, 200 and 400 μm), both with and without the TRPV1 antagonists

(Figure 4.5). Detailed quantification of the data shows that neither 10 μM CPZ nor 3 μM IRTX significantly influenced pre-scratch basal levels of calcium compared to vehicle (Figure 4.5 and 4.6A). Both TRPV1 antagonists did, however, slow the time to peak calcium levels following scratch wound (Figure 4.5 and 4.6B). Compared to vehicle-treated astrocytes, 3 μM IRTX slowed the time to peak by over three-fold at 50, 100 and 200 μm from the scratch wound ($p \leq 0.007$). Treatment with 10 μM CPZ also slowed the time to peak more than two-fold at 100 μm from the wound ($p = 0.025$). The same trend of slower time to peak by CPZ was also seen at 50 μm and 200 μm, but this was not significant ($p \geq 0.063$). At 400 μm from the scratch, the times to peak for the antagonists did not differ significantly from vehicle.

In addition to slowing the time to peak, treatment with 3 μM IRTX also reduced the overall magnitude of calcium influx following scratch compared to vehicle at all four distances from the wound that were quantified (Figure 4.6C). In the time interval 5-30 seconds following scratch, IRTX reduced the change in calcium ratio by 55-80% at all distances from the injury site ($p \leq 0.04$). The decrease in calcium influx following injury with IRTX was also observed at subsequent intervals (40-70 seconds and 75-105 seconds) following injury, although the reductions were not significant ($p \geq 0.062$; Figure 4.6C). Treatment with CPZ, while generally slowing the time to peak (Figure 4.6B), had little effect on the magnitude of the change in calcium following scratch ($p \geq 0.39$; Figure 4.6C).

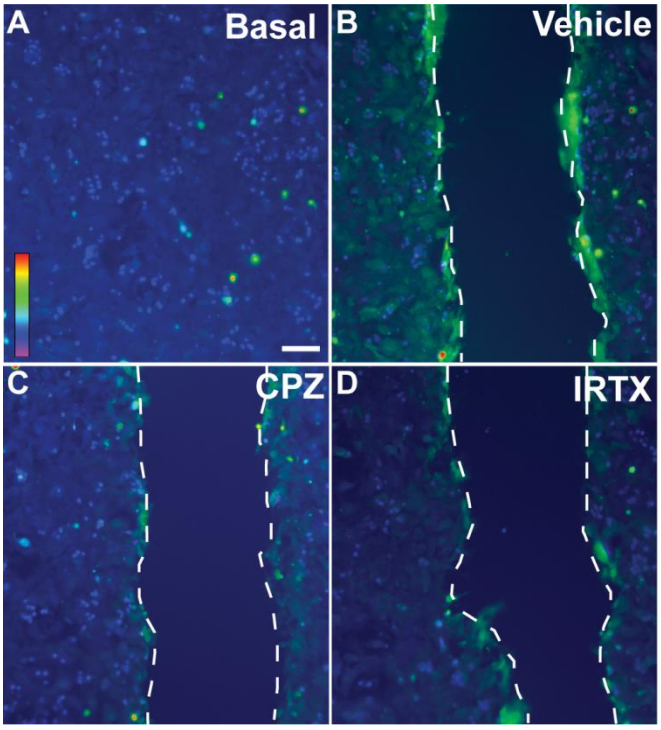

Figure 4.4. Injury-induced calcium changes with addition of TRPV1 antagonists. Scratch injury increases intracellular calcium in astrocytes. Fluorescent image of astrocytes loaded with the calcium indicator, fura-2 AM shows modest basal intracellular levels. The scale shows 340/380 nm ratio from low (violet-blue) to high (orange-red) basal calcium levels (**A**). Immediately following scratch wound (10 seconds), vehicle astrocytes (**B**) demonstrate increased intracellular calcium especially near the leading edge (dotted line); 10 μM CPZ (**C**) and 3 μM IRTX (**D**) appear to reduce this increase. Scale: 100 μm.

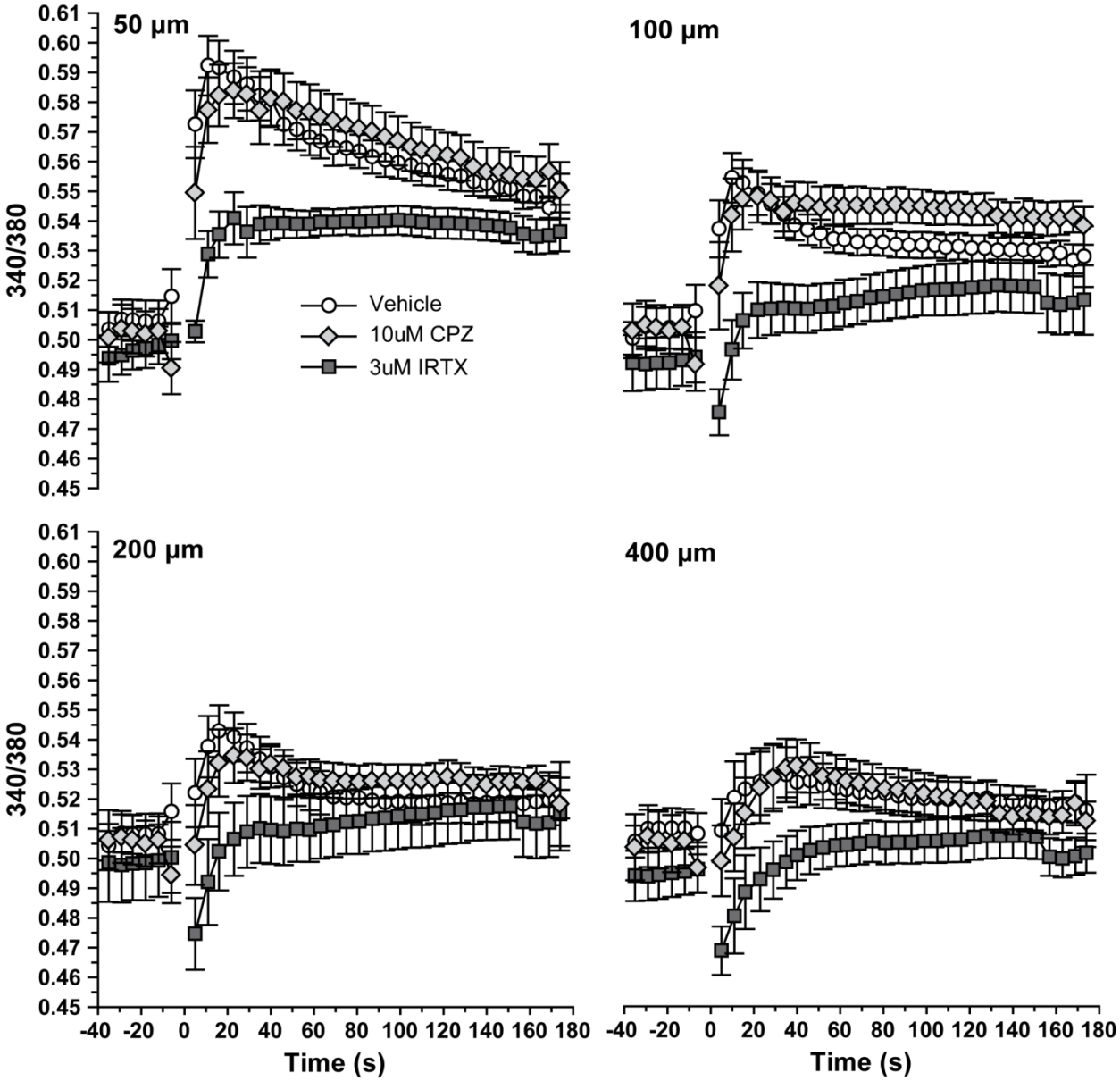

Figure 4.5. Real time calcium changes following injury and with TRPV1 antagonism. Levels of astrocyte intracellular calcium are expressed as the 340/380 nm fluorescence ratio before and following scratch injury (time = 0 seconds) for cells treated with vehicle, 10 µM CPZ and 3 µM IRTX. Measurements were taken at 50, 100, 200 and 400 µm from the scratch leading edge.

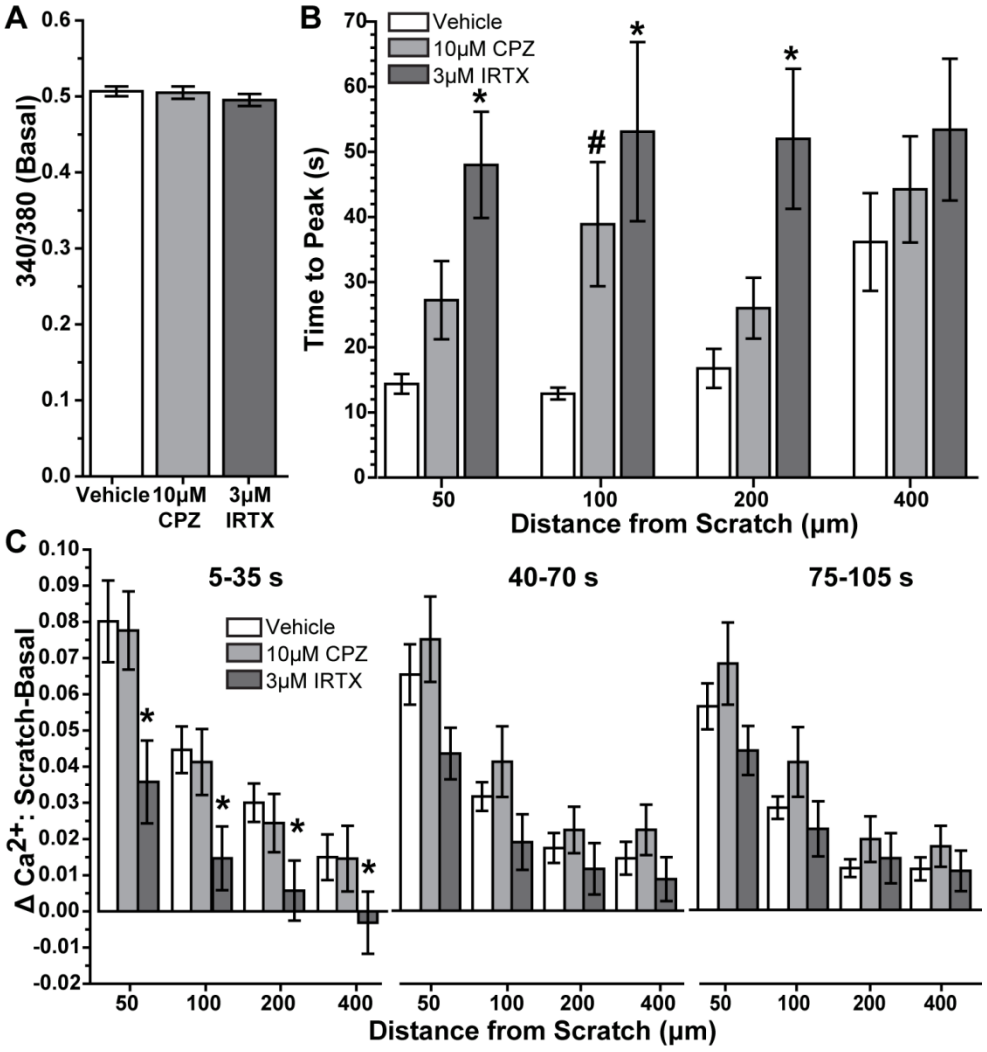

Figure 4.6. Quantification of calcium dynamics with TRPV1 antagonism. Fura-2 AM 340/380 ratio prior to scratch wound shows astrocytes treated with vehicle, 10 μM CPZ and 3 μM IRTX have similar basal levels of intracellular calcium **(A)**. Bar charts show time to reach peak 340/380 calcium ratio following scratch injury for each treatment at 50, 100, 200 and 400 μm from the leading edge of the wound **(B)**. Significance compared to vehicle: *, $p \leq 0.007$ for IRTX; #, $p = 0.025$ for CPZ. Data show the average difference between scratch and basal 340/380 calcium ratio determined for time intervals 5-35, 40-70, and 75-105 seconds post-

scratch at each distance from the injury **(C)**. Significance compared to vehicle: *, $p \leq 0.04$. All data: mean ± SEM.

Effects of TRPV1knockout on intracellular calcium influx with injury

Scratch injury induced a rise in intracellular calcium that was reduced with TRPV1 antagonism. Next, I wanted to determine if TRPV1-/- astrocytes exhibit a change in calcium with scratch injury. Optic nerve astrocytes from TRPV1-/- and C57 mice were loaded with fura-2. Genotype did not appear to affect basal levels of calcium (Figure 4.7A and B). Scratch injury induced an increase in calcium that was highest at the leading edge and dissipated with increasing distance for both C57 and TRPV1-/- astrocytes (Figure 4.7C and D).

Detailed analysis of calcium imaging shows that C57 and TRPV1-/- astrocytes had similar basal levels of calcium (Figure 4.8 and 4.9A). The time to reach peak calcium increased for both C57 and TRPV1-/- as distance from the scratch injury increased (Figure 4.8 and 4.9B). Although there was a trend towards a shorter time to peak for TRPV1-/- astrocytes compared to C57, this was not significant ($p \geq 0.210$). The change in calcium following scratch injury was also similar between C57 and TRPV1-/- astrocytes at the distances and time intervals tested (Figure 4.8 and 4.9C).

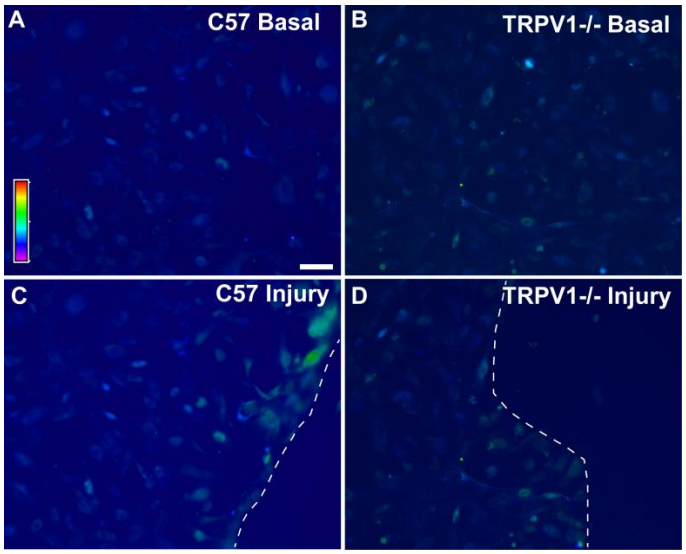

Figure 4.7. Calcium changes in C57 and TRPV1-/- astrocytes following injury. Fluorescent micrographs show basal levels of calcium for astrocytes from C57 (**A**) and TRPV1-/- optic nerves (**B**). The scale shows 340/380 nm ratio from low (violet-blue) to high (orange-red) calcium levels. Scratch injury induced an increase in calcium at the leading edge (dotted line) for both C57 (**C**) and TRPV1-/- (**D**) astrocytes. Scale 100 µm.

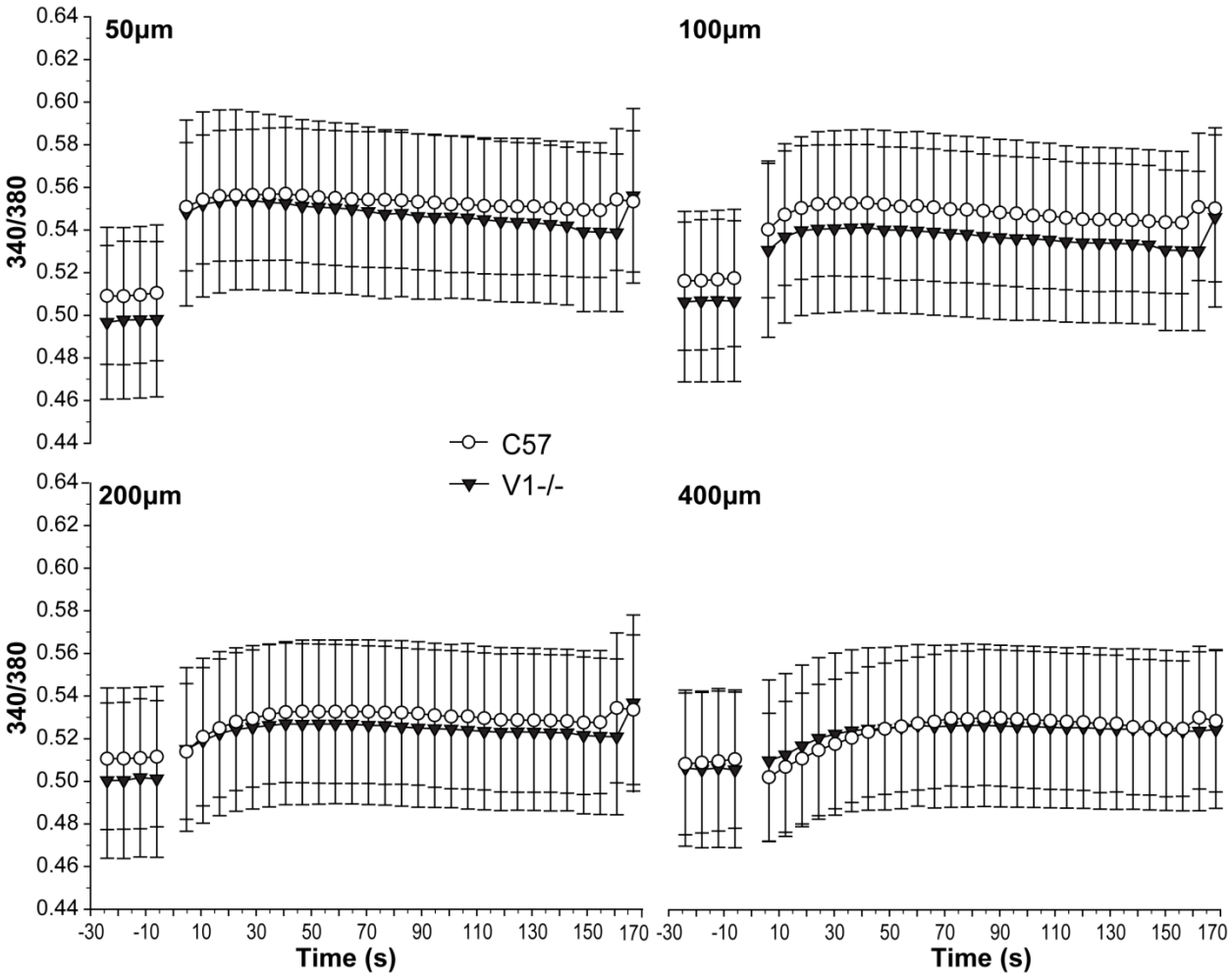

Figure 4.8. Real time calcium dynamics in TRPV1-/- astrocytes following injury. Calcium levels expressed as the 340/380 ratio are shown before and after scratch injury (time = 0 seconds) for C57 and TRPV1-/- astrocytes. Measurements were taken at 50, 100, 200 and 400 µm from the injury site.

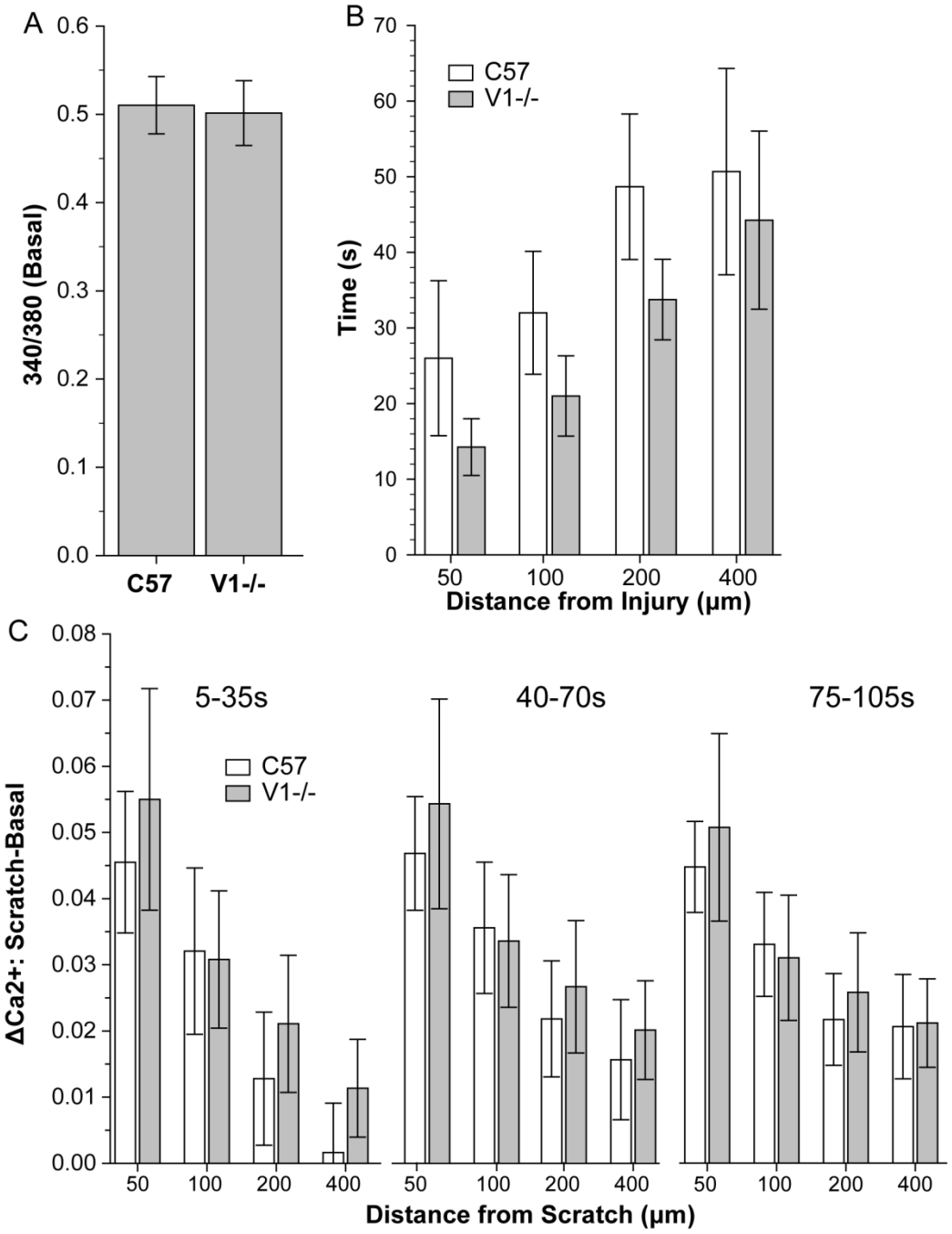

Figure 4.9. Quantification of calcium changes in TRPV1-/- astrocytes following injury. C57 and TRPV1-/- astrocytes have similar basal levels of intracellular calcium **(A)**. Bar charts show time to reach peak 340/380 calcium ratio following scratch injury for both C57 and TRPV1-/- optic nerve astrocytes at 50, 100, 200 and 400 μm from the leading edge of the wound **(B)**. Data

show the average difference between scratch and basal 340/380 calcium ratio determined for time intervals 5-35, 40-70, and 75-105 seconds post-scratch at each distance from the injury for both genotypes **(C)**. All data: mean ± SEM.

Microtubule stabilization has modest effects on intracellular calcium influx with injury

Scratch injury in astrocytes induces an increased intracellular calcium influx and cell migration, both of which were reduced with addition of TRPV1 antagonists (Figure 4.6, 3.6 and 3.7). One link between calcium and migration is changes in cytoskeletal dynamics, and TRPV channels are known to interact with the cytoskeleton. Goswami et al. showed that TRPV4 can bind microtubules and stabilize them, and that taxol treatment to stabilize microtubules reduced calcium influx via TRPV4 (Goswami et al., 2010). Stabilization of microtubules with taxol also reduces the amplitude of calcium transients and calcium release from the sarcoplasmic reticulum, while disruption of microtubules can increase the amplitude of calcium transients and its decay in myocytes (Howarth et al., 1999; Kerfant et al., 2001). Additionally, TRPV1 activation results in the disassembly of dynamic microtubules, thus contributing to cytoskeletal remodeling (Goswami et al., 2006). Given the link between TRPV channels, calcium and the cytoskeleton, I next determined whether addition of taxol to stabilize astrocyte microtubules affected calcium influx following injury. Initially, I based taxol concentrations on a published report that treated cultured primary astrocytes with 5 μM taxol (Cvetkovic et al., 2004). However, pilot studies using 5 and 50 μM taxol in the scratch wound assay showed that these concentrations induced cell detachment (data not shown). Therefore, a concentration of 500 nM taxol was used in the calcium imaging analysis.

Similar to previous experiments, astrocytes were loaded with fura-2 to measure calcium levels. Astrocytes treated with either vehicle or 500 nM taxol appeared to exhibit similar basal calcium levels (Figure 4.10A and B). Scratch wound injury induced an increase in calcium that was highest at the wound edge for both vehicle and 500 nM taxol (Figure 4.10C and D). Detailed quantification showed that basal levels of calcium were similar in vehicle and 500 nM taxol treated cells (Figure 4.11 and 4.12A). The time to peak for 500 nM taxol was also not significantly different from vehicle ($p \geq 0.181$; Figure 4.11 and 4.12B). Similar to the previous experiments, the change in calcium following injury was highest at 50 μm from the wound edge and diminished with increasing distance (Figure 4.11 and 4.12C). The injury-induced increase in calcium was sustained. The calcium changes at 5-35, 40-70 and 75-105 seconds following injury were similar. Although treatment with 500 nM taxol appears to reduce calcium influx compared to vehicle at 50 and 100 μm from the injury site at the time intervals tested, this decrease was not significant ($p > 0.07$; Figure 4.12C). As distance from the wound edge increased to 200 and 400 μm, the changes in calcium were also similar between vehicle and 500 nM taxol (Figure 4.12C).

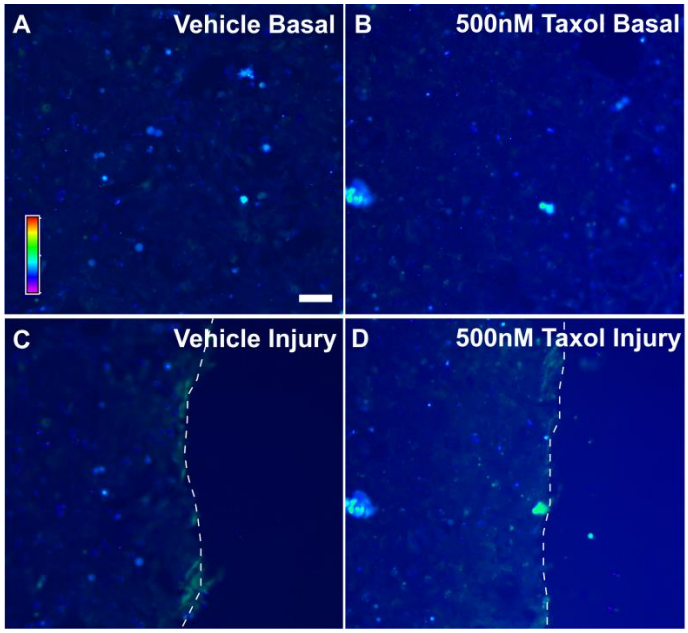

Figure 4.10. Effects of taxol on astrocyte calcium influx after injury. Fluorescent micrographs show basal levels of calcium for astrocytes from vehicle (**A**) and 500 nM taxol (**B**) treatments. The scale shows 340/380 nm ratio from low (violet-blue) to high (orange-red) calcium levels (**A**). Scratch injury induced an increase in calcium at the leading edge (dotted line) for both vehicle (**C**) and 500 nM taxol (**D**). Scale 100 µm.

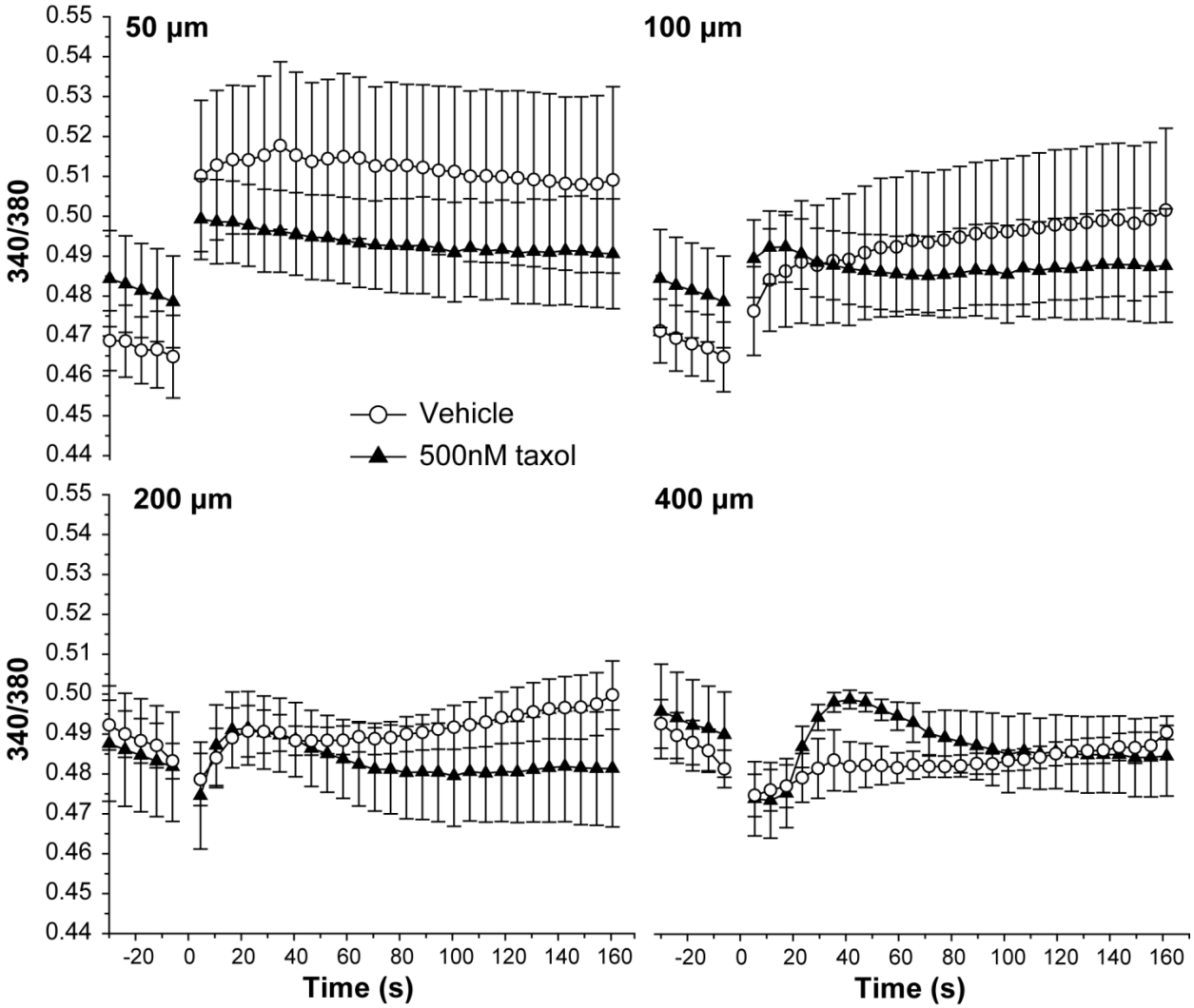

Figure 4.11. Real time calcium changes after injury and with taxol treatment. Calcium levels expressed as the 340/380 ratio are shown before and after scratch injury (time = 0 seconds) for astrocytes treated with vehicle and 500 nM taxol. Measurements were taken at 50, 100, 200 and 400 µm from the injury site.

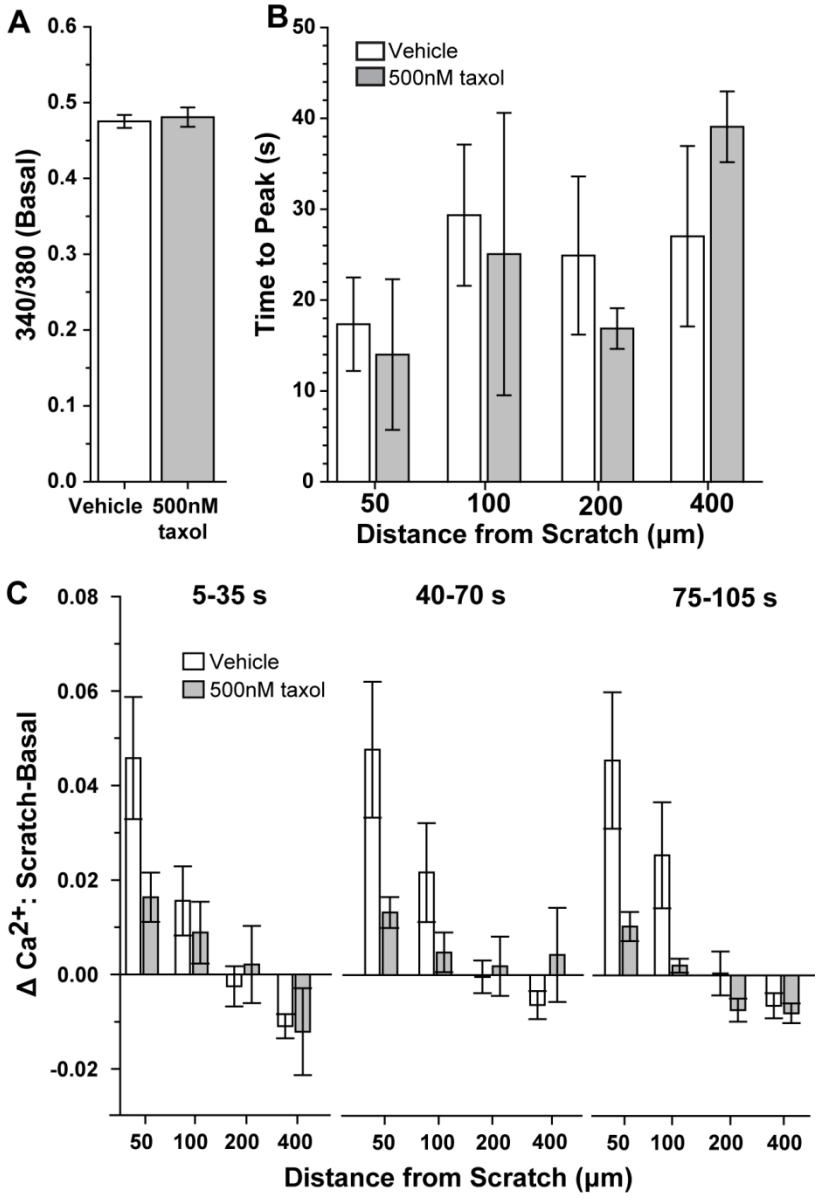

Figure 4.12. Quantification of calcium dynamics with addition of taxol. Vehicle and 500 nM taxol treatments have similar basal levels of intracellular calcium (**A**). Bar charts show time to reach peak 340/380 calcium ratio following scratch injury for both vehicle and 500 nM taxol at 50, 100, 200 and 400 μm from the leading edge of the wound (**B**). Data show the average difference between scratch and basal 340/380 calcium ratio determined for time intervals 5-35, 40-70, and 75-105 seconds post-scratch at each distance from the injury for both treatments (**C**). All data: mean ± SEM.

4.4 Discussion

In a previous chapter, I demonstrated that TRPV1 modulation influenced astrocyte migration following injury. As TRPV1 can flux calcium, and calcium is an important mediator of cell migration, this chapter examined the calcium dynamics in astrocytes with TRPV1 modulation and following injury. TRPV1 is regarded as a calcium-preferring channel where activation contributes to an increase in intracellular calcium. However, I found that addition of TRPV1 agonists CAP or RTX had only a modest effect on intracellular calcium compared to vehicle (Figure 4.2 and 4.3). This was unexpected as activation of other members of the TRP family, including TRPA and TRPC, can increase intracellular calcium in astrocytes (Malarkey et al., 2008; Shigetomi et al., 2012). Moreover, CAP and RTX have been shown to increase calcium in other cells types including retinal ganglion cells, microglia, dorsal root ganglion neurons, endothelial cells and dopaminergic neurons (Kim et al., 2005; Marshall et al., 2003; Sappington and Calkins, 2008; Sappington et al., 2009; Yang et al., 2010a). Interestingly, in cortical astrocytes TRPV1 activation by low pH can induce a change in current that is mediated by sodium influx rather than calcium (Huang et al., 2010). While TRPV1 exhibits a 10-fold higher selectivity for calcium versus sodium (Caterina and Julius, 2001), it is possible that activation of TRPV1 in retinal astrocytes by CAP or RTX under physiological conditions might induce an influx of sodium, rather than of calcium. This is a hypothesis that certainly warrants future examination.

I found that in retinal astrocytes, scratch injury increases intracellular calcium (Figures 4.4-4.6). The antagonist CPZ had only modest effects on scratch-induced calcium elevations, which was significantly reduced with IRTX. This could be due to a species-dependent difference in efficacy that has been observed for CPZ, as this antagonist only weakly inhibits

calcium currents in rat TRPV1 compared to human TRPV1 (McIntyre et al., 2001; Phillips et al., 2004). IRTX, however, does not have this selectivity and has far greater efficacy (Correll et al., 2004). Similar differences in calcium responses have been shown for TRPV1 agonists as well, emphasizing the complexity of TRPV subunit pharmacology. For example, Toth et al. found that there were qualitative differences in calcium influx when cells are treated with various TRPV1 agonists (Toth et al., 2005). In response to CAP, cells exhibited an immediate increase in calcium, but with RTX, there was minimal initial increase but a sharp subsequent increase, suggesting a latency in cellular responses to RTX. Furthermore, higher concentrations of CAP increased the maximal amount of calcium influx, an effect not seen with RTX treatment. Rather, the number of cells that responded increased with higher RTX concentrations. A similar difference in calcium response to CAP and RTX has also been observed in dorsal root ganglion neurons. Addition of RTX produced a prolonged increase in calcium compared to the sharp transient increase from CAP, even when the RTX concentration was 1000-fold less (Karai et al., 2004). As CPZ and IRTX are analogs of CAP and RTX, respectively, it is possible the qualitative differences in calcium influx seen with the agonists might be extrapolated to the antagonists (Wahl et al., 2001; Weber et al., 2008).

In the scratch wound experiments in Chapter 3, there was a greater reduction in migration with CPZ than IRTX. The opposite was seen in the calcium imaging experiments in this chapter – IRTX induced a greater decrease in calcium compared to CPZ. The complexity of the injury milieu and the different mechanisms of the antagonists might contribute to the effects seen in the migration and calcium experiments. In addition to activation by CAP and RTX, TRPV1 can also be activated by a variety of other effectors, including pH, heat and endocannabinoids, which can be blocked by both CPZ and IRTX in various systems (Korolainen et al., 2005; Sarthy et al.,

1998; Seabrook et al., 2002; Tura et al., 2009). This suggests the presence of multiple binding sites for the antagonists in addition to the vanilloid binding sites. The ability of antagonists to inhibit these stimuli can also vary. For example, CPZ can block pH activation in guinea pigs but not in rats (McIntyre et al., 2001; Sun et al., 2013).

The environment of TRPV1 can also influence its activation and regulation. For example, TRPV1 contains multiple phosphorylation sites for PKA, PKC and protein phosphatase 2B that sensitize and desensitize the channel (Shibasaki et al., 2013). Addition of cyclosporin A, an inhibitor for protein phosphatase 2B, increases the potency of TRPV1 agonists 1.1-fold for RTX to as much as 7.8-fold for DA-5018. The potency for capsaicin increased 2.1-fold. Similar to the agonists, cyclosporin A increased antagonist potencies from 1.1-fold to 2.5-fold (Bai and Lipski, 2010). This suggests that the signaling environment and phosphorylation state of TRPV1 have profound effects on the channel's sensitivity to ligands. In the injury milieu, cross-talk between a variety of effectors, receptors, and signaling pathways could modulate the structure and state of TRPV1, potentially affecting the efficacy of TRPV1 pharmacological agents. Together, these differences could explain why CPZ had the greater inhibitory effect on migration, while IRTX had the more robust effect on intracellular calcium levels. To further investigate this incongruity, I examined calcium changes in optic nerve astrocytes from C57 and TRPV1-/- mice following injury. Like in the migration experiments however, TRPV1-/- did not significantly change calcium influx following injury compared to C57 wild-type. One possible explanation for these results is that loss of TRPV1 might have been compensated during development by other calcium channels or other TRP channels, including TRPA1 and TRPC channels (Beskina et al., 2007; Grimaldi et al., 2003; Malarkey et al., 2008; Miyano et al., 2010; Shigetomi et al., 2012).

Calcium influx also can be influenced by cytoskeletal dynamics, and this chapter examined the effects of taxol, which stabilizes microtubules, on injury-induced calcium influx in astrocytes. Calcium imaging analysis indicates that addition of 500 nM taxol did not significantly affect calcium dynamics (Figure 4.10-4.12), even though microtubules can gate channels and modulate calcium influx. Microtubule stabilization with taxol reduces the amplitude of calcium transients and calcium release in myocytes, while disruption of microtubules with colchicine can increase the amplitude of calcium transients and hasten its decay (Howarth et al., 1999; Kerfant et al., 2001). Microtubules can also influence the kinetics of calcium channels. Taxol can increase the probability of being in the open state and prolong the average open time of L-type calcium channels, while colchicine has the opposite effects and increases the closed state probability (Galli and DeFelice, 1994). However, taxol [10 to 100 μM] decreases the activity of voltage-gated calcium channels, while microtubule depolymerization induced by offchicine and vinblastine increases the current amplitude, which indicates greater channel activity (Unno et al., 1999). In my experiments, concentrations greater than 5 μM induced cell detachment (data not shown). Testing higher concentrations of taxol without disrupting cellular morphology might have induced a significant change in calcium following injury, and this is a possible avenue for future experiments. Since stabilization of microtubules with taxol had only modest effects on calcium influx (Figure 4.10-4.12), it would also be interesting to examine whether agents like nocodazole and colchicine that promote microtubule disassembly would change scratch-induced calcium entry.

Like microtubules, the actin cytoskeleton can also mediate calcium transients. Actin rather than microtubules mediates calcium influx in gingival fibroblast following stretch activation. Addition of cytochalasin C to inhibit actin polymerization reduced calcium influx

while taxol did not change calcium levels compared to controls (Wu et al., 1999). Cytochalasin C can also decrease agonist-induced calcium influx as well as alter the shape of the endoplasmic reticulum (Ribeiro et al., 1997). Since addition of taxol did not significantly change calcium dynamics following scratch wound (Figure 4.10-4.12), one potential future experiment is to examine whether modulating actin assembly/disassembly affects astrocyte calcium levels following scratch injury.

Calcium can activate multiple downstream signaling pathways that influence astrocyte function including migration, as chelation of extracellular calcium reduces astrocyte migration (Chapter 3). Since TRPV1 is a calcium-selective ion channel and its inhibition reduces migration, this chapter examined the changes in calcium dynamics induced by TRPV1 modulation. Cytoskeletal changes are important driving forces behind migration, and these changes are mediated by multiple calcium-mediated pathways. Together, these data (Chapter 3 and 4) suggest TRPV1 mediates a calcium-dependent stress response that results in astrocyte migration following injury. This response likely involves cytoskeletal changes, which is the focus of Chapter 5.

CHAPTER V

TRPV1 IN CYTOSKELETAL REMODELING OF ASTROCYTES FOLLOWING INJURY*

5.1 Introduction

The astrocyte cytoskeleton is comprised of three main types of filaments: actin, microtubules and intermediate filaments. The cytoskeleton is important in not only providing the structural framework of the cell, but it also facilitates vesicular trafficking and regulates many aspects of astrocyte function including cell migration (Cotrina et al., 1998; Couchie et al., 1985; Eliasson et al., 1999; Etienne-Manneville, 2004, 2006; Goetschy et al., 1986; Goldstein and Yang, 2000; Herrmann et al., 2007; Johnson and Byerly, 1993; Lascola et al., 1998; Middeldorp and Hol, 2011; Nogales, 2000; Sorci et al., 2000). During migration, cell protrusion occurs at the front of the cell to form the filopodia, which is comprised of parallel actin fibers and lamellipodia, which is made up on of a dense actin meshwork. In astrocytes however, the lamellopodia is limited and the cells form a leading edge that contains primarily microtubules rather than actin. During astrocyte migration, a large density of microtubules assembles near the leading edge to protrude the cell (Etienne-Manneville, 2013). Depolymerization of microtubules can inhibit cell protrusion and formation of the leading edge (Etienne-Manneville, 2013). Actin, however can also mediate protrusion in astrocytes, as inhibiting actin polymerization with cytochalasin affects membrane protrusion (Baorto et al., 1992). Generally, cell protrusion results from the forces generated from actin and microtubule polymerization.

In order to migrate, cells also need to contact the extracellular matrix to establish contractile forces to pull the cell. This is mediated by the formation of stress fibers comprised of actin and myosin II to facilitate contraction, and focal adhesions that anchor stress fibers allowing the cell to adhere to the extracellular matrix (for review, see (Gardel et al., 2010). Although not directly a part of this contractility machinery, microtubules are involved in this process and can regulate signaling pathways, such as Rho that mediate contractility (Bershadsky et al., 1996; Liu et al., 1998). For example, microtubule disruption increases stress fiber and focal adhesion formation resulting in greater contractility, while microtubule growth leads to focal adhesion disassembly (Bershadsky et al., 1996; Liu et al., 1998).

Migration also requires that a cell establish polarity for both direction of migration and orientation of the cytoskeleton. Cells sense direction in response to a chemoattractant, and the cytoskeleton becomes polarized so that the protrusive and contractile forces are formed at the proper locations. Microtubules are key in establishing polarity, as cells treated with nocodazole to inhibit microtubule polymerization lose polarity and lamellipodia formation (Omelchenko et al., 2002). Polarity of microtubules is established by the MTOC which stabilizes the minus ends of microtubule filaments. In astrocytes, the MTOC is located near the nucleus and reorients towards the direction of migration following scratch injury (Etienne-Manneville, 2006).

In addition to the cytoskeleton, cell migration is mediated by a variety of receptors, proteins and signaling pathways. One such protein is the Rho GTP-ase CDC42, which mediates process formation and polarity during migration. Following injury, CDC42 accumulates at the leading edge via vesicular trafficking in astrocytes (Osmani et al., 2010). CDC42 is essential for cell protrusion and establishing directionality and can target the proteins mPar6 and PKCζ to polarize the MTOC in astrocytes (Etienne-Manneville and Hall, 2001). Astrocytes at the leading

edge also increase expression and release of tenascin C, an extracellular matrix glycoprotein, following injury (Nishio et al., 2005). Exogenous addition of tenascin C increases both astrocyte migration and proliferation, while blocking tenascin C induces morphological changes – astrocytes become flatter and wider rather than thin with processes (Nishio et al., 2003; Nishio et al., 2005). Vinculin is a cytoskeletal protein involved in the formation of focal adhesions and helps link actin to the extracellular matrix. Following endothelin-1 induced gliosis, reactive astrocytes increase vinculin protein (Egnaczyk et al., 2003). Astrocytes treated with the cytokine TNF-α, however exhibited reduced levels of vinculin (van Strien et al., 2011).

Calcium is a key regulator of the cytoskeletal reorganization that mediates cell motility. Indeed, calcium initiates many of the signaling cascades that contribute to actin remodeling, retraction of the trailing edge and turnover of adhesion molecules (Conklin et al., 2005; Easley et al., 2008; Lee et al., 1999; Martini and Valdeolmillos, 2010). By modulating calcium levels, TRPV1 activation can lead to cytoskeletal rearrangement including disassembly of microtubules and reorganization of F-actin to drive changes in cell migration (Goswami et al., 2007; Han et al., 2007; Martin et al., 2012). In a dorsal root ganglion cell line, TRPV1 expression is concentrated at filopodia tips where the channel mediates filopodia formation (Goswami and Hucho, 2007). TRPV1 can mediate migration of pulmonary arterial smooth muscle cells through actin rearrangement (Martin et al., 2012). As I have shown that TRPV1 activation can modulate astrocyte migration (Chapter 3) and that calcium influx via TRPV1 is involved in this process (Chapter 4), this chapter will examine the effects of TRPV1 on cytoskeletal dynamics in astrocytes following injury.

5.2 Methods

Western blots

Primary cell isolations and scratch wound were performed as described in Chapter II and III. Western blotting was performed as described in Chapter II with the following modifications. Cells were grown on 6-well plates until confluent, and then serum starved in 0.5% FBS. Cells were pre-incubated for 15 minutes with 5 μM CPZ prior to scratch. Four parallel wounds with 200 μL pipet tips were made through the astrocyte culture. Cells were washed and incubated with 5 μM CPZ in astrocyte media with 0.5% FBS. Protein lysates were collected and concentrations were measured as previously described in Chapter II. Western blots were performed with the following primary antibodies and concentrations: GFAP (EMD Millipore, Billerica, MA, 1:5000), GAPDH (Cell Signaling, Danvers, MA, 1:1000), actin (Sigma-Aldrich, St. Louis, MO, 1:2000), α-tubulin (Sigma-Aldrich, St. Louis, MO, 1:2000), tenascin C (Cell Signaling, Danvers, MA, 1:1000), Cdc42 (Santa Cruz, Dallas, TX, 1:500) and vinculin (Sigma-Aldrich, St. Louis, MO, 1:2000). Proteins were detected with the Li-Cor system as described in Chapter II.

Immunocytochemistry

The following modifications were made to the protocol for immunocytochemistry outlined in Chapter II. Following scratch wound, retinal or optic nerve astrocytes were fixed in extraction buffer (1 mM EGTA, 1 mM $MgCl_2$, 80 mM PIPES, 0.1% saponin, 3% paraformaldehyde) for cytoskeletal proteins (Howell et al., 2013) for 20 minutes at room temperature. A test of different types of buffers showed that fixation in extraction buffer produced more intense cytoskeletal labeling than 4% paraformaldehyde with 1% glutaraldehyde,

while addition of 10% glycerol did not seem to produce a significant change (Figure 5.1). Primary antibodies used were anti-α-tubulin (Sigma-Aldrich, St. Louis, MO, 1:500; (Sorci et al., 1998) and vinculin (Sigma-Aldrich, St. Louis, MO, 1:500). Proteins were visualized with the appropriate DyLight-conjugated secondary antibodies (Jackson Immunoresearch, West Grove, PA 1:150). Filamentous actin were labeled with Alexa Fluor 488-phalloidin (Life Technologies, Grand Island, NY, 1:150) in phosphate-buffered saline with 1% bovine serum albumin (Gionfriddo et al., 2009). Staining with 4',6-diamidino-2-phenylindole (DAPI; Life Technologies, Grand Island, NY, 1:100) in water was also performed to visualize nuclei. Confocal images were taken as previously described and settings were kept constant for all treatments so that comparisons in fluorescence intensity could be made. Measurements of cell size and intensity were done using ImageJ (Schneider et al., 2012).

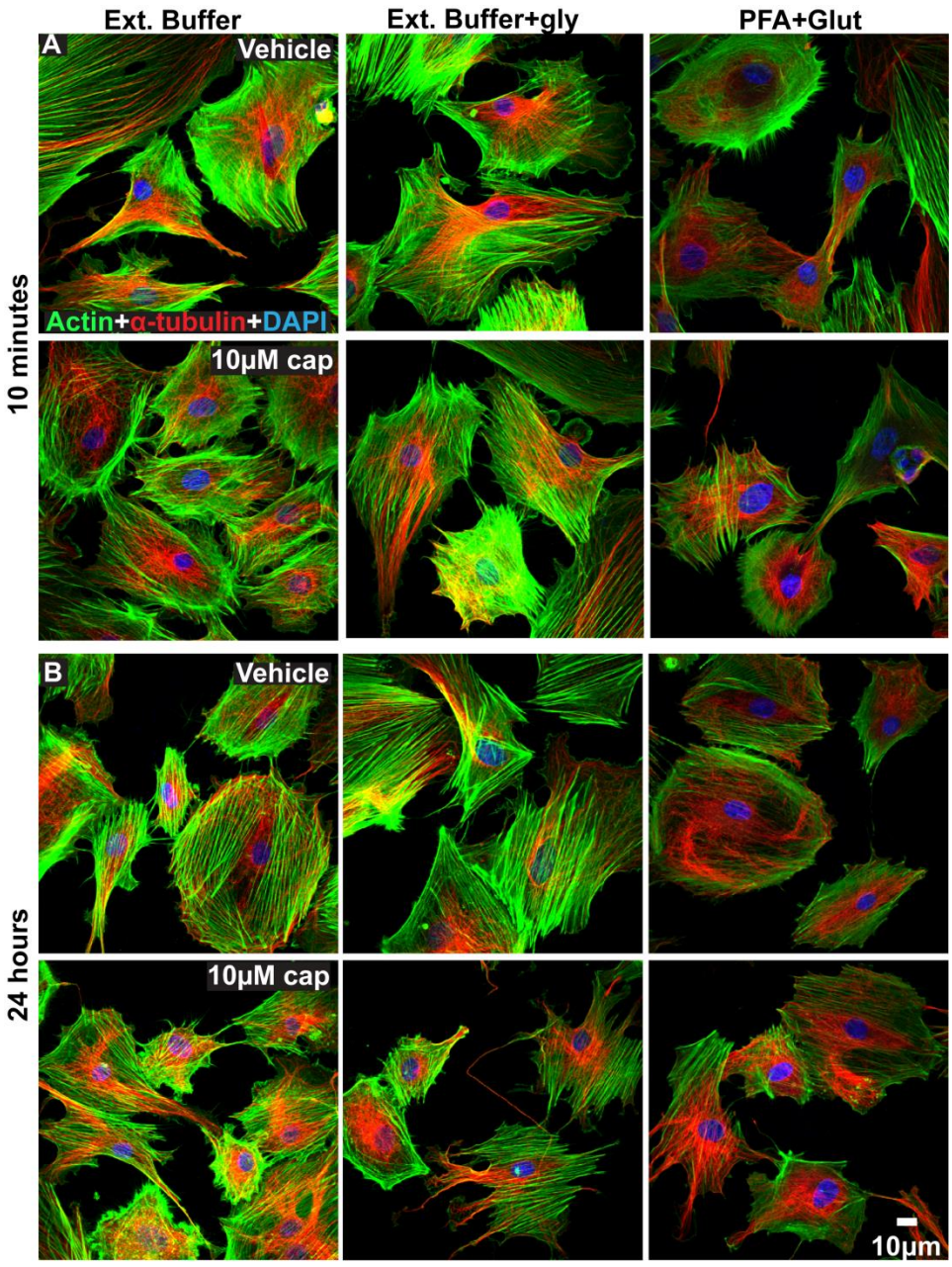

Figure 5.1. Effects of fixation on the preservation of the cytoskeleton. Astrocytes were treated with vehicle or 10 μM CAP for 10 minutes **(A)** and 24 hours **(B)**. Cells were then fixed in extraction buffer (*left*), extraction buffer with 10% glycerol (*center*) or 4% paraformaldehyde with 1% glutaraldehyde (*right*) and then labeled for actin (green), α-tubulin (red) and DAPI (blue) to observe cytoskeletal arrangement.

5.3 Results

Effects of TRPV1antagonism on levels of proteins involved in migration

Since TRPV1 can influence both migration and intracellular calcium in retinal astrocytes, I hypothesized that the channel also plays a role in the expression and localization of cytoskeletal components after injury. I collected protein from cultures containing injured astrocytes at 12 hours after scratch and naïve unscratched astrocytes and then performed Western blot analysis for cytoskeletal proteins and migration-related proteins (Figure 5.2). I chose this time point based on the divergence of closure progression in our antagonist migration assays (Chapter 3) and on literature showing peak expression of GFAP and tenascin C secretion at 12 hours following scratch injury (Gao et al., 2013; Nishio et al., 2005). Vehicle treatment following scratch injury produced a slight non-significant increase in expression of the cytoskeletal components, α-tubulin, actin and GFAP, about 5- 13% compared to unscratched naïve astrocytes ($p \geq 0.147$). Similarly, the expression of proteins involved in focal adhesion and migration — tenascin C, Cdc42 and vinculin — was modestly increased 10-20% following scratch ($p \geq 0.206$). Treatment with 5 μM CPZ reduced the expression of cytoskeletal and migration-related proteins 3-18% compared to vehicle ($p \geq 0.224$), with the exception of GFAP which remained slightly elevated.

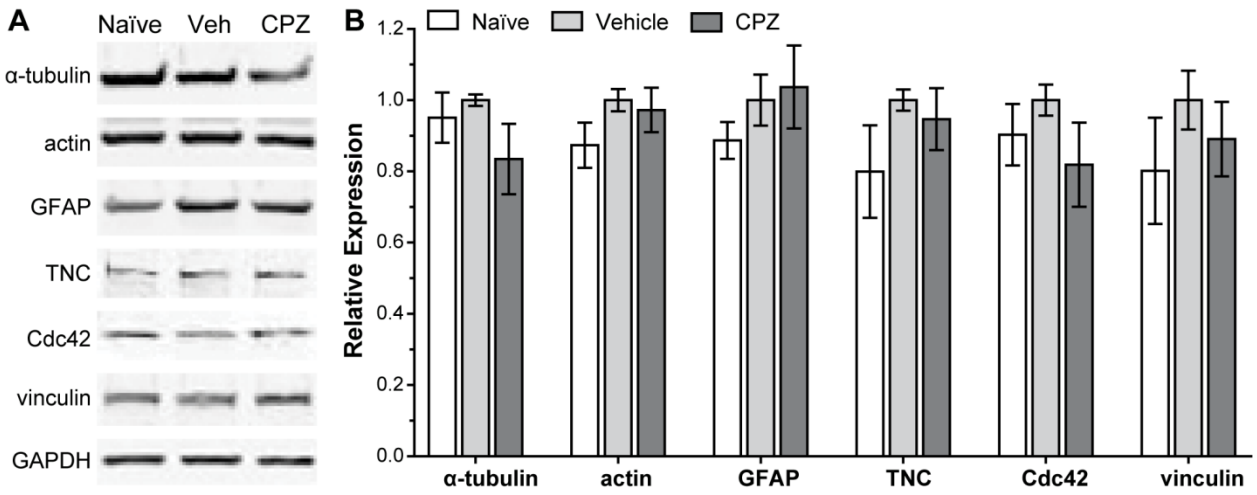

Figure 5.2. Effects of TRPV1 antagonism on levels of cytoskeletal and migration-related proteins following injury. Western blots (**A**) and quantification (**B**) demonstrates a trend towards increased expression of cytoskeletal proteins (α-tubulin, actin and GFAP) and migration-related proteins (tenascin C, CDC42 and vinculin) in cultured astrocytes 12 hours after scratch injury for vehicle treatments compared to naïve. Treatment with 5 μM CPZ had modest effects on expression of cytoskeletal and migration-related proteins compared to vehicle.

Effects of TRPV1 antagonism on cell area and cytoskeletal components

Although multiple scratches were made through the astrocyte monolayer, protein lysates were collected from cells at both the leading edge and farther away from the injury site. This might have minimized the changes in protein expression measured by Western blotting, so I used confocal microscopy to specifically examine cytoskeletal changes occurring in cells at the leading edge. To determine if there are cytoskeletal changes in astrocytes located at the leading edge compared to cells farther from the injury site, I used confocal microscopy to visualize astrocytes at 36 hours following scratch wound with and without the addition of 5 and 10 μM CPZ (Figure 5.3). Low magnification (10X) images show that astrocytes at the leading edge

display a distribution of F-actin and α-tubulin that was qualitatively similar to cells farther away from the wound edge for vehicle (Figure 5.3). A similar distribution of cytoskeletal filaments is also seen in cultures treated with CPZ. Treatment with 5 and 10 μM CPZ, however resulted in a larger cell-free area compared to vehicle, indicating that TRPV1 antagonists reduced the rate of migration as shown in Chapter III.

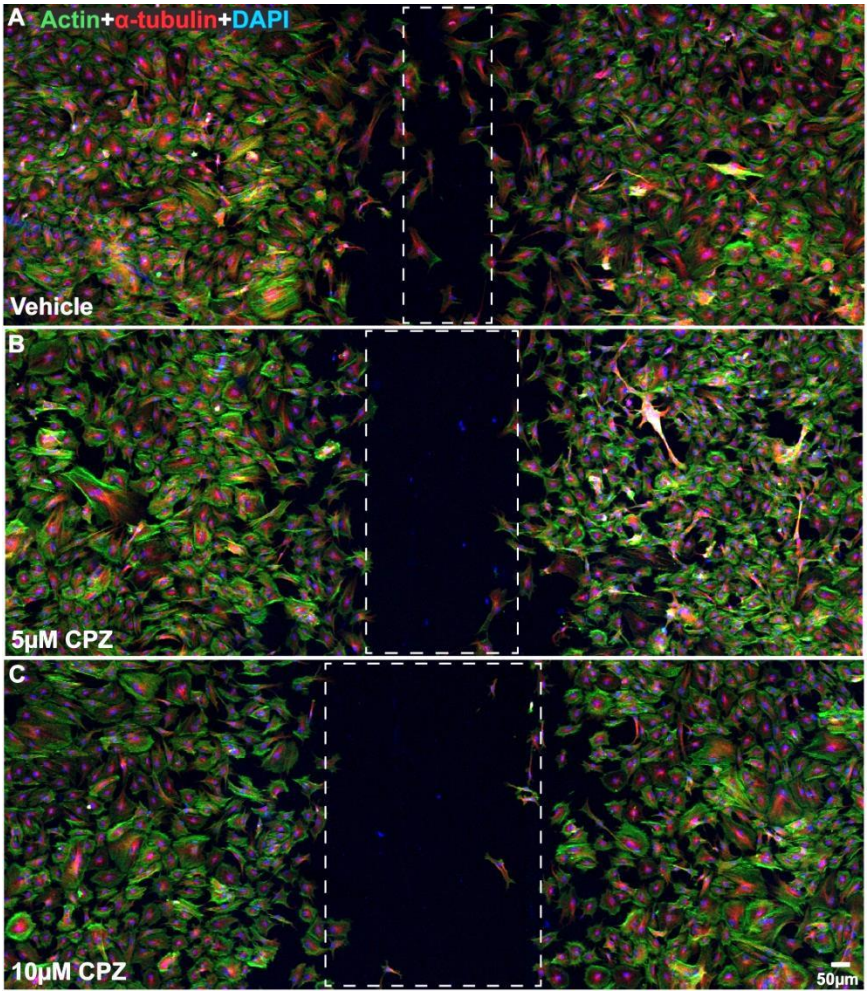

Figure 5.3. Actin and tubulin expression with increasing distance from the injury. Confocal micrographs (10X) show astrocytes at 36 hours following injury for vehicle **(A)**, 5 μM CPZ **(B)**

and 10 μM CPZ **(C)** and labeled for actin (green), a-tubulin (red) and DAPI (blue). Dotted boxes indicate cell free area.

Higher magnification (40X) images at the leading edge of the scratch injury reveal unique localization patterns for α-tubulin and F-actin (Figure 5.4). At 36 hours post-scratch, immunolabeling for α-tubulin in vehicle-treated cells appeared concentrated in the perinuclear region, with microtubules extending into astrocyte processes (Figure 5.4A and 5.4B, red). F-actin microfilaments distributed throughout the cytoplasm in parallel arrays that extended out into astrocyte processes (Figure 5.4A and 5.4B, green). There was little co-localization between α-tubulin and F-actin. Treatment with 10 μM CPZ appeared to reduce the size of the astrocytes, though the pattern of F-actin and α-tubulin labeling was similar to vehicle-treated cells (Figure 5.4A). Astrocytes treated with 3 μM IRTX did not appear to contract (Figure 5.4B), but both F-actin and α-tubulin labeling appeared more intense with more extensive co-localization. When quantified in Figure 5.4C, addition of 5 and 10 μM CPZ reduced astrocyte cytoplasmic area by 42% and 29%, respectively, relative to vehicle ($p \leq 0.003$). Although 3 μM IRTX also reduced cell area 12% relative to vehicle-treated cells, this was not significant ($p = 0.20$). Levels of α-tubulin were reduced by 17% with 10 μM CPZ ($p = 0.006$, Figure 5.4D), while IRTX had no significant effect ($p = 0.078$). In contrast, F-actin intensities were similar for CPZ compared to vehicle ($p \geq 0.11$), but increased 26% for 3 μM IRTX (Figure 5.4D; $p < 0.0001$).

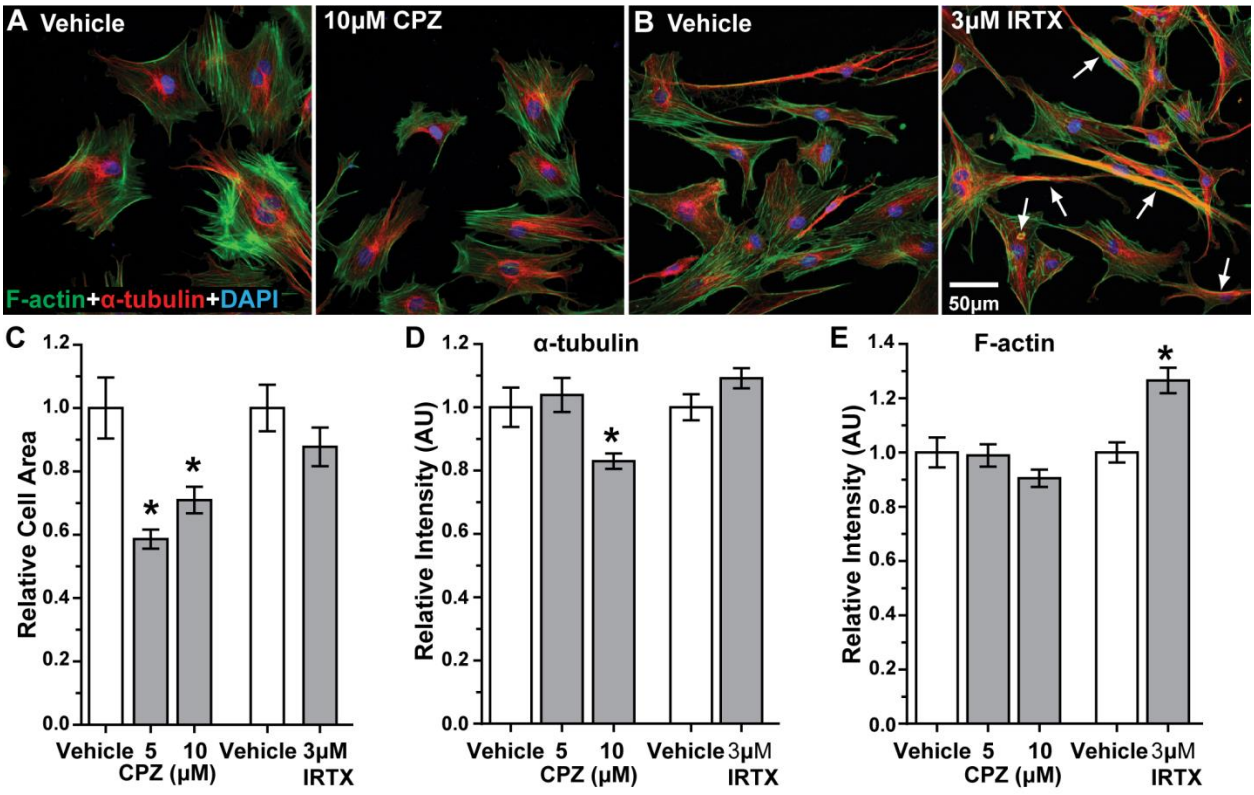

Figure 5.4. Effects of TRPV1 antagonism on cell area and α-tubulin and F-actin intensity. Confocal images (40X) show astrocytes near the leading edge 36 hours following scratch wound labeled for F-actin (green), α-tubulin (red) and DAPI (blue) for vehicle and 10 μM CPZ treatments **(A)**. Astrocytes treated with 3 μM IRTX after scratch injury have increased co-localization of F-actin and a-tubulin (arrows; **B)**. Bar graph shows average astrocyte cytoplasmic area **(C)** normalized to vehicle for 5 and 10 μM CPZ and 3 μM IRTX treatments 36 hours post-injury. *$p < 0.003$ compared with vehicle (n=51 cells). Bar graphs show the relative intensities of α-tubulin **(D)** and F-actin **(E)** normalized to vehicle for CPZ and IRTX treatments. *$p < 0.006$ compared with vehicle for α-tubulin (n=51 cells); *$p < 0.0001$ compared with vehicle for F-actin (n = 84 cells). All data: mean ± SEM.

Antagonism, but not agonism, of TRPV1 affects α-tubulin rearrangement following injury

To better understand the changes in the subcellular localization of cytoskeletal proteins during injury-induced migration, I captured higher magnification (80X) confocal micrographs of α-tubulin in astrocytes at the leading edge of the scratch wound following treatment with TRPV1 agonists or antagonists. Astrocytes treated with vehicle and immunolabeled for α-tubulin show clearly defined microtubules that radiate out from the MTOC near the nucleus and extend into cell processes at the leading edge (asterisk; Figure 5.5A). This rearrangement of the MTOC toward the leading edge establishes cell polarity and directs migration toward the cell-free area (Robel et al., 2011a). Higher magnification (240X) shows tubulin localization is most intense in processes extending toward the leading edge (Figure 5.5B). Cells treated with 1 nM CAP or 10 nM RTX had a tubulin arrangement similar to that of vehicle with microtubules radiating from the MTOC that extend into the astrocyte processes. A range of concentrations for TRPV1 agonists was used to observe possible effects on α-tubulin and representative results are shown. (Figure 5.5).

A comparable distribution of α-tubulin was observed in scratched astrocytes treated with vehicle in the antagonist experiments. Representative images of cells treated with vehicle or antagonists at the leading edge are shown in Figure 5.6. Again, microtubules radiated out from the MTOC and extended into astrocyte processes, thus directing cell migration to close the wound area. In cells treated with CPZ, microtubules are clearly defined near the MTOC, which is oriented toward the leading edge similar to what is observed in vehicle-treated cells (Figure 5.6A). However, microtubules in individual processes near the leading edge appear less intense in CPZ-treated cells (Figure 5.6A). Higher magnification (240X) of cells treated with 5 μM CPZ shows that closer to the edge of individual processes (dotted line, Figure 5.6B;) microtubules

appear less defined and take on a fragmented appearance that is exacerbated with a higher dose of CPZ (10 μM). Astrocytes treated with 3 μM IRTX had clearly defined microtubules extending from the MTOC into processes (Figure 5.6). The retraction and fragmentation observed with CPZ treatment was not observed in IRTX-treated cells.

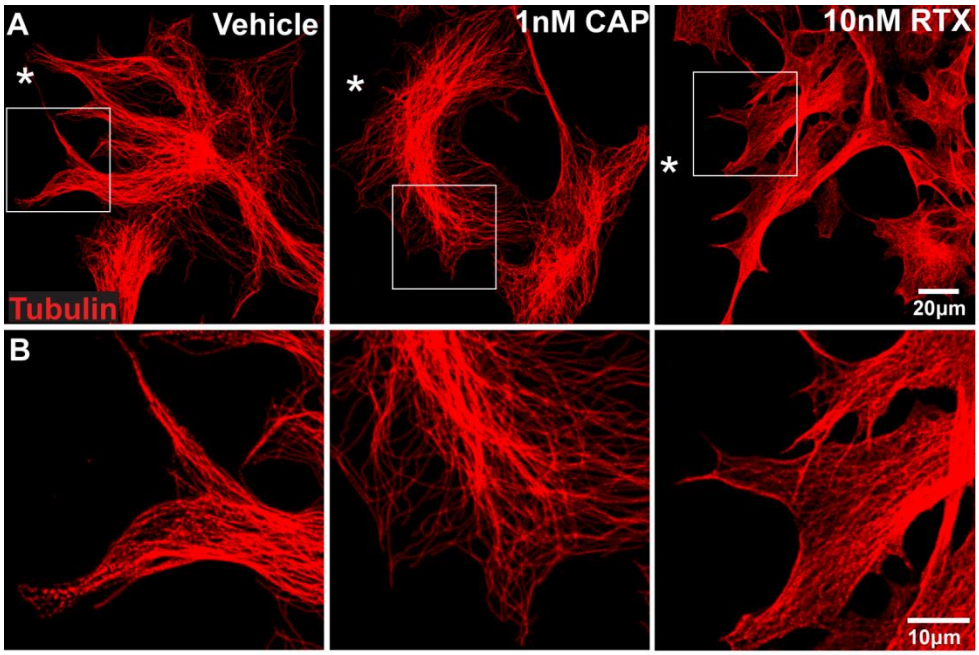

Figure 5.5. Agonism of TRPV1 and subcellular localization of α-tubulin. High magnification (80X) confocal images show astrocytes labeled for α-tubulin (red) near the leading edge (*) of the wound after scratch injury **(A)**. High magnification (240X) views of boxed areas are shown in B. Cells were scratched in the presence of vehicle, 1 nM CAP or 10 nM RTX and then fixed in an extraction buffer for cytoskeletal proteins before labeling.

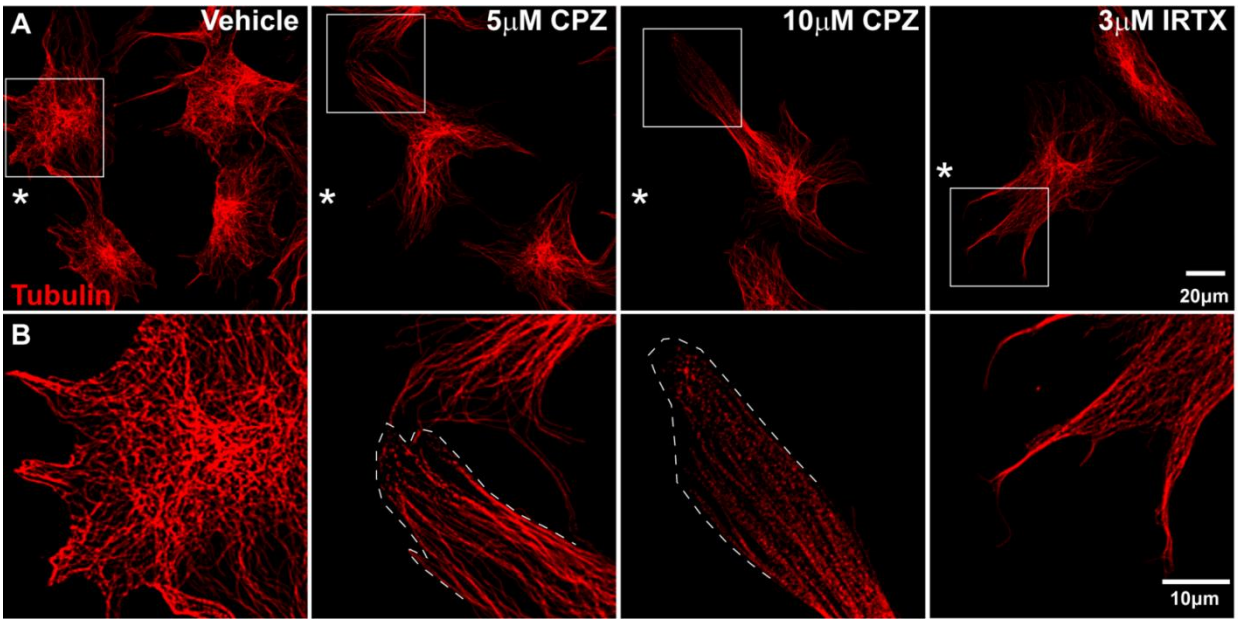

Figure 5.6. Antagonism of TRPV1 and retraction of α-tubulin. High magnification (80X) confocal images show astrocytes labeled for α-tubulin (red) near the leading edge (*) of the wound after scratch injury **(A)**. High magnification (240X) views of boxed areas are shown in B. Cells were scratched in the presence of vehicle, 5 μM or 10 μM CPZ, or 3 μM IRTX. Dotted lines represent cell edge.

Antagonism, but not agonism, of TRPV1 affects actin rearrangement following injury

In addition to tubulin, I also examined actin rearrangement at the leading edge following injury with and without TRPV1 modulation. Labeling for F-actin in vehicle-treated astrocytes shows intense localization at filopodia extending toward the leading edge and cell periphery (Figure 5.7 and 5.8). This reorganization of actin filaments following injury provides the contractile force necessary to drive cell migration (Le Clainche and Carlier, 2008). A range of concentrations for TRPV1 agonists were used and representative figures are shown. Addition of 1 μM CAP had a modest effect on actin rearrangement (Figure 5.7), similar to the result seen

with tubulin. Actin is localized throughout the cell and extended into the astrocyte processes. A result similar to CAP treatment was obtained with 10 nM RTX. Cells treated with RTX exhibited extensive actin expression throughout the soma and also in astrocyte processes (Figure 5.7).

In the antagonist experiments, injured astrocytes treated with vehicle demonstrated intense actin expression throughout the cell, especially in the cell periphery, that extended into the astrocyte processes. Representative images of cells treated with vehicle and antagonists at the leading edge are shown in Figure 5.8. In cells treated with CPZ, actin intensity appeared reduced, especially its localization to the leading edge (Figure 5.8A). Higher magnification (240X) images of cells treated with 5 μM CPZ indicate that compared to vehicle, actin expression and intensity in astrocytes processes is reduced, which is exacerbated with 10 μM CPZ (dotted line, Figure 5.8B). In cells treated with IRTX, F-actin intensity appeared similar to vehicle and extended into astrocyte processes but localization was more perinuclear and less pronounced near the cell periphery (Figure 5.8). Together, these results indicate that with injury, TRPV1 activation is associated with moderate cytoskeletal remodeling in astrocytes at the leading edge.

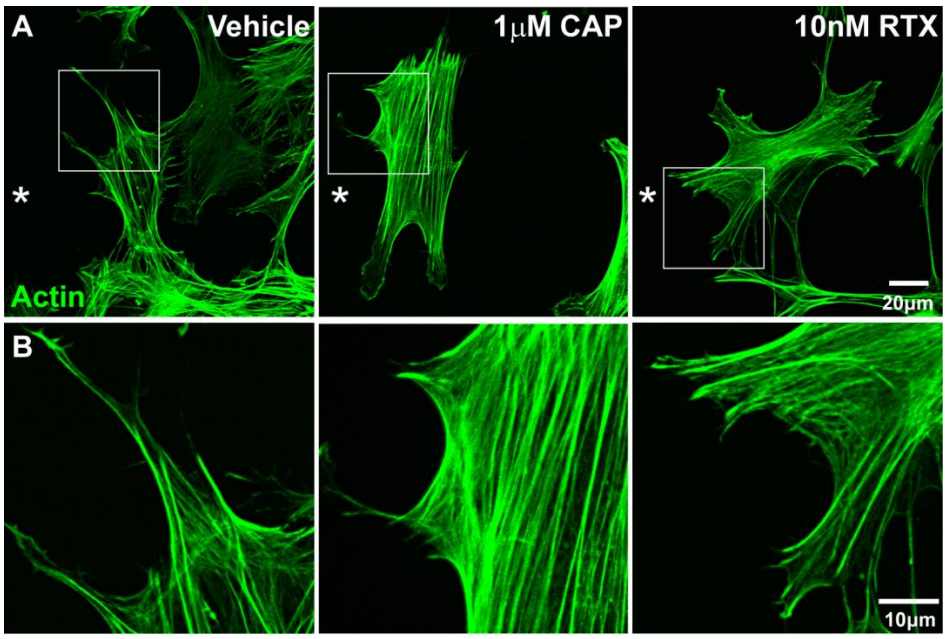

Figure 5.7. Agonism of TRPV1 and the subcellular localization of actin. High magnification (80X) confocal images show astrocytes labeled for actin (green) near the leading edge (*) of the wound after scratch injury **(A)**. High magnification (240X) views of boxed areas are shown in B. Cells were scratched in the presence of vehicle, 1 nM CAP or 10 nM RTX.

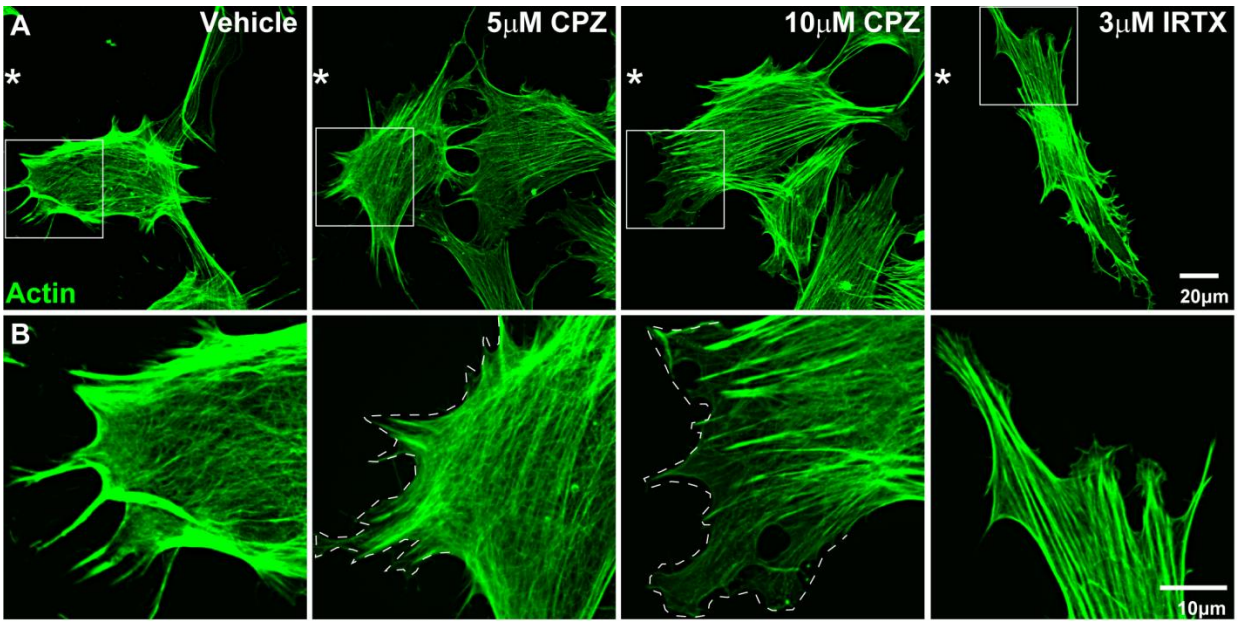

Figure 5.8. Antagonism of TRPV1 and retraction of actin. High magnification (80X) confocal images show astrocytes labeled for actin (green) near the leading edge (*) of the wound **(A)**. High magnification (240X) views of boxed areas are shown in B. Cells were scratched in the presence of vehicle, 5 μM or 10 μM CPZ, or 3 μM IRTX and then fixed in an extraction buffer for cytoskeletal proteins before labeling. Dotted lines represent the cell edge.

Knockout of TRPV1 has modest effects on cytoskeletal rearrangement following injury

To complement the pharmacological experiments, I next determined whether knockout of TRPV1 affected cytoskeletal rearrangement in optic nerve astrocytes 24 hours following scratch injury. Although these astrocytes were isolated from optic nerves and the astrocytes used in the pharmacological experiments were isolated from retina, both cell populations exhibited a similar tubulin orientation following injury. Astrocytes from C57 mice displayed an intense distribution of microtubules radiating from the MTOC and extending into the leading edge of astrocytes (Figure 5.9A). Higher magnification (240X) images of the leading edge (Figure 5.9B, C) show microtubules extending out to the edges of the processes. Following scratch injury, α-tubulin distribution in TRPV1-/- astrocytes resembled that observed in C57 astrocytes (Figure 5.9). Microtubules appeared less intense in TRPV1-/- astrocytes, yet there did not appear to be retraction or fragmentation within the astrocyte processes as seen with CPZ treatment (Figure 5.6 and Figure 5.9). Next, I determined whether TRPV1 knockout affected actin rearrangement in astrocytes following injury (Figure 5.10). Actin filaments in C57 wild-type astrocytes at 24 hours post-scratch were localized throughout the cell and extended into astrocyte processes (Figure 5.10). Again, actin distribution in C57 optic nerve astrocytes was comparable to that observed in retinal astrocytes (Figures 5.8 and 5.10). Actin intensity appeared diminished in

TRPV1-/- astrocytes (Figure 5.10), although actin did not appear to retract at the leading edge as it did with CPZ treatment (Figure 5.8).

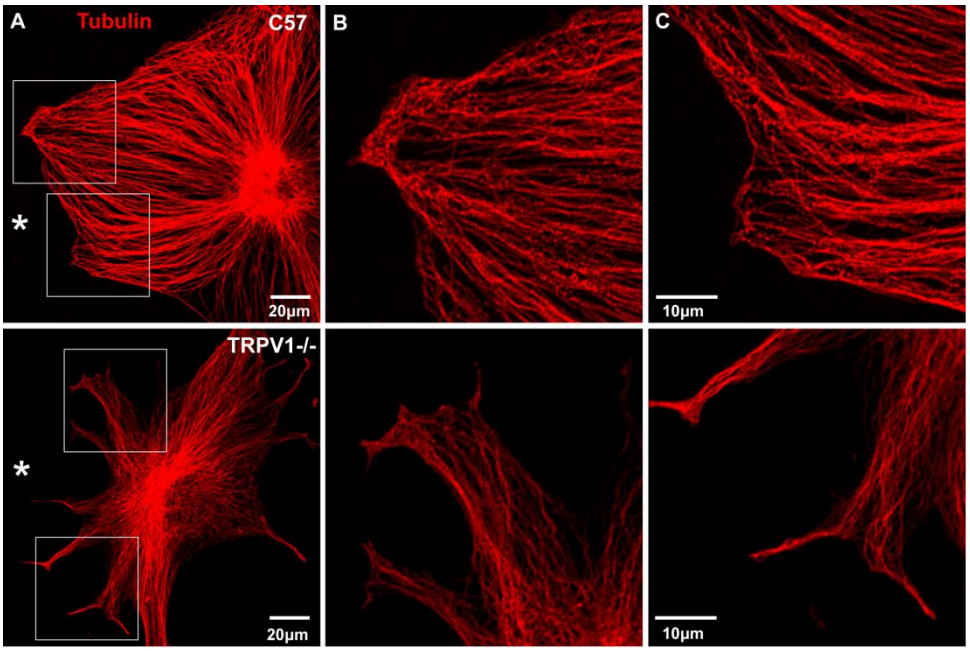

Figure 5.9. Effects of TRPV1 knockout on the subcellular localization of α-tubulin. High magnification (80X) confocal images show astrocytes labeled for α-tubulin (red) near the leading edge (*) of the wound **(A)**. High magnification (240X) views of boxed areas are shown **(B** and **C)**.

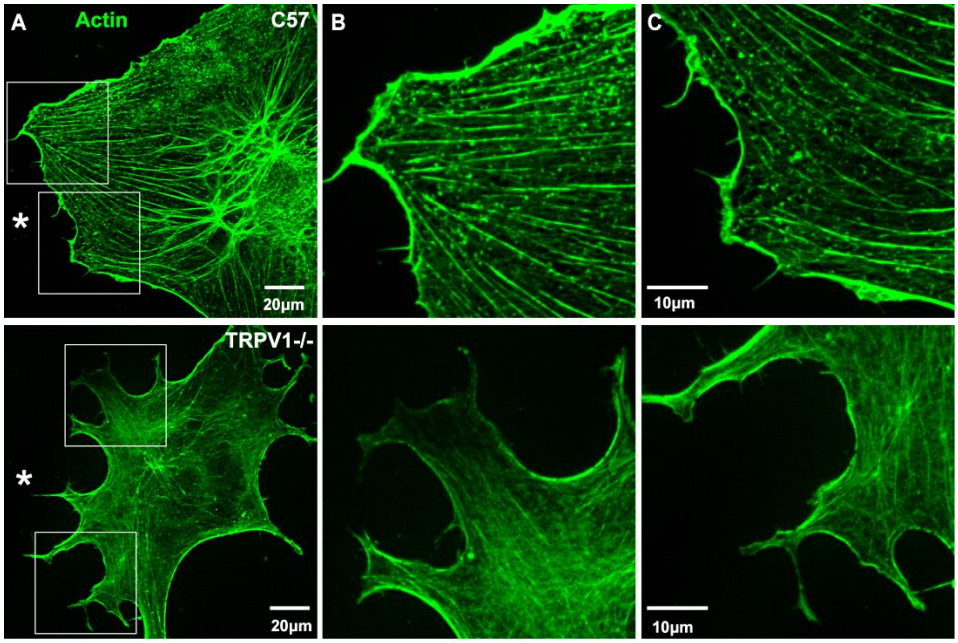

Figure 5.10. Effects of TRPV1 knockout on the localization of actin. High magnification (80X) confocal images show astrocytes labeled for actin (green) near the leading edge (*) of the wound after scratch **(A)**. High magnification (240X) views of boxed areas are shown **(B** and **C)**.

Antagonism of TRPV1 reduces the number of focal adhesions

Focal adhesions link the cytoskeleton of a cell to the extracellular matrix to help mediate adhesion. Since focal adhesion formation can be modulated by calcium, I next determined whether injury and TRPV1 modulation affected expression of vinculin, a protein present in the focal adhesion complex. In naïve (unscratched) retinal astrocytes that are confluent, vinculin expression is punctate and distributed within the cell body and along cell edges (Figure 5.11). Following injury in astrocytes treated with vehicle, vinculin appeared to distribute more toward the cell periphery or along cell-to-cell borders. Vinculin distribution appeared similar in RTX-treated cells. However, in injured astrocytes treated with IRTX, vinculin expression was

diminished. These results suggest that TRPV1 antagonism might reduce focal adhesion expression in astrocytes following injury.

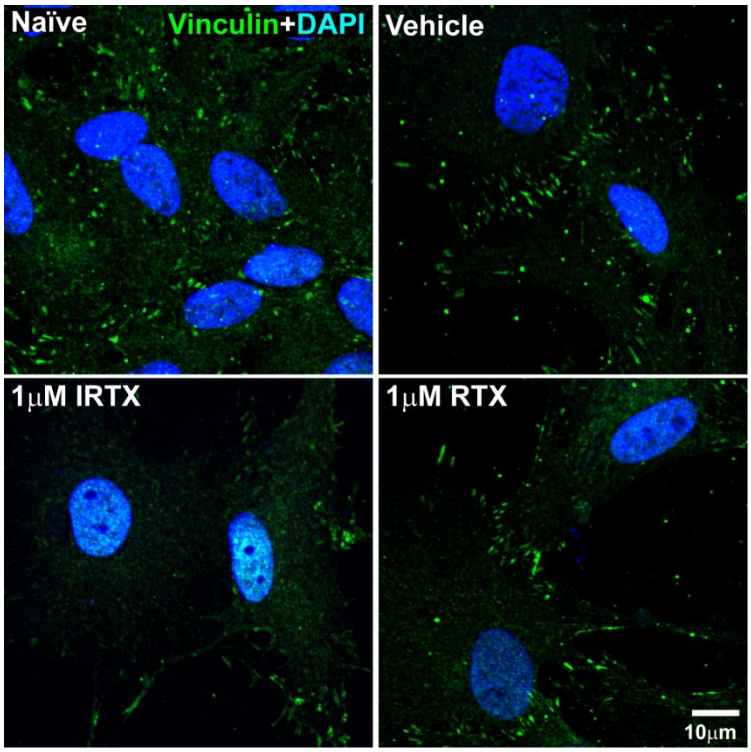

Figure 5.11. Effects of TRPV1 on vinculin expression following injury. Naïve astrocytes or injured astrocytes at 24 to 36 hours treated with vehicle, 1 μM IRTX or 1 μM RTX were labeled for vinculin (green) and DAPI (blue).

5.4 Discussion

This chapter examined the role of TRPV1 in modulating cytoskeletal rearrangement in astrocytes following injury. Antagonism of TRPV1 induced moderate cytoskeletal rearrangement – CPZ reduced astrocyte cell area and decreased α-tubulin levels, while IRTX increased actin levels (Figure 5.4). Addition of CPZ also resulted in actin and tubulin retraction within astrocyte processes, an effect not seen with IRTX treatment (Figures 5.6 and 5.8). Treatment with the

TRPV1 agonists only had minimal effects on actin and tubulin subcellular rearrangement (Figures 5.5 and 5.7). Cytoskeletal rearrangement following injury was similar in optic nerve astrocytes from C57 mice compared to rat retinal astrocytes (Figures 5.5 to 5.10). Knockout of TRPV1 only slightly reduced actin intensity compared to C57 astrocytes (Figure 5.9 and 5.10). Finally, preliminary results suggest that IRTX might also reduce focal adhesion formation in astrocytes following injury (Figure 5.11).

TRPV1 is a cation channel with a high calcium permeability, and calcium regulates multiple downstream signaling cascades that influence cytoskeletal remodeling (Ridley et al., 2003). It is not surprising therefore, that TRPV1 has been shown to modulate cytoskeletal rearrangement in various systems. For example, activation of TRPV1 by capsaicin can lead to cytoskeletal remodeling involving rearrangement of F-actin and tubulin networks (Goswami et al., 2006; Martin et al., 2012). The C-terminus of TRPV1 can bind both tubulin dimers and polymerized microtubules in a calcium-mediated manner (Goswami et al., 2004). In a submandibular gland cell line, capsaicin induces cytoskeletal rearrangement by decreasing the amount of actin and increasing the space between each filament (Cong et al., 2013). In pulmonary smooth muscle cells and neutrophils, however, capsaicin increased actin levels but had no significant effect on the tubulin cytoskeleton (Martin et al., 2012; Wang et al., 2005a). TRPV1 also localizes to the tips of filopodia and induces filopodia formation and microtubule disassembly in a dorsal root ganglia cell line (Goswami et al., 2006; Goswami and Hucho, 2007). Inhibition of TRPV1 following scratch-wound increased F-actin levels but decreased α-tubulin in migrating astrocytes (Figure 5.4). Higher magnification images of astrocytes at the leading edge following TRPV1 antagonism showed microtubule fragmentation and retraction from the cell edge (Figure 5.6 and 5.8) suggesting TRPV1 modulates cytoskeletal rearrangement and

subcellular localization after injury. Although actin intensity might be diminished in TRPV1-/- astrocytes, there was no apparent microtubule or actin retraction following scratch injury (Figure 5.9 and 5.10). This might be due to genetic or developmental compensation, or through pathways not mediated by TRPV1. The lack of discernable cytoskeletal changes between C57 and TRPV1-/- suggests that TRPV1 might only have a modest role in the development of the cytoskeleton.

Although the focus of this chapter is on modulation of actin and microtubule proteins by TRPV1, there is some evidence that TRPV1 might also modulate intermediate filaments. In pulmonary arterial smooth muscle cells, the network of vimentin filaments localized to the perinuclear region and density was increased with capsaicin (Martin et al., 2012). Following induction of inflammatory and neuropathic pain, GFAP expression was significantly reduced in TRPV1-/- animals (Chen et al., 2009). TRPV1 activation with capsaicin can also increase GFAP expression in the retina (Leonelli et al., 2010). This suggests that TPRV1 might also modulate intermediate filament rearrangement. Although changes in GFAP levels were not observed with Western blots (Figure 5.2), there might be changes in the spatial distribution and organization of intermediate filaments that were not detected. One possible experiment is to use high magnification imaging to observe changes in the distribution of intermediate filaments following scratch injury and whether this is affected with TRPV1 pharmacological agents. CPZ induced retraction of actin and tubulin from astrocyte processes even though changes in the levels were not observed with Western blots (Figure 5.2). This suggests that although total GFAP levels were not affected by injury or CPZ, there might be changes in the spatial distribution of GFAP within the cell following injury.

In order for a cell to migrate, it must form cell protrusions, establish directionality, and contact and adhere to the extracellular matrix. I examined the expression of CDC42, a protein that mediates protrusion formation and polarity, in injured astrocytes with and without TRPV1 modulation. Scratch injury did not significantly affect total levels of CDC42 (Figure 5.2). Future experiments, however, could examine CDC42 localization and active state rather than protein levels. Following scratch injury, GFP-tagged CDC42 localizes to the leading edge of astrocytes (Osmani et al., 2010). It would be interesting to determine whether a similar change in CDC42 localization is observed in my astrocyte cultures and if this is mediated by TRPV1. High magnification imaging would be useful in elucidating changes in CDC42 localization following injury and with TRPV1 modulation. CDC42 is a Rho GTPase that is active when bound by GTP and inactive when bound by GDP (Etienne-Manneville and Hall, 2002). CDC42 activity can be analyzed by precipitating GTP-bound CDC42 and then immunoblotting to determine levels. One possible future direction would be to determine changes in levels of GTP-bound CDC42 following scratch injury or with TRPV1 modulation.

Tenascin C is an extracellular matrix glycoprotein that mediates cell adhesion. Expression of this protein is increased in astrocytes following injury, although I did not observe this in my western blot (Figure 5.2). Again, high magnification imaging of tenascin C within the cell following scratch injury and with TRPV1 modulation may better determine the role of this protein in injury-induced migration. Tenascin C can also bind fibronectin, an extracellular matrix protein (Ghert et al., 2001). In trigeminal neurons, TRPV1 colocalizes with integrins, which bind fibronectin to regulate cell adhesion (Jeske et al., 2009a). Fibronectin has been shown to activate src kinase to phosphorylate and increase expression of TRPV1 at the plasma membrane (Jeske et al., 2009a). TRPV1 contains multiple phosphorylation sites and is highly

regulated by phosphorylation. My data suggests antagonism of TRPV1 might reduce expression of vinculin, suggesting TRPV1 may mediate changes in cell adhesion (Figure 5.11). Since TRPV1 phosphorylation can influence expression at the plasma membrane and TRPV1 colocalizes with integrins, it would be interesting to observe whether there are changes in TRPV1 phosphorylation following injury and whether this affects integrin expression and localization, thereby affecting focal adhesion formation.

TRPV1 could mediate cytoskeletal changes during migration via proteins and pathways that are activated by calcium. One such protein is calpain, a calcium-dependent protease. Calpains can cleave focal adhesion kinase and talin, a protein that links the actin cytoskeleton to focal adhesions to regulate cell adhesion (Chan et al., 2010; Franco et al., 2004). Calpain activation can also lead to focal adhesion turnover and disassembly to promote cell detachment from the extracellular matrix (Ramirez et al., 2001). Inhibitors of calpains reduce cell migration by stabilizing focal adhesions and reducing the rate of cell detachment from the extracellular matrix (Bhatt et al., 2002; Huttenlocher et al., 1997). TRPV1 modulation of calpain activity in injury-induced gliosis to facilitate migration is quite possible, as calpain-mediated adhesion can be influenced by localized calcium entry through TRPM7, another member of the TRP family (Su et al., 2006). In my experiments, antagonism of TRPV1 might reduce expression of vinculin, a protein present in the focal adhesion complex, suggesting that TRPV1 might also be mediating cell adhesion (Figure 5.11). Astrocytes express calpains, and levels increase in reactive astrocytes (Konig et al., 2003; Li et al., 1996; Shields et al., 1998). Since calpains are known to modulate focal adhesion dynamics, TRPV1 activation and the subsequent increase in calcium might lead to calpain activation to regulate vinculin expression. One possible experiment would be to determine if calpain expression and activity is increased following

scratch injury and whether this is modulated by TRPV1. Expression could be observed with immunolabeling or Western blots, and calpain activity can be determined by the production of calpain cleavage products. It would also be interesting to determine whether calpain inhibitors affect vinculin expression following scratch injury.

This chapter examines the cytoskeletal changes that occur following scratch injury and with TRPV1 modulation. Although the levels of various proteins involved in migration were not significantly changed, the spatial localization and orientation of the cytoskeleton was altered with TRPV1 inhibition. Addition of TRPV1 antagonists induced retraction of actin and tubulin from astrocyte processes as well as reduced the presence of focal adhesions. This suggests that TRPV1-mediated changes in cytoskeletal dynamics might contribute to reduced astrocyte migration after injury.

CHAPTER VI

DISCUSSION AND CONCLUSION

6.1 Discussion

Motility is one component of the astrocyte stress response and a functional consequence of reactivity. In order for a cell to migrate effectively, a convergence of signaling pathways occurs to mediate aspects of migration including protrusion of the leading edge, cell contraction and adhesion. Calcium serves as an important signaling regulator of migration by modulating cytoskeletal rearrangement and focal adhesion dynamics. Because calcium is an essential second messenger under both physiological and pathophysiological conditions, astrocytes express multiple channels and receptors including TRPV1 to regulate calcium levels.

Our lab has found that TRPV1 is an important component of the intrinsic stress response of RGCs. Although the channel is also expressed in retinal astrocytes, its function there is unknown. The purpose of this dissertation was to elucidate the role of TRPV1 in modulating an aspect of the astrocyte stress response – migration and the mechanisms that contribute to this phenomenon. Since relatively little is known regarding the role of TRPV1 in astrocytes, Chapter II provided a detailed characterization of TRPV1 expression in retinal and optic nerve astrocytes. Although TRPV1 is expressed throughout mouse and rat astrocytes in the retina, its expression in the optic nerve is species-dependent and ranged from diffuse to punctate. With the expression of TRPV1 in astrocytes established, the purpose of Chapter III was to elucidate the contribution of TRPV1 to astrocyte migration. Using the scratch wound model, I found that antagonism of

TRPV1 reduced astrocyte migration while agonism had minimal effect. This suggests a possible ceiling effect and that the scratch itself or the injury milieu might be activating TRPV1. Injury-induced astrocyte migration was dependent on extracellular calcium. Since calcium is important in migration and TRPV1 is a channel with a high calcium conductance, calcium dynamics in astrocytes were examined in Chapter IV. While TRPV1 had modest effects on astrocyte calcium influx under physiological conditions, injury induced an increase in intracellular calcium that was attenuated with TRPV1 antagonism but not microtubule stabilization. Calcium is also an important regulator of cytoskeletal rearrangement; therefore Chapter V examined the effects of TRPV1 modulation on cytoskeletal dynamics following injury. TRPV1 antagonism caused retraction of actin and tubulin from the leading edge, while agonism had minimal effects.

One observation that is prevalent throughout this dissertation is the disparate effects of CPZ and IRTX, both well-characterized TRPV1 antagonists. While CPZ and IRTX both reduced migration, IRTX caused a greater reduction in calcium influx and CPZ induced more cytoskeletal retraction from the leading edge. Possible explanations for these differences between the two antagonists have been discussed in Chapter IV. In addition, although TRPV1 has a high selectivity for calcium, TRPV1 has been shown to mediate sodium influx in cortical astrocytes (Huang et al., 2010). It is possible that the events downstream of CPZ treatment might be mediated by an influx of sodium. Unlike calcium, sodium is not widely regarded as an important second messenger but has been shown to mediate migration. Blocking or down-regulation of voltage-gated sodium channels by tetrodotoxin or siRNA respectively, can reduce migration of aortic smooth muscle cells (Meguro et al., 2009). The sodium-hydrogen transporter, NHE1 is localized to the lamellopodia in fibroblasts, where it mediates cytoskeletal anchoring, polarity and focal adhesion dynamics (Denker and Barber, 2002). This suggests that

sodium influx can mediate migration. The modest change in calcium as well as the greater cytoskeletal retraction observed in retinal astrocytes with CPZ addition might due to an influx of sodium, and warrants further analysis. Furthermore, sodium is important in establishing membrane potential. Influx of sodium would depolarize the cell to activate voltage-gated channels including ones that are selective for calcium. Moreover, although CPZ has been used extensively to study TRPV1 function and TRPV1-mediated effects on migration, CPZ has been shown to have non-TRPV1 mediated effects. CPZ can also bind voltage-gated calcium channels, TRPM8 and nicotinic acetylcholine receptors (Docherty et al., 1997; Malkia et al., 2009).

In addition to the differential effects of TRPV1 antagonists, another prevalent result throughout the dissertation is the modest effects observed with TRPV1-/- astrocytes. Astrocytes from TRPV1-/- mice were isolated to supplement the pharmacological experiments. Unlike astrocytes in the presence of TRPV1 antagonists, TRPV1-/- astrocytes did not exhibit changes in migration, calcium or cytoskeletal retraction following injury when compared to wild-type astrocytes. This might be due to genetic compensation by other channels. For example, astrocytes express other TRP channels, including members of the TRPC family that mediate calcium influx (Verkhratsky et al., 2014). Also, the cultures used in the pharmacological and knockout experiments were fundamentally different. The pharmacological experiments utilized astrocytes isolated from post-natal rat retinas while the knockout experiments used astrocytes from young adult mouse optic nerves. Although both pools of cells are astrocytes, inherent differences exist between the two populations (see Chapter II discussion). One interesting avenue of investigation would be to determine the functional differences between retinal and optic nerve astrocytes. For example, the TRPV1 pharmacological experiments can be repeated with rat optic nerve astrocytes. TRPV1 antagonists reduced migration and calcium influx and

caused cytoskeletal retraction in rat retinal astrocytes. It would be interesting to determine if the same results are observed in rat optic nerve astrocytes. A similar approach can be taken with mouse retinal astrocytes. Alternatively, inducible knockouts of TRPV1 or siRNA-mediated TRPV1 knockdown can be used to overcome potential genetic compensation. It is also possible that TRPV1 might only have a modest role in astrocytes, and the effects seen are mediated by other channels or receptors.

Despite the points described above, the results presented in this dissertation suggest a role for TRPV1 in modulating astrocyte migration via calcium influx and cytoskeletal dynamics following injury (Figure 6.1). Following scratch injury, TRPV1 is activated, most likely by endogenous activators within the injury milieu like endocannabinoids or pH changes. This induces an influx of calcium that leads to a relocalization of actin and tubulin within the cells. Other mediators of migration like tenascin C, CDC42 and vinculin can relocalize to the leading edge. Ultimately, these events drive cell migration.

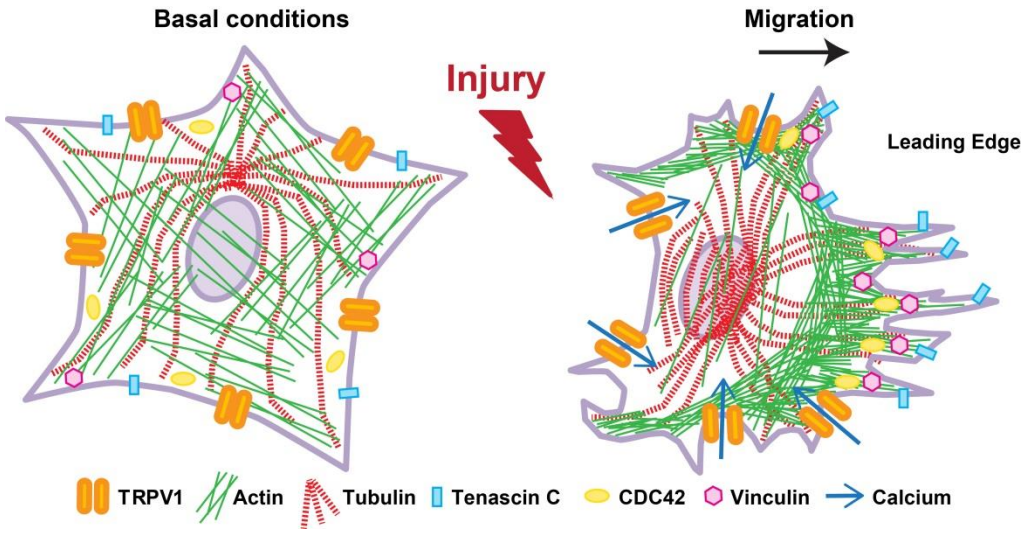

Figure 6.1. Intracellular changes that occur to modulate cell migration. Following injury, TRPV1 channels open to increase intracellular calcium. Calcium mediates cytoskeletal rearrangement and localization of migration proteins to influence motility.

6.2 Conclusion

Astrocyte migration can be modulated by TRPV1, a channel known for sensing extracellular stimuli and mediating cellular responses. Previous studies by our lab have shown that in a model of optic neuropathy, TRPV1 is neuroprotective in RGCs. Astrocyte reactivity and neuronal loss underlie many neurodegenerative diseases, and extensive communication exists between the two cell types. Since TRPV1 mediates stress responses in both RGCs and astrocytes, modulating TRPV1 activity might serve as a viable therapeutic option to target both neuronal and glial functions in disease. Reducing glial reactivity and migration while increasing neuronal survival could significantly improve outcomes in neurodegenerative diseases.

REFERENCES

Aarts, M.M., and Tymianski, M. (2005). TRPMs and neuronal cell death. Pflugers Arch *451*, 243-249.

Abbott, N.J., Ronnback, L., and Hansson, E. (2006). Astrocyte-endothelial interactions at the blood-brain barrier. Nat Rev Neurosci *7*, 41-53.

Agapova, O.A., Ricard, C.S., Salvador-Silva, M., and Hernandez, M.R. (2001). Expression of matrix metalloproteinases and tissue inhibitors of metalloproteinases in human optic nerve head astrocytes. Glia *33*, 205-216.

Agulhon, C., Sun, M.Y., Murphy, T., Myers, T., Lauderdale, K., and Fiacco, T.A. (2012). Calcium Signaling and Gliotransmission in Normal vs. Reactive Astrocytes. Frontiers in pharmacology *3*, 139.

Ahlemeyer, B., Kehr, K., Richter, E., Hirz, M., Baumgart-Vogt, E., and Herden, C. (2013). Phenotype, differentiation, and function differ in rat and mouse neocortical astrocytes cultured under the same conditions. J Neurosci Methods *212*, 156-164.

Akerman, K.E. (1978). Changes in membrane potential during calcium ion influx and efflux across the mitochondrial membrane. Biochim Biophys Acta *502*, 359-366.

Allan, S.M., Tyrrell, P.J., and Rothwell, N.J. (2005). Interleukin-1 and neuronal injury. Nat Rev Immunol *5*, 629-640.

Allen, A., and Messier, C. (2013). Plastic changes in the astrocyte GLUT1 glucose transporter and beta-tubulin microtubule protein following voluntary exercise in mice. Behav Brain Res *240*, 95-102.

Amadesi, S., Cottrell, G.S., Divino, L., Chapman, K., Grady, E.F., Bautista, F., Karanjia, R., Barajas-Lopez, C., Vanner, S., Vergnolle, N., *et al.* (2006). Protease-activated receptor 2 sensitizes TRPV1 by protein kinase Cepsilon- and A-dependent mechanisms in rats and mice. J Physiol *575*, 555-571.

Amantini, C., Mosca, M., Nabissi, M., Lucciarini, R., Caprodossi, S., Arcella, A., Giangaspero, F., and Santoni, G. (2007). Capsaicin-induced apoptosis of glioma cells is mediated by TRPV1 vanilloid receptor and requires p38 MAPK activation. J Neurochem *102*, 977-990.

Anderova, M., Kubinova, S., Mazel, T., Chvatal, A., Eliasson, C., Pekny, M., and Sykova, E. (2001). Effect of elevated K(+), hypotonic stress, and cortical spreading depression on astrocyte swelling in GFAP-deficient mice. Glia *35*, 189-203.

Appel, E., Kolman, O., Kazimirsky, G., Blumberg, P.M., and Brodie, C. (1997). Regulation of GDNF expression in cultured astrocytes by inflammatory stimuli. Neuroreport *8*, 3309-3312.

Bai, J.Z., and Lipski, J. (2010). Differential expression of TRPM2 and TRPV4 channels and their potential role in oxidative stress-induced cell death in organotypic hippocampal culture. Neurotoxicology *31*, 204-214.

Baorto, D.M., Mellado, W., and Shelanski, M.L. (1992). Astrocyte process growth induction by actin breakdown. J Cell Biol *117*, 357-367.

Barbeito, L.H., Pehar, M., Cassina, P., Vargas, M.R., Peluffo, H., Viera, L., Estevez, A.G., and Beckman, J.S. (2004). A role for astrocytes in motor neuron loss in amyotrophic lateral sclerosis. Brain Res Brain Res Rev *47*, 263-274.

Basu, S., and Srivastava, P. (2005). Immunological role of neuronal receptor vanilloid receptor 1 expressed on dendritic cells. Proc Natl Acad Sci U S A *102*, 5120-5125.

Bay, V., and Butt, A.M. (2012). Relationship between glial potassium regulation and axon excitability: a role for glial Kir4.1 channels. Glia *60*, 651-660.

Belanger, M., Allaman, I., and Magistretti, P.J. (2011). Brain energy metabolism: focus on astrocyte-neuron metabolic cooperation. Cell Metab *14*, 724-738.

Benfenati, V., Amiry-Moghaddam, M., Caprini, M., Mylonakou, M.N., Rapisarda, C., Ottersen, O.P., and Ferroni, S. (2007). Expression and functional characterization of transient receptor potential vanilloid-related channel 4 (TRPV4) in rat cortical astrocytes. Neuroscience *148*, 876-892.

Berchtold, M.W., Brinkmeier, H., and Muntener, M. (2000). Calcium ion in skeletal muscle: its crucial role for muscle function, plasticity, and disease. Physiol Rev *80*, 1215-1265.

Bershadsky, A., Chausovsky, A., Becker, E., Lyubimova, A., and Geiger, B. (1996). Involvement of microtubules in the control of adhesion-dependent signal transduction. Curr Biol *6*, 1279-1289.

Beskina, O., Miller, A., Mazzocco-Spezzia, A., Pulina, M.V., and Golovina, V.A. (2007). Mechanisms of interleukin-1beta-induced Ca2+ signals in mouse cortical astrocytes: roles of store- and receptor-operated Ca2+ entry. Am J Physiol Cell Physiol *293*, C1103-1111.

Bevan, S., Hothi, S., Hughes, G., James, I.F., Rang, H.P., Shah, K., Walpole, C.S., and Yeats, J.C. (1992). Capsazepine: a competitive antagonist of the sensory neurone excitant capsaicin. Br J Pharmacol *107*, 544-552.

Bhatt, A., Kaverina, I., Otey, C., and Huttenlocher, A. (2002). Regulation of focal complex composition and disassembly by the calcium-dependent protease calpain. J Cell Sci *115*, 3415-3425.

Bhave, G., Zhu, W., Wang, H., Brasier, D.J., Oxford, G.S., and Gereau, R.W.t. (2002). cAMP-dependent protein kinase regulates desensitization of the capsaicin receptor (VR1) by direct phosphorylation. Neuron *35*, 721-731.

Bonnington, J.K., and McNaughton, P.A. (2003). Signalling pathways involved in the sensitisation of mouse nociceptive neurones by nerve growth factor. J Physiol *551*, 433-446.

Boukhelifa, M., Hwang, S.J., Valtschanoff, J.G., Meeker, R.B., Rustioni, A., and Otey, C.A. (2003). A critical role for palladin in astrocyte morphology and response to injury. Mol Cell Neurosci *23*, 661-668.

Bradley, S.J., and Challiss, R.A. (2012). G protein-coupled receptor signalling in astrocytes in health and disease: a focus on metabotropic glutamate receptors. Biochem Pharmacol *84*, 249-259.

Bressler, J.P., Grotendorst, G.R., Levitov, C., and Hjelmeland, L.M. (1985). Chemotaxis of rat brain astrocytes to platelet derived growth factor. Brain Res *344*, 249-254.

Broussard, J.A., Webb, D.J., and Kaverina, I. (2008). Asymmetric focal adhesion disassembly in motile cells. Curr Opin Cell Biol *20*, 85-90.

Brundage, R.A., Fogarty, K.E., Tuft, R.A., and Fay, F.S. (1991). Calcium gradients underlying polarization and chemotaxis of eosinophils. Science *254*, 703-706.

Buffo, A., Rolando, C., and Ceruti, S. (2010). Astrocytes in the damaged brain: molecular and cellular insights into their reactive response and healing potential. Biochem Pharmacol *79*, 77-89.

Butenko, O., Dzamba, D., Benesova, J., Honsa, P., Benfenati, V., Rusnakova, V., Ferroni, S., and Anderova, M. (2012). The increased activity of TRPV4 channel in the astrocytes of the adult rat hippocampus after cerebral hypoxia/ischemia. PLoS One *7*, e39959.

Butt, A.M., Duncan, A., and Berry, M. (1994). Astrocyte associations with nodes of Ranvier: ultrastructural analysis of HRP-filled astrocytes in the mouse optic nerve. J Neurocytol *23*, 486-499.

Cahoy, J.D., Emery, B., Kaushal, A., Foo, L.C., Zamanian, J.L., Christopherson, K.S., Xing, Y., Lubischer, J.L., Krieg, P.A., Krupenko, S.A., *et al.* (2008). A transcriptome database for astrocytes, neurons, and oligodendrocytes: a new resource for understanding brain development and function. J Neurosci *28*, 264-278.

Cai, R., Ding, X., Zhou, K., Shi, Y., Ge, R., Ren, G., Jin, Y., and Wang, Y. (2009). Blockade of TRPC6 channels induced G2/M phase arrest and suppressed growth in human gastric cancer cells. International journal of cancer Journal international du cancer *125*, 2281-2287.

Calkins, D.J. (2012). Critical pathogenic events underlying progression of neurodegeneration in glaucoma. Prog Retin Eye Res *31*, 702-719.

Calzada, J.I., Jones, B.E., Netland, P.A., and Johnson, D.A. (2002). Glutamate-induced excitotoxicity in retina: neuroprotection with receptor antagonist, dextromethorphan, but not with calcium channel blockers. Neurochem Res *27*, 79-88.

Caterina, M.J., and Julius, D. (2001). The vanilloid receptor: a molecular gateway to the pain pathway. Annu Rev Neurosci *24*, 487-517.

Caterina, M.J., Leffler, A., Malmberg, A.B., Martin, W.J., Trafton, J., Petersen-Zeitz, K.R., Koltzenburg, M., Basbaum, A.I., and Julius, D. (2000). Impaired nociception and pain sensation in mice lacking the capsaicin receptor. Science *288*, 306-313.

Caterina, M.J., Schumacher, M.A., Tominaga, M., Rosen, T.A., Levine, J.D., and Julius, D. (1997). The capsaicin receptor: a heat-activated ion channel in the pain pathway. Nature *389*, 816-824.

Catterall, W.A., and Few, A.P. (2008). Calcium channel regulation and presynaptic plasticity. Neuron *59*, 882-901.

Chan, K.T., Bennin, D.A., and Huttenlocher, A. (2010). Regulation of adhesion dynamics by calpain-mediated proteolysis of focal adhesion kinase (FAK). J Biol Chem *285*, 11418-11426.

Chang, L., and Goldman, R.D. (2004). Intermediate filaments mediate cytoskeletal crosstalk. Nat Rev Mol Cell Biol *5*, 601-613.

Chard, P.S., Bleakman, D., Savidge, J.R., and Miller, R.J. (1995). Capsaicin-induced neurotoxicity in cultured dorsal root ganglion neurons: involvement of calcium-activated proteases. Neuroscience *65*, 1099-1108.

Charles, A.C., Merrill, J.E., Dirksen, E.R., and Sanderson, M.J. (1991). Intercellular signaling in glial cells: calcium waves and oscillations in response to mechanical stimulation and glutamate. Neuron *6*, 983-992.

Chavez, A.E., Chiu, C.Q., and Castillo, P.E. (2010). TRPV1 activation by endogenous anandamide triggers postsynaptic long-term depression in dentate gyrus. Nat Neurosci *13*, 1511-1518.

Chen, Y., Willcockson, H.H., and Valtschanoff, J.G. (2009). Influence of the vanilloid receptor TRPV1 on the activation of spinal cord glia in mouse models of pain. Exp Neurol *220*, 383-390.

Chesler, M. (2003). Regulation and modulation of pH in the brain. Physiol Rev *83*, 1183-1221.

Christensen, A.P., and Corey, D.P. (2007). TRP channels in mechanosensation: direct or indirect activation? Nat Rev Neurosci *8*, 510-521.

Chrzanowska-Wodnicka, M., and Burridge, K. (1996). Rho-stimulated contractility drives the formation of stress fibers and focal adhesions. J Cell Biol *133*, 1403-1415.

Chung, C.Y., Murphy-Ullrich, J.E., and Erickson, H.P. (1996). Mitogenesis, cell migration, and loss of focal adhesions induced by tenascin-C interacting with its cell surface receptor, annexin II. Mol Biol Cell *7*, 883-892.

Chung, W.S., Clarke, L.E., Wang, G.X., Stafford, B.K., Sher, A., Chakraborty, C., Joung, J., Foo, L.C., Thompson, A., Chen, C., *et al.* (2013). Astrocytes mediate synapse elimination through MEGF10 and MERTK pathways. Nature *504*, 394-400.

Clapham, D.E., Runnels, L.W., and Strubing, C. (2001). The TRP ion channel family. Nat Rev Neurosci *2*, 387-396.

Codeluppi, S., Fernandez-Zafra, T., Sandor, K., Kjell, J., Liu, Q., Abrams, M., Olson, L., Gray, N.S., Svensson, C.I., and Uhlen, P. (2014). Interleukin-6 secretion by astrocytes is dynamically regulated by PI3K-mTOR-calcium signaling. PLoS One *9*, e92649.

Colombo, J.A. (1996). Interlaminar astroglial processes in the cerebral cortex of adult monkeys but not of adult rats. Acta Anat (Basel) *155*, 57-62.

Colombo, J.A., Yanez, A., Puissant, V., and Lipina, S. (1995). Long, interlaminar astroglial cell processes in the cortex of adult monkeys. J Neurosci Res *40*, 551-556.

Cong, X., Zhang, Y., Yang, N.Y., Li, J., Ding, C., Ding, Q.W., Su, Y.C., Mei, M., Guo, X.H., Wu, L.L., *et al.* (2013). Occludin is required for TRPV1-modulated paracellular permeability in the submandibular gland. J Cell Sci *126*, 1109-1121.

Conklin, M.W., Lin, M.S., and Spitzer, N.C. (2005). Local calcium transients contribute to disappearance of pFAK, focal complex removal and deadhesion of neuronal growth cones and fibroblasts. Dev Biol *287*, 201-212.

Cornell-Bell, A.H., Finkbeiner, S.M., Cooper, M.S., and Smith, S.J. (1990). Glutamate induces calcium waves in cultured astrocytes: long-range glial signaling. Science *247*, 470-473.

Correll, C.C., Phelps, P.T., Anthes, J.C., Umland, S., and Greenfeder, S. (2004). Cloning and pharmacological characterization of mouse TRPV1. Neurosci Lett *370*, 55-60.

Cotrina, M.L., Lin, J.H., and Nedergaard, M. (1998). Cytoskeletal assembly and ATP release regulate astrocytic calcium signaling. J Neurosci *18*, 8794-8804.

Couchie, D., Fages, C., Bridoux, A.M., Rolland, B., Tardy, M., and Nunez, J. (1985). Microtubule-associated proteins and in vitro astrocyte differentiation. J Cell Biol *101*, 2095-2103.

Crabtree, G.R. (2001). Calcium, calcineurin, and the control of transcription. J Biol Chem *276*, 2313-2316.

Crish, S.D., Dapper, J.D., MacNamee, S.E., Balaram, P., Sidorova, T.N., Lambert, W.S., and Calkins, D.J. (2013). Failure of axonal transport induces a spatially coincident increase in astrocyte BDNF prior to synapse loss in a central target. Neuroscience *229*, 55-70.

Crish, S.D., Sappington, R.M., Inman, D.M., Horner, P.J., and Calkins, D.J. (2010). Distal axonopathy with structural persistence in glaucomatous neurodegeneration. Proc Natl Acad Sci U S A *107*, 5196-5201.

Cui, K., and Yuan, X. (2007). TRP Channels and Axon Pathfinding.

Cvetkovic, I., Miljkovic, D., Vuckovic, O., Harhaji, L., Nikolic, Z., Trajkovic, V., and Mostarica Stojkovic, M. (2004). Taxol activates inducible nitric oxide synthase in rat astrocytes: the role of MAP kinases and NF-kappaB. Cell Mol Life Sci *61*, 1167-1175.

Demuth, T., and Berens, M.E. (2004). Molecular mechanisms of glioma cell migration and invasion. J Neurooncol *70*, 217-228.

den Dekker, E., Hoenderop, J.G., Nilius, B., and Bindels, R.J. (2003). The epithelial calcium channels, TRPV5 & TRPV6: from identification towards regulation. Cell Calcium *33*, 497-507.

Denker, S.P., and Barber, D.L. (2002). Cell migration requires both ion translocation and cytoskeletal anchoring by the Na-H exchanger NHE1. J Cell Biol *159*, 1087-1096.

Derouiche, A., and Rauen, T. (1995). Coincidence of L-glutamate/L-aspartate transporter (GLAST) and glutamine synthetase (GS) immunoreactions in retinal glia: evidence for coupling of GLAST and GS in transmitter clearance. J Neurosci Res *42*, 131-143.

DeWitt, D.A., Perry, G., Cohen, M., Doller, C., and Silver, J. (1998). Astrocytes regulate microglial phagocytosis of senile plaque cores of Alzheimer's disease. Exp Neurol *149*, 329-340.

Di Giovanni, S., Movsesyan, V., Ahmed, F., Cernak, I., Schinelli, S., Stoica, B., and Faden, A.I. (2005). Cell cycle inhibition provides neuroprotection and reduces glial proliferation and scar formation after traumatic brain injury. Proc Natl Acad Sci U S A *102*, 8333-8338.

Dickenson, A.H., and Dray, A. (1991). Selective antagonism of capsaicin by capsazepine: evidence for a spinal receptor site in capsaicin-induced antinociception. Br J Pharmacol *104*, 1045-1049.

Docherty, R.J., Yeats, J.C., and Piper, A.S. (1997). Capsazepine block of voltage-activated calcium channels in adult rat dorsal root ganglion neurones in culture. Br J Pharmacol *121*, 1461-1467.

Doly, S., Fischer, J., Salio, C., and Conrath, M. (2004). The vanilloid receptor-1 is expressed in rat spinal dorsal horn astrocytes. Neurosci Lett *357*, 123-126.

Dominguez, R., and Holmes, K.C. (2011). Actin structure and function. Annu Rev Biophys *40*, 169-186.

Dong, Y., and Benveniste, E.N. (2001). Immune function of astrocytes. Glia *36*, 180-190.

Dorf, M.E., Berman, M.A., Tanabe, S., Heesen, M., and Luo, Y. (2000). Astrocytes express functional chemokine receptors. J Neuroimmunol *111*, 109-121.

Dorrell, M.I., Aguilar, E., and Friedlander, M. (2002). Retinal vascular development is mediated by endothelial filopodia, a preexisting astrocytic template and specific R-cadherin adhesion. Invest Ophthalmol Vis Sci *43*, 3500-3510.

Dorrell, M.I., Aguilar, E., Jacobson, R., Trauger, S.A., Friedlander, J., Siuzdak, G., and Friedlander, M. (2010). Maintaining retinal astrocytes normalizes revascularization and prevents vascular pathology associated with oxygen-induced retinopathy. Glia *58*, 43-54.

dos Remedios, C.G., Chhabra, D., Kekic, M., Dedova, I.V., Tsubakihara, M., Berry, D.A., and Nosworthy, N.J. (2003). Actin binding proteins: regulation of cytoskeletal microfilaments. Physiol Rev *83*, 433-473.

Dourdin, N., Bhatt, A.K., Dutt, P., Greer, P.A., Arthur, J.S., Elce, J.S., and Huttenlocher, A. (2001). Reduced cell migration and disruption of the actin cytoskeleton in calpain-deficient embryonic fibroblasts. J Biol Chem *276*, 48382-48388.

Downs, J.C., Roberts, M.D., and Burgoyne, C.F. (2008). Mechanical environment of the optic nerve head in glaucoma. Optom Vis Sci *85*, 425-435.

Du, S., Rubin, A., Klepper, S., Barrett, C., Kim, Y.C., Rhim, H.W., Lee, E.B., Park, C.W., Markelonis, G.J., and Oh, T.H. (1999). Calcium influx and activation of calpain I mediate acute reactive gliosis in injured spinal cord. Exp Neurol *157*, 96-105.

Dunn, T.A., Storm, D.R., and Feller, M.B. (2009). Calcium-dependent increases in protein kinase-A activity in mouse retinal ganglion cells are mediated by multiple adenylate cyclases. PLoS One *4*, e7877.

Dupin, I., Sakamoto, Y., and Etienne-Manneville, S. (2011). Cytoplasmic intermediate filaments mediate actin-driven positioning of the nucleus. J Cell Sci *124*, 865-872.

Easley, C.A.t., Brown, C.M., Horwitz, A.F., and Tombes, R.M. (2008). CaMK-II promotes focal adhesion turnover and cell motility by inducing tyrosine dephosphorylation of FAK and paxillin. Cell Motil Cytoskeleton *65*, 662-674.

Eckes, B., Dogic, D., Colucci-Guyon, E., Wang, N., Maniotis, A., Ingber, D., Merckling, A., Langa, F., Aumailley, M., Delouvee, A., *et al.* (1998). Impaired mechanical stability, migration and contractile capacity in vimentin-deficient fibroblasts. J Cell Sci *111 (Pt 13)*, 1897-1907.

Edwards, J.G., Gibson, H.E., Jensen, T., Nugent, F., Walther, C., Blickenstaff, J., and Kauer, J.A. (2012). A novel non-CB1/TRPV1 endocannabinoid-mediated mechanism depresses excitatory synapses on hippocampal CA1 interneurons. Hippocampus *22*, 209-221.

Efendiev, R., Bavencoffe, A., Hu, H., Zhu, M.X., and Dessauer, C.W. (2013). Scaffolding by A-kinase anchoring protein enhances functional coupling between adenylyl cyclase and TRPV1 channel. J Biol Chem *288*, 3929-3937.

Egnaczyk, G.F., Pomonis, J.D., Schmidt, J.A., Rogers, S.D., Peters, C., Ghilardi, J.R., Mantyh, P.W., and Maggio, J.E. (2003). Proteomic analysis of the reactive phenotype of astrocytes following endothelin-1 exposure. Proteomics *3*, 689-698.

Ehtesham, M., Black, K.L., and Yu, J.S. (2004). Recent progress in immunotherapy for malignant glioma: treatment strategies and results from clinical trials. Cancer Control *11*, 192-207.

Eliasson, C., Sahlgren, C., Berthold, C.H., Stakeberg, J., Celis, J.E., Betsholtz, C., Eriksson, J.E., and Pekny, M. (1999). Intermediate filament protein partnership in astrocytes. J Biol Chem *274*, 23996-24006.

Ellingson, J.M., Silbaugh, B.C., and Brasser, S.M. (2009). Reduced oral ethanol avoidance in mice lacking transient receptor potential channel vanilloid receptor 1. Behavior genetics *39*, 62-72.

Elobeid, A., Bongcam-Rudloff, E., Westermark, B., and Nister, M. (2000). Effects of inducible glial fibrillary acidic protein on glioma cell motility and proliferation. J Neurosci Res *60*, 245-256.

Emsley, J.G., and Macklis, J.D. (2006). Astroglial heterogeneity closely reflects the neuronal-defined anatomy of the adult murine CNS. Neuron Glia Biol *2*, 175-186.

Etienne-Manneville, S. (2004). Cdc42--the centre of polarity. J Cell Sci *117*, 1291-1300.

Etienne-Manneville, S. (2006). In vitro assay of primary astrocyte migration as a tool to study Rho GTPase function in cell polarization. Methods Enzymol *406*, 565-578.

Etienne-Manneville, S. (2013). Microtubules in cell migration. Annu Rev Cell Dev Biol *29*, 471-499.

Etienne-Manneville, S., and Hall, A. (2001). Integrin-mediated activation of Cdc42 controls cell polarity in migrating astrocytes through PKCzeta. Cell *106*, 489-498.

Etienne-Manneville, S., and Hall, A. (2002). Rho GTPases in cell biology. Nature *420*, 629-635.

Etienne-Manneville, S., and Hall, A. (2003). Cdc42 regulates GSK-3beta and adenomatous polyposis coli to control cell polarity. Nature *421*, 753-756.

Farin, A., Suzuki, S.O., Weiker, M., Goldman, J.E., Bruce, J.N., and Canoll, P. (2006). Transplanted glioma cells migrate and proliferate on host brain vasculature: a dynamic analysis. Glia *53*, 799-808.

Fernandez, D.C., Pasquini, L.A., Dorfman, D., Aldana Marcos, H.J., and Rosenstein, R.E. (2012a). Early distal axonopathy of the visual pathway in experimental diabetes. Am J Pathol *180*, 303-313.

Fernandez, D.C., Pasquini, L.A., Dorfman, D., Aldana Marcos, H.J., and Rosenstein, R.E. (2012b). Ischemic conditioning protects from axoglial alterations of the optic pathway induced by experimental diabetes in rats. PLoS One *7*, e51966.

Ferrini, F., Salio, C., Vergnano, A.M., and Merighi, A. (2007). Vanilloid receptor-1 (TRPV1)-dependent activation of inhibitory neurotransmission in spinal substantia gelatinosa neurons of mouse. Pain *129*, 195-209.

Figiel, I. (2008). Pro-inflammatory cytokine TNF-alpha as a neuroprotective agent in the brain. Acta Neurobiol Exp (Wars) *68*, 526-534.

Fiorio Pla, A., and Gkika, D. (2013). Emerging role of TRP channels in cell migration: from tumor vascularization to metastasis. Front Physiol *4*, 311.

Flicek, P., Amode, M.R., Barrell, D., Beal, K., Billis, K., Brent, S., Carvalho-Silva, D., Clapham, P., Coates, G., Fitzgerald, S., *et al.* (2014). Ensembl 2014. Nucleic Acids Research *42*, D749-D755.

Fok-Seang, J., Mathews, G.A., ffrench-Constant, C., Trotter, J., and Fawcett, J.W. (1995). Migration of oligodendrocyte precursors on astrocytes and meningeal cells. Dev Biol *171*, 1-15.

Frame, M.C., Fincham, V.J., Carragher, N.O., and Wyke, J.A. (2002). v-Src's hold over actin and cell adhesions. Nat Rev Mol Cell Biol *3*, 233-245.

Franco, S.J., Rodgers, M.A., Perrin, B.J., Han, J., Bennin, D.A., Critchley, D.R., and Huttenlocher, A. (2004). Calpain-mediated proteolysis of talin regulates adhesion dynamics. Nat Cell Biol *6*, 977-983.

Fresu, L., Dehpour, A., Genazzani, A.A., Carafoli, E., and Guerini, D. (1999). Plasma membrane calcium ATPase isoforms in astrocytes. Glia *28*, 150-155.

Fukuda, A.M., and Badaut, J. (2012). Aquaporin 4: a player in cerebral edema and neuroinflammation. J Neuroinflammation *9*, 279.

Fumagalli, M., Brambilla, R., D'Ambrosi, N., Volonte, C., Matteoli, M., Verderio, C., and Abbracchio, M.P. (2003). Nucleotide-mediated calcium signaling in rat cortical astrocytes: Role of P2X and P2Y receptors. Glia *43*, 218-203.

Galli, A., and DeFelice, L.J. (1994). Inactivation of L-type Ca channels in embryonic chick ventricle cells: dependence on the cytoskeletal agents colchicine and taxol. Biophys J *67*, 2296-2304.

Gao, K., Wang, C.R., Jiang, F., Wong, A.Y., Su, N., Jiang, J.H., Chai, R.C., Vatcher, G., Teng, J., Chen, J., *et al.* (2013). Traumatic scratch injury in astrocytes triggers calcium influx to activate the JNK/c-Jun/AP-1 pathway and switch on GFAP expression. Glia *61*, 2063-2077.

Garcia-Sanz, N., Fernandez-Carvajal, A., Morenilla-Palao, C., Planells-Cases, R., Fajardo-Sanchez, E., Fernandez-Ballester, G., and Ferrer-Montiel, A. (2004). Identification of a tetramerization domain in the C terminus of the vanilloid receptor. J Neurosci *24*, 5307-5314.

Gardel, M.L., Schneider, I.C., Aratyn-Schaus, Y., and Waterman, C.M. (2010). Mechanical integration of actin and adhesion dynamics in cell migration. Annu Rev Cell Dev Biol *26*, 315-333.

Gavva, N.R., Klionsky, L., Qu, Y., Shi, L., Tamir, R., Edenson, S., Zhang, T.J., Viswanadhan, V.N., Toth, A., Pearce, L.V., *et al.* (2004). Molecular determinants of vanilloid sensitivity in TRPV1. J Biol Chem *279*, 20283-20295.

Gazzieri, D., Trevisani, M., Springer, J., Harrison, S., Cottrell, G.S., Andre, E., Nicoletti, P., Massi, D., Zecchi, S., Nosi, D., *et al.* (2007). Substance P released by TRPV1-expressing neurons produces reactive oxygen species that mediate ethanol-induced gastric injury. Free Radic Biol Med *43*, 581-589.

Geisert, E.E., Jr., Johnson, H.G., and Binder, L.I. (1990). Expression of microtubule-associated protein 2 by reactive astrocytes. Proc Natl Acad Sci U S A *87*, 3967-3971.

Ghert, M.A., Qi, W.N., Erickson, H.P., Block, J.A., and Scully, S.P. (2001). Tenascin-C splice variant adhesive/anti-adhesive effects on chondrosarcoma cell attachment to fibronectin. Cell Struct Funct *26*, 179-187.

Giaume, C., Koulakoff, A., Roux, L., Holcman, D., and Rouach, N. (2010). Astroglial networks: a step further in neuroglial and gliovascular interactions. Nat Rev Neurosci *11*, 87-99.

Gibson, H.E., Edwards, J.G., Page, R.S., Van Hook, M.J., and Kauer, J.A. (2008). TRPV1 channels mediate long-term depression at synapses on hippocampal interneurons. Neuron *57*, 746-759.

Gionfriddo, J.R., Freeman, K.S., Groth, A., Scofield, V.L., Alyahya, K., and Madl, J.E. (2009). alpha-Luminol prevents decreases in glutamate, glutathione, and glutamine synthetase in the retinas of glaucomatous DBA/2J mice. Vet Ophthalmol *12*, 325-332.

Glading, A., Lauffenburger, D.A., and Wells, A. (2002). Cutting to the chase: calpain proteases in cell motility. Trends in cell biology *12*, 46-54.

Goetschy, J.F., Ulrich, G., Aunis, D., and Ciesielski-Treska, J. (1986). The organization and solubility properties of intermediate filaments and microtubules of cortical astrocytes in culture. J Neurocytol *15*, 375-387.

Goldman, R.S., Finkbeiner, S.M., and Smith, S.J. (1991). Endothelin induces a sustained rise in intracellular calcium in hippocampal astrocytes. Neurosci Lett *123*, 4-8.

Goldman, W.F., Yarowsky, P.J., Juhaszova, M., Krueger, B.K., and Blaustein, M.P. (1994). Sodium/calcium exchange in rat cortical astrocytes. J Neurosci *14*, 5834-5843.

Goldstein, L.S., and Yang, Z. (2000). Microtubule-based transport systems in neurons: the roles of kinesins and dyneins. Annu Rev Neurosci *23*, 39-71.

Golovina, V.A. (2005). Visualization of localized store-operated calcium entry in mouse astrocytes. Close proximity to the endoplasmic reticulum. J Physiol *564*, 737-749.

Goswami, C., Dreger, M., Jahnel, R., Bogen, O., Gillen, C., and Hucho, F. (2004). Identification and characterization of a Ca2+ -sensitive interaction of the vanilloid receptor TRPV1 with tubulin. J Neurochem *91*, 1092-1103.

Goswami, C., Dreger, M., Otto, H., Schwappach, B., and Hucho, F. (2006). Rapid disassembly of dynamic microtubules upon activation of the capsaicin receptor TRPV1. J Neurochem *96*, 254-266.

Goswami, C., and Hucho, T. (2007). TRPV1 expression-dependent initiation and regulation of filopodia. J Neurochem *103*, 1319-1333.

Goswami, C., Kuhn, J., Heppenstall, P.A., and Hucho, T. (2010). Importance of non-selective cation channel TRPV4 interaction with cytoskeleton and their reciprocal regulations in cultured cells. PLoS One *5*, e11654.

Goswami, C., Schmidt, H., and Hucho, F. (2007). TRPV1 at nerve endings regulates growth cone morphology and movement through cytoskeleton reorganization. FEBS J *274*, 760-772.

Griffith, L.C. (2004). Regulation of calcium/calmodulin-dependent protein kinase II activation by intramolecular and intermolecular interactions. J Neurosci *24*, 8394-8398.

Grimaldi, M., Maratos, M., and Verma, A. (2003). Transient receptor potential channel activation causes a novel form of [Ca 2+]I oscillations and is not involved in capacitative Ca 2+ entry in glial cells. J Neurosci *23*, 4737-4745.

Grueter, B.A., Brasnjo, G., and Malenka, R.C. (2010). Postsynaptic TRPV1 triggers cell type-specific long-term depression in the nucleus accumbens. Nat Neurosci *13*, 1519-1525.

Guthrie, P.B., Knappenberger, J., Segal, M., Bennett, M.V., Charles, A.C., and Kater, S.B. (1999). ATP released from astrocytes mediates glial calcium waves. J Neurosci *19*, 520-528.

Hagenacker, T., Ledwig, D., and Busselberg, D. (2008). Feedback mechanisms in the regulation of intracellular calcium ([Ca2+]i) in the peripheral nociceptive system: role of TRPV-1 and pain related receptors. Cell Calcium *43*, 215-227.

Hamilton, N., Vayro, S., Kirchhoff, F., Verkhratsky, A., Robbins, J., Gorecki, D.C., and Butt, A.M. (2008). Mechanisms of ATP- and glutamate-mediated calcium signaling in white matter astrocytes. Glia *56*, 734-749.

Hamilton, N.B., and Attwell, D. (2010). Do astrocytes really exocytose neurotransmitters? Nat Rev Neurosci *11*, 227-238.

Han, P., McDonald, H.A., Bianchi, B.R., Kouhen, R.E., Vos, M.H., Jarvis, M.F., Faltynek, C.R., and Moreland, R.B. (2007). Capsaicin causes protein synthesis inhibition and microtubule disassembly through TRPV1 activities both on the plasma membrane and intracellular membranes. Biochem Pharmacol *73*, 1635-1645.

Hassan, S., Eldeeb, K., Millns, P.J., Bennett, A.J., Alexander, S.P., and Kendall, D.A. (2014). Cannabidiol enhances microglial phagocytosis via transient receptor potential (TRP) channel activation. Br J Pharmacol *171*, 2426-2439.

Hellal, F., Hurtado, A., Ruschel, J., Flynn, K.C., Laskowski, C.J., Umlauf, M., Kapitein, L.C., Strikis, D., Lemmon, V., Bixby, J., *et al.* (2011). Microtubule stabilization reduces scarring and causes axon regeneration after spinal cord injury. Science *331*, 928-931.

Hernandez, M.R. (1992). Ultrastructural immunocytochemical analysis of elastin in the human lamina cribrosa. Changes in elastic fibers in primary open-angle glaucoma. Invest Ophthalmol Vis Sci *33*, 2891-2903.

Hernandez, M.R. (2000). The optic nerve head in glaucoma: role of astrocytes in tissue remodeling. Prog Retin Eye Res *19*, 297-321.

Hernandez, M.R., Miao, H., and Lukas, T. (2008). Astrocytes in glaucomatous optic neuropathy. Prog Brain Res *173*, 353-373.

Hernandez, M.R., Wang, N., Hanley, N.M., and Neufeld, A.H. (1991). Localization of collagen types I and IV mRNAs in human optic nerve head by in situ hybridization. Invest Ophthalmol Vis Sci *32*, 2169-2177.

Herrmann, H., Bar, H., Kreplak, L., Strelkov, S.V., and Aebi, U. (2007). Intermediate filaments: from cell architecture to nanomechanics. Nat Rev Mol Cell Biol *8*, 562-573.

Hicks, D., and Courtois, Y. (1990). The growth and behaviour of rat retinal Muller cells in vitro. 1. An improved method for isolation and culture. Exp Eye Res *51*, 119-129.

Himi, N., Hamaguchi, A., Hashimoto, K., Koga, T., Narita, K., and Miyamoto, O. (2012). Calcium influx through the TRPV1 channel of endothelial cells (ECs) correlates with a stronger adhesion between monocytes and ECs. Adv Med Sci *57*, 224-229.

Ho, K.W., Ward, N.J., and Calkins, D.J. (2012). TRPV1: a stress response protein in the central nervous system. Am J Neurodegener Dis *1*, 1-14.

Hochstim, C., Deneen, B., Lukaszewicz, A., Zhou, Q., and Anderson, D.J. (2008). Identification of positionally distinct astrocyte subtypes whose identities are specified by a homeodomain code. Cell *133*, 510-522.

Holliday, J., and Gruol, D.L. (1993). Cytokine stimulation increases intracellular calcium and alters the response to quisqualate in cultured cortical astrocytes. Brain Res *621*, 233-241.

Howarth, F.C., Calaghan, S.C., Boyett, M.R., and White, E. (1999). Effect of the microtubule polymerizing agent taxol on contraction, Ca2+ transient and L-type Ca2+ current in rat ventricular myocytes. J Physiol *516 (Pt 2)*, 409-419.

Howell, G.R., Soto, I., Libby, R.T., and John, S.W. (2013). Intrinsic axonal degeneration pathways are critical for glaucomatous damage. Exp Neurol *246*, 54-61.

Hsu, J.Y., Bourguignon, L.Y., Adams, C.M., Peyrollier, K., Zhang, H., Fandel, T., Cun, C.L., Werb, Z., and Noble-Haeusslein, L.J. (2008). Matrix metalloproteinase-9 facilitates glial scar formation in the injured spinal cord. J Neurosci *28*, 13467-13477.

Huang, C., Hu, Z.L., Wu, W.N., Yu, D.F., Xiong, Q.J., Song, J.R., Shu, Q., Fu, H., Wang, F., and Chen, J.G. (2010). Existence and distinction of acid-evoked currents in rat astrocytes. Glia *58*, 1415-1424.

Huang, G.N., Zeng, W., Kim, J.Y., Yuan, J.P., Han, L., Muallem, S., and Worley, P.F. (2006). STIM1 carboxyl-terminus activates native SOC, I(crac) and TRPC1 channels. Nat Cell Biol *8*, 1003-1010.

Huttenlocher, A., Palecek, S.P., Lu, Q., Zhang, W., Mellgren, R.L., Lauffenburger, D.A., Ginsberg, M.H., and Horwitz, A.F. (1997). Regulation of cell migration by the calcium-dependent protease calpain. J Biol Chem *272*, 32719-32722.

Hyduk, S.J., Chan, J.R., Duffy, S.T., Chen, M., Peterson, M.D., Waddell, T.K., Digby, G.C., Szaszi, K., Kapus, A., and Cybulsky, M.I. (2007). Phospholipase C, calcium, and calmodulin are critical for alpha4beta1 integrin affinity up-regulation and monocyte arrest triggered by chemoattractants. Blood *109*, 176-184.

Inman, D.M., and Horner, P.J. (2007). Reactive nonproliferative gliosis predominates in a chronic mouse model of glaucoma. Glia *55*, 942-953.

Jeske, N.A., Diogenes, A., Ruparel, N.B., Fehrenbacher, J.C., Henry, M., Akopian, A.N., and Hargreaves, K.M. (2008). A-kinase anchoring protein mediates TRPV1 thermal hyperalgesia through PKA phosphorylation of TRPV1. Pain *138*, 604-616.

Jeske, N.A., Patwardhan, A.M., Henry, M.A., and Milam, S.B. (2009a). Fibronectin stimulates TRPV1 translocation in primary sensory neurons. J Neurochem *108*, 591-600.

Jeske, N.A., Patwardhan, A.M., Ruparel, N.B., Akopian, A.N., Shapiro, M.S., and Henry, M.A. (2009b). A-kinase anchoring protein 150 controls protein kinase C-mediated phosphorylation and sensitization of TRPV1. Pain *146*, 301-307.

Jiang, B., Liou, G.I., Behzadian, M.A., and Caldwell, R.B. (1994). Astrocytes modulate retinal vasculogenesis: effects on fibronectin expression. J Cell Sci *107 (Pt 9)*, 2499-2508.

Jiang, C.Y., Fujita, T., Yue, H.Y., Piao, L.H., Liu, T., Nakatsuka, T., and Kumamoto, E. (2009). Effect of resiniferatoxin on glutamatergic spontaneous excitatory synaptic transmission in substantia gelatinosa neurons of the adult rat spinal cord. Neuroscience *164*, 1833-1844.

John, G.R., Chen, L., Rivieccio, M.A., Melendez-Vasquez, C.V., Hartley, A., and Brosnan, C.F. (2004). Interleukin-1beta induces a reactive astroglial phenotype via deactivation of the Rho GTPase-Rock axis. J Neurosci *24*, 2837-2845.

Johnson, B.D., and Byerly, L. (1993). A cytoskeletal mechanism for Ca2+ channel metabolic dependence and inactivation by intracellular Ca2+. Neuron *10*, 797-804.

Jordt, S.E., and Julius, D. (2002). Molecular basis for species-specific sensitivity to "hot" chili peppers. Cell *108*, 421-430.

Jordt, S.E., Tominaga, M., and Julius, D. (2000). Acid potentiation of the capsaicin receptor determined by a key extracellular site. Proc Natl Acad Sci U S A *97*, 8134-8139.

Jost, V., Kuhn, I., Rogalla, K., Theiss, U., and Lucker, P.W. (1992). Gastric potential difference measurement as a quantification of gastrointestinal tolerability comparing a buffered acetylsalicylic acid formulation versus plain acetylsalicylic acid. Arzneimittelforschung *42*, 650-653.

Jung, J., Hwang, S.W., Kwak, J., Lee, S.Y., Kang, C.J., Kim, W.B., Kim, D., and Oh, U. (1999). Capsaicin binds to the intracellular domain of the capsaicin-activated ion channel. J Neurosci *19*, 529-538.

Jung, J., Lee, S.Y., Hwang, S.W., Cho, H., Shin, J., Kang, Y.S., Kim, S., and Oh, U. (2002). Agonist recognition sites in the cytosolic tails of vanilloid receptor 1. J Biol Chem *277*, 44448-44454.

Jung, J., Shin, J.S., Lee, S.Y., Hwang, S.W., Koo, J., Cho, H., and Oh, U. (2004). Phosphorylation of vanilloid receptor 1 by Ca2+/calmodulin-dependent kinase II regulates its vanilloid binding. J Biol Chem *279*, 7048-7054.

Kanemaru, K., Kubota, J., Sekiya, H., Hirose, K., Okubo, Y., and Iino, M. (2013). Calcium-dependent N-cadherin up-regulation mediates reactive astrogliosis and neuroprotection after brain injury. Proc Natl Acad Sci U S A *110*, 11612-11617.

Karai, L.J., Russell, J.T., Iadarola, M.J., and Olah, Z. (2004). Vanilloid receptor 1 regulates multiple calcium compartments and contributes to Ca2+-induced Ca2+ release in sensory neurons. J Biol Chem *279*, 16377-16387.

Karlsson, U., Sundgren-Andersson, A.K., Johansson, S., and Krupp, J.J. (2005). Capsaicin augments synaptic transmission in the rat medial preoptic nucleus. Brain Res *1043*, 1-11.

Kauer, J.A., and Gibson, H.E. (2009). Hot flash: TRPV channels in the brain. Trends Neurosci *32*, 215-224.

Keeble, J.E., and Brain, S.D. (2006). Capsaicin-induced vasoconstriction in the mouse knee joint: a study using TRPV1 knockout mice. Neurosci Lett *401*, 55-58.

Kerfant, B.G., Vassort, G., and Gomez, A.M. (2001). Microtubule disruption by colchicine reversibly enhances calcium signaling in intact rat cardiac myocytes. Circ Res *88*, E59-65.

Kim, S.R., Kim, S.U., Oh, U., and Jin, B.K. (2006). Transient receptor potential vanilloid subtype 1 mediates microglial cell death in vivo and in vitro via Ca2+-mediated mitochondrial damage and cytochrome c release. J Immunol *177*, 4322-4329.

Kim, S.R., Lee, D.Y., Chung, E.S., Oh, U.T., Kim, S.U., and Jin, B.K. (2005). Transient receptor potential vanilloid subtype 1 mediates cell death of mesencephalic dopaminergic neurons in vivo and in vitro. J Neurosci *25*, 662-671.

Klepper, S., Naftolin, F., and Piepmeier, J.M. (1995). Verapamil treatment attenuates immunoreactive GFAP at cerebral cortical lesion site. Brain Res *695*, 245-249.

Kobayashi, S., Vidal, I., Pena, J.D., and Hernandez, M.R. (1997). Expression of neural cell adhesion molecule (NCAM) characterizes a subpopulation of type 1 astrocytes in human optic nerve head. Glia *20*, 262-273.

Koller, H., Thiem, K., and Siebler, M. (1996). Tumour necrosis factor-alpha increases intracellular Ca2+ and induces a depolarization in cultured astroglial cells. Brain *119 (Pt 6)*, 2021-2027.

Konig, N., Raynaud, F., Feane, H., Durand, M., Mestre-Frances, N., Rossel, M., Ouali, A., and Benyamin, Y. (2003). Calpain 3 is expressed in astrocytes of rat and Microcebus brain. J Chem Neuroanat *25*, 129-136.

Koplas, P.A., Rosenberg, R.L., and Oxford, G.S. (1997). The role of calcium in the desensitization of capsaicin responses in rat dorsal root ganglion neurons. J Neurosci *17*, 3525-3537.

Koprich, J.B., Reske-Nielsen, C., Mithal, P., and Isacson, O. (2008). Neuroinflammation mediated by IL-1beta increases susceptibility of dopamine neurons to degeneration in an animal model of Parkinson's disease. J Neuroinflammation *5*, 8.

Korolainen, M.A., Auriola, S., Nyman, T.A., Alafuzoff, I., and Pirttila, T. (2005). Proteomic analysis of glial fibrillary acidic protein in Alzheimer's disease and aging brain. Neurobiol Dis *20*, 858-870.

Kraft, A.W., Hu, X., Yoon, H., Yan, P., Xiao, Q., Wang, Y., Gil, S.C., Brown, J., Wilhelmsson, U., Restivo, J.L., *et al.* (2013). Attenuating astrocyte activation accelerates plaque pathogenesis in APP/PS1 mice. FASEB J *27*, 187-198.

Kuang, C.Y., Yu, Y., Wang, K., Qian, D.H., Den, M.Y., and Huang, L. (2012). Knockdown of transient receptor potential canonical-1 reduces the proliferation and migration of endothelial progenitor cells. Stem cells and development *21*, 487-496.

Kuroi, T., Shimizu, T., Shibata, M., Toriumi, H., Funakubo, M., Iwashita, T., Sato, H., Koizumi, K., and Suzuki, N. (2012). Alterations in microglia and astrocytes in the trigeminal nucleus caudalis by repetitive TRPV1 stimulation on the trigeminal nociceptors. Neuroreport *23*, 560-565.

Laczko, R., Szauter, K.M., Jansen, M.K., Hollosi, P., Muranyi, M., Molnar, J., Fong, K.S., Hinek, A., and Csiszar, K. (2007). Active lysyl oxidase (LOX) correlates with focal adhesion kinase (FAK)/paxillin activation and migration in invasive astrocytes. Neuropathol Appl Neurobiol *33*, 631-643.

Lamb, J.A., Allen, P.G., Tuan, B.Y., and Janmey, P.A. (1993). Modulation of gelsolin function. Activation at low pH overrides Ca2+ requirement. J Biol Chem *268*, 8999-9004.

Lambert, W., Agarwal, R., Howe, W., Clark, A.F., and Wordinger, R.J. (2001). Neurotrophin and neurotrophin receptor expression by cells of the human lamina cribrosa. Invest Ophthalmol Vis Sci *42*, 2315-2323.

Lascola, C.D., Nelson, D.J., and Kraig, R.P. (1998). Cytoskeletal actin gates a Cl- channel in neocortical astrocytes. J Neurosci *18*, 1679-1692.

Latour, I., Hamid, J., Beedle, A.M., Zamponi, G.W., and Macvicar, B.A. (2003). Expression of voltage-gated Ca2+ channel subtypes in cultured astrocytes. Glia *41*, 347-353.

Lau, S.Y., Procko, E., and Gaudet, R. (2012). Distinct properties of Ca2+-calmodulin binding to N- and C-terminal regulatory regions of the TRPV1 channel. J Gen Physiol *140*, 541-555.

Laukaitis, C.M., Webb, D.J., Donais, K., and Horwitz, A.F. (2001). Differential dynamics of alpha 5 integrin, paxillin, and alpha-actinin during formation and disassembly of adhesions in migrating cells. J Cell Biol *153*, 1427-1440.

Lee, D.A., and Higginbotham, E.J. (2005). Glaucoma and its treatment: a review. Am J Health Syst Pharm *62*, 691-699.

Lee, J., Ishihara, A., Oxford, G., Johnson, B., and Jacobson, K. (1999). Regulation of cell movement is mediated by stretch-activated calcium channels. Nature *400*, 382-386.

Lefranc, F., Rynkowski, M., DeWitte, O., and Kiss, R. (2009). Present and potential future adjuvant issues in high-grade astrocytic glioma treatment. Adv Tech Stand Neurosurg *34*, 3-35.

Leonelli, M., Martins, D.O., and Britto, L.R. (2010). TRPV1 receptors are involved in protein nitration and Muller cell reaction in the acutely axotomized rat retina. Exp Eye Res *91*, 755-768.

Leonelli, M., Martins, D.O., and Britto, L.R. (2011). TRPV1 receptors modulate retinal development. Int J Dev Neurosci.

Leonelli, M., Martins, D.O., and Britto, L.R. (2013). Retinal cell death induced by TRPV1 activation involves NMDA signaling and upregulation of nitric oxide synthases. Cellular and molecular neurobiology *33*, 379-392.

Leonelli, M., Martins, D.O., Kihara, A.H., and Britto, L.R. (2009). Ontogenetic expression of the vanilloid receptors TRPV1 and TRPV2 in the rat retina. Int J Dev Neurosci *27*, 709-718.

Lepekhin, E.A., Eliasson, C., Berthold, C.H., Berezin, V., Bock, E., and Pekny, M. (2001). Intermediate filaments regulate astrocyte motility. J Neurochem *79*, 617-625.

Levkovitch-Verbin, H. (2004). Animal models of optic nerve diseases. Eye (Lond) *18*, 1066-1074.

Li, H.B., Mao, R.R., Zhang, J.C., Yang, Y., Cao, J., and Xu, L. (2008). Antistress effect of TRPV1 channel on synaptic plasticity and spatial memory. Biol Psychiatry *64*, 286-292.

Li, Z., Hogan, E.L., and Banik, N.L. (1996). Role of calpain in spinal cord injury: increased calpain immunoreactivity in rat spinal cord after impact trauma. Neurochem Res *21*, 441-448.

Li, Z.H., and Bresnick, A.R. (2006). The S100A4 metastasis factor regulates cellular motility via a direct interaction with myosin-IIA. Cancer research *66*, 5173-5180.

Liang, C.C., Park, A.Y., and Guan, J.L. (2007). In vitro scratch assay: a convenient and inexpensive method for analysis of cell migration in vitro. Nat Protoc *2*, 329-333.

Lilja, J., Lindegren, H., and Forsby, A. (2007). Surfactant-induced TRPV1 activity--a novel mechanism for eye irritation? Toxicol Sci *99*, 174-180.

Ling, T.L., Mitrofanis, J., and Stone, J. (1989). Origin of retinal astrocytes in the rat: evidence of migration from the optic nerve. J Comp Neurol *286*, 345-352.

Lishko, P.V., Procko, E., Jin, X., Phelps, C.B., and Gaudet, R. (2007). The ankyrin repeats of TRPV1 bind multiple ligands and modulate channel sensitivity. Neuron *54*, 905-918.

Liu, B., and Neufeld, A.H. (2000). Expression of nitric oxide synthase-2 (NOS-2) in reactive astrocytes of the human glaucomatous optic nerve head. Glia *30*, 178-186.

Liu, B., Zhang, C., and Qin, F. (2005). Functional recovery from desensitization of vanilloid receptor TRPV1 requires resynthesis of phosphatidylinositol 4,5-bisphosphate. J Neurosci *25*, 4835-4843.

Liu, B.P., Chrzanowska-Wodnicka, M., and Burridge, K. (1998). Microtubule depolymerization induces stress fibers, focal adhesions, and DNA synthesis via the GTP-binding protein Rho. Cell Adhes Commun *5*, 249-255.

Liu, L., Chen, L., Liedtke, W., and Simon, S.A. (2007). Changes in osmolality sensitize the response to capsaicin in trigeminal sensory neurons. J Neurophysiol *97*, 2001-2015.

Liu, L., and Simon, S.A. (1997). Capsazepine, a vanilloid receptor antagonist, inhibits nicotinic acetylcholine receptors in rat trigeminal ganglia. Neurosci Lett *228*, 29-32.

Lohr, C., Heil, J.E., and Deitmer, J.W. (2005). Blockage of voltage-gated calcium signaling impairs migration of glial cells in vivo. Glia *50*, 198-211.

Luheshi, N.M., Rothwell, N.J., and Brough, D. (2009). Dual functionality of interleukin-1 family cytokines: implications for anti-interleukin-1 therapy. Br J Pharmacol *157*, 1318-1329.

Luo, J.H., and Weinstein, I.B. (1993). Calcium-dependent activation of protein kinase C. The role of the C2 domain in divalent cation selectivity. J Biol Chem *268*, 23580-23584.

Maione, S., Cristino, L., Migliozzi, A.L., Georgiou, A.L., Starowicz, K., Salt, T.E., and Di Marzo, V. (2009). TRPV1 channels control synaptic plasticity in the developing superior colliculus. J Physiol *587*, 2521-2535.

Malagarie-Cazenave, S., Olea-Herrero, N., Vara, D., and Diaz-Laviada, I. (2009). Capsaicin, a component of red peppers, induces expression of androgen receptor via PI3K and MAPK pathways in prostate LNCaP cells. FEBS Lett *583*, 141-147.

Malarkey, E.B., Ni, Y., and Parpura, V. (2008). Ca2+ entry through TRPC1 channels contributes to intracellular Ca2+ dynamics and consequent glutamate release from rat astrocytes. Glia *56*, 821-835.

Malathi, K., Li, X., Krizanova, O., Ondrias, K., Sperber, K., Ablamunits, V., and Jayaraman, T. (2005). Cdc2/cyclin B1 interacts with and modulates inositol 1,4,5-trisphosphate receptor (type 1) functions. J Immunol *175*, 6205-6210.

Malkia, A., Pertusa, M., Fernandez-Ballester, G., Ferrer-Montiel, A., and Viana, F. (2009). Differential role of the menthol-binding residue Y745 in the antagonism of thermally gated TRPM8 channels. Mol Pain *5*, 62.

Mandadi, S., Numazaki, M., Tominaga, M., Bhat, M.B., Armati, P.J., and Roufogalis, B.D. (2004). Activation of protein kinase C reverses capsaicin-induced calcium-dependent desensitization of TRPV1 ion channels. Cell Calcium *35*, 471-478.

Mandadi, S., Tominaga, T., Numazaki, M., Murayama, N., Saito, N., Armati, P.J., Roufogalis, B.D., and Tominaga, M. (2006). Increased sensitivity of desensitized TRPV1 by PMA occurs through PKCepsilon-mediated phosphorylation at S800. Pain *123*, 106-116.

Mandal, A., Shahidullah, M., and Delamere, N.A. (2010). Hydrostatic pressure-induced release of stored calcium in cultured rat optic nerve head astrocytes. Invest Ophthalmol Vis Sci *51*, 3129-3138.

Mannari, T., Morita, S., Furube, E., Tominaga, M., and Miyata, S. (2013). Astrocytic TRPV1 ion channels detect blood-borne signals in the sensory circumventricular organs of adult mouse brains. Glia *61*, 957-971.

Maragakis, N.J., and Rothstein, J.D. (2004). Glutamate transporters: animal models to neurologic disease. Neurobiol Dis *15*, 461-473.

Mariani, L., Beaudry, C., McDonough, W.S., Hoelzinger, D.B., Demuth, T., Ross, K.R., Berens, T., Coons, S.W., Watts, G., Trent, J.M., *et al.* (2001). Glioma cell motility is associated with reduced transcription of proapoptotic and proliferation genes: a cDNA microarray analysis. J Neurooncol *53*, 161-176.

Marinelli, S., Di Marzo, V., Berretta, N., Matias, I., Maccarrone, M., Bernardi, G., and Mercuri, N.B. (2003). Presynaptic facilitation of glutamatergic synapses to dopaminergic neurons of the rat substantia nigra by endogenous stimulation of vanilloid receptors. J Neurosci *23*, 3136-3144.

Marinelli, S., Pascucci, T., Bernardi, G., Puglisi-Allegra, S., and Mercuri, N.B. (2005). Activation of TRPV1 in the VTA excites dopaminergic neurons and increases chemical- and noxious-induced dopamine release in the nucleus accumbens. Neuropsychopharmacology *30*, 864-870.

Marinelli, S., Vaughan, C.W., Christie, M.J., and Connor, M. (2002). Capsaicin activation of glutamatergic synaptic transmission in the rat locus coeruleus in vitro. J Physiol *543*, 531-540.

Marsch, R., Foeller, E., Rammes, G., Bunck, M., Kossl, M., Holsboer, F., Zieglgansberger, W., Landgraf, R., Lutz, B., and Wotjak, C.T. (2007). Reduced anxiety, conditioned fear, and hippocampal long-term potentiation in transient receptor potential vanilloid type 1 receptor-deficient mice. J Neurosci *27*, 832-839.

Marshall, I.C., Owen, D.E., Cripps, T.V., Davis, J.B., McNulty, S., and Smart, D. (2003). Activation of vanilloid receptor 1 by resiniferatoxin mobilizes calcium from inositol 1,4,5-trisphosphate-sensitive stores. Br J Pharmacol *138*, 172-176.

Martin, E., Dahan, D., Cardouat, G., Gillibert-Duplantier, J., Marthan, R., Savineau, J.P., and Ducret, T. (2012). Involvement of TRPV1 and TRPV4 channels in migration of rat pulmonary arterial smooth muscle cells. Pflugers Arch *464*, 261-272.

Martini, F.J., and Valdeolmillos, M. (2010). Actomyosin contraction at the cell rear drives nuclear translocation in migrating cortical interneurons. J Neurosci *30*, 8660-8670.

Matsuda, H., Noma, A., Kurachi, Y., and Irisawa, H. (1982). Transient depolarization and spontaneous voltage fluctuations in isolated single cells from guinea pig ventricles. Calcium-mediated membrane potential fluctuations. Circ Res *51*, 142-151.

Matyash, M., Matyash, V., Nolte, C., Sorrentino, V., and Kettenmann, H. (2002). Requirement of functional ryanodine receptor type 3 for astrocyte migration. FASEB J *16*, 84-86.

Matyash, V., and Kettenmann, H. (2010). Heterogeneity in astrocyte morphology and physiology. Brain Res Rev *63*, 2-10.

McGeer, P.L., and McGeer, E.G. (2008). Glial reactions in Parkinson's disease. Mov Disord *23*, 474-483.

McIntyre, P., McLatchie, L.M., Chambers, A., Phillips, E., Clarke, M., Savidge, J., Toms, C., Peacock, M., Shah, K., Winter, J., *et al.* (2001). Pharmacological differences between the human and rat vanilloid receptor 1 (VR1). Br J Pharmacol *132*, 1084-1094.

Medvedeva, Y.V., Kim, M.S., and Usachev, Y.M. (2008). Mechanisms of prolonged presynaptic Ca2+ signaling and glutamate release induced by TRPV1 activation in rat sensory neurons. J Neurosci *28*, 5295-5311.

Meguro, K., Iida, H., Takano, H., Morita, T., Sata, M., Nagai, R., and Nakajima, T. (2009). Function and role of voltage-gated sodium channel NaV1.7 expressed in aortic smooth muscle cells. Am J Physiol Heart Circ Physiol *296*, H211-219.

Mena, M.A., and Garcia de Yebenes, J. (2008). Glial cells as players in parkinsonism: the "good," the "bad," and the "mysterious" glia. Neuroscientist *14*, 544-560.

Miao, H., Crabb, A.W., Hernandez, M.R., and Lukas, T.J. (2010). Modulation of factors affecting optic nerve head astrocyte migration. Invest Ophthalmol Vis Sci *51*, 4096-4103.

Middeldorp, J., and Hol, E.M. (2011). GFAP in health and disease. Prog Neurobiol *93*, 421-443.

Midwood, K.S., and Schwarzbauer, J.E. (2002). Tenascin-C modulates matrix contraction via focal adhesion kinase- and Rho-mediated signaling pathways. Mol Biol Cell *13*, 3601-3613.

Miller, R.H., David, S., Patel, R., Abney, E.R., and Raff, M.C. (1985). A quantitative immunohistochemical study of macroglial cell development in the rat optic nerve: in vivo evidence for two distinct astrocyte lineages. Dev Biol *111*, 35-41.

Miller, R.H., and Raff, M.C. (1984). Fibrous and protoplasmic astrocytes are biochemically and developmentally distinct. J Neurosci *4*, 585-592.

Milner, R., Huang, X., Wu, J., Nishimura, S., Pytela, R., Sheppard, D., and ffrench-Constant, C. (1999). Distinct roles for astrocyte alphavbeta5 and alphavbeta8 integrins in adhesion and migration. J Cell Sci *112 (Pt 23)*, 4271-4279.

Mitchison, T.J., and Cramer, L.P. (1996). Actin-based cell motility and cell locomotion. Cell *84*, 371-379.

Miyano, K., Morioka, N., Sugimoto, T., Shiraishi, S., Uezono, Y., and Nakata, Y. (2010). Activation of the neurokinin-1 receptor in rat spinal astrocytes induces Ca2+ release from IP3-sensitive Ca2+ stores and extracellular Ca2+ influx through TRPC3. Neurochem Int *57*, 923-934.

Mogi, M., Togari, A., Kondo, T., Mizuno, Y., Komure, O., Kuno, S., Ichinose, H., and Nagatsu, T. (2000). Caspase activities and tumor necrosis factor receptor R1 (p55) level are elevated in the substantia nigra from parkinsonian brain. J Neural Transm *107*, 335-341.

Mohapatra, D.P., and Nau, C. (2003). Desensitization of capsaicin-activated currents in the vanilloid receptor TRPV1 is decreased by the cyclic AMP-dependent protein kinase pathway. J Biol Chem *278*, 50080-50090.

Mohapatra, D.P., and Nau, C. (2005). Regulation of Ca2+-dependent desensitization in the vanilloid receptor TRPV1 by calcineurin and cAMP-dependent protein kinase. J Biol Chem *280*, 13424-13432.

Moiseenkova-Bell, V.Y., Stanciu, L.A., Serysheva, II, Tobe, B.J., and Wensel, T.G. (2008). Structure of TRPV1 channel revealed by electron cryomicroscopy. Proc Natl Acad Sci U S A *105*, 7451-7455.

Montell, C. (2005). TRP channels in Drosophila photoreceptor cells. J Physiol *567*, 45-51.

Morgan, J.E. (2000). Optic nerve head structure in glaucoma: astrocytes as mediators of axonal damage. Eye (Lond) *14 (Pt 3B)*, 437-444.

Morganti-Kossmann, M.C., Kossmann, T., Brandes, M.E., Mergenhagen, S.E., and Wahl, S.M. (1992). Autocrine and paracrine regulation of astrocyte function by transforming growth factor-beta. J Neuroimmunol *39*, 163-173.

Morino, I., Hiscott, P., McKechnie, N., and Grierson, I. (1990). Variation in epiretinal membrane components with clinical duration of the proliferative tissue. Br J Ophthalmol *74*, 393-399.

Morrison, J.C. (2006). Integrins in the optic nerve head: potential roles in glaucomatous optic neuropathy (an American Ophthalmological Society thesis). Trans Am Ophthalmol Soc *104*, 453-477.

Morrison, J.C., Dorman-Pease, M.E., Dunkelberger, G.R., and Quigley, H.A. (1990). Optic nerve head extracellular matrix in primary optic atrophy and experimental glaucoma. Arch Ophthalmol *108*, 1020-1024.

Munsch, T., Freichel, M., Flockerzi, V., and Pape, H.C. (2003). Contribution of transient receptor potential channels to the control of GABA release from dendrites. Proc Natl Acad Sci U S A *100*, 16065-16070.

Musella, A., De Chiara, V., Rossi, S., Prosperetti, C., Bernardi, G., Maccarrone, M., and Centonze, D. (2009). TRPV1 channels facilitate glutamate transmission in the striatum. Mol Cell Neurosci *40*, 89-97.

Mustafa, S., and Oriowo, M. (2005). Cooling-induced contraction of the rat gastric fundus: mediation via transient receptor potential (TRP) cation channel TRPM8 receptor and Rho-kinase activation. Clinical and experimental pharmacology & physiology *32*, 832-838.

Nagele, R.G., Wegiel, J., Venkataraman, V., Imaki, H., and Wang, K.C. (2004). Contribution of glial cells to the development of amyloid plaques in Alzheimer's disease. Neurobiol Aging *25*, 663-674.

Nagelhus, E.A., Veruki, M.L., Torp, R., Haug, F.M., Laake, J.H., Nielsen, S., Agre, P., and Ottersen, O.P. (1998). Aquaporin-4 water channel protein in the rat retina and optic nerve: polarized expression in Muller cells and fibrous astrocytes. J Neurosci *18*, 2506-2519.

Nakagawa, M., Fukata, M., Yamaga, M., Itoh, N., and Kaibuchi, K. (2001). Recruitment and activation of Rac1 by the formation of E-cadherin-mediated cell-cell adhesion sites. J Cell Sci *114*, 1829-1838.

Nakanishi, M., Hata, K., Nagayama, T., Sakurai, T., Nishisho, T., Wakabayashi, H., Hiraga, T., Ebisu, S., and Yoneda, T. (2010). Acid activation of Trpv1 leads to an up-regulation of calcitonin gene-related peptide expression in dorsal root ganglion neurons via the CaMK-CREB cascade: a potential mechanism of inflammatory pain. Mol Biol Cell *21*, 2568-2577.

Neumann, H., Schweigreiter, R., Yamashita, T., Rosenkranz, K., Wekerle, H., and Barde, Y.A. (2002). Tumor necrosis factor inhibits neurite outgrowth and branching of hippocampal neurons by a rho-dependent mechanism. J Neurosci *22*, 854-862.

Newman, E.A. (2001). Propagation of intercellular calcium waves in retinal astrocytes and Muller cells. J Neurosci *21*, 2215-2223.

Newman, E.A., and Zahs, K.R. (1998). Modulation of neuronal activity by glial cells in the retina. J Neurosci *18*, 4022-4028.

Nickells, R.W., Howell, G.R., Soto, I., and John, S.W. (2012). Under pressure: cellular and molecular responses during glaucoma, a common neurodegeneration with axonopathy. Annu Rev Neurosci *35*, 153-179.

Nishio, T., Kawaguchi, S., Iseda, T., Kawasaki, T., and Hase, T. (2003). Secretion of tenascin-C by cultured astrocytes: regulation of cell proliferation and process elongation. Brain Res *990*, 129-140.

Nishio, T., Kawaguchi, S., Yamamoto, M., Iseda, T., Kawasaki, T., and Hase, T. (2005). Tenascin-C regulates proliferation and migration of cultured astrocytes in a scratch wound assay. Neuroscience *132*, 87-102.

Nizzardo, M., Simone, C., Rizzo, F., Ruggieri, M., Salani, S., Riboldi, G., Faravelli, I., Zanetta, C., Bresolin, N., Comi, G.P., *et al.* (2014). Minimally invasive transplantation of iPSC-derived ALDHhiSSCloVLA4+ neural stem cells effectively improves the phenotype of an amyotrophic lateral sclerosis model. Human molecular genetics *23*, 342-354.

Nobes, C.D., and Hall, A. (1995). Rho, rac, and cdc42 GTPases regulate the assembly of multimolecular focal complexes associated with actin stress fibers, lamellipodia, and filopodia. Cell *81*, 53-62.

Noegel, A., Witke, W., and Schleicher, M. (1987). Calcium-sensitive non-muscle alpha-actinin contains EF-hand structures and highly conserved regions. FEBS Lett *221*, 391-396.

Nogales, E. (2000). Structural insights into microtubule function. Annu Rev Biochem *69*, 277-302.

Nucci, C., Gasperi, V., Tartaglione, R., Cerulli, A., Terrinoni, A., Bari, M., De Simone, C., Agro, A.F., Morrone, L.A., Corasaniti, M.T., *et al.* (2007). Involvement of the endocannabinoid system in retinal damage after high intraocular pressure-induced ischemia in rats. Invest Ophthalmol Vis Sci *48*, 2997-3004.

Numazaki, M., Tominaga, T., Takeuchi, K., Murayama, N., Toyooka, H., and Tominaga, M. (2003). Structural determinant of TRPV1 desensitization interacts with calmodulin. Proc Natl Acad Sci U S A *100*, 8002-8006.

Oberheim, N.A., Takano, T., Han, X., He, W., Lin, J.H., Wang, F., Xu, Q., Wyatt, J.D., Pilcher, W., Ojemann, J.G., *et al.* (2009). Uniquely hominid features of adult human astrocytes. J Neurosci *29*, 3276-3287.

Ogden, T.E. (1978). Nerve fiber layer astrocytes of the primate retina: morphology, distribution, and density. Invest Ophthalmol Vis Sci *17*, 499-510.

Ogier, C., Bernard, A., Chollet, A.M., T, L.E.D., Hanessian, S., Charton, G., Khrestchatisky, M., and Rivera, S. (2006). Matrix metalloproteinase-2 (MMP-2) regulates astrocyte motility in connection with the actin cytoskeleton and integrins. Glia *54*, 272-284.

Ohgaki, H., and Kleihues, P. (2005). Epidemiology and etiology of gliomas. Acta Neuropathol *109*, 93-108.

Okada, S., Nakamura, M., Katoh, H., Miyao, T., Shimazaki, T., Ishii, K., Yamane, J., Yoshimura, A., Iwamoto, Y., Toyama, Y., *et al.* (2006). Conditional ablation of Stat3 or Socs3 discloses a dual role for reactive astrocytes after spinal cord injury. Nat Med *12*, 829-834.

Omelchenko, T., Vasiliev, J.M., Gelfand, I.M., Feder, H.H., and Bonder, E.M. (2002). Mechanisms of polarization of the shape of fibroblasts and epitheliocytes: Separation of the roles of microtubules and Rho-dependent actin-myosin contractility. Proc Natl Acad Sci U S A *99*, 10452-10457.

Osmani, N., Peglion, F., Chavrier, P., and Etienne-Manneville, S. (2010). Cdc42 localization and cell polarity depend on membrane traffic. J Cell Biol *191*, 1261-1269.

Osmani, N., Vitale, N., Borg, J.P., and Etienne-Manneville, S. (2006). Scrib controls Cdc42 localization and activity to promote cell polarization during astrocyte migration. Curr Biol *16*, 2395-2405.

Panner, A., and Wurster, R.D. (2006). T-type calcium channels and tumor proliferation. Cell Calcium *40*, 253-259.

Park, E.S., Kim, S.R., and Jin, B.K. (2012). Transient receptor potential vanilloid subtype 1 contributes to mesencephalic dopaminergic neuronal survival by inhibiting microglia-originated oxidative stress. Brain research bulletin *89*, 92-96.

Parpura, V., and Verkhratsky, A. (2012). Astrocytes revisited: concise historic outlook on glutamate homeostasis and signaling. Croat Med J *53*, 518-528.

Parsons, J.T., and Parsons, S.J. (1997). Src family protein tyrosine kinases: cooperating with growth factor and adhesion signaling pathways. Curr Opin Cell Biol *9*, 187-192.

Perea, G., Navarrete, M., and Araque, A. (2009). Tripartite synapses: astrocytes process and control synaptic information. Trends Neurosci *32*, 421-431.

Perego, C., Vanoni, C., Bossi, M., Massari, S., Basudev, H., Longhi, R., and Pietrini, G. (2000). The GLT-1 and GLAST glutamate transporters are expressed on morphologically distinct astrocytes and regulated by neuronal activity in primary hippocampal cocultures. J Neurochem *75*, 1076-1084.

Petravicz, J., Fiacco, T.A., and McCarthy, K.D. (2008). Loss of IP3 receptor-dependent Ca2+ increases in hippocampal astrocytes does not affect baseline CA1 pyramidal neuron synaptic activity. J Neurosci *28*, 4967-4973.

Phillips, E., Reeve, A., Bevan, S., and McIntyre, P. (2004). Identification of species-specific determinants of the action of the antagonist capsazepine and the agonist PPAHV on TRPV1. J Biol Chem *279*, 17165-17172.

Price, T.J., Jeske, N.A., Flores, C.M., and Hargreaves, K.M. (2005). Pharmacological interactions between calcium/calmodulin-dependent kinase II alpha and TRPV1 receptors in rat trigeminal sensory neurons. Neurosci Lett *389*, 94-98.

Puntambekar, P., Van Buren, J., Raisinghani, M., Premkumar, L.S., and Ramkumar, V. (2004). Direct interaction of adenosine with the TRPV1 channel protein. J Neurosci *24*, 3663-3671.

Puschmann, T.B., Dixon, K.J., and Turnley, A.M. (2010). Species differences in reactivity of mouse and rat astrocytes in vitro. Neurosignals *18*, 152-163.

Quigley, H.A., Addicks, E.M., Green, W.R., and Maumenee, A.E. (1981). Optic nerve damage in human glaucoma. II. The site of injury and susceptibility to damage. Arch Ophthalmol *99*, 635-649.

Quigley, H.A., and Broman, A.T. (2006). The number of people with glaucoma worldwide in 2010 and 2020. Br J Ophthalmol *90*, 262-267.

Raff, M.C., Abney, E.R., Cohen, J., Lindsay, R., and Noble, M. (1983). Two types of astrocytes in cultures of developing rat white matter: differences in morphology, surface gangliosides, and growth characteristics. J Neurosci *3*, 1289-1300.

Raftopoulou, M., and Hall, A. (2004). Cell migration: Rho GTPases lead the way. Dev Biol *265*, 23-32.

Raisinghani, M., Pabbidi, R.M., and Premkumar, L.S. (2005). Activation of transient receptor potential vanilloid 1 (TRPV1) by resiniferatoxin. J Physiol *567*, 771-786.

Ramirez, J.M., Ramirez, A.I., Salazar, J.J., de Hoz, R., and Trivino, A. (2001). Changes of astrocytes in retinal ageing and age-related macular degeneration. Exp Eye Res *73*, 601-615.

Reilly, C.A., Johansen, M.E., Lanza, D.L., Lee, J., Lim, J.O., and Yost, G.S. (2005). Calcium-dependent and independent mechanisms of capsaicin receptor (TRPV1)-mediated cytokine production and cell death in human bronchial epithelial cells. J Biochem Mol Toxicol *19*, 266-275.

Ribeiro, C.M., Reece, J., and Putney, J.W., Jr. (1997). Role of the cytoskeleton in calcium signaling in NIH 3T3 cells. An intact cytoskeleton is required for agonist-induced [Ca2+]i signaling, but not for capacitative calcium entry. J Biol Chem *272*, 26555-26561.

Ricard, C.S., Kobayashi, S., Pena, J.D., Salvador-Silva, M., Agapova, O., and Hernandez, M.R. (2000). Selective expression of neural cell adhesion molecule (NCAM)-180 in optic nerve head astrocytes exposed to elevated hydrostatic pressure in vitro. Brain Res Mol Brain Res *81*, 62-79.

Ridley, A.J., and Hall, A. (1992). The small GTP-binding protein rho regulates the assembly of focal adhesions and actin stress fibers in response to growth factors. Cell *70*, 389-399.

Ridley, A.J., Schwartz, M.A., Burridge, K., Firtel, R.A., Ginsberg, M.H., Borisy, G., Parsons, J.T., and Horwitz, A.R. (2003). Cell migration: integrating signals from front to back. Science *302*, 1704-1709.

Robel, S., Bardehle, S., Lepier, A., Brakebusch, C., and Gotz, M. (2011a). Genetic deletion of cdc42 reveals a crucial role for astrocyte recruitment to the injury site in vitro and in vivo. J Neurosci *31*, 12471-12482.

Robel, S., Berninger, B., and Gotz, M. (2011b). The stem cell potential of glia: lessons from reactive gliosis. Nat Rev Neurosci *12*, 88-104.

Roberts, J.C., Davis, J.B., and Benham, C.D. (2004). [3H]Resiniferatoxin autoradiography in the CNS of wild-type and TRPV1 null mice defines TRPV1 (VR-1) protein distribution. Brain Res *995*, 176-183.

Robinson, S.R., and Dreher, Z. (1989). Evidence for three morphological classes of astrocyte in the adult rabbit retina: functional and developmental implications. Neurosci Lett *106*, 261-268.

Rodnight, R., Goncalves, C.A., Wofchuk, S.T., and Leal, R. (1997). Control of the phosphorylation of the astrocyte marker glial fibrillary acidic protein (GFAP) in the immature rat hippocampus by glutamate and calcium ions: possible key factor in astrocytic plasticity. Braz J Med Biol Res *30*, 325-338.

Rodriguez, J.J., Olabarria, M., Chvatal, A., and Verkhratsky, A. (2009). Astroglia in dementia and Alzheimer's disease. Cell Death Differ *16*, 378-385.

Rosenbaum, T., and Simon, S.A. (2007). TRPV1 Receptors and Signal Transduction.

Rothaeusler, K., and Baumgarth, N. (2007). Assessment of cell proliferation by 5-bromodeoxyuridine (BrdU) labeling for multicolor flow cytometry. Curr Protoc Cytom *Chapter 7*, Unit7 31.

Rousseau, E., Cloutier, M., Morin, C., and Proteau, S. (2005). Capsazepine, a vanilloid antagonist, abolishes tonic responses induced by 20-HETE on guinea pig airway smooth muscle. Am J Physiol Lung Cell Mol Physiol *288*, L460-470.

Rowin, M.E., Whatley, R.E., Yednock, T., and Bohnsack, J.F. (1998). Intracellular calcium requirements for beta1 integrin activation. J Cell Physiol *175*, 193-202.

Ryskamp, D.A., Witkovsky, P., Barabas, P., Huang, W., Koehler, C., Akimov, N.P., Lee, S.H., Chauhan, S., Xing, W., Renteria, R.C., *et al.* (2011). The polymodal ion channel transient receptor potential vanilloid 4 modulates calcium flux, spiking rate, and apoptosis of mouse retinal ganglion cells. J Neurosci *31*, 7089-7101.

Ryu, S., Liu, B., Yao, J., Fu, Q., and Qin, F. (2007). Uncoupling proton activation of vanilloid receptor TRPV1. J Neurosci *27*, 12797-12807.

Rzigalinski, B.A., Weber, J.T., Willoughby, K.A., and Ellis, E.F. (1998). Intracellular free calcium dynamics in stretch-injured astrocytes. J Neurochem *70*, 2377-2385.

Saadoun, S., Papadopoulos, M.C., Watanabe, H., Yan, D., Manley, G.T., and Verkman, A.S. (2005). Involvement of aquaporin-4 in astroglial cell migration and glial scar formation. J Cell Sci *118*, 5691-5698.

Saha, R.N., Liu, X., and Pahan, K. (2006). Up-regulation of BDNF in astrocytes by TNF-alpha: a case for the neuroprotective role of cytokine. J Neuroimmune Pharmacol *1*, 212-222.

Sakamoto, K., Kuroki, T., Okuno, Y., Sekiya, H., Watanabe, A., Sagawa, T., Ito, H., Mizuta, A., Mori, A., Nakahara, T., *et al.* (2014). Activation of the TRPV1 channel attenuates N-methyl-D-aspartic acid-induced neuronal injury in the rat retina. European journal of pharmacology *733*, 13-22.

Sanchez, A.M., Sanchez, M.G., Malagarie-Cazenave, S., Olea, N., and Diaz-Laviada, I. (2006). Induction of apoptosis in prostate tumor PC-3 cells and inhibition of xenograft prostate tumor growth by the vanilloid capsaicin. Apoptosis *11*, 89-99.

Sanz-Salvador, L., Andres-Borderia, A., Ferrer-Montiel, A., and Planells-Cases, R. (2012). Agonist- and Ca2+-dependent desensitization of TRPV1 channel targets the receptor to lysosomes for degradation. J Biol Chem *287*, 19462-19471.

Sappington, R.M., and Calkins, D.J. (2008). Contribution of TRPV1 to microglia-derived IL-6 and NFkappaB translocation with elevated hydrostatic pressure. Invest Ophthalmol Vis Sci *49*, 3004-3017.

Sappington, R.M., Carlson, B.J., Crish, S.D., and Calkins, D.J. (2010). The microbead occlusion model: a paradigm for induced ocular hypertension in rats and mice. Invest Ophthalmol Vis Sci *51*, 207-216.

Sappington, R.M., Chan, M., and Calkins, D.J. (2006). Interleukin-6 protects retinal ganglion cells from pressure-induced death. Invest Ophthalmol Vis Sci *47*, 2932-2942.

Sappington, R.M., Sidorova, T., Long, D.J., and Calkins, D.J. (2009). TRPV1: contribution to retinal ganglion cell apoptosis and increased intracellular Ca2+ with exposure to hydrostatic pressure. Invest Ophthalmol Vis Sci *50*, 717-728.

Sarthy, V.P., Brodjian, S.J., Dutt, K., Kennedy, B.N., French, R.P., and Crabb, J.W. (1998). Establishment and characterization of a retinal Muller cell line. Invest Ophthalmol Vis Sci *39*, 212-216.

Sasamura, T., Sasaki, M., Tohda, C., and Kuraishi, Y. (1998). Existence of capsaicin-sensitive glutamatergic terminals in rat hypothalamus. Neuroreport *9*, 2045-2048.

Scemes, E., and Giaume, C. (2006). Astrocyte calcium waves: what they are and what they do. Glia *54*, 716-725.

Scheller, J., Chalaris, A., Schmidt-Arras, D., and Rose-John, S. (2011). The pro- and anti-inflammatory properties of the cytokine interleukin-6. Biochim Biophys Acta *1813*, 878-888.

Schneider, C.A., Rasband, W.S., and Eliceiri, K.W. (2012). NIH Image to ImageJ: 25 years of image analysis. Nat Methods *9*, 671-675.

Schnizler, K., Shutov, L.P., Van Kanegan, M.J., Merrill, M.A., Nichols, B., McKnight, G.S., Strack, S., Hell, J.W., and Usachev, Y.M. (2008). Protein kinase A anchoring via AKAP150 is essential for TRPV1 modulation by forskolin and prostaglandin E2 in mouse sensory neurons. J Neurosci *28*, 4904-4917.

Scholzen, T., and Gerdes, J. (2000). The Ki-67 protein: from the known and the unknown. J Cell Physiol *182*, 311-322.

Schreiner, A.E., Berlinger, E., Langer, J., Kafitz, K.W., and Rose, C.R. (2013). Lesion-induced alterations in astrocyte glutamate transporter expression and function in the hippocampus. ISRN Neurol *2013*, 893605.

Seabrook, G.R., Sutton, K.G., Jarolimek, W., Hollingworth, G.J., Teague, S., Webb, J., Clark, N., Boyce, S., Kerby, J., Ali, Z., *et al.* (2002). Functional properties of the high-affinity TRPV1 (VR1) vanilloid receptor antagonist (4-hydroxy-5-iodo-3-methoxyphenylacetate ester) iodo-resiniferatoxin. J Pharmacol Exp Ther *303*, 1052-1060.

Shen, Y., and Schaller, M.D. (1999). Focal adhesion targeting: the critical determinant of FAK regulation and substrate phosphorylation. Mol Biol Cell *10*, 2507-2518.

Shibasaki, K., Ishizaki, Y., and Mandadi, S. (2013). Astrocytes express functional TRPV2 ion channels. Biochem Biophys Res Commun *441*, 327-332.

Shields, D.C., Tyor, W.R., Deibler, G.E., Hogan, E.L., and Banik, N.L. (1998). Increased calpain expression in activated glial and inflammatory cells in experimental allergic encephalomyelitis. Proc Natl Acad Sci U S A *95*, 5768-5772.

Shigetomi, E., Tong, X., Kwan, K.Y., Corey, D.P., and Khakh, B.S. (2012). TRPA1 channels regulate astrocyte resting calcium and inhibitory synapse efficacy through GAT-3. Nat Neurosci *15*, 70-80.

Shirakawa, H., Sakimoto, S., Nakao, K., Sugishita, A., Konno, M., Iida, S., Kusano, A., Hashimoto, E., Nakagawa, T., and Kaneko, S. (2010). Transient receptor potential canonical 3 (TRPC3) mediates thrombin-induced astrocyte activation and upregulates its own expression in cortical astrocytes. J Neurosci *30*, 13116-13129.

Sickmann, H.M., Waagepetersen, H.S., Schousboe, A., Benie, A.J., and Bouman, S.D. (2010). Obesity and type 2 diabetes in rats are associated with altered brain glycogen and amino-acid homeostasis. J Cereb Blood Flow Metab *30*, 1527-1537.

Sikand, P., and Premkumar, L.S. (2007). Potentiation of glutamatergic synaptic transmission by protein kinase C-mediated sensitization of TRPV1 at the first sensory synapse. J Physiol *581*, 631-647.

Silver, J., and Miller, J.H. (2004). Regeneration beyond the glial scar. Nat Rev Neurosci *5*, 146-156.

Simard, J.M., Tarasov, K.V., and Gerzanich, V. (2007). Non-selective cation channels, transient receptor potential channels and ischemic stroke. Biochim Biophys Acta *1772*, 947-957.

Smyth, J.T., Hwang, S.Y., Tomita, T., DeHaven, W.I., Mercer, J.C., and Putney, J.W. (2010). Activation and regulation of store-operated calcium entry. J Cell Mol Med *14*, 2337-2349.

Sofroniew, M.V. (2009). Molecular dissection of reactive astrogliosis and glial scar formation. Trends Neurosci *32*, 638-647.

Sofroniew, M.V., and Vinters, H.V. (2010). Astrocytes: biology and pathology. Acta Neuropathol *119*, 7-35.

Son, J.L., Soto, I., Oglesby, E., Lopez-Roca, T., Pease, M.E., Quigley, H.A., and Marsh-Armstrong, N. (2010). Glaucomatous optic nerve injury involves early astrocyte reactivity and late oligodendrocyte loss. Glia *58*, 780-789.

Song, Z.H., and Zhong, M. (2000). CB1 cannabinoid receptor-mediated cell migration. J Pharmacol Exp Ther *294*, 204-209.

Sorci, G., Agneletti, A.L., Bianchi, R., and Donato, R. (1998). Association of S100B with intermediate filaments and microtubules in glial cells. Biochim Biophys Acta *1448*, 277-289.

Sorci, G., Agneletti, A.L., and Donato, R. (2000). Effects of S100A1 and S100B on microtubule stability. An in vitro study using triton-cytoskeletons from astrocyte and myoblast cell lines. Neuroscience *99*, 773-783.

Strokin, M., Sergeeva, M., and Reiser, G. (2003). Docosahexaenoic acid and arachidonic acid release in rat brain astrocytes is mediated by two separate isoforms of phospholipase A2 and is differently regulated by cyclic AMP and Ca2+. Br J Pharmacol *139*, 1014-1022.

Su, L.T., Agapito, M.A., Li, M., Simonson, W.T., Huttenlocher, A., Habas, R., Yue, L., and Runnels, L.W. (2006). TRPM7 regulates cell adhesion by controlling the calcium-dependent protease calpain. J Biol Chem *281*, 11260-11270.

Sumioka, T., Okada, Y., Reinach, P.S., Shirai, K., Miyajima, M., Yamanaka, O., and Saika, S. (2014). Impairment of corneal epithelial wound healing in a TRPV1-deficient mouse. Invest Ophthalmol Vis Sci *55*, 3295-3302.

Sun, F.J., Guo, W., Zheng, D.H., Zhang, C.Q., Li, S., Liu, S.Y., Yin, Q., Yang, H., and Shu, H.F. (2013). Increased expression of TRPV1 in the cortex and hippocampus from patients with mesial temporal lobe epilepsy. J Mol Neurosci *49*, 182-193.

Suter, M.R., Berta, T., Gao, Y.J., Decosterd, I., and Ji, R.R. (2009). Large A-fiber activity is required for microglial proliferation and p38 MAPK activation in the spinal cord: different effects of resiniferatoxin and bupivacaine on spinal microglial changes after spared nerve injury. Mol Pain *5*, 53.

Szallasi, A., and Blumberg, P.M. (1989). Resiniferatoxin, a phorbol-related diterpene, acts as an ultrapotent analog of capsaicin, the irritant constituent in red pepper. Neuroscience *30*, 515-520.

Szallasi, A., Goso, C., Blumberg, P.M., and Manzini, S. (1993). Competitive inhibition by capsazepine of [3H]resiniferatoxin binding to central (spinal cord and dorsal root ganglia) and peripheral (urinary bladder and airways) vanilloid (capsaicin) receptors in the rat. J Pharmacol Exp Ther *267*, 728-733.

Talbot, S., Dias, J.P., Lahjouji, K., Bogo, M.R., Campos, M.M., Gaudreau, P., and Couture, R. (2012). Activation of TRPV1 by capsaicin induces functional kinin B(1) receptor in rat spinal cord microglia. J Neuroinflammation *9*, 16.

Tamatani, M., Che, Y.H., Matsuzaki, H., Ogawa, S., Okado, H., Miyake, S., Mizuno, T., and Tohyama, M. (1999). Tumor necrosis factor induces Bcl-2 and Bcl-x expression through NFkappaB activation in primary hippocampal neurons. J Biol Chem *274*, 8531-8538.

Tasdemir-Yilmaz, O.E., and Freeman, M.R. (2014). Astrocytes engage unique molecular programs to engulf pruned neuronal debris from distinct subsets of neurons. Genes & development *28*, 20-33.

Tawil, N., Wilson, P., and Carbonetto, S. (1993). Integrins in point contacts mediate cell spreading: factors that regulate integrin accumulation in point contacts vs. focal contacts. J Cell Biol *120*, 261-271.

Tawil, N.J., Wilson, P., and Carbonetto, S. (1994). Expression and distribution of functional integrins in rat CNS glia. J Neurosci Res *39*, 436-447.

Taylor, J.M., and Simpson, R.U. (1992). Inhibition of cancer cell growth by calcium channel antagonists in the athymic mouse. Cancer research *52*, 2413-2418.

Tezel, G., Edward, D.P., and Wax, M.B. (1999). Serum autoantibodies to optic nerve head glycosaminoglycans in patients with glaucoma. Arch Ophthalmol *117*, 917-924.

Tezel, G., Hernandez, M.R., and Wax, M.B. (2001a). In vitro evaluation of reactive astrocyte migration, a component of tissue remodeling in glaucomatous optic nerve head. Glia *34*, 178-189.

Tezel, G., Li, L.Y., Patil, R.V., and Wax, M.B. (2001b). TNF-alpha and TNF-alpha receptor-1 in the retina of normal and glaucomatous eyes. Invest Ophthalmol Vis Sci *42*, 1787-1794.

Tezel, G., and Wax, M.B. (2000). Increased production of tumor necrosis factor-alpha by glial cells exposed to simulated ischemia or elevated hydrostatic pressure induces apoptosis in cocultured retinal ganglion cells. J Neurosci *20*, 8693-8700.

Tezel, G., Yang, X., Luo, C., Cai, J., and Powell, D.W. (2012). An astrocyte-specific proteomic approach to inflammatory responses in experimental rat glaucoma. Invest Ophthalmol Vis Sci *53*, 4220-4233.

Tominaga, M., Wada, M., and Masu, M. (2001). Potentiation of capsaicin receptor activity by metabotropic ATP receptors as a possible mechanism for ATP-evoked pain and hyperalgesia. Proc Natl Acad Sci U S A *98*, 6951-6956.

Tomono, M., Toyoshima, K., Ito, M., Amano, H., and Kiss, Z. (1998). Inhibitors of calcineurin block expression of cyclins A and E induced by fibroblast growth factor in Swiss 3T3 fibroblasts. Archives of biochemistry and biophysics *353*, 374-378.

Toth, A., Wang, Y., Kedei, N., Tran, R., Pearce, L.V., Kang, S.U., Jin, M.K., Choi, H.K., Lee, J., and Blumberg, P.M. (2005). Different vanilloid agonists cause different patterns of calcium response in CHO cells heterologously expressing rat TRPV1. Life Sci *76*, 2921-2932.

Tower, D.B., and Young, O.M. (1973). The activities of butyrylcholinesterase and carbonic anhydrase, the rate of anaerobic glycolysis, and the question of a constant density of glial cells in cerebral cortices of various mammalian species from mouse to whale. J Neurochem *20*, 269-278.

Tura, A., Schuettauf, F., Monnier, P.P., Bartz-Schmidt, K.U., and Henke-Fahle, S. (2009). Efficacy of Rho-kinase inhibition in promoting cell survival and reducing reactive gliosis in the rodent retina. Invest Ophthalmol Vis Sci *50*, 452-461.

Turner, C.E. (2000). Paxillin and focal adhesion signalling. Nat Cell Biol *2*, E231-236.

Turner, H., Fleig, A., Stokes, A., Kinet, J.P., and Penner, R. (2003). Discrimination of intracellular calcium store subcompartments using TRPV1 (transient receptor potential channel, vanilloid subfamily member 1) release channel activity. Biochem J *371*, 341-350.

Ufret-Vincenty, C.A., Klein, R.M., Hua, L., Angueyra, J., and Gordon, S.E. (2011). Localization of the PIP2 sensor of TRPV1 ion channels. J Biol Chem *286*, 9688-9698.

Unno, T., Komori, S., and Ohashi, H. (1999). Microtubule cytoskeleton involvement in muscarinic suppression of voltage-gated calcium channel current in guinea-pig ileal smooth muscle. Br J Pharmacol *127*, 1703-1711.

Van Buren, J.J., Bhat, S., Rotello, R., Pauza, M.E., and Premkumar, L.S. (2005). Sensitization and translocation of TRPV1 by insulin and IGF-I. Mol Pain *1*, 17.

van der Vaart, B., Akhmanova, A., and Straube, A. (2009). Regulation of microtubule dynamic instability. Biochemical Society transactions *37*, 1007-1013.

van Landeghem, F.K., Weiss, T., Oehmichen, M., and von Deimling, A. (2006). Decreased expression of glutamate transporters in astrocytes after human traumatic brain injury. J Neurotrauma *23*, 1518-1528.

van Strien, M.E., Breve, J.J., Fratantoni, S., Schreurs, M.W., Bol, J.G., Jongenelen, C.A., Drukarch, B., and van Dam, A.M. (2011). Astrocyte-derived tissue transglutaminase interacts with fibronectin: a role in astrocyte adhesion and migration? PLoS One *6*, e25037.

Varga, A., Bolcskei, K., Szoke, E., Almasi, R., Czeh, G., Szolcsanyi, J., and Petho, G. (2006). Relative roles of protein kinase A and protein kinase C in modulation of transient receptor potential vanilloid type 1 receptor responsiveness in rat sensory neurons in vitro and peripheral nociceptors in vivo. Neuroscience *140*, 645-657.

Vellani, V., Zachrisson, O., and McNaughton, P.A. (2004). Functional bradykinin B1 receptors are expressed in nociceptive neurones and are upregulated by the neurotrophin GDNF. J Physiol *560*, 391-401.

Verkhratsky, A., Reyes, R.C., and Parpura, V. (2014). TRP Channels Coordinate Ion Signalling in Astroglia. Rev Physiol Biochem Pharmacol *166*, 1-22.

Vicente-Manzanares, M., Ma, X., Adelstein, R.S., and Horwitz, A.R. (2009). Non-muscle myosin II takes centre stage in cell adhesion and migration. Nat Rev Mol Cell Biol *10*, 778-790.

Volterra, A., Liaudet, N., and Savtchouk, I. (2014). Astrocyte Ca(2)(+) signalling: an unexpected complexity. Nat Rev Neurosci *15*, 327-335.

Vyklicky, L., Novakova-Tousova, K., Benedikt, J., Samad, A., Touska, F., and Vlachova, V. (2008). Calcium-dependent desensitization of vanilloid receptor TRPV1: a mechanism possibly involved in analgesia induced by topical application of capsaicin. Physiol Res *57 Suppl 3*, S59-68.

Wahl, P., Foged, C., Tullin, S., and Thomsen, C. (2001). Iodo-resiniferatoxin, a new potent vanilloid receptor antagonist. Mol Pharmacol *59*, 9-15.

Walpole, C.S., Bevan, S., Bovermann, G., Boelsterli, J.J., Breckenridge, R., Davies, J.W., Hughes, G.A., James, I., Oberer, L., Winter, J., *et al.* (1994). The discovery of capsazepine, the first

competitive antagonist of the sensory neuron excitants capsaicin and resiniferatoxin. J Med Chem *37*, 1942-1954.

Walter, L., Franklin, A., Witting, A., Moller, T., and Stella, N. (2002). Astrocytes in culture produce anandamide and other acylethanolamides. J Biol Chem *277*, 20869-20876.

Walz, W. (2000). Role of astrocytes in the clearance of excess extracellular potassium. Neurochem Int *36*, 291-300.

Wang, C.Y., Mayo, M.W., Korneluk, R.G., Goeddel, D.V., and Baldwin, A.S., Jr. (1998). NF-kappaB antiapoptosis: induction of TRAF1 and TRAF2 and c-IAP1 and c-IAP2 to suppress caspase-8 activation. Science *281*, 1680-1683.

Wang, F., Smith, N.A., Xu, Q., Fujita, T., Baba, A., Matsuda, T., Takano, T., Bekar, L., and Nedergaard, M. (2012). Astrocytes modulate neural network activity by Ca(2)+-dependent uptake of extracellular K+. Sci Signal *5*, ra26.

Wang, G.X., and Poo, M.M. (2005). Requirement of TRPC channels in netrin-1-induced chemotropic turning of nerve growth cones. Nature *434*, 898-904.

Wang, J.P., Tseng, C.S., Sun, S.P., Chen, Y.S., Tsai, C.R., and Hsu, M.F. (2005a). Capsaicin stimulates the non-store-operated Ca2+ entry but inhibits the store-operated Ca2+ entry in neutrophils. Toxicol Appl Pharmacol *209*, 134-144.

Wang, K., Bekar, L.K., Furber, K., and Walz, W. (2004). Vimentin-expressing proximal reactive astrocytes correlate with migration rather than proliferation following focal brain injury. Brain Res *1024*, 193-202.

Wang, M., Kong, Q., Gonzalez, F.A., Sun, G., Erb, L., Seye, C., and Weisman, G.A. (2005b). P2Y nucleotide receptor interaction with alpha integrin mediates astrocyte migration. J Neurochem *95*, 630-640.

Waning, J., Vriens, J., Owsianik, G., Stuwe, L., Mally, S., Fabian, A., Frippiat, C., Nilius, B., and Schwab, A. (2007). A novel function of capsaicin-sensitive TRPV1 channels: involvement in cell migration. Cell Calcium *42*, 17-25.

Ward, M.M., Jobling, A.I., Puthussery, T., Foster, L.E., and Fletcher, E.L. (2004). Localization and expression of the glutamate transporter, excitatory amino acid transporter 4, within astrocytes of the rat retina. Cell Tissue Res *315*, 305-310.

Ward, N.J., Ho, K.W., Lambert, W.S., Weitlauf, C., and Calkins, D.J. (2014). Absence of transient receptor potential vanilloid-1 accelerates stress-induced axonopathy in the optic projection. J Neurosci *34*, 3161-3170.

Watanabe, T., and Raff, M.C. (1988). Retinal astrocytes are immigrants from the optic nerve. Nature *332*, 834-837.

Weber, A.J., Harman, C.D., and Viswanathan, S. (2008). Effects of optic nerve injury, glaucoma, and neuroprotection on the survival, structure, and function of ganglion cells in the mammalian retina. J Physiol *586*, 4393-4400.

Wei, C., Wang, X., Chen, M., Ouyang, K., Song, L.S., and Cheng, H. (2009). Calcium flickers steer cell migration. Nature *457*, 901-905.

Wei, C., Wang, X., Zheng, M., and Cheng, H. (2012). Calcium gradients underlying cell migration. Curr Opin Cell Biol *24*, 254-261.

West, H., Richardson, W.D., and Fruttiger, M. (2005). Stabilization of the retinal vascular network by reciprocal feedback between blood vessels and astrocytes. Development *132*, 1855-1862.

Westenbroek, R.E., Bausch, S.B., Lin, R.C., Franck, J.E., Noebels, J.L., and Catterall, W.A. (1998). Upregulation of L-type Ca2+ channels in reactive astrocytes after brain injury, hypomyelination, and ischemia. J Neurosci *18*, 2321-2334.

Wilby, M.J., Muir, E.M., Fok-Seang, J., Gour, B.J., Blaschuk, O.W., and Fawcett, J.W. (1999). N-Cadherin inhibits Schwann cell migration on astrocytes. Mol Cell Neurosci *14*, 66-84.

Wilhelmsson, U., Li, L., Pekna, M., Berthold, C.H., Blom, S., Eliasson, C., Renner, O., Bushong, E., Ellisman, M., Morgan, T.E., *et al.* (2004). Absence of glial fibrillary acidic protein and vimentin prevents hypertrophy of astrocytic processes and improves post-traumatic regeneration. J Neurosci *24*, 5016-5021.

Wozniak, M.A., Modzelewska, K., Kwong, L., and Keely, P.J. (2004). Focal adhesion regulation of cell behavior. Biochim Biophys Acta *1692*, 103-119.

Wu, T.T., Peters, A.A., Tan, P.T., Roberts-Thomson, S.J., and Monteith, G.R. (2014). Consequences of activating the calcium-permeable ion channel TRPV1 in breast cancer cells with regulated TRPV1 expression. Cell Calcium *56*, 59-67.

Wu, Z., Wong, K., Glogauer, M., Ellen, R.P., and McCulloch, C.A. (1999). Regulation of stretch-activated intracellular calcium transients by actin filaments. Biochem Biophys Res Commun *261*, 419-425.

Xing, J., and Li, J. (2007). TRPV1 receptor mediates glutamatergic synaptic input to dorsolateral periaqueductal gray (dl-PAG) neurons. J Neurophysiol *97*, 503-511.

Yamamoto, H., Kawamata, T., Ninomiya, T., Omote, K., and Namiki, A. (2006). Endothelin-1 enhances capsaicin-evoked intracellular Ca2+ response via activation of endothelin a receptor in a protein kinase Cepsilon-dependent manner in dorsal root ganglion neurons. Neuroscience *137*, 949-960.

Yang, D., Luo, Z., Ma, S., Wong, W.T., Ma, L., Zhong, J., He, H., Zhao, Z., Cao, T., Yan, Z., *et al.* (2010a). Activation of TRPV1 by dietary capsaicin improves endothelium-dependent vasorelaxation and prevents hypertension. Cell Metab *12*, 130-141.

Yang, F., Ma, L., Cao, X., Wang, K., and Zheng, J. (2014). Divalent cations activate TRPV1 through promoting conformational change of the extracellular region. J Gen Physiol *143*, 91-103.

Yang, H., Wang, Z., Capo-Aponte, J.E., Zhang, F., Pan, Z., and Reinach, P.S. (2010b). Epidermal growth factor receptor transactivation by the cannabinoid receptor (CB1) and transient receptor potential vanilloid 1 (TRPV1) induces differential responses in corneal epithelial cells. Exp Eye Res *91*, 462-471.

Ye, H., and Hernandez, M.R. (1995). Heterogeneity of astrocytes in human optic nerve head. J Comp Neurol *362*, 441-452.

Yuan, J.P., Zeng, W., Huang, G.N., Worley, P.F., and Muallem, S. (2007). STIM1 heteromultimerizes TRPC channels to determine their function as store-operated channels. Nat Cell Biol *9*, 636-645.

Yuan, L., and Neufeld, A.H. (2000). Tumor necrosis factor-alpha: a potentially neurodestructive cytokine produced by glia in the human glaucomatous optic nerve head. Glia *32*, 42-50.

Yuan, Y.M., and He, C. (2013). The glial scar in spinal cord injury and repair. Neurosci Bull *29*, 421-435.

Zaidel-Bar, R., Ballestrem, C., Kam, Z., and Geiger, B. (2003). Early molecular events in the assembly of matrix adhesions at the leading edge of migrating cells. J Cell Sci *116*, 4605-4613.

Zeng, W., Yuan, J.P., Kim, M.S., Choi, Y.J., Huang, G.N., Worley, P.F., and Muallem, S. (2008). STIM1 gates TRPC channels, but not Orai1, by electrostatic interaction. Mol Cell *32*, 439-448.

Zhang, F., Yang, H., Wang, Z., Mergler, S., Liu, H., Kawakita, T., Tachado, S.D., Pan, Z., Capo-Aponte, J.E., Pleyer, U., *et al.* (2007). Transient receptor potential vanilloid 1 activation induces inflammatory cytokine release in corneal epithelium through MAPK signaling. J Cell Physiol *213*, 730-739.

Zhang, N., Inan, S., Cowan, A., Sun, R., Wang, J.M., Rogers, T.J., Caterina, M., and Oppenheim, J.J. (2005a). A proinflammatory chemokine, CCL3, sensitizes the heat- and capsaicin-gated ion channel TRPV1. Proc Natl Acad Sci U S A *102*, 4536-4541.

Zhang, X., Huang, J., and McNaughton, P.A. (2005b). NGF rapidly increases membrane expression of TRPV1 heat-gated ion channels. EMBO J *24*, 4211-4223.

Zhang, X., Li, L., and McNaughton, P.A. (2008). Proinflammatory mediators modulate the heat-activated ion channel TRPV1 via the scaffolding protein AKAP79/150. Neuron *59*, 450-461.

Zhou, J., and Sutherland, M.L. (2004). Glutamate transporter cluster formation in astrocytic processes regulates glutamate uptake activity. J Neurosci *24*, 6301-6306.

Zimov, S., and Yazulla, S. (2004). Localization of vanilloid receptor 1 (TRPV1/VR1)-like immunoreactivity in goldfish and zebrafish retinas: restriction to photoreceptor synaptic ribbons. J Neurocytol *33*, 441-452.

Zimov, S., and Yazulla, S. (2007). Vanilloid receptor 1 (TRPV1/VR1) co-localizes with fatty acid amide hydrolase (FAAH) in retinal amacrine cells. Vis Neurosci *24*, 581-591.